hhu

Heinrich Heine
Universität Düsseldorf

Aus der Klinik für Nephrologie
der Heinrich-Heine-Universität Düsseldorf

Direktor: Prof. Dr. Lars Christian Rump

Bedeutung des Renin-Angiotensin-Systems für renovaskuläre Dysfunktion und arterielle Hypertonie

Habilitationsschrift

zur Erlangung der Venia Legendi für Innere Medizin an der
Heinrich-Heine-Universität Düsseldorf

vorgelegt von

Dr. med. Sebastian Alexander Potthoff

2022

Inhaltsverzeichnis

Der Habilitationsschrift liegen folgende Arbeiten zugrunde:

I.   *Sitek B, **Potthoff S**, Schulenborg T, Stegbauer J, Vinke T, Rump LC, Meyer HE, Vonend O, Stühler K. *(contributed equally as first authors)

"Novel approaches to analyse glomerular proteins from smallest scale murine and human samples using DIGE saturation labeling."

Proteomics. 2006

PMID: 16819728

II.   **Potthoff SA**, Sitek B, Stegbauer J, Schulenborg T, Marcus K, Quack I, Rump LC, Meyer HE, Stühler K, Vonend O.

"The glomerular proteome in a model of chronic kidney disease."

Proteomics Clin Appl. 2008

PMID: 21136910

III.   *Stegbauer J, **Potthoff SA**, Quack I, Mergia E, Clasen T, Friedrich S, Vonend O, Woznowski M, Königshausen E, Sellin L, Rump LC *(contributed equally as first authors)

"Chronic treatment with angiotensin-(1-7) improves renal endothelial dysfunction in apolipoproteinE-deficient mice."

Br J Pharmacol. 2011

PMID: 21371005

IV.   **Potthoff SA**, Fähling M, Clasen T, Mende S, Ishak B, Suvorava T, Stamer S, Thieme M, Sivritas SH, Kojda G, Patzak A, Rump LC, Stegbauer J.

"Angiotensin-(1-7) modulates renal vascular resistance through inhibition of p38 mitogen-activated protein kinase in apolipoprotein E-deficient mice."

Hypertension. 2014

PMID: 24191281

V.   **Potthoff SA**, Stamer S, Grave K, Koenigshausen E, Sivritas SH, Thieme E, Mori Y, Woznowski M, Rump LC, Stegbauer J.

"Chronic p38 mitogen-activated protein kinase inhibition improves vascular function and remodeling in angiotensin II dependent hypertension."

J Renin Angiotensin Aldosterone Syst. 2016

PMID: 27407119

VI.   Broekmans K, Stegbauer J, **Potthoff SA**, Russwurm M, Koesling D, Mergia E.

"Angiotensin II-induced hypertension is attenuated by reduction of sympathetic output in NO-sensitive guanylyl cyclase1 knock-out mice."

J Pharmacol Exp Ther. 2016

PMID: 26559126

VII.   Thieme M, Sivritas SH, Mergia E, **Potthoff SA**, Yang G, Hering L, Grave K, Hoch H, Rump LC, Stegbauer J.

"Phosphodiesterase 5 inhibition ameliorates angiotensin II-dependent hypertension and renal vascular dysfunction."

Am J Physiol Renal Physiol. 2017

PMID: 28052870

VIII.   Stegbauer J, Friedrich S, **Potthoff SA**, Broekmans K, Cortese-Krott MM, Quack I, Rump LC, Koesling D, Mergia E.

"Phosphodiesterase 5 attenuates the vasodilatory response in renovascular hypertension."

PLoS One. 2013

PMID: 24260450

IX. Königshausen E, Zierhut UM, Ruetze M, **Potthoff SA**, Stegbauer J, Woznowski M, Quack I, Rump LC, Sellin L.

"Angiotensin II increases glomerular permeability by β-arrestin mediated nephrin endocytosis."

Sci Rep. 2016

PMID: 28004760

X. Haase R, **Potthoff SA**, Meyer-Schwesinger C, Frosch C, Wiech T, Panzer U, Königshausen E, Stegbauer J, Sellin L, Rump LC, Quack I, Woznowski M.

"A novel in vivo method to quantify slit diaphragm protein abundance in murine proteinuric kidney disease."
PLoS One. 2017

PMID: 28604827

geteilte Erstautorenschaft

Abkürzungsverzeichnis

ACE	Angiotensin-Converting Enzym
ACE2	Angiotensin-Converting Enzym 2
Akt	Protein-Kinase B
Ang-(1-7)	Angiotensin-(1-7)
Ang II	Angiotensin II
ApoE	Apolipoprotein E
AT1-R	Angiotensin-II-Typ-1-Rezeptor
AT2-R	Angiotensin-II-Typ-2-Rezeptor
Ca	Calcium
cGMP	cyclisches Guanosinmonophosphat
CPI17	17-kDa-PKC-potenziertes inhibitorisches Protein der Typ-1-Proteinphosphatase
DG	Diacylglycerol
eNOS	endotheliale NO-Synthase
$G\alpha_{q11}$	G-Protein-alpha-Untereinheit q11
IP3	Inosit-1,4,5-trisphosphat
kD	Kilodalton
KO	Knock-Out
L-NAME	NO-Synthase-Inhibitor
MAP-Kinase	Mitogen-Activated-Protein-Kinase
Mas-R	Mas-Rezeptor
MLC	Myosin-Leichtkette
MLCK	Myosin-Leichtkette-Kinase
MLCP	Myosin-Leichtkette-Phosphatase
eNOS	endotheliale NO-Synthase
NEP	neutrale Endopepdidase
NO	Stickstoff
NO-GC	NO-abhängige cGMP-bildende Guanylylzyklase
NOX	NADPH-Oxidase
PBS	Phosphat-gepufferte Salzlösung
PDE	Phosphodiesterase
PI3K	Phosphoinositid-3-Kinasen

PKC	Protein-Kinase C
PKG	cGMP-abhängige Proteinkinasen
PLC	Phospholipase C
PLD	Phospholipase D
RAS	Renin-Angiotensin-System
RAAS	Renin-Angiotensin-Aldosteron-System
ROS	Reaktive Sauerstoff-Spezies
sGC	lösliche Guanylylzyklase
SHP-2	Src homology-2 domain-containing phosphatase
T	Threonin
TNF-α	Tumor-Nekrose-Faktor-α
VSMC	Glatte Gefäßmuskelzellen
WT	Wildtyp
Y	Tyrosin
2K1C	2 Kidney 1 Clip

1. Einleitung

1.1 Das Renin-Angiotensin-System und die Gefäßfunktion

Die Niere erfüllt eine Vielzahl an lebensnotwendigen Funktionen. Sie ist für die Exkretion harnpflichtiger Substanzen verantwortlich, die endogen entstehen oder exogen zugeführt und gegebenenfalls verstoffwechselt werden. Die Niere sorgt für die Aufrechterhaltung der Homöostase des Wasser-, Elektrolyt- und Säure-Basen-Haushaltes und ist zentrales Organ in der Regulation des Renin-Angiotensin-Aldosteron-Systems. Es nimmt damit eine zentrale Stellung in der Blutdruckregulation ein.

Die grundlegende anatomische Einheit zur Umsetzung von Exkretion und Homöostase ist das Nephron. Dieses besteht aus einem Glomerulum mit seinen Vas afferens und Vas efferens als zentrale Filtereinheit sowie dem Tubulussystem, welches die Zusammensetzung des Urins bestimmt und somit wesentlichen Einfluss auf den Flüssigkeits-, Elektrolyt- und Säure-Basen-Haushalt hat. Dem Glomerulum vor-geschaltet sind die sogenannten präglomerulären Gefäße. Diese Gefäße stellen Widerstandsgefäße dar. Da ein Fünftel des Herzzeitvolumens durch die Nieren fließt, hat die Funktion dieser Gefäße einen erheblichen Einfluss auf die Blutdruckregulation. In ihrer Funktion als Widerstandgefäße regeln sie den renalen Plasmafluss und die glomeruläre Hämodynamik, wodurch die glomeruläre Filtrationsrate, die Natrium- und Wasser-Exkretion beeinflusst werden. Vas afferens und Vas efferens liegen mit ihrem Gefäßpol einem Abschnitt der Pars recta des distalen Tubulus an, der den sogenannten juxtaglomerulären Apparat bildet. Diese endokrine Struktur hoch-spezialisierter Zellen dient der Bildung des Enzyms Renin. Renin stellt den Ausgangs-punkt des Renin-Angiotensin-System (RAS) dar, welches ein zentraler Effektor der Blutdruckregulation und des Elektrolyt- und Wasserhaushaltes ist.

Durch Hydrolyse von Angiotensinogen durch Renin entsteht das Dekapeptid Angiotensin I. Durch das Angiotensin-Converting-Enzym (ACE), eine Metalloproteinase, werden zwei Aminosäuren vom Carboxy-Ende des Angiotensin I abgespalten. Durch diesen Prozess entsteht das Oktapeptid Angiotensin II (Abb. 1).
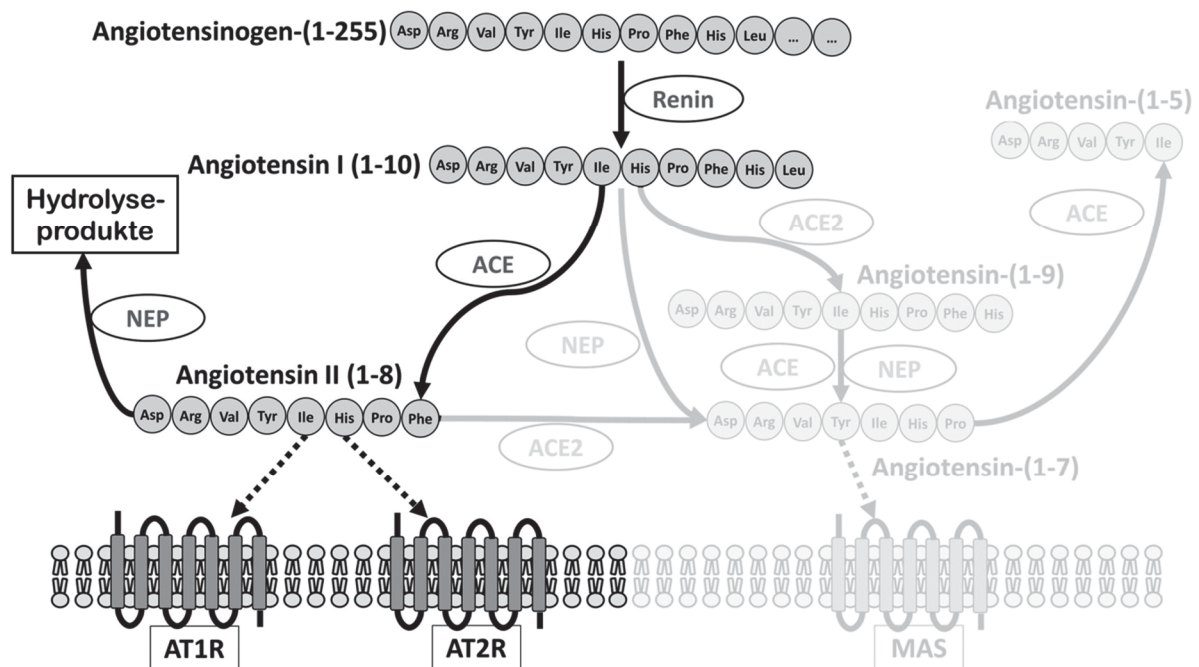

Abbildung 1: Das „klassische" Renin-Angiotensin-System (RAS). (siehe Text – „erweiterter Anteil" des RAS ausgegraut. (modifiziert nach [1] – Reproduktion und Nutzung genehmigt durch den Verlag und Rechteinhaber, *Mary Ann Liebert, Inc., New Rochelle, NY*)

Ang II ist der Haupteffektor des Renin-Angiotensin-Systems. Es nimmt eine zentrale Rolle in der Steuerung des Blutdrucks ein. Kommt es zu einer gesteigerten Aktivierung des RAS und damit zu einer vermehrten Bildung von Ang II, führt dies in der Regel zum Anstieg des arteriellen Blutdrucks. Bei Erkrankungen der Niere aber auch bei einer chronisch gesteigerten sympathischen Aktivität kommt es zu einer dauerhaften Aktivierung des RAS und damit zur Ausbildung einer Ang-II-abhängigen Hypertonie.

Die Wirkung von Ang II wird über zwei G-Protein-gekoppelte Rezeptoren vermittelt, der Angiotensin-II-Typ-1 (AT1)-Rezeptor und der Angiotensin-II-Typ-2 (AT2)-Rezeptor. [2] Diese Rezeptoren sind auf unterschiedlichen Zellen einzelner Organsysteme wie Niere, Herz, Gefäße, Gehirn, Lymphozyten exprimiert. Tier-experimentelle Arbeiten mit selektiven AT1- und AT2-Rezeptorantagonisten und genetisch veränderten Tieren konnten zeigen, dass für die Ang-II-vermittelten Effekte im Wesentlichen die Signaltransduktion über den AT1-Rezeptor verantwortlich ist. Die Aktivierung des AT1-Rezeptors bewirkt eine arterielle Blutdruckerhöhung durch Vasokonstriktion. Dabei führt die Aktivierung des AT1-Rezeptors zum einen zur Aktivierung von Phospholipase C und in Folge zur Bildung von Inositol-Trisphosphat (IP3). IP3 führt zur Aktivierung von membranständigen Calcium-Kanälen und zur Freisetzung von Calcium aus dem sarkoplasmatischen Retikulum. Der zytosolische Calcium-Influx führt zur Aktivierung der Myosin-Leichtkette-Kinase (MLCK), welche letztlich die Kontraktion der Myofilamente bewirkt. Die AT1-Rezeptor-Aktivierung führt zudem zur Aktivierung des RhoA/Rho-Kinase-Signalweges. Zusammen mit der Aktivierung der Proteinkinase C (PKC) führen diese beiden Wege zur Hemmung der Myosin-Leichtkette-Phosphatase (MLCP). Hierdurch kommt es indirekt zur Steigerung der kontraktilen Wirkung, wodurch die Kontraktion der glatten Gefäßzelle verstärkt wird (Abb. 2). [3]
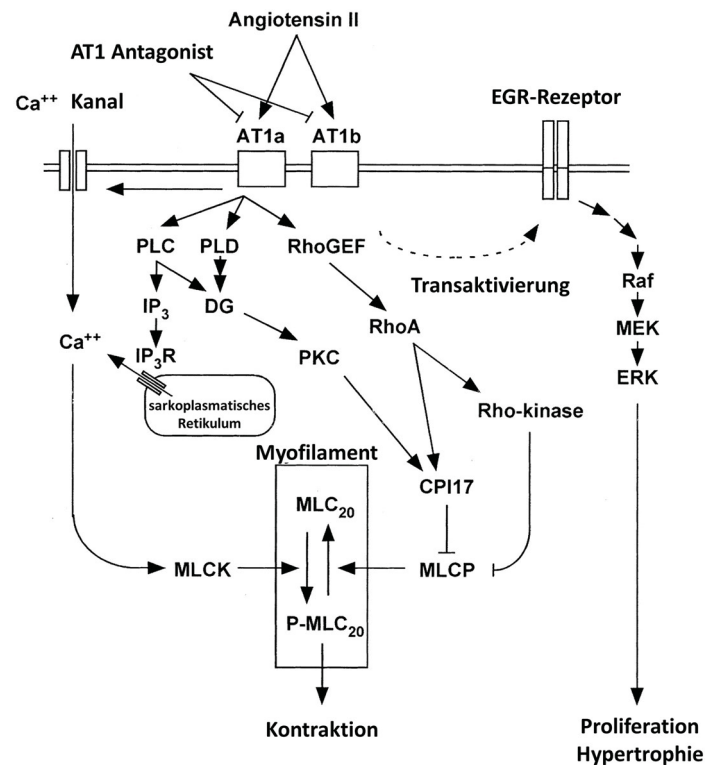
Abbildung 2: Signaltransduktionswege nach Aktivierung des AT1-Rezeptors mit Fokus auf die Erregungs-Kontraktions-Kopplung in der glatten Gefäßmuskulatur. Die Stimulierung des AT1-Rezeptors aktiviert Phospholipase C (PLC) und produziert Inosit-1,4,5-trisphosphat (IP3) und Diacylglycerol (DG). IP3 induziert die Freisetzung von Ca^{2+} aus den intrazellulären Speichern durch den IP3-Rezeptor (IP3R). Die AT1-Rezeptor-Aktivierung vermittelt den Ca^{2+}-Influx durch Kanäle der Plasmamembran. Die Erhöhung der zytosolischen Ca^{2+}-Konzentration aktiviert die Myosin-Leichtkette-Kinase (MLCK) und phosphoryliert dadurch Myosin, das die Kontraktion der glatten Muskulatur induziert. DG wird zudem durch die Aktivierung von Phospholipase D (PLD) gebildet. DG aktiviert Proteinkinase C (PKC). Eines seiner Substrate ist ein 17-kDa-PKC-potenziertes inhibitorisches Protein der Typ-1-Proteinphosphatase (CPI17), das die Aktivität der Myosin-Leichtkette-Phosphatase (MLCP) direkt hemmt. Die AT1-Rezeptor-Aktivierung führt auch zur Stimulation des RhoA/Rho-Kinase-

Weges, der die MLCP-Aktivität hemmt. CPI17 ist auch ein Substrat der Rho-Kinase. Die Hemmung von MLCP verursacht bei einer gegebenen Erhöhung von Ca2$^+$ ein größeres Ausmaß an Myosinphosphorylierung, was zur Sensibilisierung des Myofilaments führt. (modifiziert nach [3] – Reproduktion und Nutzung genehmigt durch den Verlag und Rechteinhaber, *Wolters Kluwer Health, Inc.*)

Neben dem unmittelbaren Effekt auf die Gefäßwand führt die AT1-Rezeptor-Aktivierung zur renalen Natrium- und Wasserretention. In der Nebenniere führt die Aktivierung des AT1-Rezeptors zur Aldosteron-Freisetzung. Zudem führt die AT1-Rezeptor-Aktivierung im vegetativen Nervensystem zur Sympathikusaktivierung. Neben dem Einfluss auf den Blutdruck beeinflusst die AT1-Rezeptor-Aktivierung die Modulation der Immunantwort.

1.2 <u>Stickstoffmonoxid (NO) und Gefäßfunktion</u>

Die Stickstoffmonoxid (NO)-abhängige Vasodilatation spielt für die Steuerung des Gefäßtonus neben dem Einfluss von Ang II eine herausragende Rolle. Das RAS mit seinem Effektor – dem Ang II – interagiert unmittelbar mit der NO-abhängigen Vasodilatation über die Modulation der Stickstoffmonoxid (NO)/zyklisches-Guanosin-monophosphat (cGMP)-Signalkaskade.

NO wird im vaskulären System in den Endothelzellen von der endothel-spezifischen NO-Synthase (eNOS) gebildet. NO wirkt unmittelbar parakrin auf die vaskuläre glatte Muskelzelle (VSMC), in der es an die lösliche Gyanylylzyklase (sGC) bindet und damit die Bildung von cGMP reguliert. Die sGC liegt als zwei Subtypen vor: alpha1- und alpha2-Subtyp. Im Gefäßsystem ist der alpha1-Subtyp vorherrschend (NO-GC1). [4]

Die Aktivierung der cGMP-abhängigen Proteinkinasen (PKG) bewirkt letztlich die Vasorelaxation (Abb. 3). Neben der Bildung von NO durch die NO-Synthase spielt sowohl die Bildung von cGMP durch die sGC als auch der Abbau von cGMP durch die Phosphodiesterasen eine entscheidende Rolle für die Vasorelaxationsfähigkeit der Widerstandsgefäße. Ang II scheint auf diesen Abbauweg ebenfalls Einfluss zu nehmen. [5]
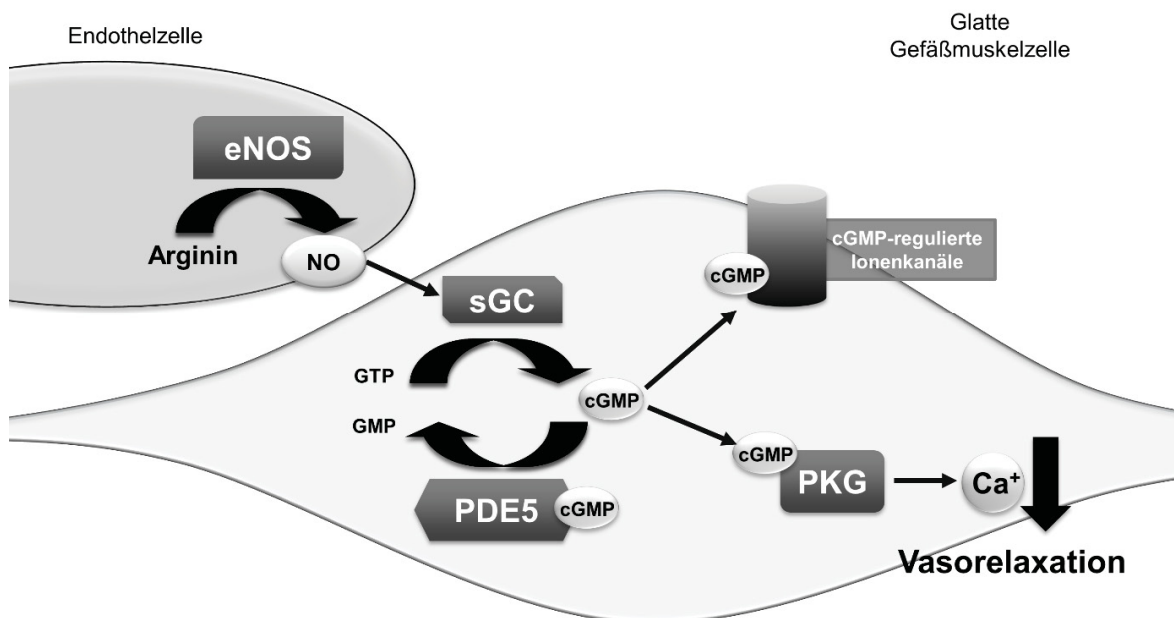

Abbildung 3: eNOS/cGMP-Signalkaskade: Die endotheliale NO-Synthase (eNOS) produziert in der Endothelzelle aus dem Substrat Arginin den Botenstoff Stickstoff-monoxid (NO). NO aktiviert in der glatten Gefäßmuskelzelle die lösliche Guanylyl-zyklase (sGC), die cGMP als second messenger bereitstellt. Dieses aktiviert in einem negativen Feedback die Phosphodiesterase 5 (PDE5) und die Protein-Kinase G (PKG) sowie cGMP-abhängige Ionenkanäle, wodurch der intrazelluläre Calcium-Gehalt abfällt und dies zur Vasorelaxation führt. (eigene Abbildung)

1.3   Bedeutung von Angiotensin II für die Entstehung von arterieller Hypertonie und Gefäßdysfunktion

Die arterielle Hypertonie stellt den wichtigsten Risikofaktor für Morbidität und Mortalität in der westlichen Welt dar. [6] Die pathologische Aktivierung des Renin-Angiotensin-Aldosteron-Systems spielt in der Genese der arteriellen Hypertonie eine wesentliche Rolle. Die Wirkung von Ang II über den AT1-Rezeptor mit Steigerung der Vasokonstriktion im vaskulären System stellt den zentralen Wirkmechanismus dieses Systems dar (siehe Abschnitt 1.1). Durch die pharmakologische Hemmung des Renin-Angiotensin-Systems durch ACE-Hemmer oder AT1-Rezeptorblocker kann der blutdrucksteigernden Wirkung des RAS entgegengewirkt werden. Diese Medikamente werden im klinischen Alltag zur Behandlung der arteriellen Hypertonie eingesetzt.

Über AT1-Rezeptor-Stimulation kann es zu einer Steigerung inflammatorischer Prozesse kommen, welche die Bildung von Atherosklerose und Organfibrose begünstigen und das Remodelling nach Myokardischämie und zerebralem Insult beeinflussen. [7, 8] Diese Prozesse spielen eine wichtige Rolle bei der Zunahme der Gefäßsteifigkeit. Die Zunahme der Gefäßsteifigkeit trägt zusätzlich zu einer vor allem isolierten systolischen Hypertonie bei, die typischerweise mit zunehmendem Alter auftritt.

Das RAS und die NO/cGMP-Signalkaskade spielen eine Schlüsselrolle bei der Regulation der Gefäßfunktion. Die gesteigerte AT1-Rezeptor-Aktivierung-vermittelte Vasokonstriktion geht mit einer verminderten oder gestörten NO/cGMP-vermittelten Vasorelaxationsfähigkeit einher. In diesem Zusammenhang fördert Ang II die Gefäßdysfunktion durch Steigerung der Vasokonstriktion, Induktion von Gefäßmuskelzellenproliferation und damit Hypertrophie der Gefäßwand und vaskuläre Inflammation mit

extrazellulärem Matrixumbau. [9] Zudem führt Ang II zur Reduktion der NO-Bioverfüg-barkeit, was zur vaskulären Dysfunktion führt. [10-12] Neben dem Einfluss von Ang II auf die Bioverfügbarkeit von NO zeigen mehrere Studien die Rolle von Ang II in der Modulation des cGMP-Abbaus durch Beeinflussung der cGMP-abbauenden Phospho-diesterasen (PDE) in glatten Gefäßmuskelzellen. Es wurde gezeigt, dass Ang II die Expression von PDE1 und PDE5 erhöht. Beide PDEs sind von besonderer Bedeutung für die Vasorelaxation von Widerstandsgefäßen. [13-15] Im Allgemeinen wird PDE1 durch zytoplasmatischen Calcium-Influx aktiviert, der während Ang-II-vermittelter Vasokonstriktion auftritt. [16, 17] PDE1 und PDE5 sind beide im vaskulären System exprimiert. Die PDE5 wird durch die Bildung von cGMP aktiviert und vermittelt auf diese Weise einen automatischen, negativen Feedback-Mechanismus (siehe Abb. 3). Beide Phosphodiesterasen können pharmakologisch inhibiert werden. Da Ang II auf die Expression und Aktivität der Phosphodiesterasen Einfluss nimmt, scheint hier ein weiterer Mechanismus zu bestehen, über welchen Ang II zur Regulation des Gefäß-tonus und damit zur Blutdrucksteuerung beiträgt. Welche Phosphodiesterase bei der Ang-II-vermittelten Vasokonstriktion und Regulation des Gefäßtonus in Widerstands-gefäßen den wesentlichen Anteil hat, wird in den vorgestellten Arbeiten untersucht.

Eine dauerhaft gesteigerte Ang-II-Freisetzung führt zudem über AT1-Rezeptor-Aktivierung intrazellulär im Bereich der Gefäßwand zur Aktivierung der p38 mitogen activated protein Kinase (MAPK). Diese MAPK spielt im vaskulären System eine wichtige Rolle. [18, 19] Die p38-MAPK wird entweder direkt durch Ang II oder über die Freisetzung von Zytokinen und Reaktive Sauerstoff-Spezies (ROS), welche bei Gefäß-schädigungen erhöht sind, aktiviert. Dabei können ROS auch Ang-II-vermittelt über die Aktivierung von NADP(H)-Oxidasen vermehrt freigesetzt werden und die Aktivierung von p38-MAPK damit indirekt begünstigen. Die Ang-II-vermittelte Aktivierung der p38-

MAPK begünstigt sehr wahrscheinlich die Hypertrophie von Gefäßmuskelzellen und fördert die vaskuläre Inflammation. Inwieweit die Ang-II-vermittelte p38-MAPK-Aktivierung zusätzlich zur Blutdrucksteigerung beiträgt, wird durch pharmakologische Inhibition von p38-MAPK bei Ang-II-induzierter arterieller Hypertonie in den vorgestellten Arbeiten dargelegt.

1.4 Rolle von Angiotensin-(1-7) im vaskulären System

1988 wurde durch Entdeckung von Angiotensin-(1-7) das klassische Renin-Angiotensin-System durch eine zusätzliche Achse erweitert. [20] Es wurde gezeigt, dass das Angiotensin-Converting-Enzym 2 (ACE2) der Hauptmediator dieser Achse des RAS ist. ACE2 ist eine Monocarboxypeptidase. Sie spaltet Phenylalanin von Ang II ab und wandelt es in Ang-(1-7) um, zudem spaltet es Leucin von Ang I ab, um es in Ang-(1-9) umzuwandeln. Außerdem wird Ang-(1-7) aus Ang-(1-9) durch ACE und die neutrale Endopeptidase (NEP) gebildet. Zusammen wirken ACE2, Ang-(1-9) und Ang-(1-7) als endogener Gegenspieler des RAS. Ang-(1-7), ein Heptapeptid, ist Ligand des sogenannten Mas-Rezeptors (Mas-R). Dabei scheint die Aktivierung des Mas-R für die Ang-(1-7)-vermittelten Effekte verantwortlich zu sein (Abb. 4). [21-23]
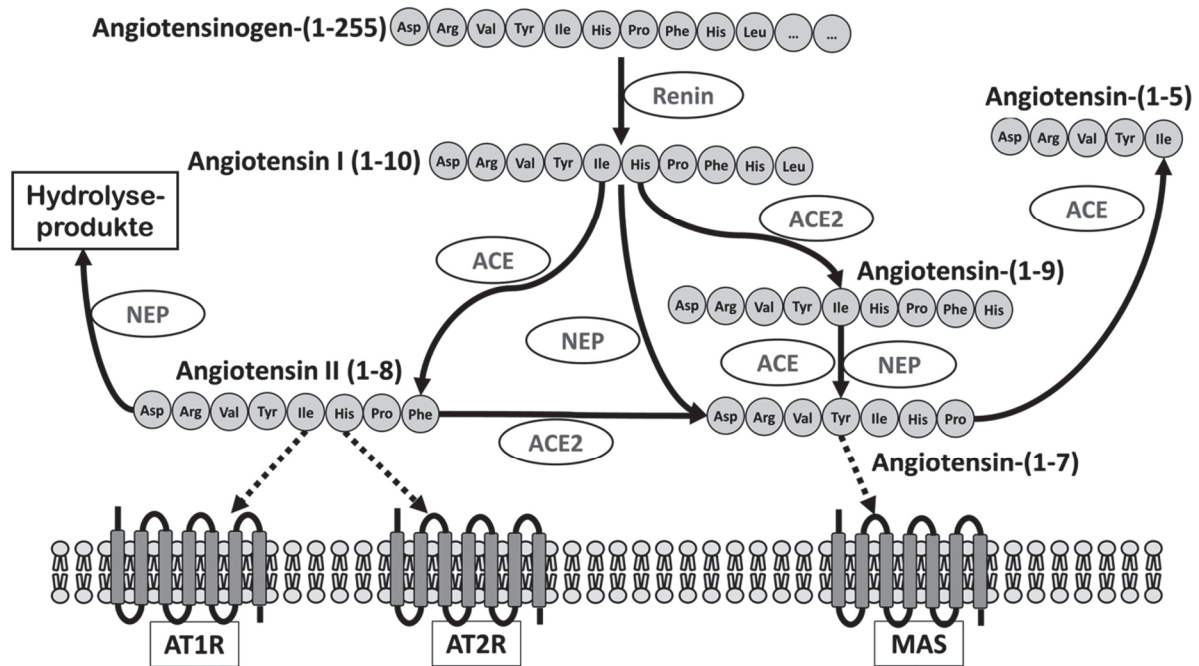
Abbildung 4: Das „erweiterte" Renin-Angiotensin-System. (siehe Text – modifiziert nach [1] – Reproduktion und Nutzung genehmigt durch den Verlag und Rechteinhaber, *Mary Ann Liebert, Inc., New Rochelle, NY*)

Ang-(1-7) hat eine protektive Wirkung auf das Gefäßsystem. Es erhöht die Bioverfügbarkeit von NO und reduziert die Bildung von ROS. Darüber hinaus führt es zur Freisetzung von vasodilatatorischen Prostanoiden. Die Ang-(1-7)-vermittelten Effekte hängen dabei von der Aktivierung des PI3K/AKT/eNOS-Signalweges ab. Zudem aktiviert Ang-(1-7) SHP-2 und führt auf diese Weise zu einer Gegenregulation des Ang-II/AT1-Signalweges. [24, 25] Die zugrunde liegenden Mechanismen, welche Ang-(1-7)-vermittelt die NO-Bioverfügbarkeit und ROS-Produktion beeinflussen, werden in den aufgeführten Arbeiten untersucht und differenziert.

Die Aktivierung des RAS spielt auch bei der Genese von Herz-Kreislauf-Erkrankungen, bei Adipositas, Diabetes mellitus und arterieller Hypertonie eine wichtige Rolle. Als

Gegenspieler zeigt Ang-(1-7) in diesen Krankheitsmodellen einen positiven Einfluss auf die zugrunde liegenden Mechanismen. Im murinen Typ-2-Diabetes-Modell führt die Behandlung mit Ang-(1-7) zur Besserung der diastolischen Dysfunktion und reduzierten Herzhypertrophie, Fibrose und interstitiellen und vaskulären Inflammation. [26, 27] Ein Verlust von ACE2 führt umgekehrt bei Adipositas zur fortschreitenden Kardiomyopathie durch Inflammation und zunehmenden Insulinresistenz des Gewebes. In den ACE2-KO-Mäusen führt die Behandlung mit Ang-(1-7) zu einer Verbesserung der kardialen Funktionsparameter. [28] Bei adipösen Patienten verbesserte die Therapie mit Ang-(1-7) die endothelabhängige Vasodilatation und reduzierte die Endothelin-1-abhängige Vasokonstriktion. [29]

Nach Myokardinfarkt unterdrückt Ang-(1-7) das Kardiomyozytenwachstum und damit eine linksventrikuläre Hypertrophie. Zudem vermindert es proinflammatorische Zytokine im Myokard und hemmt dadurch eine anhaltende Inflammation. [30, 31] Die Ang-(1-7)-vermittelte Aktivierung des Mas-R führt über Aktivierung von PI3K/Akt zur Stimulation der eNOS, zur Hemmung der Protein-Kinase C (PKC) / p38-MAPK-Achse und Hemmung der Produktion von Reaktiver Sauerstoff-Spezies. Durch Hemmung der Kollagenexpression wird einer Myokardfibrose entgegengewirkt. [25, 32-35]

Die beschriebenen Mechanismen wirken alle den pathologischen Effekten der „klassischen" RAS-Aktivierung mit dem Effektor Ang II entgegen.

1.5   Renale Schädigung und Albuminurie

Erkrankungen wie der Diabetes Mellitus oder die arterielle Hypertonie führen häufig zur renalen Schädigung. Einer der frühesten Marker dieser Schädigung ist die Albuminurie.

Für das Auftreten von Albumin im Urin ist eine Schädigung des Glomerulums als zentrale Filtereinheit der Niere verantwortlich. Diese Filtereinheit ist für die Entstehung des Primärharns verantwortlich. Das Glomerulum besteht aus einem Vas afferens und einem Vas efferens, zwischen welchen sich ein Kapillargeflecht ausbildet. Dieses Geflecht ist umschlossen von der sogenannten Bowman'schen Kapsel, welche in das Tubulussystem mündet (Abb. 5).
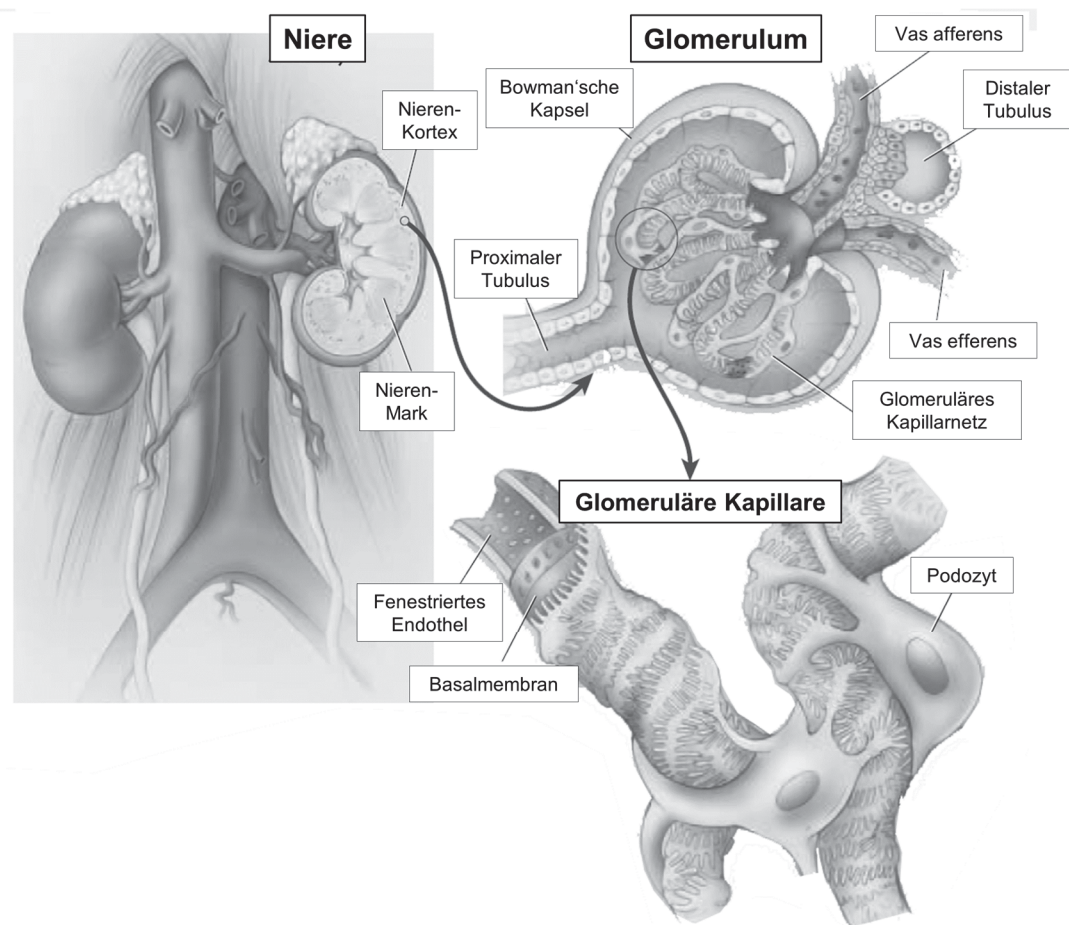

Abbildung 5: Schematische Darstellung des anatomischen Aufbaus der Niere. (modifiziert nach [36] – Reproduktion und Nutzung genehmigt durch den Rechteinhaber, *Copyright Massachusetts Medical Society*)

Die eigentliche Filtereinheit des Glomerulums wird durch das fenestrierte Endothel der Kapillaren, die glomeruläre Basalmembran und den auf den Kapillaren aufliegenden Podozyten gebildet. Die Podozyten selbst interdigitieren mit ihren Fußfortsätzen. Zwischen diesen Fußfortsätzen spannt sich die sogenannte podozytäre Schlitzmembran auf (Abb. 6).
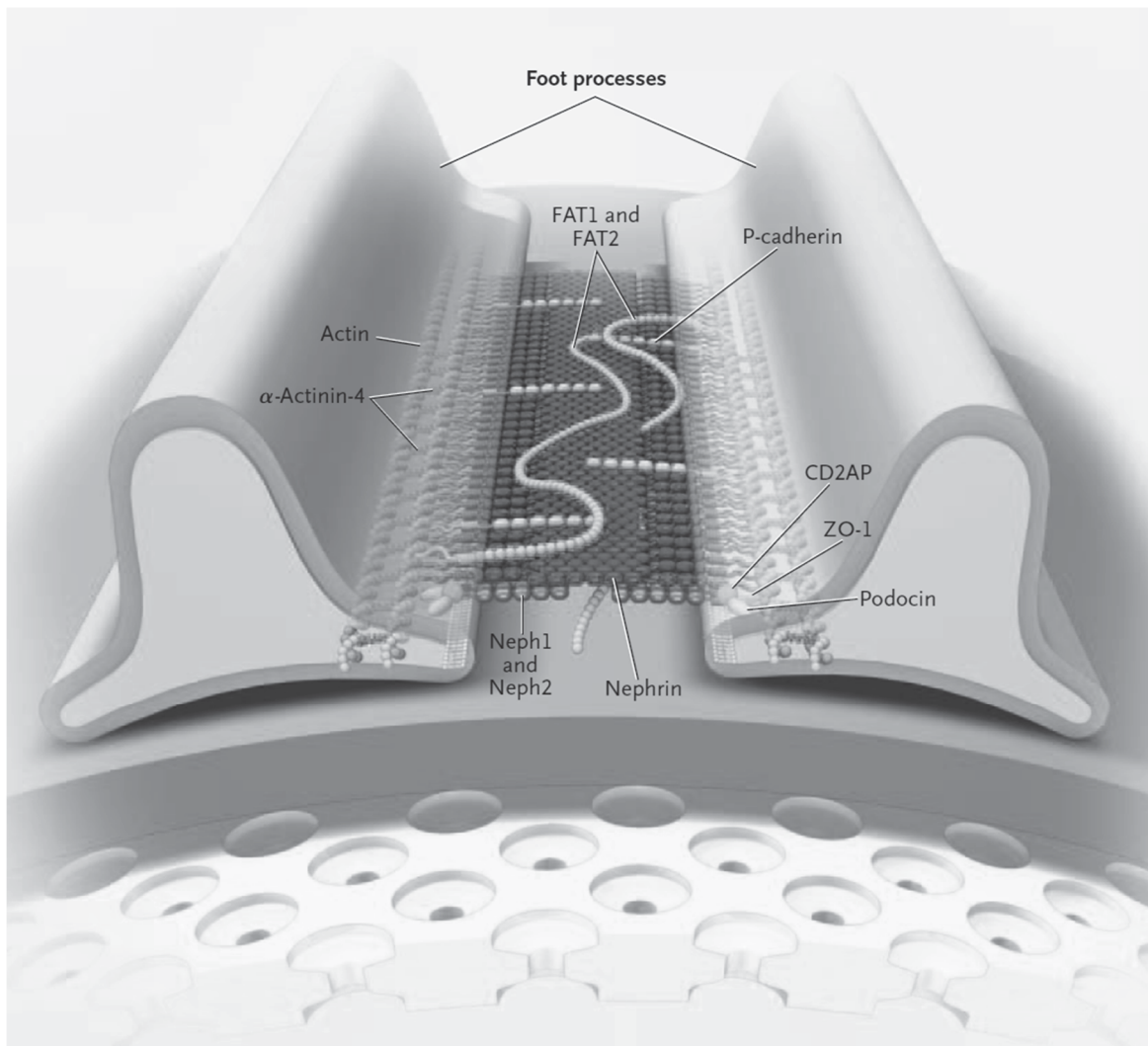

Abbildung 6: Schematische Darstellung der podozytären Schlitzmembran. Die Schlitzmembran wird durch Interaktion von membranständigen Proteinen gebildet, die intrazellulär verankert sind. Für die extrazelluläre Ausbildung der Schlitzmembran sind vor allem die Proteine Nephrin, NEPH1 und NEPH2 sowie FAT1 und FAT2 und P-Cadherin verantwortlich. (modifiziert nach [36] – Reproduktion und Nutzung genehmigt durch den Rechteinhaber, *Copyright Massachusetts Medical Society*)

Die Integrität der podozytären Schlitzmembran ist entscheidend für den Rückhalt von Makroproteinen. Sie stellt eine Barriere für größere Proteine ab ca. 60 kD dar. Diese können nicht in den Primärharn übertreten. Das Auftreten einer Albuminurie (66kD) zeigt daher eine Schädigung der glomerulären Filtereinheit an.

Nephrin, als Bestandteil des extrazellulären Aufbaus der podozytären Schlitz-membran, spielt eine entscheidende Rolle in der Aufrechterhaltung der Filterfunktion. So konnte gezeigt werden, dass Nephrin durch die intrazelluläre Bindung von β-Arrestin2 zur Endozytose und somit zur Disruption der Schlitzmembran und zum Auftreten einer Proteinurie führt. [37] Im Rahmen von Erkrankungen, die mit einer Albuminurie einhergehen, scheint dieser Mechanismus eine zentrale Rolle bei der Aufrechterhaltung der Integrität der podozytären Schlitzmembran zu spielen. Das Auftreten einer Albuminurie bei Diabetes mellitus stellt einen wichtigen Hinweis der renalen Schädigung dar. Es konnte gezeigt werden, dass die Hyperglykämie direkt die Nephrin-Endozytose durch Regulation der β-Arrestin2-Nephrin-Interaktion via PKCα steigert. [38]

Auch bei arterieller Hypertonie stellt die Albuminurie einen frühen renalen Schädi-gungsmarker dar. Inwieweit Ang II als wichtiger Mediator der arteriellen Hypertonie Einfluss auf die podozytäre Schlitzmembran nimmt, wird in den vorgestellten Arbeiten dargelegt.

2. Darstellung und Diskussion eigener Ergebnisse

2.1 Methoden zur Charakterisierung renaler Funktionseinheiten *(Publikation I, II, IV, X)*

Als hochspezialisiertes Organ muss die Niere eine Vielzahl von Aufgaben über-
nehmen. Dies spiegelt die komplexe histologische Kompartimentalisierung der Niere
wider. Diese ausgeprägte Spezialisierung einzelner Funktionseinheiten erschwert eine
exakte Untersuchung der Niere und ihrer Kompartimente als Ganzes. Dabei spielen
die präglomerulären Gefäße als Teil des Widerstandsgefäßsystems eine heraus-
ragende Rolle bei der Blutdruckregulation. Zudem beeinflussen sie maßgeblich den
glomerulären Blutfluss und haben damit einen wesentlichen Einfluss auf die
glomeruläre Filtration. Eine Dysfunktion dieser Gefäße wirkt sich somit sowohl auf die
Blutdruckregulation als auch die Nierenfunktion aus und hat damit eine hohe Relevanz
bei der Entwicklung einer chronischen Niereninsuffizienz. Um diese renalen Gefäß-
abschnitte im Einzelnen exakt funktionell und auch molekularbiologisch zu unter-
suchen, ist es notwendig, Untersuchungsmethoden einzusetzen, welche die renale
Kompartimentalisierung überwinden. Daher haben wir mehrere Untersuchungs-
techniken etabliert, um die einzelnen Komponenten der renalen Funktionseinheiten
gesondert untersuchen zu können. In den folgenden Abschnitten werden diese
Methoden dargestellt, welche die Grundlage der im Weiteren dargestellten Ergebnisse
bilden.

2.1.1 Isolation renaler Gefäßabschnitte zur selektiven Analyse

Durch Embolisation mit unterschiedlich großen, ferromagnetischen Partikeln lassen
sich die einzelnen Gefäßabschnitte der Nierengefäße isolieren und selektiv analy-
sieren. [19, 39-43] Es wurden präglomeruläre Widerstandsgefäße isoliert, um wichtige

Regulatoren der vaskulären Funktion renaler Widerstandgefäße genauer zu analysieren. [19, 43] Zudem konnten in zwei Arbeiten die Analyse des glomerulären Proteoms als Methode und Analyseverfahren etabliert werden (Abb. 7). [39, 40]
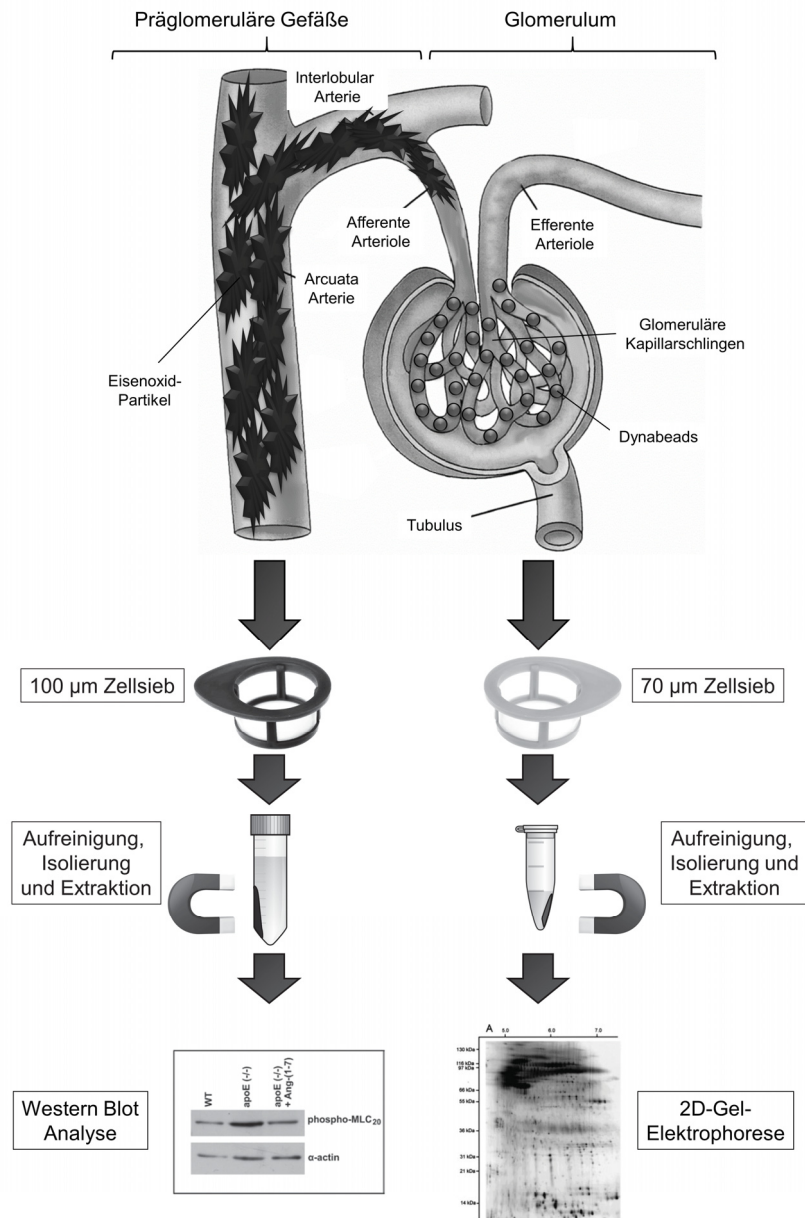

Abbildung 7: Extraktion und Analyse renaler Widerstandsgefäße mittels Eisenoxidpartikel (links) und Glomeruli mittels Dynabeads (rechts).

Murine Glomeruli wurden mittels Technik der isoliert-perfundierten Niere und Perfusion mit Magnetpartikeln mit einem Durchmesser von 4.5 µm perfundiert (Dynabeads,

Invitrogen/Thermofischer, Deutschland). Aufgrund der Größe embolisieren diese Magnetpartikel vor allem in den Kapillarschlingen des Glomerulums (Abb. 7). Nach stattgehabter Perfusion und Zerkleinern der Nieren wurde das Gewebe gesiebt (100 μm Sieb) und mehrfach mit PBS gewaschen. Durch einen Magnetfänger und wiederholte Waschschritte konnte auf diese Weise die Reinheit isolierter Glomeruli in der Gewebesuspension auf über 90 % erhöht werden. Zirka 40 μg glomerulären Proteins konnte so aus je einer Nierenpräparation gewonnen werden. (eigene Abbildung)

Um nun eine differenzierte Analyse des Proteoms und Unterschiede zu unterschiedlichen Proben darzustellen, wurden die Proteine mit einem Fluoreszenzfarbstoff markiert und dann mittels 2D-Gelelektrophorese aufgetrennt. Durch unterschiedliche Fluoreszenzfarbstoffe (Cy3, Cy5) können gleichzeitig zwei Proben untersucht werden, um die Unterschiede im Proteom vergleichend zu erfassen. In einem ersten Schritt wurde hierfür glomeruläres murines Protein mit murinem Cortex-Proteinlysat (keine differenzierte Isolierung einzelner Kompartimente) verglichen. Im Weiteren wurden differenziert exprimierte Proteine aus dem 2D-Gel isoliert und einer massenspektrometrischen Analyse zur Identifikation zugeführt (MS nanoLC-ESI-MS/MS).

Insgesamt konnten mittels 2D-Gelelektrophorese ca. 2800 verschiedene Proteine isoliert werden. Im Vergleich zwischen glomerulärem Proteinlysat und Cortexlysat zeigten in dieser Pilotarbeit 48 Proteine einen mindestens 1,5-fachen Expressionsunterschied ($p < 0.05$). Mittels nanoLCESI-MS/MS konnten 23 dieser Proteine identifiziert werden.

Mit dieser Methode wurde zum einen der Nachweis erbracht, auch aus kleinsten Gewebeproben eine differenzierte Proteinanalyse zu ermöglichen. Die Anwendung von Magnetpartikeln ermöglichte zudem als synergistisches Verfahren die Analyse einzelner renaler Kompartimente, wie dem Glomerulum, die bisher in dieser Größenordnung nicht möglich war. In einem zweiten Schritt wurde dieses Verfahren in der Analyse des murinen glomerulären Proteoms in einem renalen Schädigungsmodell (5/6 Nephrektomie) angewendet. [40]

Die renalen Widerstandsgefäße sind in das histologische Gefüge der Niere eingebettet und lassen sich als Ganzes durch die Extraktion mittels Eisenoxid-Partikel-Embolisation untersuchen. [19, 42] Die Perfusion mittels größerer Eisenoxid-Partikel ermöglicht die gezielte Isolierung dieser präglomerulären Kapillaren, um sie weiteren molekularbiologischen Analyseverfahren zukommen zu lassen. Dieses Verfahren ermöglicht die isolierte Analyse des Kompartimentes der renalen Widerstandgefäße und Minimierung möglicher störender Einflüsse durch andere Gewebearten der Niere. Beispielsweise konnte mit diesem Verfahren die Expression von NADP(H)-Untereinheiten und damit die Charakterisierung unterschiedlicher ROS-produzierender NOX-Enzyme in renalen Widerstandsgefäßen von ApoE(−/−) erfolgen. [43]

2.1.2 Funktionelle Untersuchung renaler Widerstandsgefäße in der isoliert-perfundierten Niere

Die Untersuchung der einzelnen Gefäßabschnitte durch isolierte Extraktion mittels Magnetpartikel lässt im Wesentlichen nur molekularbiologische Analyseverfahren zu. Funktionelle Untersuchungen renaler Widerstandsgefäße sind nur am intakten Organ möglich und lassen sich funktionell im ex-vivo Modell der isoliert-perfundierten Niere untersuchen (Abb. 8). [44]
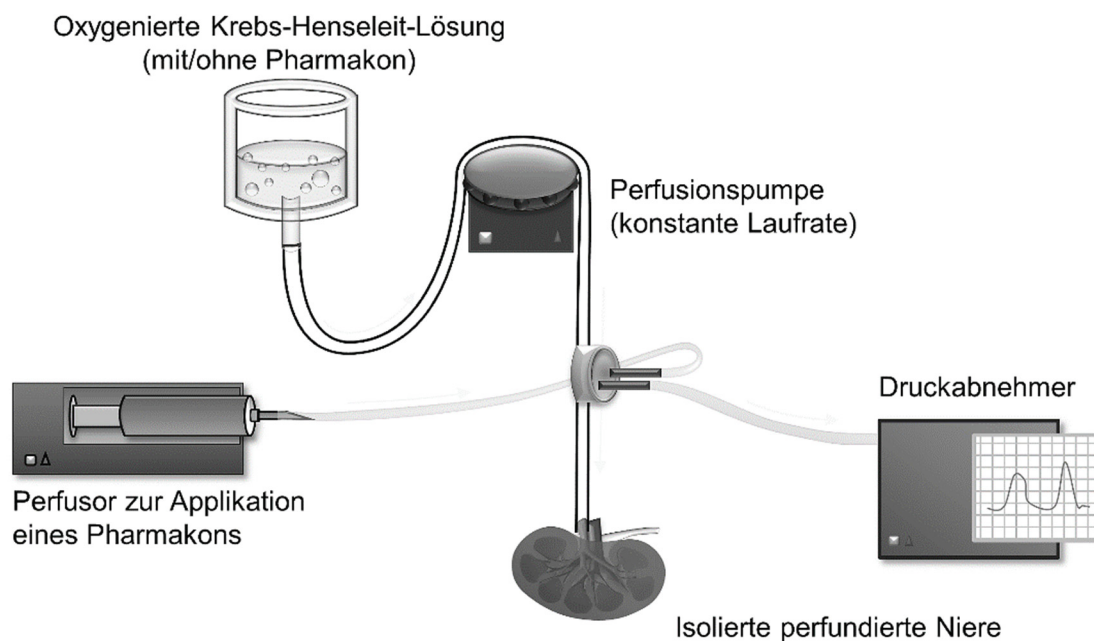

Abbildung 8: Modell der isoliert-perfundierten Mausniere: Die Nierenarterie wird an ein geschlossenes Perfusorsystem mit Druckabnehmer angeschlossen. Über eine Perfusionspumpe wird unter konstanter Laufrate die Niere mit oxygenierter Krebs-Henseleit-Lösung perfundiert, welche ggf. mit einem Pharmakon versehen ist. Mittels Perfusor können dann unmittelbar Pharmaka in ansteigender Konzentration dem System zugeführt werden. Die Reaktion der Widerstandsgefäße wird als Druck-änderung registriert und aufgezeichnet. (eigene Abbildung)

Hierbei wird die Nierenarterie über ein Schlauchsystem perfundiert. Die Flussrate wird durch eine Pumpe kontinuierlich aufrechterhalten. Die Perfusionslösung besteht dabei aus einer gepufferten Krebs-Henseleit-Lösung, welche präoxygeniert wird. Durch Applikation von Pharmaka über ein Infusionsstück kann in Abhängigkeit von der Konzentration die pharmakologische Wirkung auf die Widerstandsgefäße im Sinne einer Vasorelaxation oder Vasokonstriktion mittels Druckabnehmer festgestellt werden. Dieses Testprinzip ermöglicht es, die Gefäßfunktion sehr genau in Abhängigkeit von bestimmten Pharmaka zu prüfen.

In chronischen Schädigungsmodellen, wie z. B. der Ang-II-induzierten Hypertonie, erlaubt dieser Versuchsaufbau, die pathologischen Veränderungen der renalen Gefäßfunktion zu definierten Zeitpunkten zu untersuchen. Dabei werden Nieren von Ang-II-behandelten Tieren im Vergleich zu Kontrollen untersucht und in Abhängigkeit von bestimmten Pharmaka die veränderte Funktion renaler Widerstandsgefäße charakterisiert. Dies lässt Rückschlüsse hinsichtlich der Pathophysiologie und möglicher Therapieansätze in diesen Modellen zu. [19, 43-45]

2.1.3 Quantifizierung von Schlitzmembranproteinen bei proteinurischer Nierenerkrankung

Die Störung des glomerulären Filters durch eine akute oder chronische Schädigung führt zur Proteinurie. Um dieses Kompartiment genauer untersuchen zu können, entwickelten wir eine Methode der In-situ-Biotinylierung von Nephrin. Dabei wurden die Nieren mit Biotin perfundiert, im Anschluss Glomeruli, wie in 2.1.1 dargestellt, isoliert, und das Protein der Wahl mittels Immunopräzipitation separiert und die Menge des oberflächlich exprimierten Nephrins mittels Western-Blot-Analyse und

Streptavidin-Färbung quantifiziert. [46, 47] Durch die zeitlich begrenzte Perfusion mit Biotin wird nur das zu diesem Zeitpunkt oberflächlich exprimierte Nephrin (und andere Oberflächenproteine) markiert. Im Vergleich mit Kontrollen stellt dies einen indirekten Marker für die Integrität der glomerulären Schlitzmembran zu diesem Zeitpunkt dar.

Diese Methode wurde in zwei renalen, proteinurischen Schädigungsmodellen untersucht. Zum einen wurde C57Bl/6-Mäusen ein Nephritis-induzierendes Serum (NTN Modell) appliziert. In diesem Modell kommt es im Verlauf nach ausgeprägter Proteinurie zum Rückgang der Eiweißausscheidung und Erholung, so dass die Tiere an Tag 1 und Tag 18 nach Induktion untersucht wurden. Zum anderen wurde in BalbC-Mäusen eine Adriamycin-induzierte Nephropathie sieben Tage nach Applikation untersucht. In diesem Modell kommt es nicht zur Erholung der glomerulären Funktion. In beiden Modellen konnte die Abnahme der oberflächlichen Nephrin-Expression und damit eine Störung der glomerulären Schlitzmembranintegrität nachgewiesen werden. Dies ging mit der Zunahme der Proteinurie einher. Im NTN-Modell konnte zudem an Tag 18 gezeigt werden, dass sich die oberflächliche Nephrin-Expression erholte, was mit einem Rückgang der Proteinurie einherging.

Mit dieser Methode ist es daher möglich, Oberflächenproteine der glomerulären Schlitzmembran zu quantifizieren und mit dem Krankheitsverlauf zu korrelieren.

2.2. Interaktion zwischen Angiotensin II und der NO/cGMP-Signalkaskade und die Bedeutung für die vaskuläre Funktion *(Publikationen VI, VII, VIII)*

Die Endothel-vermittelte Vasorelaxation ist im Wesentlichen von der Bereitstellung von NO abhängig. Die eNOS, welche in den Endothelzellen exprimiert wird, spielt dabei eine entscheidende Rolle (siehe auch Abschnitt 1.2.). In mehreren Arbeiten untersuchten wir den Einfluss von Ang II und Ang-II-vermittelter Hypertonie wie auch den Einfluss des „Gegenspielers" Ang-(1-7) auf dieses System. [45, 48, 49]

Das „2 Kidney 1 Clip"-Hypertonie-Modell (2K1C) führt zu einer Aktivierung des RAS. Dieses Modell wurde angewandt, um den Einfluss des RAS auf die NO/cGMP-Signalkaskade und die NO-abhängige Vasorelaxation zu untersucht. Das Modell führt durch Reduktion des renalen Blutflusses zur Aktivierung des RAS und dadurch zur Entwicklung einer arteriellen, renovaskulären Hypertonie. [50] Wir untersuchten den Einfluss der induzierten Hypertonie auf den NO/cGMP-Stoffwechsel in Wildtyp- und NO-GC1-KO-Mäusen. [45]

Durch Charakterisierung der Funktion renaler Widerstandsgefäße in der isoliert-perfundierten Niere konnten wir zeigen, dass in unbehandelten NO-GC1 KO im Vergleich zu unbehandelten WT-Tieren die PDE5-Aktivität unverändert, die Vaso-relaxation auf Carbachol jedoch reduziert war. Dabei wird in NO-GC1 KO im Vergleich zu WT sehr wenig cGMP gebildet, welches für die PDE5-Aktivierung verantwortlich ist. Entsprechend zeigte sich die NO-GC-Aktivität in Nierenlysaten der NO-GC1-KO-Tiere in diesem Modell erwartungsgemäß deutlich erniedrigt.

Im Rahmen der Behandlung mit dem 2K1C-Modell entwickelten die Tiere im Verlauf von vier Wochen in gleichem Ausmaß eine arterielle Hypertonie bei ebenfalls gleichen Ausgangswerten (SBP - WT: 128 ±2 mmHg; NO-GC1 KO: 128 ±1 mmHg).

In den behandelten Tieren zeigte sich in der isoliert-perfundierten Niere, dass die induzierte Hypertonie die vaskuläre Relaxation in den WT-Tieren reduzierte. In den NO-GC1-KO-Tieren blieb jedoch die bereits eingeschränkte NO-abhängige Vasorelaxation unverändert. Die induzierte Hypertonie führte in den NO-GC1-KO-Tieren somit zu keiner zusätzlichen Funktionseinschränkung der Vasorelaxation.

In den WT-Tieren war die eingeschränkte Relaxation nicht auf eine geringere NO-GC1-Aktivität oder Expression zurückzuführen. Da durch die Behandlung mit Sildenafil (PDE5-Inhibitor) die eingeschränkte Vasorelaxation in den WT-Tieren wiederhergestellt werden konnte, muss eine erhöhte PDE5-Aktivität dafür verantwortlich sein. Entsprechend hatte die systemische Behandlung mit Sildenafil einen stärkeren blutdrucksenkenden Effekt in WT-Tieren nach 2K1C-OP als bei NO-GC1-KO-Tieren.

Die RAS-Aktivierung im 2K1C-Modell stellt den entscheidenden Pathomechanismus für die Entwicklung der arteriellen Hypertonie dar. Um die Rolle von Ang II bei der Störung der Vasorelaxation weiter zu beschreiben, wurde in einem weiteren Modell die Hypertonie durch eine chronische Ang-II-Infusion induziert (osmotische Minipumpen). [49]

Zwar entwickelten sowohl Wildtyp- als auch NO-GC1-KO-Tiere einen signifikanten Blutdruckanstieg innerhalb des 14-tägigen Beobachtungszeitraums, jedoch zeigte die Ausprägung der Hypertonie keinen signifikanten Unterschied. Unter der Behandlung kam es zu einer deutlichen Herzhypertrophie, die jedoch ebenfalls im Vergleich der Gruppen keinen signifikanten Unterschied zeigte. Die NO-GC1-Defizienz führt somit nicht zur unmittelbaren Beeinflussung der Ang-II-induzierten Hypertonie.

Die NO-abhängige Vasorelaxation in Aortenringen war sowohl in WT- als auch KO-Tieren unter Behandlung mit Ang II im Vergleich zu nicht-Behandlung signifikant

reduziert. Zudem war die Bioverfügbarkeit von cGMP unter Ang-II-induzierter Hypertonie ebenfalls reduziert. Die NO-GC1-Defizienz führte zu einer deutlicheren Einschränkung der NO-abhängigen Vasorelaxation im Vergleich zu WT-Tieren. Die Reduktion der Vasorelaxationsfähigkeit in der Ang-II-abhängigen Hypertonie im Vergleich zu unbehandelten Tieren war jedoch in beiden Gruppen (WT vs. KO) identisch. Ang II scheint somit zumindest in Aortenringen keinen zusätzlichen Einfluss auf die cGMP-vermittelte Modulation der Gefäßfunktion zu haben.

Um zu klären, welche Phosphodiesterase (PDE1 oder PDE5) im renalen Gefäßbett – also in Widerstandsgefäßen – entscheidend für die Regulation der NO/cGMP-Signalkaskade ist, führten wir akute Ang-II-Infusionen mit gleichzeitiger Messung des renalen Blutflusses durch. [48] Ang II führt wie in den Aortenringen zu einer deutlichen Verschlechterung der NO-abhängigen Vasorelaxation. Wir konnten zeigen, dass unter Ang-II-Gabe die Inhibition der PDE5 (durch Sildenafil) jedoch nicht der PDE1 (durch Vinpocetin) mit einem erhöhten renalen Blutfluss und einer Druckreduktion einherging. Die gestörte NO-abhängige Vasorelaxation in renalen Widerstandsgefäßen bei Ang-II-induzierter Hypertonie (osmotische Minipumpen) konnte in WT-Tieren zudem durch PDE5-Inhibition (Sildenafil) wiederhergestellt werden. PDE1-Inhibition hatte im Vergleich dazu keine signifikante Wirkung. (Abb. 9)
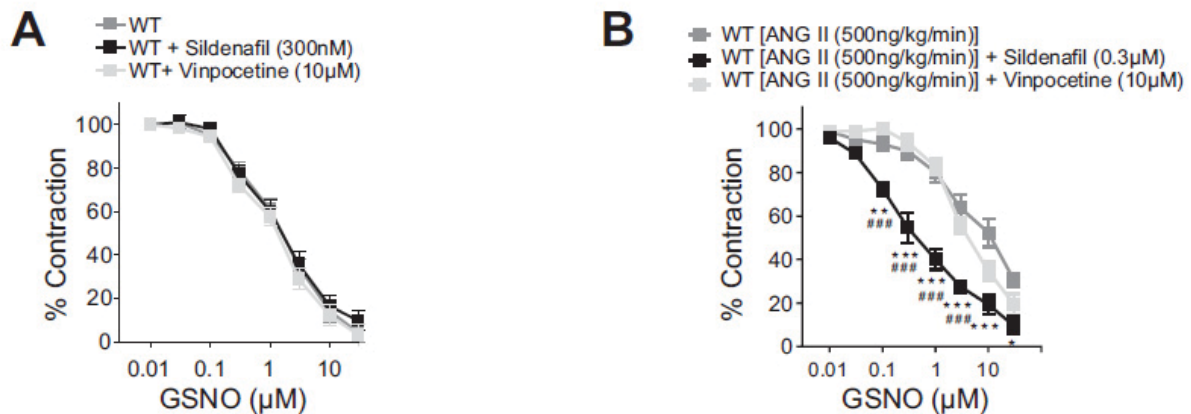
Abbildung 9: Akute Gabe von Sildenafil verbessert die glattmuskuläre Vasorelaxation in Nieren von Ang-II-behandelten WT-Mäusen. A, Die Gabe von Sildenafil oder Vinpocetin verbesserte nicht die glattmuskuläre Vasorelaxation durch GSNO in isoliert-perfundierten Nieren von unbehandelten WT-Mäusen (n = 5-9). B, Die Gabe von Sildenafil jedoch nicht von Vinpocetin verbesserte GSNO-induzierte Vasorelaxation in isoliert-perfundierten Nieren von chronisch Ang-II-behandelten WT-Mäusen (n = 5-6). Mittelwerte ± SE. *P 0.001, Ang II (500 ng/kg/min) vs. Ang II (500 ng/kg/min) + Vinpocetin; #P 0.001, Ang II (500 ng/kg/min) vs. Ang II (500 ng/kg/min) + Sildenafil; **P 0.01 und ***P 0.001 vs. WT [Ang II (500 ng/kg/min)]; ###P 0.001 vs. WT Ang II (500 ng/kg/min) + Vinpocetin. Two-way ANOVA gefolgt von Bonferroni-multiple-comparison-post-hoc-Test. (modifiziert nach [48] – Reproduktion und Nutzung genehmigt durch den Rechteinhaber, *American Physiological Society*)

Zusammenfassend zeigt dies, dass in der Ang-II-induzierten Hypertonie die NO-GC1-Defizienz lediglich die NO-abhängige Vasorelaxation, jedoch damit nicht indirekt die Ang-II-abhängige Vasokonstriktion beeinflusst. Ang II reduziert deutlich die Fähigkeit der NO-abhängigen Vasorelaxation. Hierfür ist eine am ehesten Ang-II-vermittelte gesteigerte Aktivität der PDE5 und nicht der PDE1 verantwortlich. Die PDE5-Inhibition

hebt diesen Effekt auf und stellt die NO-abhängige Vasorelaxationsfähigkeit wieder her. Dies zeigt, dass PDE5 eine Schlüsselrolle bei Ang-II-vermittelter Hypertonie einnimmt.

2.3 Rolle der p38-MAP-Kinase in der Angiotensin-II-abhängigen Hypertonie
(Publikationen IV, V)

In mehreren Ansätzen wurde die Rolle der Widerstandsgefäße und deren Dysfunktion in der Entwicklung einer arteriellen Hypertonie untersucht. Neben der eingeschränkten Vasorelaxation durch Störung der NO-Signalkaskade spielt die gesteigerte Kontraktilität eine wichtige Rolle. Neben der unmittelbaren arteriellen Blutdrucksteigerung vermittelt Ang II einen zunehmenden Umbau der Gefäßwand mit Zunahme der Gefäßsteifigkeit. Diese Prozesse führen zu einem Verlust der kapazitiven Eigenschaft zentraler Gefäße, welche normalerweise zu einer Abschwächung des systolischen Blutdruckanstiegs führt. Dieser Verlust trägt zur Augmentation des systolischen Blutdrucks und damit zur Entstehung einer arteriellen Hypertonie bei. [51-53] Die Augmentation mit Zunahme der Gefäßsteifigkeit ist ein Prädiktor für das kardiovaskuläre Risiko und die kardiovaskuläre Mortalität. [54, 55] Dieser Prozess wird durch eine vaskuläre Inflammation und Fibrosierung vorangetrieben. [56, 57] Hierbei kommt es Ang-II-vermittelt zur Zunahme von Reaktiven Sauerstoff-Spezies (ROS) und zur Inflammation im Bereich der Gefäßwand mit Freisetzung profibrotischer und proinflammatorischer Zytokine. Dies kann zu einer Aktivierung der p38-MAPK führen. [58, 59] Ob die chronische p38-MAPK-Inhibition bei der Ang-II-vermittelten Hypertonie eine Rolle spielt, wurde in mehreren Arbeiten genauer untersucht. [19, 44]

In C57Bl/6J-Mäusen wurde durch fortlaufende Gabe von Ang II mittels osmotischer Minipumpe eine Hypertonie induziert. Die Behandlung mit Ang II erfolgte über 14 Tage. Die Tiere wurden zudem mit dem oralen p38-MAPK-Inhibitor BIRB796 oder Vehikel behandelt. Die Gefäßfunktion wurde in vivo als auch ex vivo analysiert.

Bei gleichem arteriellen Ausgangsblutdruck zu Anfang der Implantation der Ang-II-Pumpen zeigte sich nach zwei Wochen ein signifikanter Unterschied des systolischen Blutdrucks der Tiere (baseline: 122 ± 2 versus 119 ± 4 mmHg; 14 Tage Ang II: 173 ± 3 versus 155 ± 3 mmHg; $p < 0.001$). Die Aktivierung von p38-MAPK in renalem Kortexgewebe durch die Ang-II-Behandlung konnte durch die BIRB796-Behandlung signifikant reduziert werden. Die Ang-II-Behandlung führte zudem zur gesteigerten 8-Isoprostan-Exkretion (Marker für ROS), die durch die BIRB796-Behandlung ebenfalls reduziert werden konnte. Die im Vergleich zur Nicht-Behandlung durch Ang II gesteigerte renale Noradrenalin-Exkretion im Urin wurde durch BIRB796 ebenfalls signifikant abgeschwächt (Abb. 10).
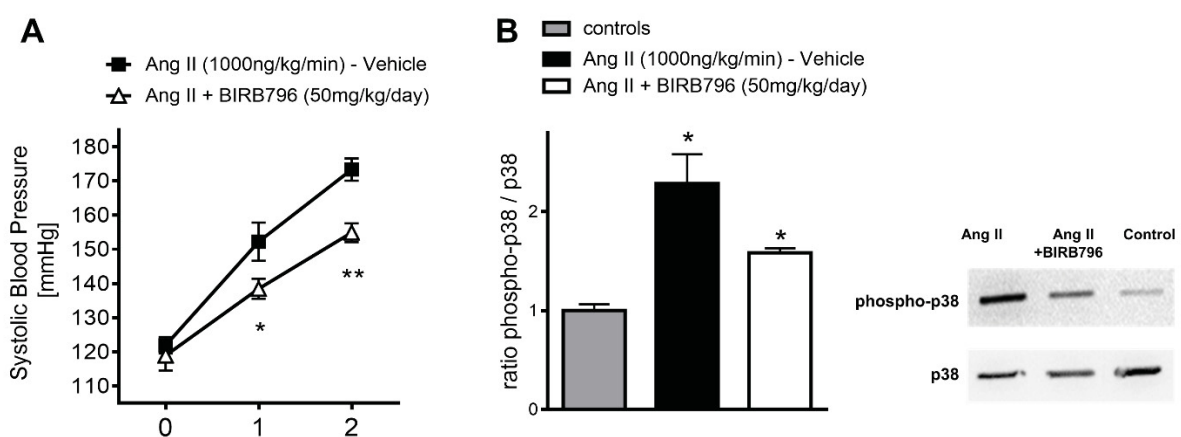

Abbildung 10: Chronische p38-MAPK-Inhibition reduziert den systolischen Blutdruck in Ang-II-induzierter Hypertonie: A, Systolischer Blutdruck (SBP) von Mäusen mit Ang-II-induzierter Hypertonie unter Behandlung mit „Vehikel" oder BIRB796, baseline („0"), Woche 1 und Woche 2 (baseline: 122 ± 2 mmHg (Vehikel) vs. 119 ± 4 mmHg

(BIRB796, 50 mg/kg BW/d); Woche 1: 152 ± 6 vs. 138 ± 3 mmHg, p < 0.01; Woche 2: 173 ± 3 vs. 155 ± 3 mmHg, p < 0.001). Mittelwerte ± SEM (vehicle n = 8; BIRB796 n = 8); *p < 0.05, **p < 0.01. One-way ANOVA gefolgt von Bonferroni-multiple-comparison-post-hoc-Test. B, Representative Immunoblots und densitometrische Analyse der p38-MAPK-Aktivität aus Nierenkortexlysaten, phospho-p38-MAPK zu Gesamt-p38-MAPK Ratio (vehicle, n = 6; BIRB796, n = 6; controls, n = 6): *p < 0.05 vehicle vs. BIRB796; *p < 0.05 vehicle vs. controls (% relative Änderung: controls 100 %, Ang II 228 %, Ang II + BIRB796 158 % (Mittelwerte)). One-way ANOVA gefolgt von Bonferroni-multiple-comparison-post-hoc-Test. (modifiziert nach [44] – Reproduktion und Nutzung genehmigt durch den Rechteinhaber, *SAGE Publications Ltd.*)

Die Reduktion des Blutdrucks durch die BIRB796-Therapie spiegelt sich in einer reduzierten Media-Lumen-Ratio der Aorta wider. In aortalen Gewebelysaten konnte entsprechend ebenfalls eine Reduktion der p38-MAPK-Aktivierung nachgewiesen werden.

Die Charakterisierung der Funktion renaler Widerstandsgefäße in der isoliert-perfundierten Niere zeigte, dass die BIRB796-Behandlung zu einer signifikant geringeren konzentrationsabhängigen Vasokonstriktion durch Ang II führte. Zudem war die Vasorelaxation auf den NO-Donator GNSO in den BIRB796-behandelten Tieren signifikant besser.

Wie dargestellt, führt die Hemmung der p38-MAPK zur geringeren kontraktilen Antwort auf Ang II. Analog dazu kann durch die unmittelbare Hemmung der p38-MAPK im Modell der isoliert-perfundierten Niere (p38-MAPK Inhibitor SB203580) die GNSO-induzierte Vasorelaxation signifikant verbessert werden. Die Hemmung der p38-MAPK

führt also sowohl akut als auch in der chronischen Behandlung zu einer Verbesserung der vaskulären Funktion von renalen Widerstandsgefäßen.

Das RAS spielt bei der Entwicklung vieler Erkrankungen des kardiovaskulären Systems eine wichtige Rolle. Neben der Aktivierung des RAS haben weitere Erkrankungen wie die Hypercholesterinämie und der Diabetes mellitus einen ungünstigen Einfluss auf die Progression von kardiovaskulären Erkrankungen. Dabei stellt die Hypercholesterinämie einen der wichtigsten kardiovaskulären Risikofaktoren dar. Neben der fortschreitenden Arteriosklerose führt sie zu einer anhaltenden Inflammation des Gefäßsystems. Diese beiden Faktoren führen zu einer gesteigerten Gefäßsteifigkeit und Vulnerabilität. Es ist daher nachvollziehbar, dass die negativen kardiovaskulären Effekte des RAS im Milieu der Hypercholesterinämie potenziert werden.

Die Apolipoprotein-E-KO-Maus (ApoE(−/−)) entwickelt aufgrund eines gestörten Lipoproteintransportes eine ausgeprägte Hyperlipoproteinämie, welche durch eine Hoch-Fett-Diät zusätzlich gesteigert werden kann. Diese Tiere entwickeln in kürzester Zeit eine ausgeprägte Arteriosklerose mit endothelialer Dysfunktion. Die endotheliale Dysfunktion ist gekennzeichnet durch eine reduzierte Verfügbarkeit von NO und erhöhtem oxidativem Stress. Dieser Zustand ist mit der Entwicklung einer Hypertonie und einem gesteigerten kardiovaskulären Risiko vergesellschaftet. [60]

Ob die vermittelte Hyperkontraktilität auf Ang II (siehe Abschnitt 2.4) in den ApoE(−/−)-Tieren auf eine p38-MAPK-Aktivierung zurückzuführen war, untersuchten wir zum einen durch Expressionsnachweis der phospho-p38-MAPK im renalen Kortex als auch in präglomerulären Kapillaren – den renalen Widerstandsgefäßen. Zudem testeten wir, ob die unmittelbare p38-Inhibiton (p38-MAPK Inhibitor SB203580) die Ang-II-vermittelte Vasokonstriktion in unbehandelten ApoE(−/−)-Tieren beeinflussen konnte.

Es zeigte sich, dass sowohl im renalen Kortex als auch in präglomerulären Kapillaren die p38-MAPK-Aktivierung in den ApoE(−/−)-Tieren gesteigert war (siehe Abschnitt 2.4). In der isoliert-perfundierten Mausniere konnte sodann gezeigt werden, dass die p38-MAPK-Inhibition auch zu einer signifikant reduzierten Druckantwort auf Ang II führte (Abb. 11).
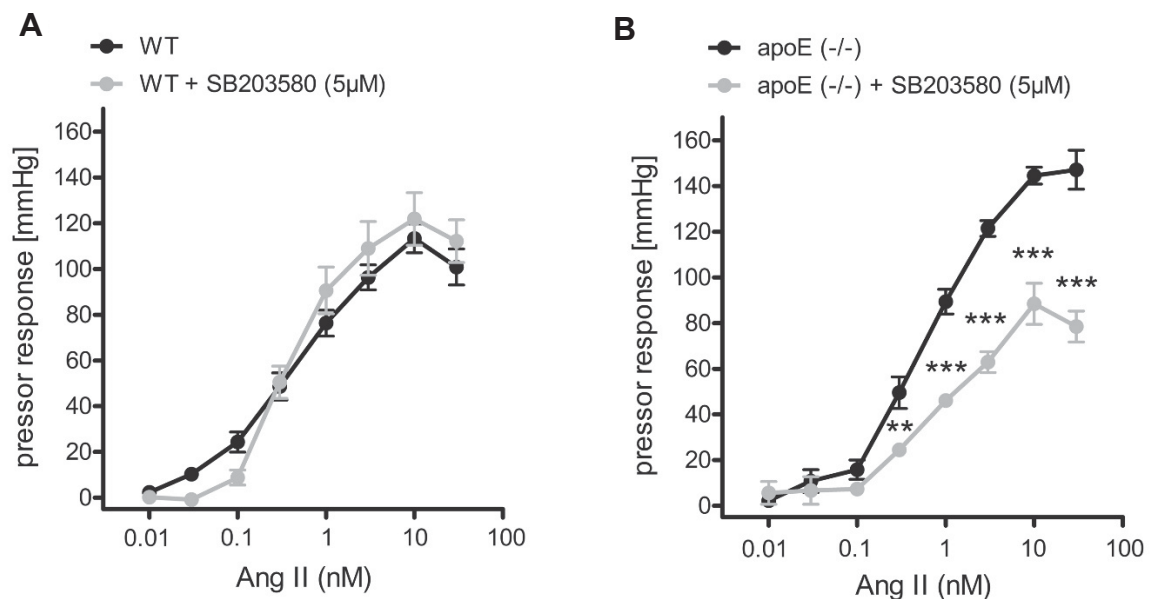

Abbildung 11: A, Die Ang-II-induzierte Druckantwort wird in isolierten Nieren von WT-Mäusen durch p38-Inhibitor (SB203580, 5 µmol/L) nicht beeinflusst. (WT, n = 23; WT+SB203580, n = 14). B, Die Ang-II-induzierte Druckantwort in Nieren von ApoE(−/−)-Mäusen wird durch p38-MAPK-Inhibition (SB203580, 5 µmol/L) signifikant abgeschwächt. (ApoE(−/−), n = 14; ApoE(−/−) + SB203580, n = 11). 2-way ANOVA gefolgt von Bonferroni-correction-post-hoc-Test. (modifiziert nach [19] – Reproduktion und Nutzung genehmigt durch den Rechteinhaber, *American Heart Association, Inc.*)

Zusammengefasst konnte gezeigt werden, dass die Aktivität der p38-MAPK eine wichtige Rolle in der Ang-II-vermittelten Vasokonstriktion spielt. Die chronische

Inhibition von p38-MAPK führt bei Ang-II-induzierter Hypertonie zur Reduktion des systolischen Blutdrucks und verbessert die Funktion renaler Widerstandsgefäße. Auch die akute Inhibition im Ex-vivo-Modell kann die akute Ang-II-Wirkung abschwächen. In der ApoE(−/−)-Maus konnte zudem gezeigt werden, dass die Hypercholesterinämie zu einer p38-MAPK-Aktivierung führt. Diese gesteigerte Aktivität führt zu einer verstärkten Ang-II-Antwort, die durch p38-MAPK-Inhibition signifikant abgeschwächt werden kann.

2.4 Protektiver Effekt von Angiotensin-(1-7) auf die renale Gefäßfunktion
(Publikationen III, IV)

Wie in der Einleitung dargestellt, ist Ang-(1-7) ein Heptapeptid, welches über seinen eigenen Rezeptor (Mas-R) eine gefäßprotektive Wirkung als Gegenspieler zu Ang II entfalten kann.

Neben der gestörten Ang-II-induzierten Vasokonstriktion untersuchten wir im ApoE-KO-Modell die Wirkung der chronischen Ang-(1-7)-Behandlung auf die Funktion renaler Widerstandsgefäße. [61]

Im Rahmen der Behandlung wurden sechs Wochen alte ApoE(−/−)-Mäuse mittels osmotischer Minipumpe entweder mit isotonischer Kochsalzlösung (Kontrolle), Ang-(1-7) allein oder Ang-(1-7) zusammen mit D-ALA-Ang-(1-7), einem spezifischen Mas-R-Antagonisten, für insgesamt sechs Wochen behandelt. Die Funktion renaler Wider-standsgefäße dieser Tiere wurde dann im Modell der isoliert-perfundierten Niere geprüft.

Ang-(1-7)-behandelte ApoE(−/−) zeigten eine signifikant gebesserte endothel-abhängige Vasorelaxation auf Carbachol im Vergleich zu unbehandelten KO-Tieren. Dabei war die Endothel-unabhängige Vasorelaxation, welche mit dem NO-Donator

GSNO getestet wurde, in allen Gruppen gleich. Dies unterstreicht die protektive Wirkung von Ang-(1-7) auf die endotheliale Dysfunktion. Der Effekt von Ang-(1-7) konnte durch D-Ala-Ang-(1-7) aufgehoben werden, womit die Abhängigkeit der Wirkung von Ang-(1-7) in der Wiederherstellung der endothel-abhängigen Relaxation vom Mas-R bewiesen werden konnte.

Um herauszufinden, wie es zu einer verbesserten NO-Bioverfügbarkeit kommt, wurde sowohl die Achse der NO-Produktion als auch die Achse des NO-Abbaus untersucht. Es konnte gezeigt werden, dass Ang-(1-7) sowohl die Expression der eNOS als auch die Menge an cGMP als second messenger in kortikalen Nierenschnitten erhöht.

ROS spielen eine entscheidende Rolle als NO-depletierendes Agens. Mit Hilfe von Tempol, das ROS abfangen kann, konnten wir zeigen, dass die endothel-abhängige Vasorelaxation in ähnlichem Maße verbessert werden konnte wie durch die Ang-(1-7)-Behandlung. In renalem Kortexgewebe wie auch im Urin der Tiere konnte nach-gewiesen werden, dass ApoE(−/−)-Tiere eine erhöhte ROS-Produktion aufweisen und die Behandlung mit Ang-(1-7) diese signifikant senken kann. Dies lässt darauf schließen, dass die positive Wirkung von Ang-(1-7) auf das Endothel zumindest teilweise durch Reduktion der ROS-Produktion zustande kommt.

Mit dem Nachweis einer reduzierten Expression von Catalase und gp91phox- und p47phox-NAD(P)H-Oxidase-Untereinheiten durch Ang-(1-7)-Behandlung konnte geschlussfolgert werden, dass Ang-(1-7) offensichtlich unmittelbar durch Expressions-änderung der ROS-produzierenden Enzyme Einfluss auf die lokale ROS-Menge nimmt. Durch diese Arbeit konnte gezeigt werden, dass sich die Ang-(1-7)-Behandlung in einem Modell der endothelialen Dysfunktion deutlich positiv auf die vaskuläre Funktion auswirkt. Dieser Effekt wurde zum einen durch Wiederherstellung der endothelialen NO-Produktion als auch durch Reduktion von ROS bewirkt. [43]

Die Wirkung von Ang-(1-7) auf die Ang-II-vermittelte Vasokonstriktion wurde ebenfalls im Modell der ApoE-KO-Maus unter Hochfett-Diät-Bedingungen untersucht. Erneut wurden die Tiere sechs Wochen mit Ang-(1-7) bzw. Kochsalzlösung als Kontrolle behandelt. Im Modell der isoliert-perfundierten Niere wurde dann die Vasokonstriktion auf ansteigende Ang-II-Konzentrationen getestet. [19]

Es zeigte sich, dass die unbehandelten ApoE(−/−)-Tiere im Vergleich zu Wildtyp-Tieren eine deutlich gesteigerte konzentrationsabhängige Vasokonstriktion auf Ang II aufwiesen. Die Ang-(1-7)-Behandlung führte zu einer signifikanten Reduktion der kontraktilen Antwort auf Ang II. Unter Ang-(1-7)-Behandlung zeigten die ApoE(−/−)-Tiere eine Senkung der Druckantwort auf das Niveau der Wildtyp-Tiere. In isolierten präglomerulären Kapillaren konnten wir nachweisen, dass dies gesteigerte Vaso-reaktivität in unbehandelten ApoE(−/−)-Tieren auf eine gesteigerte Phosphorylierung der Myosin-Leichtkette 20 (MLC20) zurückzuführen war. Durch die Ang-(1-7)-Behandlung konnte die Phosphorylierung der MLC20 signifikant auf das Niveau von Wildtyp-Tieren gesenkt werden (Abb. 12).
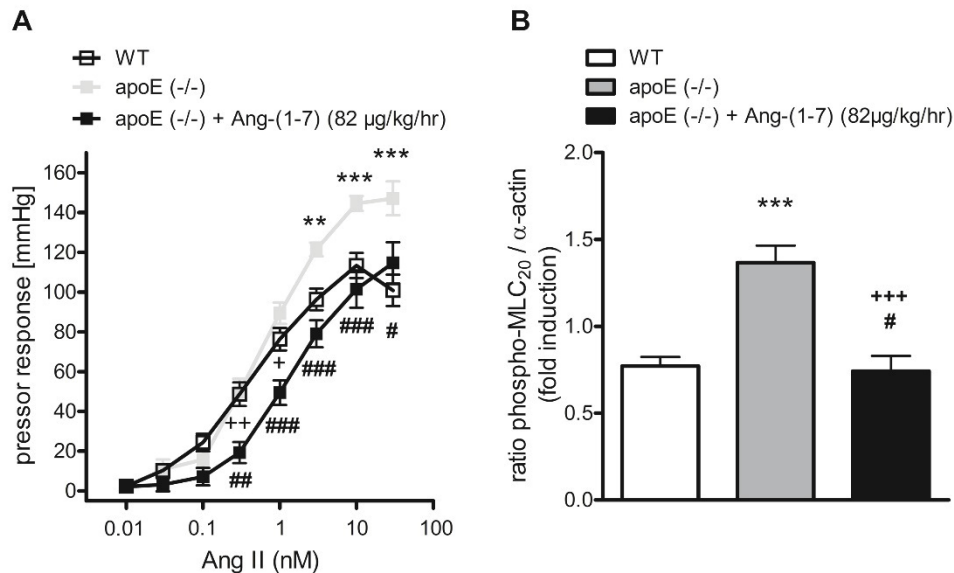
Abbildung 12: A, Die Ang-II-induzierte Druckantwort in Nieren von ApoE(−/−)-Mäusen (n = 14) ist im Vergleich zu WT-Mäusen (n = 23) deutlich gesteigert. Die chronische Ang-(1-7)-Behandlung senkt die Ang-II–induzierte Druckantwort in Nieren von ApoE(−/−) (n = 9) auf WT-Niveau. Mittelwert ± SEM. **P < 0.01, ***P < 0.001: WT vs. ApoE(−/−). +P < 0.05, ++P < 0.01 WT vs. ApoE(−/−) + [Ang-(1-7)], #P < 0.05, ##P < 0.01, ###P < 0.001 ApoE(−/−) vs. ApoE(−/−) + Ang-(1-7). 2-way ANOVA gefolgt von Bonferroni-correction-post-hoc-Test. B, Western Blot Analyse der MLC20 aus präglomerulären Gefäßlysaten. WT vs. ApoE(−/−): 0.77 ± 0.05 vs. 1.37 ± 0.10, ***P < 0.001; ApoE(−/−) vs. ApoE(−/−) + Ang-(1-7): 1.37 ± 0.10 vs. 0.74 ± 0.09, +++P < 0.001; WT vs. ApoE(−/−) + Ang-(1-7): 0.77 ± 0.05 vs. 0.74 ± 0.09, #P = NS; n = 8. Mittelwert ± SEM. 1-way ANOVA gefolgt von Bonferroni-multiple-comparison-post-hoc-Test. (modifiziert nach [19] – Reproduktion und Nutzung genehmigt durch den Rechteinhaber, *American Heart Association, Inc.*)

Ob die vermittelte Hyperkontraktilität auf Ang II und die Aktivierung der MCL20 in den ApoE(−/−)-Tieren auf eine p38-MAPK-Aktivierung zurückzuführen sein könnte, untersuchten wir zum einen durch Expressionsnachweis der phospho-p38-MAPK im

renalen Kortex als auch in präglomerulären Kapillaren – den renalen Widerstandsgefäßen. Zudem testeten wir, ob der spezifische p38-MAPK-Inhibitor SB203580 die Ang-II-vermittelte Vasokonstriktion in den unbehandelten ApoE(−/−)-Tieren beeinflussen würde. Es zeigte sich, dass sowohl im renalen Kortex als auch in präglomerulären Kapillaren die p38-MAPK-Aktivierung in unbehandelten ApoE(−/−)- im Vergleich zu WT-Tieren signifikant gesteigert war. Durch Ang-(1-7) Behandlung wurde diese Aktivierung in ApoE(−/−)-Tieren signifikant abgeschwächt. In der isoliert-perfundierten Mausniere konnte sodann gezeigt werden, dass die p38-MAPK-Inhibition bei gleichzeitiger Ang-(1-7)-Behandlung keine zusätzliche Wirkung zeigte. (Ohne Ang-(1-7)-Behandlung zeigte die p38-MAPK-Inhibition eine sehr deutliche Reduktion der Druckantwort (siehe Abschnitt 2.3)).

Aus den Versuchen bezüglich der endothel-abhängigen Vasorelaxation (siehe Abschnitt 2.2) wussten wir, dass ROS eine wichtige Rolle bei der Ang-(1-7)-vermittelten Verbesserung der Gefäßfunktion spielen. Daher untersuchten wir in einem weiteren Schritt Marker für ROS (Urinausscheidung von 8-Isoprostan, Lucigenin-verstärkte Chemilumineszenz als Maß für die ROS-Produktion in Nierenkortex-gewebe). Es zeigte sich, dass diese Marker durch Ang-(1-7)-Behandlung auch in diesem Versuchsumfeld signifikant reduziert wurden. Zudem konnte erneut gezeigt werden, dass die Überexpression der NADP(H)-Oxidase-Untereinheit p47phox in unbehandelten ApoE(−/−)-Tieren durch Ang-(1-7) auf das Niveau von Wildtyp-Tieren reduziert werden konnte. Die p47phox-NADP(H)-Oxidase-Untereinheit kann durch Ang II induziert werden und spielt daher in der Ang-II-vermittelten Hypertonie eine exponierte Rolle. [62]

Mit Hilfe von ApoE/Mas-R-Doppel-KO-Mäusen (Mas(−/−)/ApoE(−/−)) konnten wir beweisen, dass die Wirkung von Ang-(1-7) spezifisch über den eigenen Rezeptor und

nicht über andere Rezeptoren vermittelt wird. In der Doppel-KO-Maus hatte die Ang-(1-7)-Behandlung keinen Einfluss auf die Kontraktilität. Auch ROS-Marker wurden durch die Ang-(1-7)-Behandlung in den Doppel-KO-Tieren nicht signifikant beeinflusst (Abb. 13).
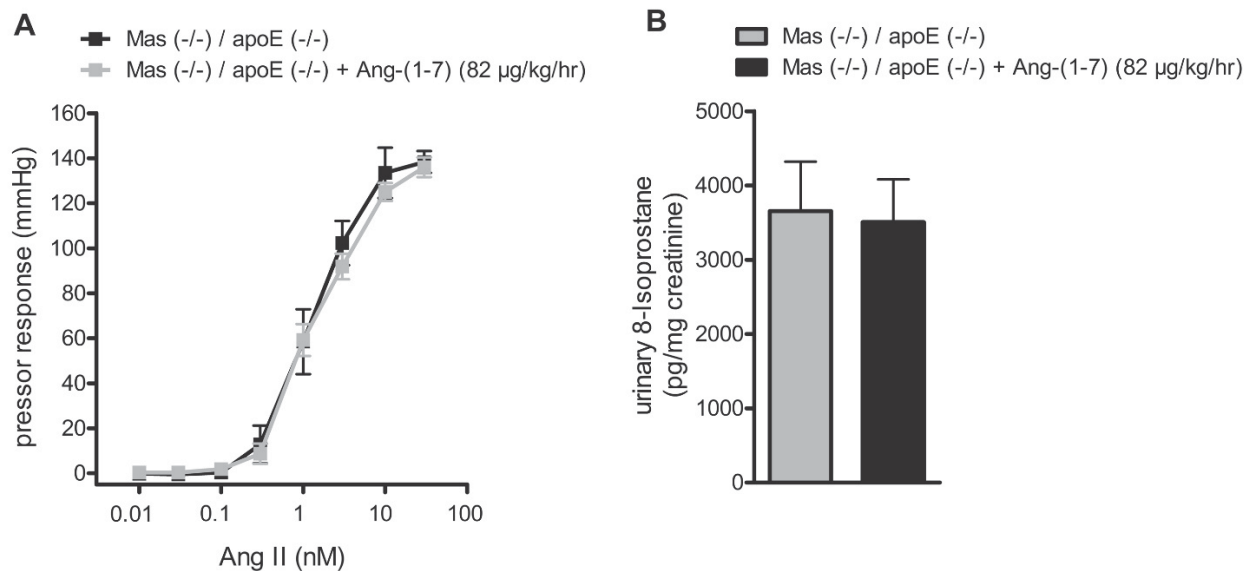

Abbildung 13: A, Die Ang-II-induzierte Druckantwort in den Mausnieren Mas(−/−)/ApoE(−/−) (n = 6) und Mas(−/−)/ApoE(−/−) + Ang-(1-7) (n = 8) ist nicht signifikant unterschiedlich. Mittelwerte ± SEM (P = NS). 2-way ANOVA gefolgt von Bonferroni-correction-post-hoc-Test. B, Die 24h 8-Isoprostan Exkretion (Urin) in den Mäusen Mas(−/−)/ApoE(−/−) (n = 8) und Mas(−/−)/ApoE(−/−) + Ang-(1-7) (n = 10) ist nicht signifikant unterschiedlich. Mittelwert ± SEM; P = NS, Mann-Whitney-U-Test (**P < 0.01, ***P < 0.001). 2-way ANOVA gefolgt von Bonferroni-correction-post-hoc-Test. (modifiziert nach [19] – Reproduktion und Nutzung genehmigt durch den Rechteinhaber, *American Heart Association, Inc.*)

Zusammenfassend zeigen die Versuche an ApoE(−/−)-und WT-Tieren, dass die Behandlung mit Ang-(1-7) einen protektiven Effekt auf die Gefäßfunktion hat. Die gesteigerte Kontraktilität auf Ang-II-Gabe und die endotheliale Dysfunktion werden in einem kardiovaskulären Risikomodell durch Ang-(1-7)-Behandlung abgeschwächt. Dabei spielen die Reduktion von ROS und die geminderte Aktivierung der p38-MAPK eine wichtige Rolle. Durch Einsatz einer Doppel-KO-Maus konnte bewiesen werden, dass die Effekte von Ang-(1-7) spezifisch über den Mas-R vermittelt werden.

2.5 Angiotensin II vermittelt den Integritätsverlust der glomerulären Schlitzmembran

(Publikation IX)

Neben dem Einfluss auf die renale Gefäßfunktion spielt Ang II auch entlang des Nephrons eine entscheidende Rolle in dessen Funktion. So führt Ang II im Tubulussystem zu einer vermehrten Natrium-Rückresorption und hat damit einen Einfluss auf den Elektrolyt- und Flüssigkeitshaushalt.

Inwieweit Ang II neben hämodynamischen Effekten auch die Integrität der glomerulären Schlitzmembran mit Rückhalt von Makroproteinen aus dem Blut beeinflusst, untersuchten wir in einer Arbeit sowohl in vivo als auch in vitro. [63]

FVB-Mäusen wurde hierfür über einen Jugular-Katheter kontinuierlich Ang II appliziert. Die Dosis wurde gering gewählt, so dass kein signifikant Blutdruck-steigernder Effekt eintrat. Über die Zeit von 60 bzw. 120 Minuten wurde der Einfluss von Ang II auf die glomeruläre Permeabilität untersucht. Hierfür wurde den Tieren FITC-Ficoll 70 intravenös appliziert und dessen Auftreten im Urin untersucht.[64]

Es konnte gezeigt werden, dass Ang II in einer Blutdruck-unabhängigen Dosierung im Vergleich zu unbehandelten Tieren die Permeabilität für FITC-Ficoll signifikant steigert.

Dieser Effekt konnte durch die vorherige Gabe eines AT1-Antagonisten (Candesartan) blockiert werden. Wie in Abschnitt 1.5 dargestellt, führt die β-Arrestin2-Bindung an Nephrin zur Endozytose von Nephrin. Durch Extraktion von Glomeruli mittels ferromagnetischer Partikel (siehe 2.1) entsprechend behandelter Tiere konnte gezeigt werden, dass die Nephrin-β-Arrestin2-Bindung durch Ang-II-Behandlung deutlich zunahm.

In einem In-vitro-Versuch mit HEK293T-Zellen, welche mit AT1-Rezeptor DNA transfiziert wurden, konnten wir zeigen, dass die membranständige Expression von Nephrin, nachgewiesen durch ein Biotin-Assay, durch die Stimulation mit Ang II über einen Zeitraum vom 60 Minuten signifikant reduziert wurde. Hinzugabe von Candesartan konnte die Reduktion der membranständigen Expression von Nephrin teilweise aufheben.

Für die Untersuchung des Ang-II-Effektes wurden immortalisierte humane Podozyten mit dem humanen AT1-Rezeptor transduziert. Wir konnten zeigen, dass die Stimulation mit Ang II von AT1-exprimierenden Podozyten zu einer signifikant gesteigerten Nephrin-β-Arrestin2-Bindung führt. Dieser Effekt konnte durch den AT1-Antagonisten Candesartan aufgehoben werden. In Podozyten, die den AT1-Rezeptor nicht exprimierten, hatte Ang II keinen Effekt auf die Nephrin-β-Arrestin2-Interaktion.

Mit Hilfe einer AT1-Rezeptor-Mutante (D125AR126L) konnte nachgewiesen werden, dass die G-Protein-gekoppelte Signaltransduktion (via $G\alpha_i$) über PLC für die verstärkte β-Arrestin2-Bindung an Nephrin verantwortlich ist. Zudem konnte durch Transfektion von Nephrin-Mutanten in HEK293T-Zellen nachgewiesen werden, dass die Phosphorylierung von Threonin 1120 und 1125 in der Nephrin-Proteinsequenz mit der konsekutiven Bindung β-Arrestin2 an dieser Stelle der entscheidende Mechanismus für die Ang-II-vermittelte Endozytose von Nephrin darstellt.

Zusätzlich konnte gezeigt werden, dass unter Ang-II-Einfluss die Verankerung von Nephrin am Zytoskelett via nck/F-Aktin-Bindung am Tyrosin 1217 durch Dephosphorylierung dieser Bindungsstelle vermindert wird.

Zusammenfassend konnte gezeigt werden, dass Ang II die Permeabilität der glomerulären Schlitzmembran für Makroproteine steigert. Die Wirkung wird dabei über den AT1-Rezeptor auf Podozyten vermittelt. Die intrazelluläre Signaltransduktion erfolgt G-Protein-vermittelt über PLC. Die konsekutive Phosphorylierung an den Motiven T1120/1125 führt zur β-Arrestin2-Bindung und nachfolgend zur Endozytose von Nephrin. Die Dephosphorylierung von Y1217 führt zusätzlich zur Destabilisierung der Nephrin-Verankerung in der Zellmembran. Diese Ang-II-vermittelten Effekte stellen einen wichtigen Mechanismus im Integritätsverlust der glomerulären Schlitzmembran und damit der Entwicklung einer Albuminurie dar (Abb. 14).
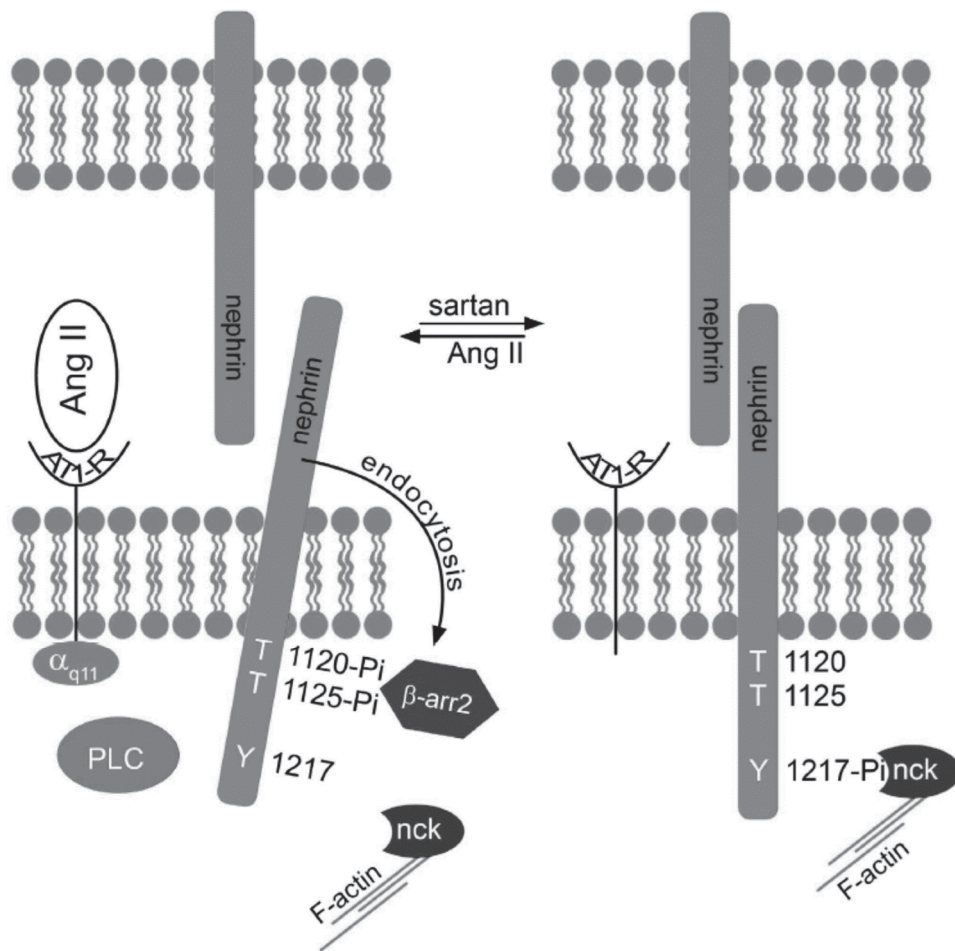
Abbildung 14: Schema der Ang-II-vermittelten Permeabilitätssteigerung an der podozytären Schlitzmembran: Ang II aktiviert den AT1-R. Der aktivierte AT1-R überträgt das Signal durch $G\alpha_{q11}$ und PLC. Nephrin wird bei T1120 / T1125 phosphoryliert und bindet an β-Arrestin2. Die Bindung von β-Arrestin2 führt zu einer erhöhten Nephrin-Endozytose. Zudem wird durch Dephosphorylierung die Bindung an nck/A-Aktin geschwächt, wodurch die Nephrin-Integrität in der Zellmembran zusätzlich abgeschwächt wird. Dies könnte neben hämodynamischen Effekten die Ang-II-vermittelte Steigerung der Permeabilität der podozytären Schlitzmembran erklären. Im Gegensatz dazu führt die AT1-Rezeptor-Hemmung durch Sartane zu einer geringeren β-Arrestin2-Nephrin-Wechselwirkung und führt zu einer geringeren Nephrin-Endozytose-vermittelten glomerulären Permeabilität. (modifiziert nach [63] – Reproduktion und Nutzung genehmigt durch den Rechteinhaber, *Springer Nature Limited*)

3.   Zusammenfassung

Die arterielle Hypertonie ist der wichtigste Risikofaktor für kardiovaskuläre Morbidität und Mortalität. Für die Entstehung und Aufrechterhaltung der arteriellen Hypertonie spielen das RAS und die NO/cGMP-Achse eine herausragende Rolle. Eine Dysbalance zwischen diesen Achsen führt zu einer Gefäßdysfunktion und kann anhaltend zu einer dauerhaften Gefäßschädigung und zu einem gesteigerten arteriellen Blutdruck führen. Begleiterkrankungen wie die Hypercholesterinämie und der Diabetes Mellitus sind dabei wichtige Modifikatoren für vaskuläre Dysfunktion. Um herauszufinden, welche Mechanismen die renale Gefäßfunktion ungünstig beein-flussen und zur Entwicklung einer arteriellen Hypertonie beitragen, wurden unter-schiedliche Modelle eingesetzt. Im Rahmen der vorgestellten Arbeiten kamen das ApoE(−/−)-Modell (Hypercholesterinämie/Atherosklerose), das NO-GC1(−/−)-Modell (Störung der NO/cGMP-Achse), das 2k1C-Modell (Induktion einer Nierenarterien-stenose mit Aktivierung des RAS), die Ang-II-induzierte Hypertonie (osmotische Mini-pumpen) sowie In-vivo- und In-vitro-Untersuchungen des Einflusses von Ang II auf die podozytäre Schlitzmembran zum Einsatz. Durch die Behandlung mit Ang-(1-7), als Gegenspieler des Angiotensin II, wurde in einzelnen Modellen dessen therapeutische Wirkung auf die vaskuläre Dysfunktion untersucht.

In den vorgestellten Arbeiten konnte gezeigt werden, dass Angiotensin II als Haupt-effektor des „klassischen" RAS einen wesentlichen Einfluss auf die renovaskuläre Dysfunktion hat. Ang II bewirkt über Beeinflussung der NO/cGMP-Achse, der ROS-Produktion und der p38-MAPK-Aktivierung eine Steigerung des Gefäßtonus. In dem dargestellten Hypercholesterinämie-Modell (ApoE(−/−)-Maus) kommt es zum einen zur eingeschränkten Bereitstellung von NO durch reduzierte eNOS-Expression als

auch zu einem Überangebot von ROS, was zu einer NO-Depletion führt. Sowohl Ang II als auch die gesteigerte vaskuläre Inflammation bei Hypercholesterinämie führen zu einer Zunahme von ROS. Dabei spielt die gesteigerte Expression von NADP(H)-Oxidasen als Quelle von ROS eine wichtige Rolle.

In der Ang-II-abhängigen Hypertonie (2K1C-Modell/Ang-II-Infusion) konnten wir nachweisen, dass auch der Abbau von cGMP als second messenger des NO über eine gesteigerte Aktivität der PDE5, als wichtigste regulierende Phosphodiesterase in den Widerstandsgefäßen, zur Entwicklung der arteriellen Hypertonie beiträgt.

Sowohl Ang-II-vermittelt als auch im Rahmen der Hypercholesterinämie wird die p38-MAPK aktiviert. Die Aktivierung kann direkt Ang-II-vermittelt erfolgen oder auch Folge einer gesteigerten ROS-Produktion sein. So konnte nachgewiesen werden, dass unter Behandlung mit einem ROS-„Scavenger" die Gefäßdysfunktion im Hypercholesterinämie-Modell gebessert ist. Die gesteigerte Aktivität und Expression der p38-MAPK führt zu einer verstärkten Phosphorylierung der MLC(20). Hierdurch wird ein gesteigerter kontraktiler Zustand der glatten Gefäßmuskelzelle bewirkt, welcher zu einer gesteigerten Vasokonstriktion führt und damit zur Entwicklung einer arteriellen Hypertonie beitragen kann. Es konnte gezeigt werden, dass sowohl die unmittelbar akute Hemmung als auch die chronische Inhibition der p38-MAPK im Rahmen einer Ang-II-induzierten Hypertonie zu einer deutlich gebesserten Gefäßfunktion und arteriellen Blutdrucksenkung im chronischen Modell führt. Dieser Effekt konnte auch in Mäusen mit Hypercholesterinämie nachgewiesen werden.

Bei Hypercholesterinämie konnte somit nachgewiesen werden, dass die Ang-II-Wirkung auf die Vasokonstriktion deutlich verstärkt wird und die Vasorelaxation signifikant eingeschränkt ist. Dabei spielt die p38-MAPK-Aktivierung im Rahmen der Hypercholesterinämie eine wichtige Rolle. Die dargestellten Mechanismen, welche zu

einer gesteigerten Ang-II-Wirkung führen, könnten zum erhöhten kardiovaskulären Risiko bei Hypercholesterinämie beitragen.

Dem Haupteffektor des RAS, dem Angiotensin II, steht das Heptapeptid Ang-(1-7) als Metabolit des erweiterten RAS entgegen. In den aufgeführten Arbeiten konnten mehrere Mechanismen identifiziert werden, die eine Gefäß-protektive Wirkung von Ang-(1-7) aufzeigen. So führt die Behandlung mit Ang-(1-7) in Mäusen mit Hypercholesterinämie durch eine gesteigerte eNOS-Expression und durch Reduktion von ROS zu einer verbesserten NO-Bioverfügbarkeit. Dies zeigt sich in einer gebesserten endothel-abhängigen Vasorelaxation. Zudem wird die verstärkte Kontraktilität bei Hypercholesterinämie in Abhängigkeit von Ang II deutlich abgeschwächt. Neben der gebesserten NO-Bioverfügbarkeit und dem Einfluss auf ROS über die reduzierte Expression von NADP(H)-Oxidasen führt die Ang-(1-7)-Behandlung in diesem Modell zusätzlich zur Reduktion der gesteigerten p38-MAPK-Aktivität. Hierdurch wird der verstärkten Phosphorylierung der MLC(20) und damit einer gesteigerten Kontraktilität der Gefäßmuskelzelle entgegengewirkt. In der Untersuchung von ApoE/Mas-Rezeptor-Doppel-KO-Mäusen konnte bewiesen werden, dass die Ang-(1-7)-vermittelten Effekte von der Signaltransduktion durch den Mas-R abhängig sind.

Ang-(1-7) stellt somit einen endogenen Gegenspieler des Angiotensin II dar. Es vermag der gesteigerten Angiotensin-II-Wirkung bei Hypercholesterinämie entgegen-zuwirken. Diese Wirkung ist im Wesentlichen von der Aktivierung des Mas-Rezeptors abhängig.

Zusätzlich zu den hämodynamischen Effekten von Ang II konnte gezeigt werden, dass Ang II die Permeabilität der podozytären Schlitzmembran direkt auf molekularer Ebene durch Steigerung der Nephrin-Endozytose und Destabilisierung der Verankerung des

Nephrins am Aktin-Zytoskelett steigert. Diese Wirkung von Ang II kann pharmakologisch durch Gabe eines AT-1-Antagonisten (Sartane) abgeschwächt werden. Dieser Mechanismus stellt einen Erklärungsansatz für die anti-proteinurische Wirkung durch RAS-Blockade bei Nierenerkrankungen dar.

Die vorgelegten Arbeiten zeigen den Einfluss von Ang II auf die renovaskuläre Dysfunktion und arterielle Hypertonie in renalen und vaskulären Schädigungsmodellen auf. Die pharmakologische Intervention mit p38-MAPK-Inhibition und die Gabe des Ang-II-Gegenspielers Ang-(1-7) können die renovaskuläre Dysfunktion und den Hypertonus über Beeinflussung der NO/cGMP-Achse und ROS günstig beeinflussen und bieten somit das Potential einer pharmakologischen Intervention.

4.   Literaturverzeichnis

1.   Yang, G., et al., *ACE2 and the Homolog Collectrin in the Modulation of Nitric Oxide and Oxidative Stress in Blood Pressure Homeostasis and Vascular Injury.* Antioxid Redox Signal, 2017. 26(12): p. 645-659.

2.   Murphy, T.J., et al., *Isolation of a cDNA encoding the vascular type-1 angiotensin II receptor.* Nature, 1991. 351(6323): p. 233-6.

3.   Kanaide, H., et al., *Cellular mechanism of vasoconstriction induced by angiotensin II: it remains to be determined.* Circ Res, 2003. 93(11): p. 1015-7.

4.   Mergia, E., et al., *Spare guanylyl cyclase NO receptors ensure high NO sensitivity in the vascular system.* J Clin Invest, 2006. 116(6): p. 1731-7.

5.   Hirai, T., et al., *Differential sympathetic nerve responses to nitric oxide synthase inhibition in anesthetized rats.* Am J Physiol, 1995. 269(4 Pt 2): p. R807-13.

6.   Lim, S.S., et al., *A comparative risk assessment of burden of disease and injury attributable to 67 risk factors and risk factor clusters in 21 regions, 1990-2010: a systematic analysis for the Global Burden of Disease Study 2010.* Lancet, 2012. 380(9859): p. 2224-60.

7.   Sparks, M.A., et al., *Classical Renin-Angiotensin system in kidney physiology.* Compr Physiol, 2014. 4(3): p. 1201-28.

8.   Stegbauer, J. and T.M. Coffman, *New insights into angiotensin receptor actions: from blood pressure to aging.* Curr Opin Nephrol Hypertens, 2011. 20(1): p. 84-8.

9.   Montezano, A.C., et al., *Angiotensin II and vascular injury.* Curr Hypertens Rep, 2014. 16(6): p. 431.

10.   Arruda, R.M., et al., *Evaluation of vascular function in apolipoprotein E knockout mice with angiotensin-dependent renovascular hypertension.* Hypertension, 2005. 46(4): p. 932-6.

11.   Heitzer, T., et al., *Increased NAD(P)H oxidase-mediated superoxide production in renovascular hypertension: evidence for an involvement of protein kinase C.* Kidney Int, 1999. 55(1): p. 252-60.

12.   Jung, O., et al., *Extracellular superoxide dismutase is a major determinant of nitric oxide bioavailability: in vivo and ex vivo evidence from ecSOD-deficient mice.* Circ Res, 2003. 93(7): p. 622-9.

13.   Giachini, F.R., et al., *Decreased cGMP level contributes to increased contraction in arteries from hypertensive rats: role of phosphodiesterase 1.* Hypertension, 2011. 57(3): p. 655-63.

14.   Kim, D., et al., *Angiotensin II increases phosphodiesterase 5A expression in vascular smooth muscle cells: a mechanism by which angiotensin II antagonizes cGMP signaling.* J Mol Cell Cardiol, 2005. 38(1): p. 175-84.

15.   Kim, D., et al., *Upregulation of phosphodiesterase 1A1 expression is associated with the development of nitrate tolerance.* Circulation, 2001. 104(19): p. 2338-43.

16.   Sonnenburg, W.K., et al., *Identification, quantitation, and cellular localization of PDE1 calmodulin-stimulated cyclic nucleotide phosphodiesterases.* Methods, 1998. 14(1): p. 3-19.

17.   Huang, C.Y., et al., *Mechanism of activation of cyclic nucleotide phosphodiesterase: requirement of the binding of four Ca2+ to calmodulin for activation.* Proc Natl Acad Sci U S A, 1981. 78(2): p. 871-4.

18.   Park, J.K., et al., *p38 mitogen-activated protein kinase inhibition ameliorates angiotensin II-induced target organ damage.* Hypertension, 2007. 49(3): p. 481-9.

19.   Potthoff, S.A., et al., *Angiotensin-(1-7) modulates renal vascular resistance through inhibition of p38 mitogen-activated protein kinase in apolipoprotein E-deficient mice.* Hypertension, 2014. 63(2): p. 265-72.

20.   Santos, R.A., et al., *Converting enzyme activity and angiotensin metabolism in the dog brainstem.* Hypertension, 1988. 11(2 Pt 2): p. I153-7.

21.   Santos, R.A., et al., *Angiotensin-(1-7) is an endogenous ligand for the G protein-coupled receptor Mas.* Proc Natl Acad Sci U S A, 2003. 100(14): p. 8258-63.

22.   Santos, R.A.S., et al., *The Renin-Angiotensin System: Going Beyond the Classical Paradigms.* Am J Physiol Heart Circ Physiol, 2019.

23.   Domenig, O., et al., *Neprilysin is a Mediator of Alternative Renin-Angiotensin-System Activation in the Murine and Human Kidney.* Sci Rep, 2016. 6: p. 33678.

24.   Sampaio, W.O., et al., *Angiotensin-(1-7) counterregulates angiotensin II signaling in human endothelial cells.* Hypertension, 2007. 50(6): p. 1093-8.

25.   Sampaio, W.O., et al., *Angiotensin-(1-7) through receptor Mas mediates endothelial nitric oxide synthase activation via Akt-dependent pathways.* Hypertension, 2007. 49(1): p. 185-92.

26.   Mori, J., et al., *Angiotensin 1-7 ameliorates diabetic cardiomyopathy and diastolic dysfunction in db/db mice by reducing lipotoxicity and inflammation.* Circ Heart Fail, 2014. 7(2): p. 327-39.

27.   Parajuli, N., et al., *Loss of NOX2 (gp91phox) prevents oxidative stress and progression to advanced heart failure.* Clin Sci (Lond), 2014. 127(5): p. 331-40.

28.   Patel, V.B., et al., *ACE2 Deficiency Worsens Epicardial Adipose Tissue Inflammation and Cardiac Dysfunction in Response to Diet-Induced Obesity.* Diabetes, 2016. 65(1): p. 85-95.

29.   Schinzari, F., et al., *Favorable Vascular Actions of Angiotensin-(1-7) in Human Obesity.* Hypertension, 2018. 71(1): p. 185-191.

30.   Qi, Y., et al., *Lentivirus-mediated overexpression of angiotensin-(1-7) attenuated ischaemia-induced cardiac pathophysiology.* Exp Physiol, 2011. 96(9): p. 863-74.

31.   Tallant, E.A., C.M. Ferrario, and P.E. Gallagher, *Angiotensin-(1-7) inhibits growth of cardiac myocytes through activation of the mas receptor.* Am J Physiol Heart Circ Physiol, 2005. 289(4): p. H1560-6.

32.   Giani, J.F., et al., *Angiotensin-(1-7) improves cardiac remodeling and inhibits growth-promoting pathways in the heart of fructose-fed rats.* Am J Physiol Heart Circ Physiol, 2010. 298(3): p. H1003-13.

33.   Gwathmey, T.M., et al., *Angiotensin-(1-7)-angiotensin-converting enzyme 2 attenuates reactive oxygen species formation to angiotensin II within the cell nucleus.* Hypertension, 2010. 55(1): p. 166-71.

34.   Patel, V.B., et al., *Cardioprotective effects mediated by angiotensin II type 1 receptor blockade and enhancing angiotensin 1-7 in experimental heart failure in angiotensin-converting enzyme 2-null mice.* Hypertension, 2012. 59(6): p. 1195-203.

35.   Zhong, J., et al., *Angiotensin-converting enzyme 2 suppresses pathological hypertrophy, myocardial fibrosis, and cardiac dysfunction.* Circulation, 2010. 122(7): p. 717-28, 18 p following 728.

36.   Tryggvason, K., J. Patrakka, and J. Wartiovaara, *Hereditary proteinuria syndromes and mechanisms of proteinuria.* N Engl J Med, 2006. 354(13): p. 1387-401.

37.   Quack, I., et al., *beta-Arrestin2 mediates nephrin endocytosis and impairs slit diaphragm integrity.* Proc Natl Acad Sci U S A, 2006. 103(38): p. 14110-5.

38.   Quack, I., et al., *PKC alpha mediates beta-arrestin2-dependent nephrin endocytosis in hyperglycemia.* J Biol Chem, 2011. 286(15): p. 12959-70.

39.   Sitek, B., et al., *Novel approaches to analyse glomerular proteins from smallest scale murine and human samples using DIGE saturation labelling.* Proteomics, 2006. 6(15): p. 4337-45.

40.   Potthoff, S.A., et al., *The glomerular proteome in a model of chronic kidney disease.* Proteomics Clin Appl, 2008. 2(7-8): p. 1127-39.

41.   Chaudhari, A. and M.A. Kirschenbaum, *A rapid method for isolating rabbit renal microvessels.* Am J Physiol, 1988. 254(2 Pt 2): p. F291-6.

42.   Patzak, A., et al., *Angiotensin II response in afferent arterioles of mice lacking either the endothelial or neuronal isoform of nitric oxide synthase.* Am J Physiol Regul Integr Comp Physiol, 2008. 294(2): p. R429-37.

43.   Stegbauer, J., et al., *Chronic treatment with angiotensin-(1-7) improves renal endothelial dysfunction in apolipoproteinE-deficient mice.* British journal of pharmacology, 2011. 163(5): p. 974-83.

44.   Potthoff, S.A., et al., *Chronic p38 mitogen-activated protein kinase inhibition improves vascular function and remodeling in angiotensin II-dependent hypertension.* J Renin Angiotensin Aldosterone Syst, 2016. 17(3).

45.   Stegbauer, J., et al., *Phosphodiesterase 5 attenuates the vasodilatory response in renovascular hypertension.* PLoS One, 2013. 8(11): p. e80674.

46.   Haase, R., et al., *A novel in vivo method to quantify slit diaphragm protein abundance in murine proteinuric kidney disease.* PLoS One, 2017. 12(6): p. e0179217.

47.   Konigshausen, E., et al., *Isolation of Glomeruli and In Vivo Labeling of Glomerular Cell Surface Proteins.* J Vis Exp, 2019(143).

48.   Thieme, M., et al., *Phosphodiesterase 5 inhibition ameliorates angiotensin II-dependent hypertension and renal vascular dysfunction.* Am J Physiol Renal Physiol, 2017. 312(3): p. F474-F481.

49.   Broekmans, K., et al., *Angiotensin II-Induced Hypertension Is Attenuated by Reduction of Sympathetic Output in NO-Sensitive Guanylyl Cyclase 1 Knockout Mice.* J Pharmacol Exp Ther, 2016. 356(1): p. 191-9.

50.   Wiesel, P., et al., *Two-kidney, one clip and one-kidney, one clip hypertension in mice.* Hypertension, 1997. 29(4): p. 1025-30.

51.   Laurent, S., et al., *Aortic stiffness is an independent predictor of fatal stroke in essential hypertension.* Stroke, 2003. 34(5): p. 1203-1206.

52.   Mattace-Raso, F.U., et al., *Arterial stiffness and risk of coronary heart disease and stroke: the Rotterdam Study.* Circulation, 2006. 113(5): p. 657-63.

53.   Palatini, P., et al., *Arterial stiffness, central hemodynamics, and cardiovascular risk in hypertension.* Vasc Health Risk Manag, 2011. 7: p. 725-39.

54.   Laurent, S., et al., *Aortic stiffness is an independent predictor of all-cause and cardiovascular mortality in hypertensive patients.* Hypertension, 2001. 37(5): p. 1236-41.

55.   Vlachopoulos, C., K. Aznaouridis, and C. Stefanadis, *Prediction of cardiovascular events and all-cause mortality with arterial stiffness: a systematic review and meta-analysis.* J Am Coll Cardiol, 2010. 55(13): p. 1318-27.

56.   Wang, M., R.E. Monticone, and E.G. Lakatta, *Proinflammation of aging central arteries: a mini-review.* Gerontology, 2014. 60(6): p. 519-29.

57.   Tsioufis, C., et al., *Low-grade inflammation and hypoadiponectinaemia have an additive detrimental effect on aortic stiffness in essential hypertensive patients.* Eur Heart J, 2007. 28(9): p. 1162-9.

58.   Ushio-Fukai, M., et al., *p38 Mitogen-activated protein kinase is a critical component of the redox-sensitive signaling pathways activated by angiotensin II. Role in vascular smooth muscle cell hypertrophy.* J Biol Chem, 1998. 273(24): p. 15022-9.

59.   Patzak, A., et al., *Adenosine enhances long term the contractile response to angiotensin II in afferent arterioles.* Am J Physiol Regul Integr Comp Physiol, 2007. 293(6): p. R2232-42.

60.   Cai, H. and D.G. Harrison, *Endothelial dysfunction in cardiovascular diseases: the role of oxidant stress.* Circ Res, 2000. 87(10): p. 840-4.

61.   Stegbauer, J., et al., *Chronic treatment with angiotensin-(1-7) improves renal endothelial dysfunction in apolipoproteinE-deficient mice.* Br J Pharmacol, 2011. 163(5): p. 974-83.

62.   Ebrahimian, T., et al., *Mitogen-activated protein kinase-activated protein kinase 2 in angiotensin II-induced inflammation and hypertension: regulation of oxidative stress.* Hypertension, 2011. 57(2): p. 245-54.

63.   Konigshausen, E., et al., *Angiotensin II increases glomerular permeability by beta-arrestin mediated nephrin endocytosis.* Sci Rep, 2016. 6: p. 39513.

64.   Konigshausen, E., et al., *Highly Sensitive Measurement of Glomerular Permeability in Mice with Fluorescein Isothiocyanate-polysucrose 70.* J Vis Exp, 2019(150).

5.   Danksagung

verdanke ich zum einen die Analyse unzähliger Proben für eine Vielzahl von Projekten, aber auch die kritische Beurteilung von Versuchen und Analyseverfahren. Ihr Einsatz und ihre Beständigkeit haben wesentlich zur Qualität der wissenschaftlichen Daten fast aller Projekte beigetragen.

Herrn Professor Dr. med. Ivo Quack, Herrn Professor Dr. med. Lorenz Sellin, Frau Dr. med. Eva Königshausen und Frau Dr. med. Magdalena Woznowski möchte ich für die Kooperation und Hilfestellung bei vielen gemeinsamen Projekten danken. Der kontinuierliche Austausch sowohl von Expertise als auch Ressourcen hat wesentlich zum Erfolg unserer gemeinsamen Projekte beigetragen. Für die fortwährende Unterstützung bin ich ihnen sehr dankbar.

Mit meinen Wegbegleitern verbindet mich auch zum Teil eine langjährige Freundschaft. Sie haben dazu beigetragen, dass Düsseldorf nach vielen Stationen meine Heimat geworden ist.

Allen Doktoranden und technischen Assistentinnen des Labors, insbesondere Frau Nicola Kuhr und Frau Christina Schwandt gilt mein Dank für die Unterstützung vieler Projekte und der langjährigen guten Zusammenarbeit.

Danken möchte ich allen Kooperationspartnern außerhalb der nephrologischen Klinik, die mit ihrer Expertise zum Gelingen vieler Projekte beigetragen haben.

Auch meinen Kollegen aus der Klinik möchte ich danken. Über die Jahre haben Sie ebenso dazu beigetragen, mir Freiräume für meine wissenschaftliche Tätigkeit zu ermöglichen.

Meinen Eltern, Herrn Professor Dr. med. Peter Christian Potthoff und Frau Karola Hildegard Potthoff, möchte ich für Ihre uneingeschränkte Unterstützung danken. Ich bedaure sehr, dass sie die Stationen meines akademischen Werdeganges nicht miterleben dürfen.

Meine neun Geschwister stehen immer an meiner Seite. Ein guter Rat, Rückhalt in jeder Lebenslage, gemeinsam feiern und das Leben genießen, diesen Dingen kann ich mir mit Ihnen immer gewiss sein. Dafür bin ich Ihnen unendlich dankbar.

A1 - Gesamtverzeichnis der eigenen Publikationen

1. B. Sitek, **S. Potthoff**, T. Schulenborg, J. Stegbauer, T. Vinke, L.C. Rump, H.E. Meyer, O. Vonend, and K. Stuhler, *Novel approaches to analyse glomerular proteins from smallest scale murine and human samples using DIGE saturation labelling.* Proteomics, 2006. 6(15): p. 4337-45.

2. **S.A. Potthoff**, B. Sitek, J. Stegbauer, T. Schulenborg, K. Marcus, I. Quack, L.C. Rump, H.E. Meyer, K. Stuhler, and O. Vonend, *The glomerular proteome in a model of chronic kidney disease.* Proteomics Clin Appl, 2008. 2(7-8): p. 1127-39.

3. H.C. Yang, S. Deleuze, Y. Zuo, **S.A. Potthoff**, L.J. Ma, and A.B. Fogo, *The PPARgamma agonist pioglitazone ameliorates aging-related progressive renal injury.* J Am Soc Nephrol, 2009. 20(11): p. 2380-8.

4. H. Hoch, J. Stegbauer, **S.A. Potthoff**, L. Hein, I. Quack, L.C. Rump, and O. Vonend, *Regulation of renal sympathetic neurotransmission by renal alpha(2A)-adrenoceptors is impaired in chronic renal failure.* Br J Pharmacol, 2011. 163(2): p. 438-46.

5. F. Mahfoud, O. Vonend, H. Bruck, W. Clasen, S. Eckert, B. Frye, H. Haller, M. Hausberg, U.C. Hoppe, J. Hoyer, K. Hahn, T. Keller, B.K. Kramer, R. Kreutz, **S.A. Potthoff**, H. Reinecke, R. Schmieder, V. Schwenger, U. Kintscher, M. Bohm, L.C. Rump, and V.u.d.D.G.f.N.V.s.d.D.H.e.V.D.H. Arbeitsgemeinschaft Herz und Niere der Deutschen Gesellschaftfur Kardiologie - Herz- und Kreislaufforschunge, *[Expert consensus statement on interventional renal sympathetic denervation for hypertension treatment].* Dtsch Med Wochenschr, 2011. 136(47): p. 2418.

6. **S.A. Potthoff**, A. Janus, H. Hoch, M. Frahnert, P. Tossios, D. Reber, M. Giessing, H.M. Klein, E. Schwertfeger, I. Quack, L.C. Rump, and O. Vonend, *PTH-receptors regulate norepinephrine release in human heart and kidney.* Regul Pept, 2011. 171(1-3): p. 35-42.

7. I. Quack, M. Woznowski, **S.A. Potthoff**, R. Palmer, E. Konigshausen, S. Sivritas, M. Schiffer, J. Stegbauer, O. Vonend, L.C. Rump, and L. Sellin, *PKC alpha mediates beta-arrestin2-dependent nephrin endocytosis in hyperglycemia.* J Biol Chem, 2011. 286(15): p. 12959-70.

8. R. Rabenalt, C. Winter, **S.A. Potthoff**, C.F. Eisenberger, K. Grabitz, P. Albers, and M. Giessing, *Retrograde balloon dilation >10 weeks after renal transplantation for transplant ureter stenosis - our experience and review of the literature.* Arab J Urol, 2011. 9(2): p. 93-9.

9. F. Riediger, I. Quack, F. Qadri, B. Hartleben, J.K. Park, **S.A. Potthoff**, D. Sohn, G. Sihn, A. Rousselle, V. Fokuhl, U. Maschke, B. Purfurst, W. Schneider, L.C. Rump, F.C. Luft, R. Dechend, M. Bader, T.B. Huber, G. Nguyen, and D.N. Muller, *Prorenin receptor is essential for podocyte autophagy and survival.* J Am Soc Nephrol, 2011. 22(12): p. 2193-202.

10. J. Stegbauer, **S.A. Potthoff**, I. Quack, E. Mergia, T. Clasen, S. Friedrich, O. Vonend, M. Woznowski, E. Konigshausen, L. Sellin, and L.C. Rump, *Chronic treatment with angiotensin-(1-7) improves renal endothelial dysfunction in apolipoproteinE-deficient mice.* Br J Pharmacol, 2011. 163(5): p. 974-83.

11. **S.A. Potthoff**, F. Beuschlein, and O. Vonend, *[Primay hyperaldosteronism--diagnostic and treatment].* Dtsch Med Wochenschr, 2012. 137(48): p. 2480-4.

12. **S.A. Potthoff** and D. Blondin, *[18 year-old woman with recurrent cerebral seizures].* Dtsch Med Wochenschr, 2012. 137(48): p. 2485-6.

13. **S.A. Potthoff**, U. Wenzel, and U. Kintscher, *[Hypertension 2012--still a challenge].* Dtsch Med Wochenschr, 2012. 137(48): p. 2475.

14. Y. Zuo, H.C. Yang, **S.A. Potthoff**, B. Najafian, V. Kon, L.J. Ma, and A.B. Fogo, *Protective effects of PPARgamma agonist in acute nephrotic syndrome.* Nephrol Dial Transplant, 2012. 27(1): p. 174-81.

15. A.K. Gitt, P. Baumgart, P. Bramlage, F. Mahfoud, **S.A. Potthoff**, J. Senges, S. Schneider, H. Buhck, R.E. Schmieder, and E.R. Group, *EARLY Treatment with azilsartan compared to ACE-inhibitors in anti-hypertensive therapy--rationale and design of the EARLY hypertension registry.* BMC Cardiovasc Disord, 2013. 13: p. 46.

16. I. Glowacka, K. Korn, **S.A. Potthoff**, U. Lehmann, H.H. Kreipe, K. Ivens, H. Barg-Hock, T.F. Schulz, and A. Heim, *Delayed seroconversion and rapid onset of lymphoproliferative disease after transmission of human T-cell lymphotropic virus type 1 from a multiorgan donor.* Clin Infect Dis, 2013. 57(10): p. 1417-24.

17. **S.A. Potthoff** and H.G. Munch, *[Safety aspects of parenteral iron supplementation therapies in patients with chronic kidney disease].* Dtsch Med Wochenschr, 2013. 138(24): p. 1312-7.

18. **S.A. Potthoff**, L.C. Rump, and O. Vonend, *The "resistant hypertension team": focus on a multidisciplinary approach to hypertension.* EuroIntervention, 2013. 9 Suppl R: p. R48-53.

19. **S.A. Potthoff**, J. Stegbauer, J. Becker, P.J. Wagenhaeuser, B. Duvnjak, L.C. Rump, and O. Vonend, *P2Y2 receptor deficiency aggravates chronic kidney disease progression.* Front Physiol, 2013. 4: p. 234.

20. J. Stegbauer, S. Friedrich, **S.A. Potthoff**, K. Broekmans, M.M. Cortese-Krott, I. Quack, L.C. Rump, D. Koesling, and E. Mergia, *Phosphodiesterase 5 attenuates the vasodilatory response in renovascular hypertension.* PLoS One, 2013. 8(11): p. e80674.

21. Y. Zuo, B. Chun, **S.A. Potthoff**, N. Kazi, T.J. Brolin, D. Orhan, H.C. Yang, L.J. Ma, V. Kon, T. Myohanen, N.E. Rhaleb, O.A. Carretero, and A.B. Fogo, *Thymosin beta4 and its degradation product, Ac-SDKP, are novel reparative factors in renal fibrosis.* Kidney Int, 2013. 84(6): p. 1166-75.

22. **S.A. Potthoff**, M. Fahling, T. Clasen, S. Mende, B. Ishak, T. Suvorava, S. Stamer, M. Thieme, S.H. Sivritas, G. Kojda, A. Patzak, L.C. Rump, and J. Stegbauer, *Angiotensin-(1-7) modulates renal vascular resistance through inhibition of p38 mitogen-activated protein kinase in apolipoprotein E-deficient mice.* Hypertension, 2014. 63(2): p. 265-72.

23. P. Bramlage, R.E. Schmieder, A.K. Gitt, P. Baumgart, F. Mahfoud, H. Buhck, T. Ouarrak, M. Ehmen, **S.A. Potthoff**, and E.R. Group, *The renin-angiotensin receptor blocker azilsartan medoxomil compared with the angiotensin-converting enzyme inhibitor ramipril in clinical trials versus routine practice: insights from the prospective EARLY registry.* Trials, 2015. 16: p. 581.

24. D. Scheiber, V. Veulemans, P. Horn, M.L. Chatrou, **S.A. Potthoff**, M. Kelm, L.J. Schurgers, and R. Westenfeld, *High-Dose Menaquinone-7 Supplementation Reduces Cardiovascular Calcification in a Murine Model of Extraosseous Calcification.* Nutrients, 2015. 7(8): p. 6991-7011.

25. R.E. Schmieder, **S.A. Potthoff**, P. Bramlage, P. Baumgart, F. Mahfoud, H. Buhck, T. Ouarrak, M. Ehmen, J. Senges, A.K. Gitt, and E.R. Group, *Patients With Newly Diagnosed Hypertension Treated With the Renin Angiotensin Receptor Blocker Azilsartan Medoxomil vs Angiotensin-Converting Enzyme Inhibitors: The Prospective EARLY Registry.* J Clin Hypertens (Greenwich), 2015. 17(12): p. 947-53.

26. K. Broekmans, J. Stegbauer, **S.A. Potthoff**, M. Russwurm, D. Koesling, and E. Mergia, *Angiotensin II-Induced Hypertension Is Attenuated by Reduction of*

Sympathetic Output in NO-Sensitive Guanylyl Cyclase 1 Knockout Mice. J Pharmacol Exp Ther, 2016. 356(1): p. 191-9.

27. A.K. Gitt, P. Bramlage, **S.A. Potthoff**, P. Baumgart, F. Mahfoud, H. Buhck, M. Ehmen, T. Ouarrak, J. Senges, R.E. Schmieder, and E.R. Group, *Azilsartan compared to ACE inhibitors in anti-hypertensive therapy: one-year outcomes of the observational EARLY registry.* BMC Cardiovasc Disord, 2016. 16: p. 56.

28. E. Konigshausen, U.M. Zierhut, M. Ruetze, **S.A. Potthoff**, J. Stegbauer, M. Woznowski, I. Quack, L.C. Rump, and L. Sellin, *Angiotensin II increases glomerular permeability by beta-arrestin mediated nephrin endocytosis.* Sci Rep, 2016. 6: p. 39513.

29. **S.A. Potthoff**, S. Stamer, K. Grave, E. Konigshausen, S.H. Sivritas, M. Thieme, Y. Mori, M. Woznowski, L.C. Rump, and J. Stegbauer, *Chronic p38 mitogen-activated protein kinase inhibition improves vascular function and remodeling in angiotensin II-dependent hypertension.* J Renin Angiotensin Aldosterone Syst, 2016. 17(3).

30. R. Haase, **S.A. Potthoff**, C. Meyer-Schwesinger, C. Frosch, T. Wiech, U. Panzer, E. Konigshausen, J. Stegbauer, L. Sellin, L.C. Rump, I. Quack, and M. Woznowski, *A novel in vivo method to quantify slit diaphragm protein abundance in murine proteinuric kidney disease.* PLoS One, 2017. 12(6): p. e0179217.

31. **S.A. Potthoff** and O. Vonend, *Multidisciplinary Approach in the Treatment of Resistant Hypertension.* Curr Hypertens Rep, 2017. 19(1): p. 9.

32. M. Thieme, S.H. Sivritas, E. Mergia, **S.A. Potthoff**, G. Yang, L. Hering, K. Grave, H. Hoch, L.C. Rump, and J. Stegbauer, *Phosphodiesterase 5 inhibition ameliorates angiotensin II-dependent hypertension and renal vascular dysfunction.* Am J Physiol Renal Physiol, 2017. 312(3): p. F474-F481.

33. E. Konigshausen, **S.A. Potthoff**, R. Haase, C. Meyer-Schwesinger, E. Kaufmann, L.C. Rump, J. Stegbauer, L. Sellin, I. Quack, and M. Woznowski, *Isolation of Glomeruli and In Vivo Labeling of Glomerular Cell Surface Proteins.* J Vis Exp, 2019(143).

34. E. Konigshausen, **S.A. Potthoff**, M. Woznowski, J. Stegbauer, L.C. Rump, and L. Sellin, *Highly Sensitive Measurement of Glomerular Permeability in Mice with Fluorescein Isothiocyanate-polysucrose 70.* J Vis Exp, 2019(150).

35. L. Hering, M. Rahman, H. Hoch, L. Marko, G. Yang, A. Reil, M. Yakoub, V. Gupta, **S.A. Potthoff**, O. Vonend, D.L. Ralph, S.B. Gurley, A.A. McDonough, L.C. Rump, and J. Stegbauer, *alpha2A-Adrenoceptors Modulate Renal Sympathetic Neurotransmission and Protect against Hypertensive Kidney Disease.* J Am Soc Nephrol, 2020. 31(4): p. 783-798.

36. L. Hering, M. Rahman, **S.A. Potthoff**, L.C. Rump, and J. Stegbauer, *Role of alpha2-Adrenoceptors in Hypertension: Focus on Renal Sympathetic Neurotransmitter Release, Inflammation, and Sodium Homeostasis.* Front Physiol, 2020. 11: p. 566871.

37. L.A. Volker, J. Kaufeld, W. Miesbach, S. Brahler, M. Reinhardt, L. Kuhne, A. Muhlfeld, A. Schreiber, J. Gaedeke, M. Tolle, W.J. Jabs, F. Ozcan, S. Markau, M. Girndt, F. Bauer, T.H. Westhoff, H. Felten, M. Hausberg, M. Brand, J. Gerth, M. Bieringer, M. Bommer, S. Zschiedrich, J. Schneider, S. Elitok, A. Gawlik, A. Gackler, A. Kribben, V. Schwenger, U. Schoenermarck, M. Roeder, J. Radermacher, J. Bramstedt, A. Morgner, R. Herbst, A. Harth, **S.A. Potthoff**, C. von Auer, R. Wendt, H. Christ, P.T. Brinkkoetter, and J. Menne, *Real-world data confirm the effectiveness of caplacizumab in acquired thrombotic thrombocytopenic purpura.* Blood Adv, 2020. 4(13): p. 3085-3092.

38.   L.A. Volker, J. Kaufeld, W. Miesbach, S. Brahler, M. Reinhardt, L. Kuhne, A. Muhlfeld, A. Schreiber, J. Gaedeke, M. Tolle, W.J. Jabs, F. Ozcan, S. Markau, M. Girndt, F. Bauer, T.H. Westhoff, H. Felten, M. Hausberg, M. Brand, J. Gerth, M. Bieringer, M. Bommer, S. Zschiedrich, J. Schneider, S. Elitok, A. Gawlik, A. Gackler, A. Kribben, V. Schwenger, U. Schoenermarck, M. Roeder, J. Radermacher, J. Bramstedt, A. Morgner, R. Herbst, A. Harth, **S.A. Potthoff**, C. von Auer, R. Wendt, H. Christ, P.T. Brinkkoetter, and J. Menne, *ADAMTS13 and VWF activities guide individualized caplacizumab treatment in patients with aTTP.* Blood Adv, 2020. 4(13): p. 3093-3101.

39.   M. Azizi, K. Sanghvi, M. Saxena, P. Gosse, J.P. Reilly, T. Levy, L.C. Rump, A. Persu, J. Basile, M.J. Bloch, J. Daemen, M.D. Lobo, F. Mahfoud, R.E. Schmieder, A.S.P. Sharp, M.A. Weber, M. Sapoval, P. Fong, A. Pathak, P. Lantelme, D. Hsi, S. Bangalore, A. Witkowski, J. Weil, B. Kably, N.C. Barman, H. Reeve-Stoffer, L. Coleman, C.K. McClure, A.J. Kirtane, and R.-H. investigators, *Ultrasound renal denervation for hypertension resistant to a triple medication pill (RADIANCE-HTN TRIO): a randomised, multicentre, single-blind, sham-controlled trial.* Lancet, 2021. 397(10293): p. 2476-2486.

40.   **S.A. Potthoff**, *Volumenmanagement bei Peritonealdialyse.* Der Nephrologe, 2022. 17(2): p. 74-84.

41.   M. Woznowski, **S.A. Potthoff**, E. Königshausen, R. Haase, H. Hoch, C. Meyer-Schwesinger, R. Wiech, J. Stegbauer, L.C. Rump, L. Sellin, and I. Quack, *Inhibition of MAPK p38 Decreases Hyperglycemia-Induced Nephrin Endocytosis and Protects against Albuminuria.* Journal of Molecular Medicine, accepted 27.02.2022 DOI 10.1007/s00109-022-02184-5

A2 - Lebenslauf

Düsseldorf, März 2022

Sebastian Alexander Potthoff

Geboren:	21. Dezember 1977
Geburtsort:	Günzburg, Bayern, Deutschland
Eltern:	Herr Prof. Dr. med. Peter C. Potthoff (†) Frau Karola Hildegard Potthoff, geborene Ansorge (†)

Akademischer Grad: Doktor der Humanmedizin (Dr. med.)

1. Schulbildung

1984-1986	Grundschule Günzburg (Bayern/Deutschland)
1986-1988	Grundschule Gelsenkirchen (NRW/ Deutschland)
1988-1997	Max-Planck-Gymnasium Gelsenkirchen (NRW/ Deutschland)
1997	Abitur

2. Ausbildung

September 1997 – Juli 2001	Ausbildung zum ADTV Tanzlehrer ADTV Tanzschule Seidel, Gelsenkirchen, Deutschland

3. Universitäre Ausbildung

Oktober 1999 – Mai 2006	**Studium der Humanmedizin** Ruhr-Universität Bochum, Deutschland
September 2004	**Famulatur** (Kardiologie/Kardiochirurgie) Saitama Medical School, Moroyama, Japan
April – August 2005	**Praktisches Jahr** (Tertial Anästhesiologie) Hopital d'Hautepierre, Strasbourg, Frankreich
September – November 2005	**Praktisches Jahr** (Tertial Chirurgie) NYU Downtown Hospital, New York, USA
Dezember 2005 – März 2006	**Praktisches Jahr** (Tertial Innere Medizin) Universitätsklinik Marienhospital, Herne, Deutschland

4. Beruflicher Werdegang

Juni 2006 – Juni 2008	**Assistenzarzt** (Innere Medizin / Nephrologie) Universitätsklinik Marienhospital, Herne, Deutschland
Juli 2008 bis November 2015	**Wissenschaftlicher Mitarbeiter/Assistenzarzt** Universitätsklinikum Düsseldorf, Klinik für Nephrologie, Heinrich-Heine-Universität Düsseldorf, Deutschland
März 2015	**Facharzt für Innere Medizin und Nephrologie** Ärztekammer Nordrhein, Düsseldorf, Deutschland
Mai 2015	**Hypertensiologe DHL** Deutsche Gesellschaft für Hypertonie und Prävention
Dezember 2015 bis Oktober 2017	**Funktionsoberarzt** Universitätsklinikum Düsseldorf, Klinik für Nephrologie, Heinrich-Heine-Universität Düsseldorf, Deutschland
Seit Oktober 2017	**Oberarzt** Universitätsklinikum Düsseldorf, Klinik für Nephrologie, Heinrich-Heine-Universität Düsseldorf, Deutschland
Juni 2021	**Zusatzbezeichnung Klinische Akut- und Notfallmedizin** Ärztekammer Nordrhein, Düsseldorf, Deutschland
August 2021	**Zusatzbezeichnung Transplantationsmedizin** Ärztekammer Nordrhein, Düsseldorf, Deutschland
Oktober 2021	**DEGUM Stufe I – Innere Medizin** Deutsche Gesellschaft für Ultraschall in der Medizin

5. Wissenschaftlicher Werdegang

2004 - 2010	**Doktorarbeit – experimentelle Nephrologie** **„Differentielle Proteomanalyse der Niere mittels 2D-Gelelektrophorese und Untersuchung des glomerlulären Proteoms in einem Mausmodell der chronischen Niereninsuffizienz" (s.c.l.)** Prof. Dr. med. L. C. Rump, Heinrich-Heine University, Düsseldorf, Deutschland
Februar 2007 – Juni 2008	**Forschungsaufenthalt - Division of Nephrology / Renal Pathology** (Stipendium der Universitätsklinik Marienhospital Herne – Ruhr-Universität Bochum) Professor Agnes Fogo Vanderbilt University, Nashville, Tennessee, USA

seit Juli 2008	**Wissenschaftlicher Mitarbeiter**
	Klinik für Nephrologie/experimentelle Nephrologie
	Univ.-Prof. Dr. med. L. C. Rump
	Heinrich-Heine-Universität, Düsseldorf, Deutschland

6. Mitgliedschaften / Ehrenamtliche Positionen

Deutsche Gesellschaft für Innere Medizin
Deutsche Gesellschaft für Hypertonie und Prävention
Deutsche Gesellschaft für Nephrologie
Deutsche Gesellschaft für Ultraschall in der Medizin
Deutsche Transplantationsgesellschaft

November 2009 – November 2017	**Vorsitzender des "Forum Junge Hypertensiologie"**
	Deutsche Gesellschaft für Hypertonie und Prävention
seit 2016	**Mitglied der wissenschaftlichen Kommission**
	Deutsche Hypertonie Akademie
	Akademie für Fortbildung der Deutschen Hochdruckliga GmbH
seit 2020	**Mitglied des Medizinisch-wissenschaftlicher Beirat**
	Das Lebenshaus e.V.

7. Preise - Stipendien

Dezember 2006	**Förderpreis der Sophia & Fritz Heinemann Stiftung**
	Ruhr-Universität Bochum
Januar 2007 – Juni 2008	**Forschungsstipendium der Ruhr-Universität-Bochum**
	Universitätsklinik Marienhospital, Herne, Deutschland
Januar – Dezember 2013	**Wissenschaftliches Förderstipendium der Deutschen Gesellschaft für Hypertonie und Prävention** (Förderzeitraum 12 Monate)
November 2007	Young Investigator Award – DHL Hypertonie Kongress 2007
November 2009	Young Investigator Award – DHL Hypertonie Kongress 2009
Juni 2010	Abstract Preis – ERA/EDTA Kongress 2010
November 2010	Young Investigator Award – DHL Hypertonie Kongress 2010
November 2011	Young Investigator Award – DHL Hypertonie Kongress 2011
November 2012	Young Investigator Award – DHL Hypertonie Kongress 2012
Dezember 2013	Young Investigator Award – DHL Hypertonie Kongress 2013

Dezember 2014   Young Investigator Award – DHL Hypertonie Kongress 2014

Januar 2016   **Walter-Clawiter-Preis 2015**

Walter-Clawiter-Stiftung Heinrich-Heine-Universität, Düsseldorf

Ausgezeichnete Publikation: "*Angiotensin-(1-7) modulates renal vascular resistance through inhibition of p38 mitogen-activated protein kinase in apolipoprotein E-deficient mice.*"

Potthoff SA, Fähling M, Clasen T, Mende S, Ishak B, Suvorava T, Stamer S, Thieme M, Sivritas SH, Kojda G, Patzak A, Rump LC, Stegbauer J., Hypertension. 2014 Feb;63(2):265-72

A3 – Publikationen der Habilitationsschrift

(Reproduktion und Nutzung im Rahmen der Habilitationsschrift genehmigt durch die einzelnen Rechteinhaber / Verlage.)

RESEARCH ARTICLE

Novel approaches to analyse glomerular proteins from smallest scale murine and human samples using DIGE saturation labelling

Barbara Sitek[1]*, Sebastian Potthoff[2]*, Thomas Schulenborg[1], Johannes Stegbauer[2], Tobias Vinke[2], Lars-Christian Rump[2], Helmut E. Meyer[1], Oliver Vonend[2]** and Kai Stühler[1]**

[1] Medical Proteom-Center, Ruhr-University, Bochum, Germany
[2] Department of Nephrology, Ruhr-University, Bochum, Germany

Loss of renal function is often associated with the injury of kidney glomeruli. It is therefore necessary to understand the mechanisms leading to progressive glomerular diseases; this may be addressed using proteomics. Until now, however, analysis of the glomeruli proteome using 2-DE has been technically hampered by low protein yields from scarce samples. To circumvent this problem, we developed a procedure which allows the human and mouse glomeruli proteome to be analysed. In this study, two different approaches were used to isolate mouse and human glomerular protein from kidney cortex. Mouse glomeruli were extracted by embolisation magnetic beads into the glomerular capillaries. Laser capture microdissection (LCM) was utilised to harvest glomeruli from human biopsy material. Human and murine samples were analysed using a fluorescence saturation labelling technique. Using 3 µg mouse glomerular protein a total of 2900 spots were resolved for differential proteome analysis. Moreover, it was also demonstrated for the first time that only ten glomeruli (0.5 µg) picked by LCM from a slide of a human kidney biopsy material were sufficient to visualise 900 spots. This novel strategy paves the way for future experiments aimed at investigating functional proteomics of glomerular diseases in humans and in mice.

1 Introduction

The kidney plays a vital physiological role in vertebrate homeostasis, *e.g.* in acid-base balance, the regulation of plasma volume and hormone secretion. These intricate mechanisms are achieved through functional compartmen- talisation of the kidney, the major functional unit of which is the nephron. Nephrons are responsible for renal function *per se* and consist of a glomerulus and a draining tubular system. In humans, glomeruli are able to produce up to 150 mL ultrafiltrate per minute and are the target of many renal diseases. One main focus of kidney research should, therefore, attempt to understand glomerular physiology and pathophysiology to prevent disease progression [1–3]. This may be addressed using proteomic and/or transcriptomic technologies; however, as levels in gene expression (mRNA)

Correspondence: Dr. Kai Stühler, Medical Proteom-Center, Ruhr-University Bochum, MA 2/046, Universitaetsstrasse 150, 44801 Bochum, Germany
E-mail: kai.stuehler@ruhr-uni-bochum.de
Fax: +49-234-32-14554

Abbreviations: LCM, laser capture microdissection; **PFF**, peptide fragment mass fingerprint

---

 * These authors contributed equally and should be considered as joint first authors.
** These authors contributed equally and should be considered as joint senior authors.

may not necessarily reflect levels in protein abundance, arguably a proteomics methodology is preferred (for review see [4]).

Animal models are commonly used to find out more about underlying mechanisms leading to disease progression. Substantial progress has been made in the past by generating knockout mice. Using these models, it became possible to study the effect of single genes, for example, on glomerulosclerosis *in vivo* [5]. The main disadvantage of using mice, however, is the limited amount of sample available; this is particularly so when analysing protein expression of glomeruli. Even though the kidney cortex is enriched in glomeruli only a small percentage of glomerular protein is expected in the kidney cortex lysate.

The problem becomes even more pronounced when human samples are analysed. In this case, small needle biopsy material of kidney cortex is the only material that is available and a maximum of only 30 glomeruli can be expected in these kinds of samples.

Very few publications are available that report the analysis of the renal proteome using 2-DE. In a pioneering study Arthur *et al.* [6] separated the glomerulus-rich cortex from the medulla to describe a differential expression pattern within the kidney. Very recently, however, Yoshida and coworkers [7] were able to profile the kidney glomerulus proteome. Employing a serial sieving technique, it was possible to separate glomeruli from kidney tissue to provide the 500 µg protein that was needed for 2-DE analysis [7]. However, these techniques require a relatively high amount of protein. This prerequisite immediately excludes 'scarce samples' such as those derived from mouse models (*e.g.* subtotal 5/6 nephrectomy) and biopsies from diseased human tissue.

To overcome these limitations, we established a protocol allowing us to analyse scarce sample amounts from mouse glomerulus preparations or human biopsy material by differential proteome analysis. The method of choice to analyse scarce sample amount using a proteomics approach is the so-called DIGE saturation labelling. This method enables complete 2-DE analysis and quantification of changes in protein abundance in scarce samples, *i.e.* approx. 2 µg protein/image. The applied dyes (Cy3 and Cy5) react via a maleimide group with all available cysteine residues in the protein sample, giving a high labelling concentration. Due to their net zero charge, there is no charge alteration of the labelled protein. As with all DIGE experiments an internal standard sample containing an equal amount of each sample is run on each gel. Sensitivity is 20-fold higher compared to silver staining. This enhanced sensitivity allows the analysis of scarce samples from murine and human glomeruli micropreparations using ferromagnetic beads and laser capture microdissection (LCM), respectively.

Sample preparation for proteome analysis is a very critical step. Therefore, we established two different approaches allowing us to select specifically for glomeruli. Working with a murine model, embolisation of ferromagnetic beads allows a fast and effective purification of glomeruli. LCM is the method of choice for isolating glomerular cells from human kidney since biopsy tissue is the only material available for diagnostic purpose.

Here, we present novel approaches to analyse scarce sample amounts from murine and human kidney glomeruli by differential proteome analysis in a range of 0.5–3 µg protein.

2 Materials and methods

2.1 Tissue preparation

2.1.1 Isolation of mouse glomeruli

White FVB mice were obtained from Janvier (Belgium). All mice were 70 ± 15 days old, and weighted between 21 and 26 g. The investigations were performed in accordance with institutional guidelines. Mice were anaesthetised intraperitoneally with Ketanest® and Xylazin® (0.168 mg and 8 µg/g body weight). The kidneys were perfused with PBS via abdominal aorta according to an amended method described previously [8]. The distal aorta was cannulated with polyethylene tubing (Portex, Germany; id 0.28 mm) and perfused *in situ* at a constant rate of 7.2 mL/min/g kidney. The proximal aorta was ligated. To ensure venous drainage, a hole was cut into the inferior cava vein. Initially, kidneys were perfused with ice-cold PBS to free the blood vessels from any remaining blood.

After preparation, kidneys were perfused with Dynabeads (diameter 4.5 µm) (Dynal Biotech/Invitrogen, Germany) in a concentration of 4×10^6/mL PBS (Fig. 1A). The kidneys were removed and minced through a 100-µm cell mesh with intermittent PBS flushing (2–3 times, 5 mL ice-cold sterile PBS). After centrifugation at $4185 \times g$ for 5 min, the cell pellet was dissolved in 2 mL cooled PBS and transferred to a 2-mL tube. Using a magnet catcher and a three-step washing procedure, the ferromagnetic beads containing glomeruli (Fig. 1A) were purified to approximately 95% homogeneity determined microscopically (Zeiss Axiovert, Germany). Approximately 40 µg glomerular protein were prepared from one single kidney.

The extracted glomeruli were lysed in 20 µL 2-DE lysis buffer (30 mM Tris-HCl, 2 M thiourea, 7 M urea, 4% CHAPS, pH 8) and sonicated (6 × 10-s pulses on ice). To remove Dynabeads, lysates were centrifuged at $9300 \times g$ for 10 min. Protein concentration was determined using the Bio-Rad protein assay (Bio-Rad). The samples were stored at −80°C.

2.1.2 Cortex tissue

Mouse kidneys were removed and placed into ice-cold PBS. Cortical tissue was manually separated from medulla. The cortex tissue was then cut into small pieces, minced in 2-DE lysis buffer, sonicated, centrifuged and stored as described above.
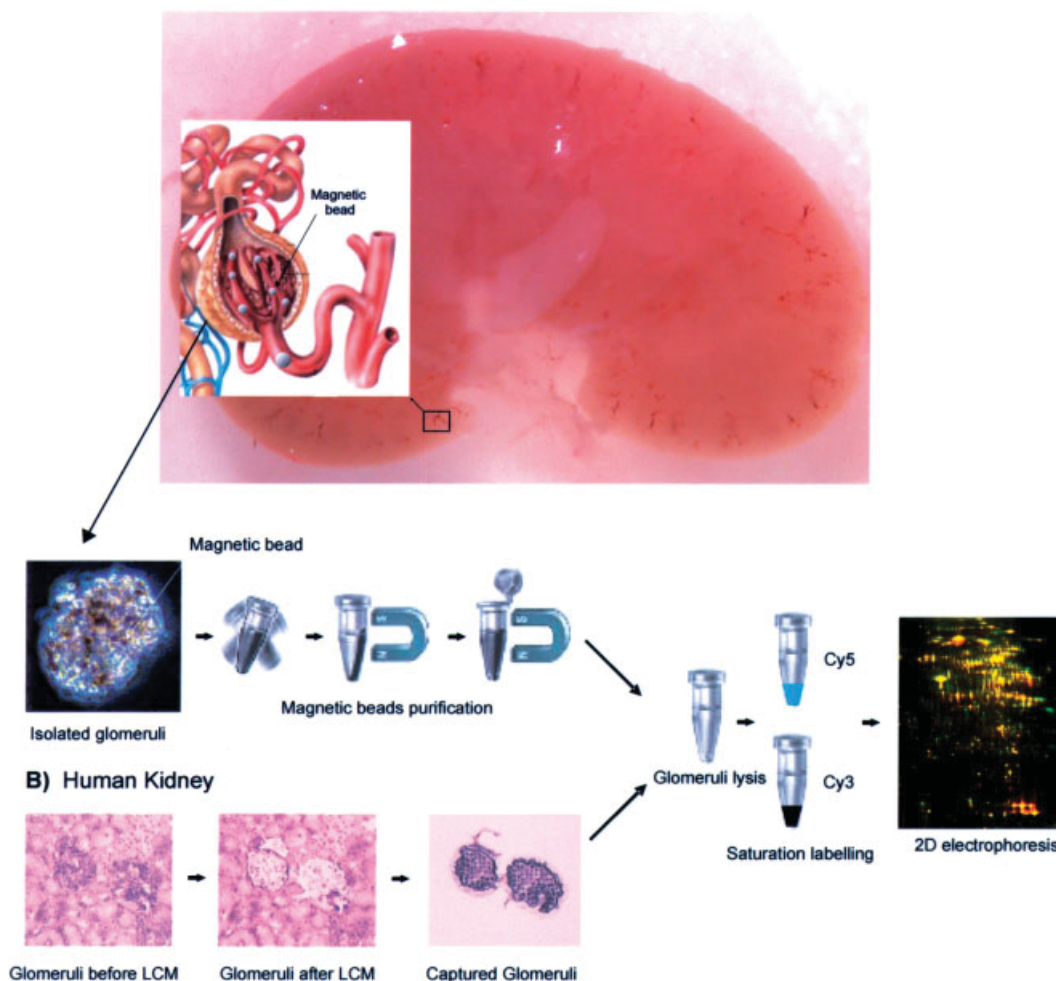
A) Mouse Kidney

Figure 1. (A) A mouse kidney cut in half and a schematic drawing of a nephron with visible dark brown microbeads, embolised in vasa afferenti and glomeruli. Glomeruli were isolated using a magnetic catcher. (B) A 6-μm section of two human glomeruli before and after LCM. Glomerular proteins were labelled, mixed with labelled internal standard and separated by 2-DE.

2.1.3 Isolation of human glomeruli

The study was approved by the Ethics Committee of the Ruhr-University Bochum. Kidney biopsy tissue was obtained from patients that underwent nephrectomy due to renal carcinoma. Material was mounted in Tissue-Tek OCT and snap frozen (−80°C). Tissue blocks were serially sectioned (6-μm sections) and stored on dry ice. Sections were fixed, stained and dehydrated using HistoGene™ LCM Frozen Section Staining Kit (Arcturus, USA) according to the supplier's manual. Glomeruli were isolated using an AutoPix™ Automated LCM System (Arcturus) (Fig. 1B). The following laser beam settings were used: Laser power 70 mW, laser time 2500 μs. The isolated glomeruli were lysed, sonicated, centrifuged and stored as described above.

2.2 Protein labelling

2.2.1 Labelling of murine proteins

To perform a differential proteome analysis, three independent isolated glomeruli and cortex preparations from three mice were considered. For cysteine reduction, cell lysates containing 3 μg protein were incubated with 1 nmol Tris (2-carboxyethyl) phosphine hydrochloride (TCEP; Sigma) at 37°C in the dark for 1 h. Saturation CyDyes™ (Amersham Biosciences/GE Healthcare, Freiburg, Germany) were diluted with anhydrous DMF p.a. (2 nmol/μL; Sigma) and 2 nmol CyDye was added to the reduced TCEP sample. The samples were vortexed, centrifuged briefly and left at 37°C in the dark for 30 min. The glomeruli and cortex lysates (3 μg) were labelled with Cy5. For internal standardi-

sation, a pool of all analysed samples (cortex and glomeruli) was created and labelled with Cy3. The labelling reaction was stopped by adding 2 μL DTT (1.08 g/mL; Bio-Rad) and finally 2 μL Ampholine 2–4 (Amersham Biosciences/GE Healthcare) was added. Before IEF, 3 μg labelled internal standard was mixed with labelled glomeruli or cortex samples. For preparative gels, 400 μg reference proteome lysate (70% kidney cortex tissue, 30% glomerular extract) was reduced with 105 nmol TCEP and labelled with 210 nmol Cy3.

2.2.2 Labelling of human proteins

For DIGE saturation labelling of microdissected human glomeruli, three different protein extracts (4.5, 2.7 and 0.5 μg) were reduced with 1 nmol TCEP and subsequently incubated with 2 nmol Cy5 and than processed as described above.

2.3 2-DE

Carrier ampholyte-based IEF was performed in a self-made IEF chamber using tube gels (20 cm × 1.5 mm) as described elsewhere [9]. After running a 21.25-h voltage gradient, the ejected tube gels were incubated in equilibration buffer (125 mM Tris, 40% glycerol, 3% SDS, 65 mM DTT, pH 6.8) for 10 min. The second dimension was performed in a Desaphor VA 300 system using polyacrylamide gels (15.2% total acrylamide, 1.3% bisacrylamide) as described elsewhere [9]. The IEF tube gels were placed onto the polyacrylamide gels (20 cm × 30 cm × 1.5 mm) and fixed using 1.0% agarose containing 0.01% bromophenol blue dye (Riedel deHaen, Seelze, Germany). For protein identification, 400 μg labelled protein sample from the reference proteome was applied on an identically sized gel system under identical conditions. Silver post-staining was performed after gel scanning using a MS-compatible protocol as described elsewhere [10].

2.4 Scanning and image analysis

After 2-DE, the gels were left between the glass plates and images were acquired using the Typhoon™ 9400 scanner (Amersham Biosciences/GE Healthcare). Excitation wavelengths and emission filters were chosen specific for each of the CyDyes according to the Typhoon user guide. Before image analysis with DeCyder software (Amersham Biosciences/GE Healthcare) the images were cropped with ImageQuant™ software (Amersham Biosciences/GE Healthcare). The intra-gel spot detection and quantification were performed using the Differential In-gel Analysis (DIA) mode of the DeCyder software. The estimated number of spots was set to 3000. An exclusion filter was applied to remove spots with a slope greater than 1.6. Images from different gels were matched using the BVA mode of DeCyder software. Protein spots represented in all gels ($n = 3$) with expression level greater then 1.5-fold change and $p < 0.05$ were defined as being differentially expressed.

To determine the degree of reproducibility of the glomerular protein preparations, the mean SD of protein quantification was ascertained. A randomly chosen number of 278 protein spots from three different 2-DE gels were checked in respect of correct matching and the intensities of protein spots were normalised considering internal standard using DeCyder image analysis software.

2.5 MS nanoLC-ESI-MS/MS

The proteins were excised from the gel, tryptically digested and afterwards preconcentrated and separated in a Dionex LC Packings HPLC system (Dionex LC Packings, Idstein, Germany) containing the components Famos™ (autosampler), the Switchos™ (loading pump and switching valves), and the Ultimate (gradient pump and UV-detector). Peptides were loaded on-line and preconcentrated with 0.1% TFA at a flow rate of 30 μL/min for 6 min on a μ-precolumn (0.3-mm id × 5 mm, 5 μm, PepMap; Dionex LC Packings) using an isocratic loading pump (Switchos; Dionex LC Packings). For separation by RP nano-HPLC (75-μm id × 250 mm 5 μm, Pep-Map; Dionex LC Packings) using the Ultimate system (Ultimate; Dionex LC Packings), a solvent system consisting of solvent A (0.1% formic acid) and solvent B (0.1% formic acid, 84% ACN) was used. A gradient of 5–50% solution B in 35 min was carried out. Flow rates were generally adjusted to 250 nL/min. During separation the second precolumn was washed with 50% ACN/0.1% TFA for 20 min plus 84% ACN/0.1% TFA for 10 min using the isocratic loading pump as described by Schaefer *et al.* [11].

ESI-MS/MS spectra were recorded using a 4000 Q Trap® (Applied Biosystems, Foster City, CA, USA) high-performance hybrid triple quadrupole/linear IT LC/MS/MS mass spectrometer equipped with NanoSpray® source and non-coated SilicaTips (FS360–20–10-N; New Objective). The needle voltage was set at 2800 V and the interface was heated to 150°C. Nitrogen was used as curtain and collision gas. Each scan cycle consist of an MS scan (EMS), an enhanced resolution scan (ER) and up to three MS/MS scans (EPI) with an overall duration of 3.5 s. The mass range of the EMS was m/z 400–1400 and m/z 100–1750 in EPI mode. To determine more precisely the m/z value and the charge state (+1 to +3), an ER scan was performed for the three most intense ions.

For protein identification, uninterpreted ESI-MS/MS-spectra were correlated with the NCBI-protein sequence database (http://www.ncbi.nlm.nih.gov) applying the SEQUEST™ algorithm [12–14] with the following search parameters: variable modification due to methionine oxidation, two maximal missed cleavage sites in case of incomplete trypsin hydrolysis and no details about 2-DE-derived protein mass and p*I*, including mass tolerances of ± 1.5 Da for parent ions and ± 0.5 Da fragment ions. Proteins were considered as identified if two peptides were explained by the spectra and had a SequestMetaScore (Proteinscape™) greater than 3.

3   Results

3.1   2-DE of glomerular protein using ferromagnetic microbeads

Embolisation of mouse glomeruli by injecting ferromagnetic microbeads is a robust method to isolate glomerular proteins suitable for 2-DE. Following the labelling process, 3.0 µg total protein from glomerular samples and the internal standard (pool of all analysed samples) were loaded onto the 2-DE gel. After electrophoresis and image acquisition using a confocal fluorescence scanner approximately 2900 protein spots were detected on an average (Fig. 2, Tables 1, 2) with a mean SD of 30.32% in protein spot quantification for three independent glomerular preparations.

3.2   Identification of differentially expressed proteins from mouse glomeruli

After establishing the protocol for a reproducible preparation of glomerular proteins using ferromagnetic microbeads, we performed a differential proteome analysis to determine proteins with aberrant expression in kidney glomerulus and cortex. Before analysing the glomerulus and cortex proteome using saturation DIGE, we optimised the labelling conditions according to the procedure as described elsewhere [15].

Table 1. Differentially expressed protein spots (n=48; p<0.05, fold change >1.5) in the cortex and glomerular proteome

No. of spots	2900
No. of spots analysed in all gels	1900
No. of high abundant spots in glomeruli (fold change >5)	4
No. of up-regulated spots in glomeruli (fold change <5 and >1.5)	23
No. of high abundant spots in cortex (fold change >5)	14
No. of up-regulated spots in cortex (fold change <5 and >1.5)	7

For differential proteome analysis, glomerulus or cortex specimens from three independently prepared samples were labelled with Cy5 and separately analysed with Cy3-labelled internal standard to achieve high accuracy in protein quantification. For the cortex proteome (Fig. 3 A) and the glomerular proteome (Fig. 3 B), 2800 and 2900 protein spots, respectively, were detected using DeCyder software (Tables 1, 2). In Fig. 3A, a representative 2-DE gel of cortex proteome
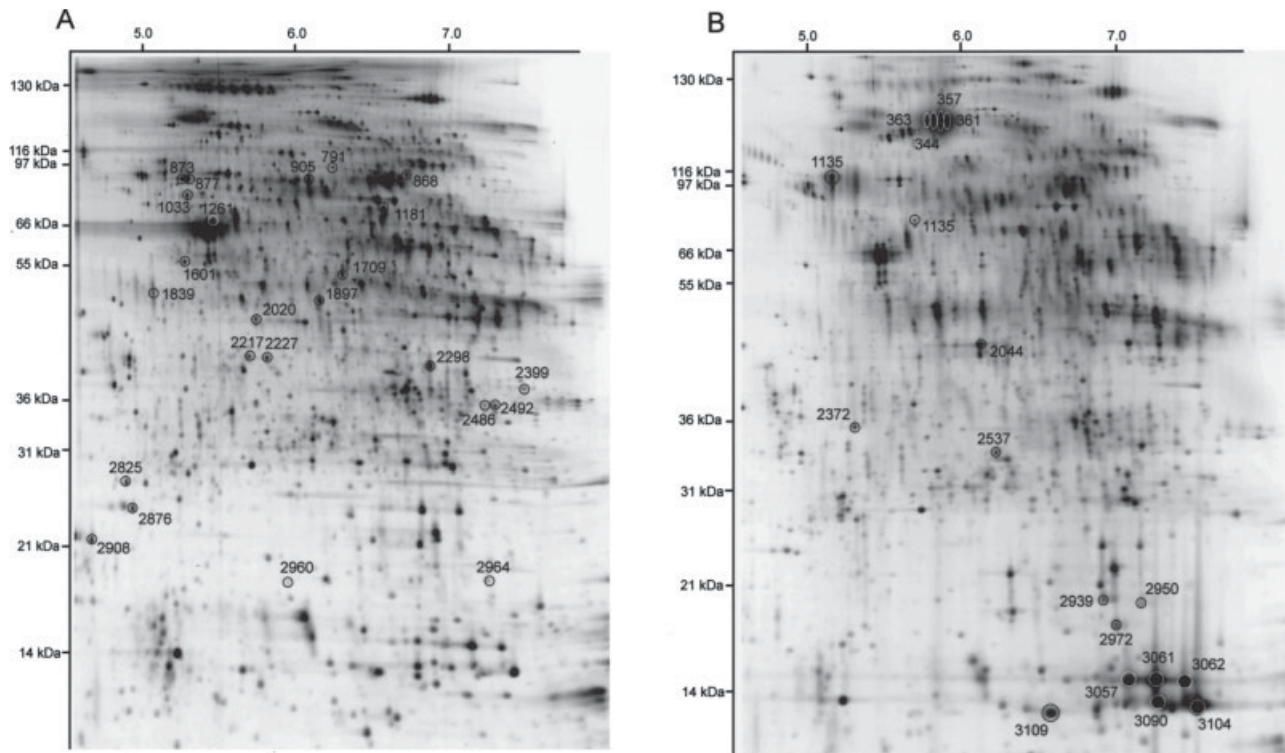

Figure 2. 2-DE gels of glomeruli lysate (A) or cortex lysate (B). Analysis of 3 µg glomeruli and 3 µg cortex revealed a pattern of 2900 (A) and 2800 (B) protein spots, respectively. Significantly up-regulated protein spots in glomeruli and cortex are numbered in gels A and B, respectively.

Table 2. Identified proteins of the differential proteome of murine kidney cortex and glomerulus

No.	Spot name	NCBI accession	Protein	Experimental		Theoretical		t-test	Fold change	Se-quence coverage (%)	Peptide count	Se-quest-Meta score
				p*I*	Mol. mass (kDa)	p*I*	Mol. mass (kDa)					
Up-regulated proteins in glomerular tissue												
1	2227	27369886	Chloride intracellular channel 5	6.0	43.1	5.5	28.3	0.012	5.59	17.1	3	17.4
2	1709	13195624	NADH dehydrogenase 1 alpha subcomplex 10 subcomnplex 10	6.9	58.5	7.7	40.6	0.0032	2.85	8.5	2	8.8
3	2298	29789289	Enoyl Coenzyme A hydratase, short chain, 1	7.2	40.1	8.8	31.3	0.022	4.14	41.3	9	72.9
4	1261	809561	Gamma-actin	5.6	71	5.6	41	0.041	6.24	11.4	3	15.8
5	868	6680027	Glutamate dehydrogenase 1	7.1	84.3	8.5	61.3	0.0054	2.86	11.5	4	22.7
6	1181	13385454	Glycine amidinotransferase	6.9	74	9	48.3	0.009	3.19	6.4	3	32.4
7	1897	21704140	3-Hyxdroxyisobutyrate dehydrogenase, mitoch. precursor genase, mitoch. precursor	6.4	52.9	8.4	35.4	0.019	4.11	8	2	18.3
8	905	54114929	D-Lactate dehydrogenase	6.3	83	6.1	51.8	0.041	3.97	5.4	2	12.9
9	791	346883	Lamin A	6.5	87.2	6.4	74.2	0.022	2.56	5.1	3	13
10	873	31982755	Vimentin	5.4	84.1	5.1	53.7	0.0041	4.46	45.5	18	130.9
11	877	31982755	Vimentin	5.4	84	5.1	53.7	0.046	3.64	52.6	16	139.3
Up-regulated proteins in cortical tissue												
12	1135	6680117	Glutathione synthetase	5.9	75.2	5.7	52.2	0.038	−6.59	9.1	2	20.1
13	3109	62185646	Heat-responsive protein 12	6.78	13.3	8.7	14.2	0.0055	−2.91	20	3	8.8
14	2044	319837	Malate dehydrogenase	6.3	51	6.3	36.5	0.014	−2.19	12	5	42.3
Contaminants												
15	3057	4760586	Haemoglobin beta-1 chain	7.3	14.5	7.7	15.8	0.0068	−24.55	14.4	2	22.4
16	3061	4760586	Haemoglobin beta-1 chain	7.5	14.5	7.7	15.8	0.055	−9.18	53.1	4	38.1
17	3062	4760586	Haemoglobin beta-1 chain	7.7	14.4	7.7	15.8	0.029	−14.96	63.7	7	52.3
18	3104	28175802	Haemoglobin alpha	7.8	13.2	8.7	15.1	0.038	−13.89	31.7	5	44.8
19	3090	4760586	Haemoglobin beta-1 chain	7.5	13.6	7.7	15.8	0.0057	−30.96	22	3	32.1
20	344	3647327	Serum albumin	6.0	106.1	5.8	68.7	0.00014	−79.82	9.5	3	24.1
21	357	3647327	Serum albumin	6.1	106.1	5.8	68.7	0.00005	−62.37	9.7	5	43.5
22	361	3647327	Serum albumin	6.1	106.1	5.8	68.7	0.00051	−23.07	8.2	4	32.5
23	363	3647327	Serum albumin	6.1	106.1	5.8	68.7	0.0016	−21.25	6.7	3	24.9

(Cy5, red labelled) *versus* internal standard (Cy3, green labelled) is shown. Figure 3B illustrates a glomerular sample (Cy5, red labelled) and internal standard (Cy3, green labelled).

Significant differences in glomerular and cortical protein expression are given in Tables 1 and 2. Altogether, 48 differentially expressed protein spots ($p<0.05$) with at least a 1.5-fold up- or down-regulation were evaluated by DeCyder software in cortex and glomerular proteome (Table 1). For 27 protein spots, a higher protein expression (positive expression ratio) was detected in the glomerular proteome, whereas 21 differentially expressed protein spots showed a higher abundance in cortical tis-

sue (negative expression ratio) (Table 1). Using nanoLC-ESI-MS/MS, we identified 23 proteins with different biological functions.

Representative gels illustrate the expression change of spot 357 and spot 2227 (Fig. 3A, B). Spot 357 is almost equally abundant in cortex and reference proteome leading to a yellow overlay. Expression of spot 357 in glomerular proteome is barely detectable, resulting in a green (reference) spot only. After protein identification we could assign this protein spot belonging to a high abundant spot cluster to contaminating serum albumin. In contrast, spot 2227 (chloride channel 5) is in low abundance in the cortex and is more highly expressed (factor 5.56) in the glomerular proteome.
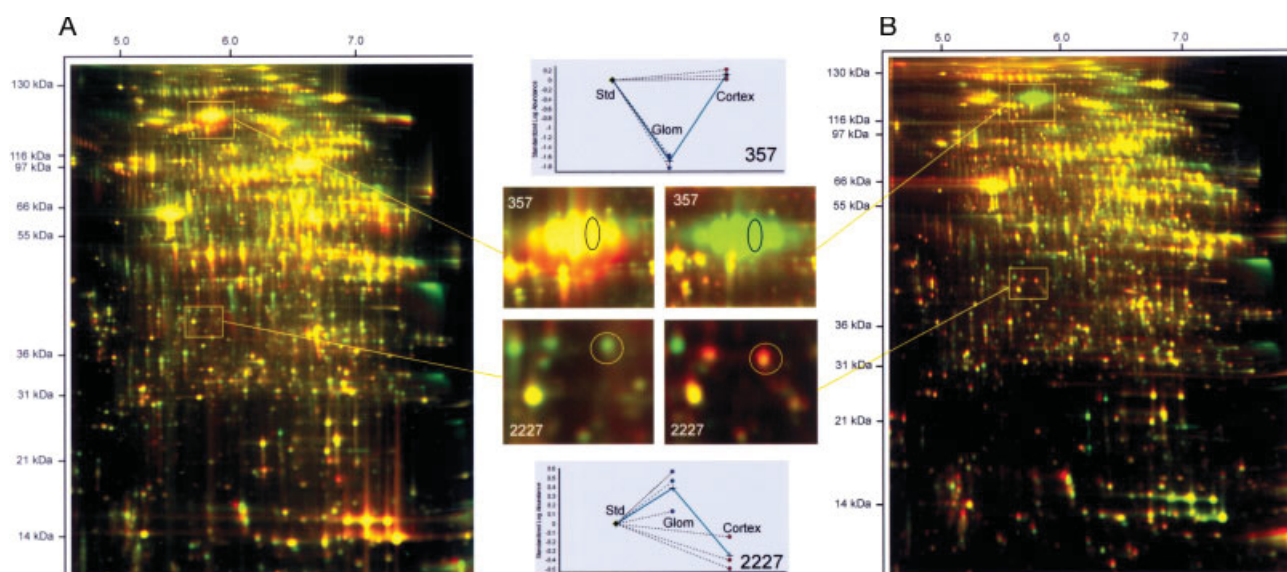
Figure 3. (A) A gel on which 3.0 µg cortex proteome (Cy5, red labelled) and 3.0 µg internal standard (Cy3, green labelled) were loaded. (B) A gel on which 3.0 µg glomerular proteome (Cy5, red labelled) and 3.0 µg internal standard (Cy3, green labelled) were loaded. The figures in between show the glomerular (Glom) and cortical (Cortex) expression levels of spot 357 and spot 2227 in comparison to the internal standard (Std) in a representative gel and statistically evaluated by DeCyder in three independent samples (three different kidney preparations). The upper evaluated spot 357 is almost equally abundant in cortex (red labelled) and reference (green labelled) proteome leading to a yellow overlay. Expression of spot 357 in glomerular (red labelled) proteome is barely detectable, resulting in a green (reference) spot only. The lower evaluated spot 2227 shows an opposite expression pattern. Spot 2227 is low abundant in cortex (red labelled) compared to reference (green labelled) proteome leading, to a green spot. Expression of spot 2227 in glomerular (red labelled) proteome is higher compared to reference (green labelled) proteome leading to a red spot.

3.3 Isolating glomeruli from cryopreserved histological slices of human kidney biopsy material using LCM

Human kidney biopsy samples were embedded in Tissue-Tek OCT and cryopreserved. Serial sections of 6 µm were cut and slices were fixed and stained. Various quantities of human glomeruli (100, 75, 10) were captured using automated LCM Arcturus autopix100™. The area captured by LCM is given by Arcturus software for every individual cap. Corresponding areas used for exemplary 2-DE shown in Fig. 4A–C were 1.53 mm^2 for 100 glomeruli (Fig. 4A, 1400 spots), 0.91 mm^2 for 75 glomeruli (Fig. 4B, 1350 spots) and 0.18 mm^2 for 10 glomeruli (Fig. 4C, 900 spots). Estimated protein amount labelled and loaded for 2-DE was 4.5, 2.7 and 0.5 µg, respectively.

4 Discussion

The present study was performed to establish a new method allowing us to perform a differential proteome analysis of kidney glomeruli from human and mouse tissue using a minimal sample amount. The expression of a variety of renal proteins, including those originating from the glomerulus, has previously been reported using Western blotting or immunohistochemistry. However, only a limited number of

proteins can be studied at a time and the existence of specific antibodies is a prerequisite. Moreover, both techniques require a prior knowledge from previous studies about the protein of interest. In contrast, 2-DE in combination with MS allows the detection and identification of many unknown marker proteins. Indeed, after numerous technical modifications as many as 10 000 polypeptide spots can be detected in one gel [9]. Furthermore, with the introduction of DIGE technology, proteome analysis of unparalleled accuracy and sensitivity can be performed [15, 16].

Even though 2-DE gives a high resolution separation of the renal proteome, a protein amount of at least 75 µg [6] and 500 µg [7] was required to visualise 1095 [6] and 1713 [7] spots, respectively. This requirement places a significant constraint on the experimental procedure, in particular when glomerular protein and not full cortex protein is to be analysed. This, however, is a basic requirement, since kidney cortex is enriched in glomeruli but only a small percentage of glomerular protein can actually be found in kidney cortex lysate. The present study was able to demonstrate the marked difference between the full-cortex and isolated glomeruli proteome.

To understand the underlying mechanisms leading to glomerular injury and, furthermore, to be able to comprehend how pharmacological treatment influences diseases progression, differential analyses of the glomerular proteome should be performed [17]. There are no data at this time correlating changes in clinical parameters with changes
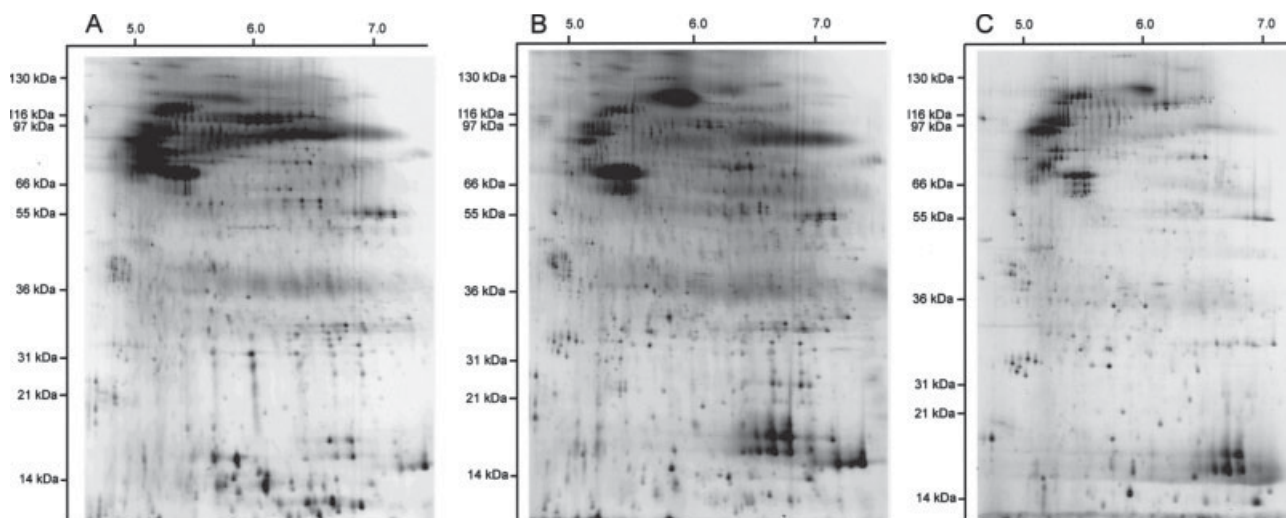
Figure 4. (A–C) Representative 2-D gels of human glomerular proteins extracted from serial sections of human kidney biopsy material using LCM. In (A), 100 glomeruli (4.5 μg, 1400 spots) were applied, in (B) 75 glomeruli (2.7 μg, 1350 spots), and in (C) 10 glomeruli (0.5 μg, 900 spots) to 2-DE.

in the glomerular proteome, either in humans or in animals. However, the protein amount available for glomerular proteome analysis is exceedingly low. We therefore established novel approaches that combine specific separation of glomerular proteins with the highly sensitive DIGE saturation labelling.

Mouse glomeruli were extracted using ferromagnetic Dynabeads (adapted method of [18]). These 4.5-μm-diameter ferromagnetic particles embolised the glomerular capillaries allowing the isolation of glomeruli with a magnetic catcher. Compared to the small organ size, a reasonable amount of glomerular protein could be provided even in subtotally (5/6) nephrectomised mice. In contrast, the classical serial sieving technique leads to a reduced yield of glomerular protein (unpublished observation). Considering the differential analysis (Table 2), we found a number of mitochondrial- and energy metabolism-associated proteins, which are highly abundant in glomeruli. The important role of intact mitochondrial function has been recently shown in glomerular endothelial cells [19]. Furthermore, the enrichment of vimentin, a protein known to be typically expressed in glomerular podocytes [20], by a factor of three to four proved the feasibility of the presented method. In contrast, interfering contaminants like serum albumin and haemoglobin were significantly depleted (by a factor 9–79). The high abundance of contaminants demonstrated again the necessity of sub-proteome analysis for in-depth elucidation of a compartment's (*e.g.* glomerulus) function.

Extraction of human glomeruli using ferromagnetic beads can not be applied since biopsies may only be performed for diagnosis. LCM has been shown to be a useful tool for performing segmental analysis of renal material [21]. However, studies demonstrating a proteome analysis of renal LCM tissue are still lacking. The major limiting factor in the past was

the low amount of protein available by LCM. Using our optimised procedure, we demonstrate for the first time that glomeruli picked from serial 6-μm-thick sections of human renal biopsy material is sufficient for further proteome analyses.

Low amount of human and murine glomerular protein in a range of 0.5–3.0 μg was analysed using a new DIGE saturation labelling technique [15]. With these techniques, we were able to increase the sensitivity of 2-DE analysis to an extent that enables glomerular protein analysis of one single section with ten human glomeruli. This offers the opportunity to plan further experiments examing the functional proteome of glomerular diseases in humans and mice. With this knowledge we will be able to elucidate those cellular mechanisms that lead to end stage renal failure, and, in addition, deduce the molecular background of new pharmacological approaches.

5 References

[1] Hieter, P., Boguski, M., *Science* 1997, *278*, 601–602.

[2] Takenaka, M., Imai, E., *Nephrol. Dial. Transplant.* 2000, *15*, 139–141.

[3] Vonend, O., Apel, T., Amann, K., Sellin, L. *et al.*, *Nephrol. Dial. Transplant.* 2004, *19*, 2217–2222.

[4] Knepper, M. A., *J. Am. Soc. Nephrol.* 2002, *13*, 1398–1408.

[5] Buzello, M., Haas, C. S., Hauptmann, F., Gross, M. L. *et al.*, *Nephrol. Dial. Transplant.* 2004, *19*, 566–573.

[6] Arthur, J. M., Thongboonkerd, V., Scherzer, J. A., Cai, J. *et al.*, *Kidney Int.* 2002, *62*, 1314–1321.

[7] Yoshida, Y., Miyazaki, K., Kamiie, J., Sato, M. *et al.*, *Proteomics* 2005, *5*, 1083–1096.

[8] Vonend, O., Stegbauer, J., Sojka, J., Habbel, S. *et al.*, *Br. J. Pharmacol.* 2005, *145*, 66–74.

[9] Klose, J., Kobalz, U., *Electrophoresis* 1995, *16*, 1034–1059.

[10] Nesterenko, M. V., Tilley, M., Upton, S. J., *J. Biochem. Biophys. Methods* 1994, *28*, 239–242.

[11] Schaefer, H., Chervet, J. P., Bunse, C., Joppich, C. *et al.*, *Proteomics* 2004, *4*, 2541–2544.

[12] Eng, J. K., McCormack, A. L., Yates, J. R. 3rd, *Am. Soc. Mass Spectrom.* 1994, *5*, 976–989.

[13] Yates, J. R. 3rd, Eng, J. K., McCormack, A. L., *Anal. Chem.* 1995, *67*, 3202–3210.

[14] Yates, J. R. 3rd, Eng, J. K., McCormack, A. L., Schieltz, D., *Anal. Chem.* 1995, *67*, 1426–1436.

[15] Sitek, B., Luttges, J., Marcus, K., Kloppel, G. *et al.*, *Proteomics* 2005, *5*, 2665–2679.

[16] Alban, A., David, S. O., Bjorkesten, L., Andersson, C. *et al.*, *Proteomics* 2003, *3*, 36–44.

[17] Bonventre, J. V., *Kidney Int.* 2002, *62*, 1470–1471.

[18] Takemoto, M., Asker, N., Gerhardt, H., Lundkvist, A. *et al.*, *Am. J. Pathol.* 2002, *161*, 799–805.

[19] Tanaka, T., Miyata, T., Inagi, R., Kurokawa, K. *et al.*, *Kidney Int.* 2003, *64*, 2020–2032.

[20] Pavenstadt, H., Kriz, W., Kretzler, M., *Physiol. Rev.* 2003, *83*, 253–307.

[21] Kohda, Y., Murakami, H., Moe, O. W., Star, R. A., *Kidney Int.* 2000, *57*, 321–331.

RESEARCH ARTICLE

The glomerular proteome in a model of chronic kidney disease

Sebastian A. Potthoff[1,2], Barbara Sitek[3]*, Johannes Stegbauer[4], Thomas Schulenborg[2],
Katrin Marcus[3], Ivo Quack[4], Lars C. Rump[4], Helmut E. Meyer[3], Kai Stühler[3]**
and Oliver Vonend[1,4]***

[1] Marienhospital Herne, Klinikum der Ruhr-Universität Bochum, Bochum, Germany
[2] Department of Pathology, Vanderbilt University, Nashville, USA
[3] Medizinisches Proteom-Center, Ruhr-Universität Bochum, Bochum, Germany
[4] Department of Nephrology, Heinrich-Heine-Universität, Düsseldorf, Germany

Adequate kidney function is crucial in sustaining vertebrate homeostasis. Certain diseases can diminish renal function and lead to end-stage renal disease. Diabetes mellitus and hypertension are the main causes of glomerulosclerosis and albuminuria in adults. The molecular mechanisms that trigger these maladaptive changes are still unsatisfyingly described. We previously introduced 2-D DIGE in combination with focused tissue isolation methods to analyze protein expression in glomeruli. Glomeruli, the crucial compartments in albuminuric renal diseases, were extracted using magnetic particles from subtotally nephrectomized FVB mice ($n = 6$); this 5/6 nephrectomy in FVB mice is a model of chronic kidney disease. Analysis of protein expression levels from glomerular protein lysates was performed using 2-D DIGE and compared with glomerular protein lysates from mice that underwent sham surgery. The comparison of about 2100 detectable spots between both groups revealed 48 protein spots that showed significant differential expression. Of those, 33 proteins could be identified using nanoLC-ESI MS. The metalloproteinase meprin 1 alpha, the beta galactoside-binding-lectin galectin-1 and dimethylarginine dimethylaminohydrolase 1, a key enzyme in NO metabolism, were found to be differentially regulated, thus implying a role in the pathogenesis and pathophysiology of progressive kidney disease. In conclusion, 2-D DIGE protein analysis of smallest sample sizes from specific organ compartments provides focused protein expression results, which help in gaining an understanding of the molecular mechanisms of chronic kidney disease.

1 Introduction

The kidney's role in acid-base balance, regulation of plasma volume and hormone secretion is crucial in sustaining vertebrate homeostasis, but can be diminished by many kidney diseases that lead to a loss of organ function. Progressive chronic kidney disease (CKD) can lead to end-stage renal disease with the necessity of dialysis.

The nephron is the essential anatomic unit within the kidney for maintaining renal function. It consists of a filter unit, the glomerulus, and a draining system, the tubulus system. In humans, intact glomeruli structure is essential for its proper function as the main filter unit of the plasma, ensuring the excretion of up to 150 mL ultrafiltrate per minute and retaining cellular and protein content within the

Correspondence: Professor Oliver Vonend, Department of Nephrology, Heinrich-Heine-Universität Düsseldorf, Moorenstrasse 5, 40225 Düsseldorf, Germany
E-mail: vonend@yahoo.com
Fax: +49-211-811-7722

Abbreviations: ADMA, asymmetric dimethylarginine; **BP**, blood pressure; **CKD**, chronic kidney disease; **DDAH**, dimethylarginine dimethylaminohydrolase 1; **eNOS**, endothelial nitric oxide synthase; **GFR**, glomerular filtration rate; **PFF**, peptide fragment mass fingerprint; **SNx**, subtotal nephrectomy

---

*   These authors contributed equally and should be considered as joint first authors.
** These authors contributed equally and should be considered as joint senior authors.

capillary lumen. The glomerulus is target of many kidney diseases that are associated with the development and the progression of renal fibrosis and glomerulosclerosis. These two entities imply a reduction of healthy and vital tissue and the accumulation of extracellular matrix with a loss in organ function; thus leading to proteinuria and a reduction of excretion. Understanding the pathophysiology leading to a progressive loss of glomerulus function due to sclerosis is the subject of ongoing research with the purpose of preventing disease progression [1–3]. Although measurement of gene expression levels (mRNA) are widely used to assess pathophysiological changes *in vivo* and *in vitro*, they may not necessarily reflect levels in protein abundance, and therefore lack a certain predictive value of changes in tissue/cellular function. In our study, a proteomics methodology is preferred to avoid this restriction [4].

We have previously shown that 2-D DIGE in combination with focused tissue isolation is a sophisticated tool to overcome the limitations of protein analysis caused by the compartmentalization of the kidney. Distinct glomerular protein analysis of smallest sample sizes can be performed by isolating glomeruli with magnetic particles or laser capture microsdissection (LCM) [5].

Recent publications using 2-DE comparing the glomerulus-rich cortex with the medulla showed differences in protein expression. Very few publications are available that report the analysis of the renal proteome using 2-DE. One of the first studies approaching the renal proteome was performed by Arthur *et al.* [6] who separated the glomerulus-rich cortex from the medulla to describe a differential expression pattern within the kidney. Yoshida and co-workers [7] were able to profile parts of the kidney proteome. Xu *et al.* [8] directly analyzed glomerular samples from LCM slides using MALDI-MS to find differences in glomerular protein expression of sclerosed and non-sclerosed glomeruli.

In this study, FVB mice were divided into two groups ($n = 6$). One group underwent 5/6 nephrectomy, the other group sham-surgery only. The loss of nephrons due to 5/6 nephrectomy leads to hyperfiltration, hypertrophy and the development and progression of glomerulosclerosis [9]. From a clinical point of view, these mice develop CKD with retention of creatinine and urea, proteinuria and hypertension [10]. At 5 weeks after surgery, glomeruli from these mice were extracted with magnetic particles as described previously [5]. The glomerular protein analysis was performed using the highly sensitive fluorescence dye protein saturation labeling (2-D DIGE) to overcome the limitation caused by the small sample size and to achieve a high resolution in the proteomic analysis [5]. In contrast to 2-D DIGE minimal labeling where three fluorescence dyes (Cy2, Cy 3 and Cy5) are available, 2-D DIGE saturation labeling utilizes only two fluorescence dyes (Cy3 and Cy5), of which Cy3 is used for internal standardization (for detailed description see [11, 12]). DIGE saturation labeling enables complete 2-DE analysis and quantification of changes in protein abundance in scarce samples, *i.e.,* ~2 µg protein/image. The applied dyes (Cy3 and Cy5) react *via* a maleimide group with all available cysteine residues in the protein sample, giving a high labeling concentration. Due to their net zero charge, there is no charge alteration of the labeled protein. As with all DIGE experiments an internal standard is run on each gel.

The main goal of the presented study was to find specific glomerular proteins that are regulated in the state of CKD due to a loss of functional tissue. These proteins are implied to play a role in the pathophysiology of the ongoing disease and offer targets for future research.

2 Materials and methods

2.1 Animal care

FVB mice were obtained from Janvier (Belgium). At the date of surgery, all mice were 65 ± 10 days old and weighed 21–26 g. The investigations and surgery were performed in accordance with institutional guidelines. The animals were housed in type III Makrolon polycarbonate cages at 45% humidity, 20–22°C temperature and a 12-h day/night cycle with free access to water and food. Standard food was Altromin (Altromin 1314: 20% protein, 0.4% NaCl; Lage/Lippe, Germany). At 2 days prior to surgery (sham and SNx) food was changed to Altromin with 40% protein and 0.6% NaCl fraction. This food was maintained during the period of study.

2.2 Subtotal nephrectomy and sham surgery

The animals were randomly allocated to two groups ($n = 6$ each); Group 1: sham-surgery control group, and group 2: subtotally nephrectomized group (SNx).

The mice were anesthetized intraperitoneally with Ketanest® and Xylazin® (0.168 mg and 8 mg/g bodyweight). Subtotal nephrectomy was performed through two dorsal incisions with complete resection of the right kidney and two-thirds removal of the left kidney by ligation of the upper and lower renal pole. Kidney weight was measured at the time of removal. Kidney weight of the completely removed kidney was assumed to measure half of the total healthy kidney weight (two kidneys) at the time of surgery. Sham surgery was performed only by skin and abdominal muscle incisions.

2.3 Preparation of urinary, serum and tissue samples

The mice were killed 35 ± 2 days after surgery. Blood samples were gathered by retro orbital vein puncture and were centrifuged for serum aliquotation. A 24-h urine was collected using metabolic cages (Techniplast, Italy). Remnant and control kidneys of pilot experiments were harvested and paraffin embedded.

2.4 Isolation of mouse glomeruli

Mice were anesthetized intraperitoneally with Ketanest® and Xylazin® (0.168 mg and 8 mg/g bodyweight). Mouse glomeruli were extracted as described previously [5]. In brief, the kidneys were perfused *in situ* with ice-cold PBS through the abdominal aorta at a constant rate of 1.8 mL/min. The aorta was ligated proximal the renal arteries and distal the canula. To ensure venous drainage, a hole was cut into the inferior cava vein on the level of the kidneys. After preparation, the kidneys were perfused with magnetic particles (Dynabeads M-450 Epoxy, Dynal Biotech/Invitrogen, Germany) in a concentration of 4×10^6/mL PBS. The kidneys were removed and minced through a 100-mm cell mesh. After centrifugation, the cell pellet was dissolved in 2 mL ice-cold PBS and transferred to a 2-mL tube. Through multiple washing steps using a magnet catcher, the glomeruli containing magnetic particles were purified to approximately 90–95% homogeneity, controlled microscopically (Zeiss Axiovert, Germany). Approximately 40 µg glomerular protein was prepared from one single healthy kidney (sham-surgery group) and approximately 10 µg glomerular protein from a single remnant kidney (SNx group). The extracted glomeruli were lysed in 20 µL 2-D DIGE lysis buffer (30 mM Tris-HCl, 2 M thiourea, 7 M urea, 4% CHAPS, pH 8) and sonicated (6×10 s pulses on ice). To remove the magnetic particles, lysates were centrifuged at $9300 \times g$ for 10 min. Protein concentration was determined using a Bradford protein assay (Bio-Rad). The samples were stored at –80°C.

2.5 Blood pressure

Blood pressure (BP) measurement was performed on trained mice 1–2 days before they were killed. Hatteras Instruments® single channel blood pressure analysis system SC1000 was used to measure BP in all mice according to the manufacturer's protocol.

2.6 Serum/urinary parameters

Measurement of creatinine levels in serum and urine were performed using a standard kit supplied by Labor&Technik®, Germany. The analysis was performed following the manufacturer's protocol.

Method of choice for measuring serum urea level was based on the urease reaction. A standard kit for urea measurement supplied by Randox®, Germany, was used and measurement was performed following manufacturer's protocol.

To measure serum albumin levels, a test kit supplied by Randox was used. Measurement was performed following manufacturer's protocol. Urinary albumin levels were measured using the Albuwell M Kit by Exocell, USA. Measurements were performed following manufacturer's protocol.

2.7 Podocyte cell culture

Podocytes were obtained from Peter Mundel (Mount Sinai Medical Center, NY, USA). The specific cell type of immortalized podocytes has been described previously [13]. The cells were cultured under described conditions and harvested for RT-PCR analysis.

2.8 RNA preparation/cDNA

Cryo-preserved glomeruli from glomeruli isolation and immortalized podocytes [13] from cell culture were analyzed for RNA expression. RNA was extracted using the guanidinium–thiocyanate–phenol–chloroform extraction method (TRIzol®, Invitrogen). Following DNA digestion (RNase-free DNase; Invitrogen, Germany), cDNA synthesis was performed using Enhanced Avian Reverse Transcriptase (eAMV-RT; Sigma-Aldrich) following the manufacturer's protocol.

2.9 Real-time PCR

Specific primer pairs were acquired from Applied Biosystems (Foster City, CA, USA). TaqMan® Gene Expression Assays (Applied Biosystems) were used with a 7300 Real-Time PCR System (Applied Biosystems). Real-time PCR was performed following the manufacturer's protocol.

All real-time PCR experiments were repeated two times to reduce technical variations. The amplification cycle, when threshold level is reached, is described as CT value and is detected automatically by the 7300 Real-Time PCR System. Comparing CT values allows the estimation of changes in mRNA (cDNA) expression level [3].

The following TaqMan® Assays were used: lectin, galactose binding, soluble 1 (galectin-1; assay ID: Mm00839408_g1); glyceraldehyde-3-phosphate dehydrogenase (GAPDH) (assay ID: Mm99999915_g1); meprin 1 α (assay ID: Mm00484970_m1).

2.10 Immunohistochemistry

Immunohistochemistry staining was based on the streptavidin-biotin-method. Sections, 2 µm thick, were deparaffinized using xylene and acetone and rehydrated in Tris buffer. Demasking of antigen structures was achieved with target retrieval solution (Dako, Germany) at 98°C (water bath). Avidin-biotin blocking was performed with a biotin-blocking system (Dako) for 15 min at room temperature. Sections were then treated with peroxidase and alkaline phosphatase blocking reagent (Dako).

The following primary antibodies were used: anti-galectin-1 antibody (Santa Cruz, sc-19277) diluted 1:100 in antibody diluent (Dako, S3022); anti-C4-antibody (Santa Cruz, sc-23483) diluted 1:50 in antibody diluent; and anti-meprin 1 α (Santa Cruz, sc-23487) diluted 1:50 in antibody diluent.

The sections were incubated for 30 min at room temperature and then rinsed with Tris buffer. Incubation for an ad-

ditional 30 min with the secondary-antibody (donkey anti-goat; Dianova, 705-065-147) diluted to 1:1000 was performed. Sections were conjugated with streptavidin (1:1000; Dianova, 016-050-084) for 30 min at room temperature. The sections were then processed with fuchsin chromogen substrate (Dako, K0625), and counterstained with hematoxylin.

2.11 Protein labeling

Protein labeling for 2-D DIGE and MS (nanoLC-ESI-MS/MS) was performed as previously described [5]. In brief, to obtain free thiol groups of cysteines, cell lysates containing 3 μg protein were reduced with 1 nmol Tris (2-carboxyethyl) phosphine hydrochloride (TCEP; Sigma) at 37°C in the dark for 1 h. Protein samples were labeled with saturation CyDyes (Amersham Biosciences/GE Healthcare, Freiburg, Germany). The glomeruli lysates (3 μg) were labeled with Cy5. For internal standardization, a pool of all analyzed samples plus kidney cortex was created and subsequently labeled with Cy3. The additional sample from kidney cortex was added to ensure a sufficient amount of sample for protein identification after in-gel digestion (reference proteome). The labeling reaction was stopped by adding 2 μL DTT (1.08 g/mL; Bio-Rad) and finally 2 μL Ampholine 2–4 (GE Healthcare) was added. Before IEF, 3 μg labeled internal standard was mixed with labeled glomeruli samples. For preparative gels, 400 μg reference proteome lysate was reduced with 105 nmol TCEP and labeled with 210 nmol Cy3.

2.12 2-D DIGE

For the separation in the first dimension (IEF) the samples were placed onto the anodic side of the carrier ampholyte (CA) mixture containing polyacrylamide tube gels (4% acrylamide, 7 M urea; 20 cm × 1.5 mm) [5, 12]. The CA-based IEF was performed in a self-made vertical IEF chamber. After running a 21.25-h voltage gradient, the ejected tube gels were incubated in equilibration buffer (125 mM Tris, 40% glycerol, 3% SDS, 65 mM DTT, pH 6.8) for 10 min. The second dimension was performed in a Desaphor VA 300 system using polyacrylamide gels (15.2% total acrylamide, 1.3% bisacrylamide) as described elsewhere [5]. The IEF tube gels were placed onto the polyacrylamide gels (20 cm × 30 cm × 1.5 mm) and fixed using 1.0% agarose containing 0.01% bromophenol blue dye (Riedel deHaen, Seelze, Germany). For protein identification, the preparative-sized gel system (IEF: 20 cm × 1.5 mm, SDS-PAGE: 20 cm × 30 cm × 1.5 mm) was applied under identical conditions. Silver post staining was performed after gel scanning using a MS-compatible protocol as described elsewhere [5, 12]

2.13 Scanning and image analysis

The 2-D DIGE protein spot pattern was acquired using the Typhoon™ 9400 scanner (GE Healthcare) with dye-specific filters. The intra-gel spot detection and quantification were performed using the Differential In-gel Analysis (DIA) mode of the DeCyder software (GE Healthcare). Images from different gels were matched using the BVA mode of DeCyder software.

The estimated number of spots was set to 3000. An exclusion filter was applied to remove spots with a slope greater than 1.6. Images from different gels were matched using the BVA mode of DeCyder software. Protein spots represented in all gels with a change in expression level greater than 1.5-fold with $p<0.05$ were defined as being differentially expressed.

2.14 MS analysis using nanoLC-ESI-MS/MS

Protein spots of interest were excised from the gel, digested with trypsin and analyzed *via* nanoLC-ESI-MS/MS as preciously described [5]. In brief, peptides were loaded on-line and pre-concentrated with 0.1% TFA at a flow rate of 30 μL/min for 6 min on a μ-pre-column (0.3 mm id × 5 mm, 5 μm, PepMap; Dionex LC Packings) using the Ultimate system (Ultimate; Dionex LC Packings). ESI-MS/MS spectra were recorded using a 4000 Q Trap® (Applied Biosystems) high performance hybrid triple quadrupole/linear ion trap LC/MS/MS mass spectrometer equipped with NanoSpray® source and non-coated SilicaTips (FS360–20–10-N; New Objective). The needle voltage was set at 2800 V and the interface was heated to 150°C. Nitrogen was used as the curtain and collision gas. Each scan cycle consisted of an MS scan (EMS), an enhanced resolution scan (ER) and up to three MS/MS scans (EPI) with an overall duration of 3.5 s. The mass range of the EMS was m/z 400–1400 and m/z 100–1750 in EPI mode. To determine more precisely the m/z value and the charge state (+1 to +3) the ER scan was performed of the three most intense ions.

For protein identification, uninterpreted ESI-MS/MS-spectra were correlated with the NCBI protein sequence database (http://www.ncbi.nlm.nih.gov) applying the SEQUEST™ and MASCOT algorithm [14–16]. Proteins were considered as identified if two peptides were explained by the spectra and had a SequestMetaScore (Proteinscape™) greater than 3 or a MASCOT score greater than 25.

3   Results

3.1 Physiological data

Various clinical parameters that were needed to confirm renal disease after 5/6 nephrectomy were monitored, including serum creatinine, urea and albumin levels as well as urine creatinine, urea and albumin levels (Table 1). The creatinine clearance was calculated from 24-h urine collections. The SNx mice showed a significant increase in albumin excretion and a distinct loss of glomerular filtration rate

Table 1. Physiological data of sham-operated (Sham) and subtotally (SNx) nephrectomized mice

		Sham $n = 6$	SNx $n = 6$
Kidney weight at surgery[a]	(mg)	195 ± 22	82 ± 13
Kidney weight 5 weeks after surgery[a]	(mg)	337 ± 11	277 ± 31
Blood pressure$_{systolic}$	(mmHg)	146 ± 7	165 ± 13*
24-h urine volume	(mL/24 h)	2.90 ± 0.7	7.52 ± 2.1*
U$_{creatinine}$	(mg/dl)	26.11 ± 5.00	4.74 ± 0.67*
U$_{urea}$	(mg/dl)	15 612 ± 2087	4015 ± 901*
U$_{albumin}$	(mg/l)	9.6 ± 4.3	151.5 ± 20.1*
Albumin excretion over 24 h	(mg/die)	0.26 ± 0.09	11.5 ± 3.55*
Albumin-creatinine-ratio	(mg/g)	370 ± 180	3270 ± 740*
S$_{creatinine}$	(mg/dl)	0.52 ± 0.14	2.22 ± 1.15*
S$_{urea}$	(mg/dl)	127.0 ± 37.4	621.7 ± 127.3*
S$_{albumin}$	(mg/dl)	19.4 ± 3.8	14.8 ± 1.4
Creatinine clearance	(mL/min)	0.104 ± 0.037	0.015 ± 0.001*

a) indicates the kidney weight of only one kidney in sham-operated mice and the one remaining remnant kidney in SNx mice.
*= $p < 0.05$.

(GFR). Urinary albumin levels rose 44-fold and GFR dropped to 15% compared to sham-surgery mice ($p < 0.05$). The mice developed polyuria with a reduced concentration of creatinine and urea in the urine (Table 1).

In addition, BP was measured in all groups at the end of the study. The mice had a significantly increased BP after subtotal nephrectomy compared to sham-surgery mice (Table 1). To determine hypertrophy in nephrectomized remnant kidneys compared to sham-surgery kidneys, the weight of the remaining remnant kidney (SNx group) or one healthy kidney (sham-surgery group) was measured on the day of sacrifice and compared to the weight of only one healthy kidney on the day of the initial surgery. SNx mice showed an approximate 230% increase in kidney mass as compared to 70% in sham-surgery mice.

3.2 2-D DIGE of protein lysates from extracted glomeruli

The extraction of mouse glomeruli using magnetic particles has been proven to be a robust alternative to the established sieving technique [5]. In particular, if scarce amounts of samples from 5/6 nephrectomized have to be analyzed the magnetic particle method can be applied very successfully in combination with fluorescence dye saturation labeling. We have shown that applying fluorescence dye saturation labeling (2-D DIGE) for the analysis of 3.0 µg total protein from glomerular samples revealed up to 2100 protein spots and that the whole procedure of sample preparation, protein labeling and 2-D DIGE with a mean SD of ~30% is highly reproducible and allowed quantitative proteome analysis studies (Fig. 1, Table 2).

3.3 Proteomic analysis: Sham surgery *vs.* subtotal nephrectomy

The differential proteome analysis of sham-surgery and subtotal nephrectomized mice ($n = 6$ in each group) revealed that subtotal nephrectomy led to a significant expression change of 48 protein spots (Table 2). Using MS we could identify 33 protein spots (Fig. 2) representing 24 non-redundant proteins (Table 3 and Supporting Information). The reason for these redundancies is not a subject of this manuscript, but the protein isoforms are probably caused either by PTMs (phosphorylation, proteolytic processing *etc.*) or charge variant isoforms [17]. For the detailed elucidation, detailed studies utilizing MS/MS experiments have to be performed. For vimentin, showing a diametric expression change for two isoforms, we assume changes in proteolytic processing as the main cause.

Altogether, a high number of protein spots (25) were found that showed an expression change of more than five-fold after subtotal nephrectomy (Table 2). Meprin 1 α showed a 14-fold decrease in glomeruli from nephrectomized mice. Whereas galectin-1 (23-fold), C4-complement (21-fold) and dimethylarginine dimethylaminohydrolase 1 (DDAH-1; 165-fold) revealed an increase of glomerular expression in the SNx group (Table 3).

3.4 Immunohistochemistry in FVB mice

For *in situ* verification of the protein expression of C4 complement, galectin-1 and meprin, immunohistochemistry was performed on 2-µm sections of paraffin-embedded kidneys (sham *vs.* SNx). Glomeruli of remnant subtotal nephrectomized kidneys show a distinct staining for complement C4 in the area of the glomerular capillaries (Figs. 3A and B).
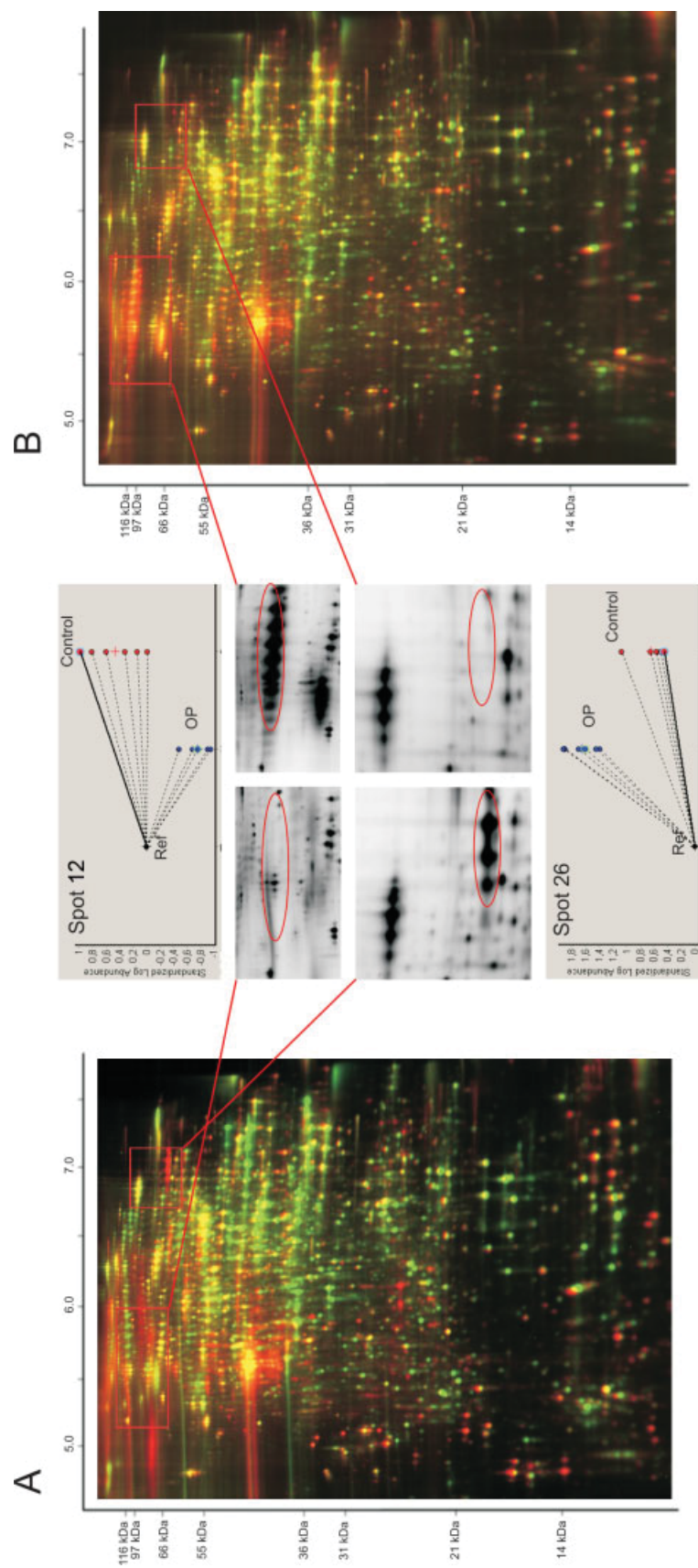
Figure 1. Representative proteome pattern from murine glomeruli preparation obtained by 2-D DIGE saturation labeling. Glomeruli preparations (3.0 μg protein) from SNx (Cy5, red labeled) (A) and sham-surgery mice (B) were separated by 2-DE together with 3.0 μg internal standard (Cy3, green labeled), respectively. The figures in between show the expression level exemplarily of spot 12 (meprin α) and spot 26 (hydroxyacyl-CoA) in SNx mice (OP) and sham-operated mice (control) in comparison to the internal standard (Ref) obtained by DeCyder image analysis software considering *n* = 6 independent samples. The spot 12 is more abundant in control mice (red-labeled) than in internal standard (green-labeled) leading to a red overlay. Expression of spot 12 in OP mice proteome (red-labeled) is barely detectable resulting in a green (reference) spot only. The lower evaluated spot 26 shows an opposite expression pattern. Spot 26 is low abundant in control mice (red-labeled) compared to reference (green-labeled) proteome leading to a green spot. Expression of spot 26 in OP mice (red-labeled) proteome is higher compared to reference (green-labeled) proteome leading to a red spot.
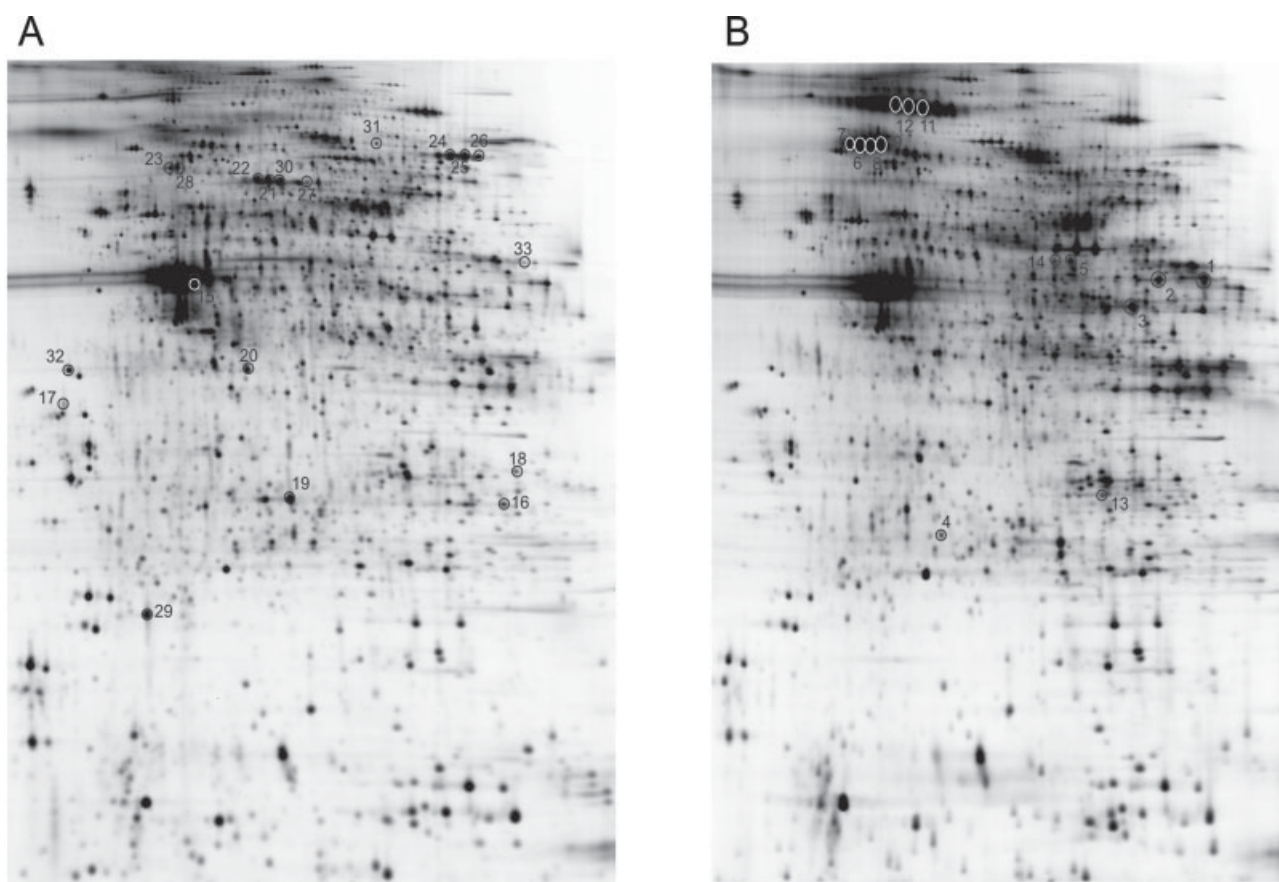
Figure 2. 2-D DIGE gels of SNx mice lysate (A) or sham-surgery mice lysate (B). In operated SNx mice significantly up- and down-regulated proteins are numbered in gel A and in gel B.

Table 2. List of 48 differentially expressed protein spots ($p<0.05$, fold change >2.0) in the sham and SNx-glomerular proteome

Number of spots analyzed in all gels	2100
Number of high abundant spots in operated mice (fold change >5)	18
Number of up-regulated spots in operated mice (fold change <5 and >2)	13
Number of highly down-regulated spots in operated mice (fold change >-5)	7
Number of down-regulated spots in operated mice (fold change <-5 and >-2)	10

Staining for galectin-1 reveals an enhancement in the area of the Bowman's capsule from subtotal nephrectomized kidneys in comparison to sham-surgery control mice (Figs. 3C and D).

Although meprin is predominantly expressed in the epithelium of the proximal tubules, immunohistochemistry shows additional reduced expression in healthy glomeruli. In SNx-mice none of the glomeruli can be stained for meprin with a reduced expression in the tubulus system (Figs. 3E and F).

3.5 Real-time PCR for galectin-1 and meprin – glomerular gene expression in FVB mice

Common housekeeping genes for real-time RT-PCR such as GAPDH and HPRT1 were not suitable for mRNA expression changes in this study due to inconsistency in their expression (regulation in 2-D DIGE analysis detected). Therefore, we directly compared the difference in CT values between the SNx group and the sham-surgery group without referring to a housekeeping gene (Table 4). In sham-surgery animals, there was almost no difference in the CT values between meprin 1 α and galectin-1, indicating comparable mRNA expression levels. Contrary to these findings, in SNx animals, the threshold level of galectin-1 was reached 3.41 cycles earlier than meprin (ΔCT meprin-galectin). Assuming doubling of cDNA in each cycle of the PCR, one can estimate a $2^{3.41}$ (~10.6-fold) higher expression of galectin-1 compared to meprin 1 α mRNA in SNx mice.

Table 3. Differentially expressed and identified proteins in the sham and SNx-glomerular proteome

Spot	NCBI accession	Protein
Down-regulated spots in SNx mice		
1	gi|21707669	Aldolase 2, B isoform
2	gi|192065	Argininosuccinate synthetase
3	gi|6996911	Argininosuccinate synthetase
4	gi|34222621	CCG1-interacting factor B
5	gi|13385454	Glycine amidinotransferase
6–9	gi|19072778	Hydrophilic CFTR-binding protein
	gi|10946938	PDZ domain containing 1
10–12	gi|31982199	Meprin 1 α
13	gi|6678413	Triosephosphate isomerase 1
14	gi|31982755	Vimentin
Up-regulated spots in SNx mice		
15	gi|17511847	ACTG1 protein
16	gi|18606328	Serine hydrolase
17	gi|30794164	Clathrin, light polypeptide (Lcb)
18	gi|467517	Collagen
29	gi|2944420	Complement C4
20	gi|38371755	Dimethylarginine dimethylaminohydrolase 1
21, 22	gi|23958822	Glucose regulated protein
23	gi|16923998	Heterogeneous nuclear ribonucleoprotein K
24–26	gi|54887356	Hydroxyacyl-coenzyme A dehydrogenase, α subunit
27	gi|15929761	Lamin A
28	gi|293689	Lamin B
29	gi|12805209	Lectin, galactose binding, soluble 1
30	gi|1083311	Protein disulfide-isomerase, ERp61 precursor
31	gi|3851614	Succinate dehydrogenase Fp subunit
32	gi|19353393	Tropomyosin 2
33	gi|31982755	Vimentin

Table 4. Differences in mRNA expression by comparing CT values: galectin-1 *vs.* meprin

	Sham	SNx
Meprin 1 α	25.1 ± 2.9	30.4 ± 3.5
Galectin-1	25.1 ± 1.6	27.0 ± 3.2
Delta (meprin–galectin)	0.04 ± 1.9	3.41 ± 0.6

3.6 Meprin expression *in vitro*

In the kidney, meprin is predominantly expressed in the brush border membrane of the tubulus system [18]. The expression of meprin in the glomerulus has not been described previously. Our proteomic approach found a change in expression in the extracted glomeruli. To verify a glomerular meprin and also galectin-1 expression, mRNA for RT-PCR was extracted from immortalized podocytes [19]. Podocytes are glomerulus-specific cells; the expression of meprin and galectin-1 in these cells support our findings in the proteomic analysis. RT-PCR was performed for the subunit meprin 1 α to verify meprin expression. GAPDH served as a control in this experiment (Fig. 4).

4 Discussion

4.1 General

In this study we focused on the analysis of the glomerular proteome in a model of CKD. Subtotal nephrectomy in rodents is a well-established model to induce CKD [20–22]. It is known that particular cellular mechanisms that involve a distinct balance in apoptosis and proliferation play a major role in the disease progression and adaptation processes that take place after the loss of functional tissue [9]. The interaction of podocytes, glomerular endothelium cells and mesangial cells, as well as local inflammatory processes with activation of cytokines and macrophages and cell-to-matrix or cell-to-cell interactions through integrins, are key players in the complexity of glomerulosclerosis. Although the pathology of these processes has been well described, the molecular mechanisms that lead to a self-sustaining progression of tissue injury at the site of the glomerulus are not very well understood.

In this study we used FVB mice to achieve a severe phenotype of disease. It has been previously described that this strain has a higher susceptibility for renal diseases compared to others [10, 23, 24].
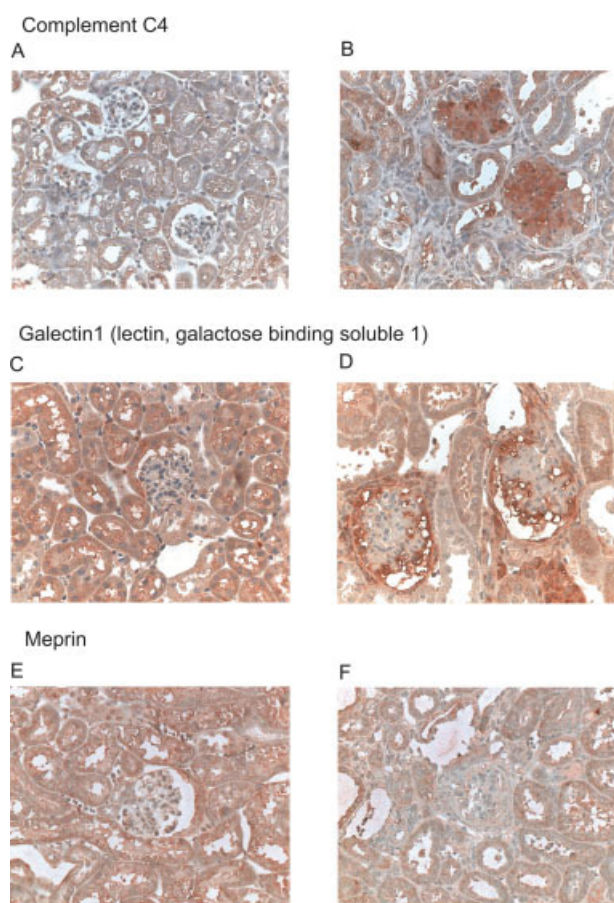
Figure 3. Immunohistochemistry of selected candidate proteins. Complement C4 protein (A, B), galectin-1 protein (C, D) and meprin α protein in murine kidney (E, F) considering tissue from sham-surgery mice (A, C, E) and SNx mice (B, D, F) in 400x magnification.
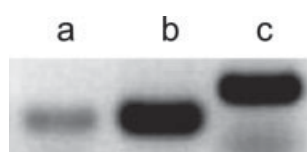

Figure 4. RT-PCR for meprin 1 α (a), galectin-1 (b) und GAPDH (c) – cDNA of immortalized podocytes.

To assess the degree of CKD, we obtained clinical parameters from both treatment groups 5 weeks after surgery (Table 1). The SNx mice developed significant albuminuria, which was found to be 44-fold higher compared to the sham-surgery group. Albuminuria is a marker for glomerular injury, indicting an alteration of its filter function, in particular the slit membrane [25–27]. The GFR measured by creatinine clearance was significantly decreased. With only 15% of GFR remaining after 5 weeks compared to the sham-surgery group, these mice suffer from stage 4 CKD if adapted to the K/DOQI criteria for humans [28]. CKD regularly leads to

increased activity of the renin-angiotensin-aldosterone system (RAAS), resulting in increased BP [29]. Compared to the sham-surgery group, the SNx mice had a significantly higher BP 5 weeks after surgery (Table 1). To support the clinical findings of CKD in our study, we assessed the histology of exemplary kidney sections, which revealed a progressed glomerulosclerosis in the SNx group (Figs. 5A and B).
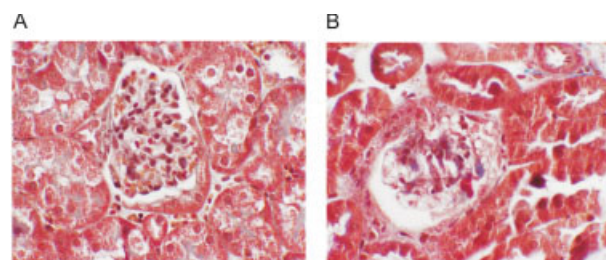
Figure 5. Masson's trichrome staining. Normal glomerulus (Sham) (A) and focal segmental glomerulosclerosis (SNx) (B) in 400 × magnification

4.2 Glomerular protein analysis

Compartmentalization is one major feature of kidney anatomy. To understand the molecular processes involved in the pathophysiology of CKD, this very unique characteristic of the kidney has to be taken into account. Our recent approach using magnetic particles for glomerular isolation in combination with 2-D DIGE proved to be a suitable tool to overcome this issue and to achieve a high-resolution protein analysis of the glomerular proteome [5]. The extraction of glomeruli from kidneys 5 weeks after subtotal nephrectomy or sham surgery, respectively, allowed us to identify 48 significantly regulated protein spots.

In the following discussion, we only focus on selected significantly regulated proteins. This selection was based on the expression level, its possible impact on the pathogenesis of CKD and the discussions found in recent literature concerning key proteins of renovascular research. However, it should be pointed out that this is a random selection and does not indicate that other non-discussed proteins are of minor importance.

4.3 Dimethylarginine dimethylaminohydrolase 1

The analysis revealed a 160-fold increase in DDAH expression in SNx mice compared to the sham-surgery group. DDAH is essential for the degradation of asymmetric dimethylarginine (ADMA) to L-citrulline and dimethylamine. ADMA serves as an endogenous inhibitor of the endothelial nitric oxide synthase (eNOS) (Fig. 6A). Besides enzymatic degradation, ADMA is eliminated through renal excretion [30].

CKD is associated with high serum levels of ADMA in rodents and humans [31]. Elevated serum levels of ADMA cause an inhibition of the eNOS and therefore a reduced
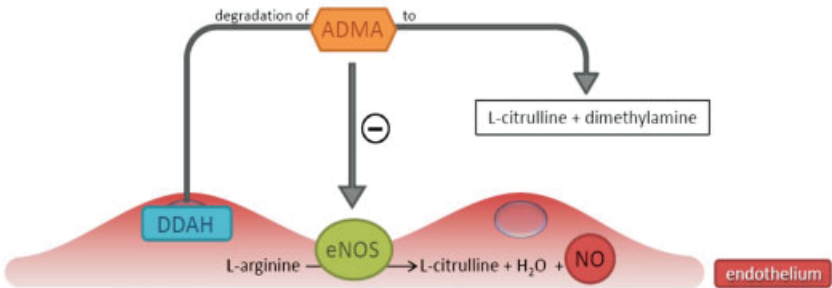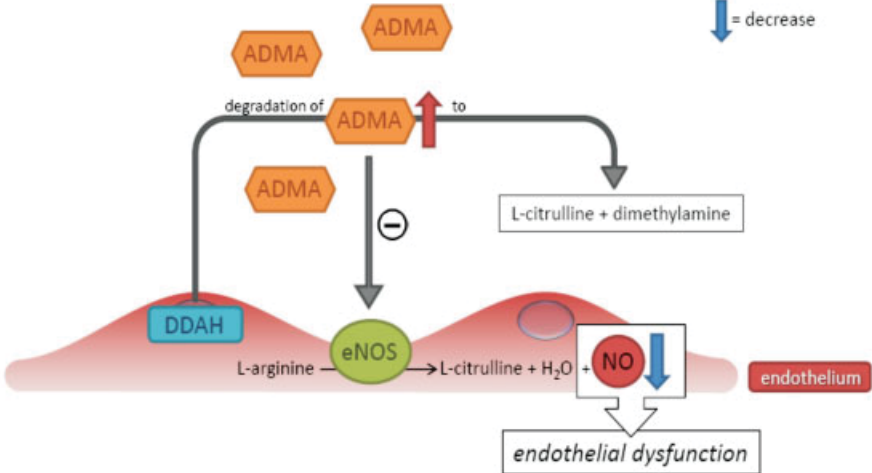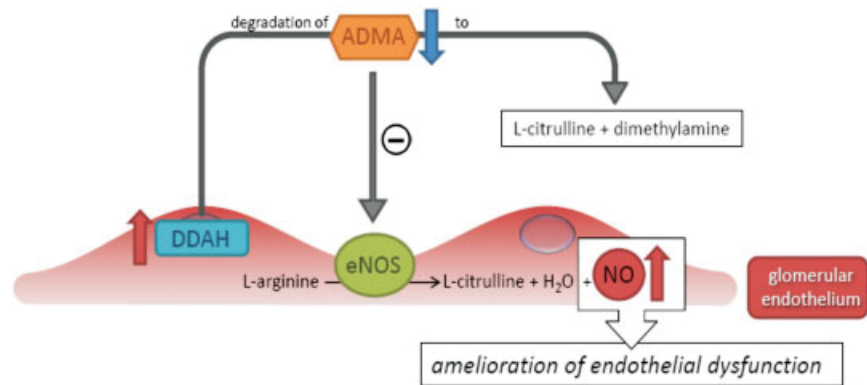
Figure 6. Illustration of the DDAH-ADMA-eNOS-NO pathway in healthy glomeruli (A), CKD (B) and the possible rescue mechanism in the analyzed glomeruli (C).

release of NO. A reduction in NO leads to increased vascular tonus and, therefore, an increase in perfusion pressure. In this context, high serum levels of ADMA have been shown to be an independent cardiovascular risk factor [32].

Previous studies have found that DDAH activity and its expression are reduced in CKD [31, 33]. It was assumed that this reduction was the cause of higher ADMA serum levels that correlate with the increase in BP and progression of CKD [31, 34] (Fig. 6B). The reduced DDAH activity in combination with higher ADMA levels further reduces the release of NO through eNOS causing further endothelial dysfunction, which might be a cause of the self-sustaining progression of CKD [35, 36].

Due to our exclusive focus on glomerular protein expression, we found that the DDAH expression is drastically increased in glomeruli of mice with CKD. Previous studies, which analyzed a homogenate of the whole kidney without taking in account the compartmentalization of the kidney, found the overall renal activity of DDAH to be decreased. It is likely that this overall reduction of DDAH activity is caused by an increase in extracellular matrix and fibrotic tissue as well as a reduction of functional tissue. A glomerular DDAH expression has been described by Tojo and coworkers [37]. They found in rat kidneys a distinct glomerular DDAH staining, in particular after challenging the animals with angiotensin II.

Our findings suggest a mechanism within the glomerular endothelium that might counteract endothelial dysfunction caused by a reduced NO release as a consequence of high ADMA serum levels and reduced availability of L-arginine [38, 39] (Fig. 6C).

4.4 Galectin-1

Galectin-1 is the first protein identified from the family of β-galactoside-binding lectins (galectins) [40]. It is a glomerular protein that showed a 23-fold up-regulation in SNx mice compared to sham-surgery mice.

Galectin-1 is involved in the regulation of a variety of processes including T cell homeostasis and immune response, inflammation, apoptosis and cell-to-cell and/or cell-to-matrix adhesion [41]. However, its specific role on the background of CKD is unclear.

An increase in galectin-1 expression has been shown in other diseases that are also associated with tissue fibrosis [42]. Its anti-inflammatory effects and influence on proliferation and apoptosis might play a role in the development and progression of glomerulosclerosis [43–45]. Its affinity to extracellular matrix proteins such as fibronectin and laminin suggest a role in cell-to-extracellular matrix adhesion and other extracellular matrix-related processes [46]. This might play a role in the interaction of glomerular cells with the glomerular basement membrane and/or the mesangial matrix. A distinct role of galectin-1 in the pathology of glomeruli is emphasized by the finding that galectin glycopro-

tein interactions are important in the maintenance of the renal epithelial phenotype [18].

It remains unclear whether the reduction in renal function after subtotal nephrectomy or the progression of tissue injury in this CKD model is the main cause of the increased expression of galectin-1. The specific role of galectin-1 in this pathology has to be elucidated in future studies.

4.5 Meprin 1 α

Meprin is a membrane-bound or secreted metalloproteinase composed of two subunits α and/or β. The homodimer serves as secreted form of meprin and is composed of two α subunits. Meprin is also expressed as a membrane-bound protein, which is composed as homodimer (β-β) or heterodimer (α-β) [47, 48]. The analysis of the glomerular proteome showed at least a 14-fold reduction of meprin 1 α expression in the SNx group compared to the sham-surgery group, which implies a reduction in secreted meprin.

In the kidney, meprin is predominantly expressed at the brush border membrane of tubules [49–52]. The results of this study show that meprin is also expressed in the glomerulus. These findings have been confirmed by immunohistochemistry (Figs. 3C and D). RT-PCR of cultured podocytes showed meprin 1 α mRNA expression in these glomerulus-specific cells (Fig. 4).

Meprin acts as a matrix-degrading metalloproteinase. A reduced expression of meprin is commonly found in kidney diseases [49, 53, 54]. This is associated with increased tissue fibrosis [27]. It is feasible that the reduction in secreted meprin and meprin expression might facilitate fibrosis.

Angiotensin-converting enzyme inhibitors (ACEI) or angiotensin receptor 1 antagonists (ARB) are known to prevent or even ameliorate glomerulosclerosis and tubulointerstitial fibrosis [55]. In the quoted study, meprin expression was increased under treatment with ACEI, suggesting a link between the anti-fibrotic effects of the inhibition of the renin-angiotensin system and meprin. This further emphasizes the role of meprin in the development of fibrosis/sclerosis. Future research will reveal the impact of meprin expression on the pathogenesis of glomerulosclerosis and glomerular disease.

In addition to the discussed proteins, other proteins that are not primarily synthesized in the glomerulus and therefore cannot be detected by mRNA analysis were accessible through 2-D DIGE. Complement C4 is one of these proteins (Table 3); glomerular-bound complement C4 is known to play a major role in various kidney diseases [56].

In contrast to previous studies that were unable to assess the compartmentalization of the kidney and/or analyze smallest sample sizes, our study reveals changes in the glomerular proteome in an disease model that do not reflect the overall change in the renal proteome shown in other studies, thus underlining the necessity of focused protein analysis for distinct tissue compartments. The specific approach used in this study allowed us to identify proteins that are implied in

the pathogenesis and pathophysiology of CKD. These proteins will be target of future research. In particular a correlation of clinical outcome and regulation of local protein expression after pharmacological interventions will help to understand the underlying mechanisms that reduce the progression of proteinuric kidney disease.

5 References

[1] Hieter, P., Boguski, M., Functional genomics: It's all how you read it. *Science* 1997, *278*, 601–602.

[2] Takenaka, M., Imai, E., Functional genomics in nephrology. *Nephrol. Dial. Transplant.* 2000, *15*, 139–141.

[3] Vonend, O., Apel, T., Amann, K., Sellin, L. *et al.*, Modulation of gene expression by moxonidine in rats with chronic renal failure. *Nephrol. Dial. Transplant.* 2004, *19*, 2217–2222.

[4] Knepper, M. A., Proteomics and the kidney. *J. Am. Soc. Nephrol.* 2002, *13*, 1398–1408.

[5] Sitek, B., Potthoff, S., Schulenborg, T., Stegbauer, J. *et al.*, Novel approaches to analyse glomerular proteins from smallest scale murine and human samples using DIGE saturation labelling. *Proteomics* 2006, *6*, 4337–4345.

[6] Arthur, J. M., Thongboonkerd, V., Scherzer, J. A., Cai, J. *et al.*, Differential expression of proteins in renal cortex and medulla: A proteomic approach. *Kidney Int.* 2002, *62*, 1314–1321.

[7] Yoshida, Y., Miyazaki, K., Kamiie, J., Sato, M. *et al.*, Two-dimensional electrophoretic profiling of normal human kidney glomerulus proteome and construction of an extensible markup language (XML)-based database. *Proteomics* 2005, *5*, 1083–1096.

[8] Xu, B. J., Shyr, Y., Liang, X., Ma, L. J. *et al.*, Proteomic patterns and prediction of glomerulosclerosis and its mechanisms. *J. Am. Soc. Nephrol.* 2005, *16*, 2967–2975.

[9] Thomas, G. L., Yang, B., Wagner, B. E., Savill, J., El Nahas, A. M., Cellular apoptosis and proliferation in experimental renal fibrosis. *Nephrol. Dial. Transplant.* 1998, *13*, 2216–2226.

[10] Ma, L. J., Fogo, A. B., Model of robust induction of glomerulosclerosis in mice: Importance of genetic background. *Kidney Int.* 2003, *64*, 350–355.

[11] Sitek, B., Luttges, J., Marcus, K., Kloppel, G. *et al.*, Application of fluorescence difference gel electrophoresis saturation labelling for the analysis of microdissected precursor lesions of pancreatic ductal adenocarcinoma. *Proteomics* 2005, *5*, 2665–2679.

[12] Sitek, B., Jung, K., Schramm, A., Stühler, K., Difference gel electrophoresis (DIGE): The next generation of two-dimensional gel electrophoresis for clinical research, in: *Proteomics in Drug Research. Methods and Principles in Medicinal Chemistry, vol. 28*, Wiley-VCH, Weinheim 2006, pp. 33–55.

[13] Mundel, P., Shankland, S. J., Podocyte biology and response to injury. *J. Am. Soc. Nephrol.* 2002, *13*, 3005–3015.

[14] Eng, J. K., McCormack, A. L., Yates, J. R. 3rd, An approach to correlate tandem mass spectral data of peptides with amino acid sequences in a protein database. *Am. Soc. Mass Spectrom.* 1994, *5*, 976–989.

[15] Yates, J. R. 3rd, Eng, J. K., McCormack, A. L., Mining genomes: Correlating tandem mass spectra of modified and unmodified peptides to sequences in nucleotide databases. *Anal. Chem.* 1995, *67*, 3202–3210.

[16] Yates, J. R. 3rd, Eng, J. K., McCormack, A. L., Schieltz, D., Method to correlate tandem mass spectra of modified peptides to amino acid sequences in the protein database. *Anal. Chem.* 1995, *67*, 1426–1436.

[17] Lutter, P., Meyer, H. E., Langer, M., Witthohn, K. *et al.*, Investigation of charge variants of rViscumin by two-dimensional gel electrophoresis and mass spectrometry. *Electrophoresis* 2001, *22*, 2888–2897.

[18] Bond, J. S., Matters, G. L., Banerjee, S., Dusheck, R. E., Meprin metalloprotease expression and regulation in kidney, intestine, urinary tract infections and cancer. *FEBS Lett.* 2005, *579*, 3317–3322.

[19] Mundel, P., Reiser, J., Zuniga Mejia Borja, A., Pavenstadt, H. *et al.*, Rearrangements of the cytoskeleton and cell contacts induce process formation during differentiation of conditionally immortalized mouse podocyte cell lines. *Exp. Cell Res.* 1997, *236*, 248–258.

[20] Shimamura, T., Morrison, A. B., A progressive glomerulosclerosis occurring in partial five-sixths nephrectomized rats. *Am. J. Pathol.* 1975, *79*, 95–106.

[21] Floege, J., Alpers, C. E., Burns, M. W., Pritzl, P. *et al.*, Glomerular cells, extracellular matrix accumulation, and the development of glomerulosclerosis in the remnant kidney model. *Lab. Invest.* 1992, *66*, 485–497.

[22] Amann, K., Koch, A., Hofstetter, J., Gross, M. L. *et al.*, Glomerulosclerosis and progression: Effect of subantihypertensive doses of alpha and beta blockers. *Kidney Int.* 2001, *60*, 1309–1323.

[23] Rumberger, B., Vonend, O., Kreutz, C., Wilpert, J. *et al.*, cDNA microarray analysis of adaptive changes after renal ablation in a sclerosis-resistant mouse strain. *Kidney Blood Press. Res.* 2007, *30*, 377–387.

[24] Pillebout, E., Burtin, M., Yuan, H. T., Briand, P. *et al.*, Proliferation and remodeling of the peritubular microcirculation after nephron reduction: Association with the progression of renal lesions. *Am. J. Pathol.* 2001, *159*, 547–560.

[25] Deckert, T., Feldt-Rasmussen, B., Borch-Johnsen, K., Jensen, T., Kofoed-Enevoldsen, A., Albuminuria reflects widespread vascular damage. The Steno hypothesis. *Diabetologia* 1989, *32*, 219–226.

[26] Keane, W. F., Shapiro, B. E., Renal protective effects of angiotensin-converting enzyme inhibition. *Am. J. Cardiol.* 1990, *65*, 49I–53I.

[27] Ma, L. J., Nakamura, S., Aldigier, J. C., Rossini, M. *et al.*, Regression of glomerulosclerosis with high-dose angio-

tensin inhibition is linked to decreased plasminogen activator inhibitor-1. *J. Am. Soc. Nephrol.* 2005, *16,* 966–976.

[28] K/DOQI clinical practice guidelines for chronic kidney disease: Evaluation, classification, and stratification. *Am. J. Kidney Dis.* 2002, *39,* S1–266.

[29] Ljutic, D., Kes, P., The role of arterial hypertension in the progression of non-diabetic glomerular diseases. *Nephrol. Dial. Transplant.* 2003, *18 Suppl 5,* V28–30.

[30] Teerlink, T., ADMA metabolism and clearance. *Vasc. Med.* 2005, *10 Suppl 1,* S73–81.

[31] Matsuguma, K., Ueda, S., Yamagishi, S., Matsumoto, Y. *et al.,* Molecular mechanism for elevation of asymmetric dimethylarginine and its role for hypertension in chronic kidney disease. *J. Am. Soc. Nephrol.* 2006, *17,* 2176–2183.

[32] Boger, R. H., Asymmetric dimethylarginine, an endogenous inhibitor of nitric oxide synthase, explains the "L-arginine paradox" and acts as a novel cardiovascular risk factor. *J. Nutr.* 2004, *134,* 2842S–2847S; discussion 2853S.

[33] Okubo, K., Hayashi, K., Wakino, S., Matsuda, H. *et al.,* Role of asymmetrical dimethylarginine in renal microvascular endothelial dysfunction in chronic renal failure with hypertension. *Hypertens. Res.* 2005, *28,* 181–189.

[34] Zoccali, C., Kielstein, J. T., Asymmetric dimethylarginine: A new player in the pathogenesis of renal disease? *Curr. Opin. Nephrol. Hypertens.* 2006, *15,* 314–320.

[35] Rennke, H. G., Glomerular adaptations to renal injury or ablation. Role of capillary hypertension in the pathogenesis of progressive glomerulosclerosis. *Blood Purif.* 1988, *6,* 230–239.

[36] Yin, Q. F., Fu, S. H., He, P., Xiong, Y., Dimethylarginine dimethylaminohydrolase inhibition and asymmetric dimethylarginine accumulation contribute to endothelial dysfunction in rats exposed to glycosylated protein: Effects of aminoguanidine. *Atherosclerosis* 2007, *190,* 53–61.

[37] Tojo, A., Kimoto, M., Wilcox, C. S., Renal expression of constitutive NOS and DDAH: Separate effects of salt intake and angiotensin. *Kidney Int.* 2000, *58,* 2075–2083.

[38] Mendes Ribeiro, A. C., Brunini, T. M., Ellory, J. C., Mann, G. E., Abnormalities in L-arginine transport and nitric oxide biosynthesis in chronic renal and heart failure. *Cardiovasc. Res.* 2001, *49,* 697–712.

[39] Ashab, I., Peer, G., Blum, M., Wollman, Y. *et al.,* Oral administration of L-arginine and captopril in rats prevents chronic renal failure by nitric oxide production. *Kidney Int.* 1995, *47,* 1515–1521.

[40] Barondes, S. H., Castronovo, V., Cooper, D. N., Cummings, R. D. *et al.,* Galectins: A family of animal beta-galactoside-binding lectins. *Cell* 1994, *76,* 597–598.

[41] Camby, I., Le Mercier, M., Lefranc, F., Kiss, R., Galectin-1: A small protein with major functions. *Glycobiology* 2006, *16,* 137R–157R.

[42] Santucci, L., Fiorucci, S., Cammilleri, F., Servillo, G. *et al.,* Galectin-1 exerts immunomodulatory and protective effects on concanavalin A-induced hepatitis in mice. *Hepatology* 2000, *31,* 399–406.

[43] Ellerhorst, J., Nguyen, T., Cooper, D. N., Lotan, D., Lotan, R., Differential expression of endogenous galectin-1 and galec-tin-3 in human prostate cancer cell lines and effects of over-expressing galectin-1 on cell phenotype. *Int. J. Oncol.* 1999, *14,* 217–224.

[44] Moiseeva, E. P., Spring, E. L., Baron, J. H., de Bono, D. P., Galectin 1 modulates attachment, spreading and migration of cultured vascular smooth muscle cells *via* interactions with cellular receptors and components of extracellular matrix. *J. Vasc. Res.* 1999, *36,* 47–58.

[45] van den Brule, F., Califice, S., Garnier, F., Fernandez, P. L. *et al.,* Galectin-1 accumulation in the ovary carcinoma peritumoral stroma is induced by ovary carcinoma cells and affects both cancer cell proliferation and adhesion to laminin-1 and fibronectin. *Lab. Invest.* 2003, *83,* 377–386.

[46] Murphy, K. M., Zalik, S. E., Endogenous galectins and effect of galectin hapten inhibitors on the differentiation of the chick mesonephros. *Dev. Dyn.* 1999, *215,* 248–263.

[47] Kumar, J. M., Bond, J. S., Developmental expression of meprin metalloprotease subunits in ICR and C3H/He mouse kidney and intestine in the embryo, postnatally and after weaning. *Biochim. Biophys. Acta* 2001, *1518,* 106–114.

[48] Marchand, P., Tang, J., Bond, J. S., Membrane association and oligomeric organization of the alpha and beta subunits of mouse meprin A. *J. Biol. Chem.* 1994, *269,* 15388–15393.

[49] Carmago, S., Shah, S. V., Walker, P. D., Meprin, a brush-border enzyme, plays an important role in hypoxic/ischemic acute renal tubular injury in rats. *Kidney Int.* 2002, *61,* 959–966.

[50] Walker, P. D., Kaushal, G. P., Shah, S. V., Meprin A, the major matrix degrading enzyme in renal tubules, produces a novel nidogen fragment *in vitro* and *in vivo*. *Kidney Int.* 1998, *53,* 1673–1680.

[51] Ricardo, S. D., Bond, J. S., Johnson, G. D., Kaspar, J., Diamond, J. R., Expression of subunits of the metalloendopeptidase meprin in renal cortex in experimental hydronephrosis. *Am. J. Physiol.* 1996, *270,* F669–676.

[52] Kieran, N. E., Doran, P. P., Connolly, S. B., Greenan, M. C. *et al.,* Modification of the transcriptomic response to renal ischemia/reperfusion injury by lipoxin analog. *Kidney Int.* 2003, *64,* 480–492.

[53] Trachtman, H., Valderrama, E., Dietrich, J. M., Bond, J. S., The role of meprin A in the pathogenesis of acute renal failure. *Biochem. Biophys. Res. Commun.* 1995, *208,* 498–505.

[54] Sadlier, D. M., Connolly, S. B., Kieran, N. E., Roxburgh, S. *et al.,* Sequential extracellular matrix-focused and baited-global cluster analysis of serial transcriptomic profiles identifies candidate modulators of renal tubulointerstitial fibrosis in murine adriamycin-induced nephropathy. *J. Biol. Chem.* 2004, *279,* 29670–29680.

[55] Mathew, R., Futterweit, S., Valderrama, E., Tarectecan, A. A. *et al.,* Meprin-alpha in chronic diabetic nephropathy: Interaction with the renin-angiotensin axis. *Am. J. Physiol. Renal Physiol.* 2005, *289,* F911–921.

[56] Sijpkens, Y. W., Joosten, S. A., Wong, M. C., Dekker, F. W. *et al.,* Immunologic risk factors and glomerular C4d deposits in chronic transplant glomerulopathy. *Kidney Int.* 2004, *65,* 2409–2418.

RESEARCH PAPER

Chronic treatment with angiotensin-(1-7) improves renal endothelial dysfunction in apolipoproteinE-deficient mice

J Stegbauer[1]*, SA Potthoff[1]*, I Quack[1], E Mergia[2], T Clasen[1], S Friedrich[1], O Vonend[1], M Woznowski[1], E Königshausen[1], L Sellin[1] and LC Rump[1]

[1]Department of Nephrology, Medical Faculty, Heinrich-Heine University Düsseldorf, Düsseldorf, Germany, and [2]Department of Pharmacology and Toxicology, Medical Faculty MA N1, Ruhr-University Bochum, Bochum, Germany

Correspondence
Johannes Stegbauer,
Klinik für Nephrologie,
Universitätsklinikum Düsseldorf,
Heinrich-Heine-Universität
Düsseldorf, Moorenstrasse 5,
40225 Düsseldorf, Germany.
E-mail: johannes.stegbauer@med.
uni-duesseldorf.de

----

*These authors contributed
equally to this study and should
be considered joint first authors.

BACKGROUND AND PURPOSE

ApolipoproteinE-deficient [apoE (–/–)] mice, a model of human atherosclerosis, develop endothelial dysfunction caused by decreased levels of nitric oxide (NO). The endogenous peptide, angiotensin-(1-7) [Ang-(1-7)], acting through its specific GPCR, the Mas receptor, has endothelium-dependent vasodilator properties. Here we have investigated if chronic treatment with Ang-(1-7) improved endothelial dysfunction in apoE (–/–) mice.

EXPERIMENTAL APPROACH

ApoE (–/–) mice fed on a lipid-rich Western diet were divided into three groups and treated via osmotic minipumps with either saline, Ang-(1-7) (82 µg·kg^{-1}·h^{-1}) or the same dose of Ang-(1-7) together with D-Ala-Ang-(1-7) (125 µg·kg^{-1}·h^{-1}) for 6 weeks. Renal vascular function was assessed in isolated perfused kidneys.

KEY RESULTS

Ang-(1-7)-treated apoE (–/–) mice showed improved renal endothelium-dependent vasorelaxation induced by carbachol and increased renal basal cGMP production, compared with untreated apoE (–/–) mice. Tempol, a reactive oxygen species (ROS) scavenger, improved endothelium-dependent vasorelaxation in kidneys of saline-treated apoE (–/–) mice whereas no effect was observed in Ang-(1-7)-treated mice. Chronic treatment with D-Ala-Ang-(1-7), a specific Mas receptor antagonist, abolished the beneficial effects of Ang-(1-7) on endothelium-dependent vasorelaxation. Renal endothelium-independent vasorelaxation showed no differences between treated and untreated mice. ROS production and expression levels of the NAD(P)H oxidase subunits gp91phox and p47phox were reduced in isolated preglomerular arterioles of Ang-(1-7)-treated mice, compared with untreated mice, whereas eNOS expression was increased.

CONCLUSION AND IMPLICATIONS

Chronic infusion of Ang-(1-7) improved renal endothelial function via Mas receptors, in an experimental model of human cardiovascular disease, by increasing levels of endogenous NO.

Abbreviations

Ang, angiotensin; apoE, apolipoproteinE; AT$_1$ receptor, angiotensin II type 1 receptor; GSNO, S-nitrosoglutathione; IBMX, 3-isobutyl-1-methylxanthine; ROS, reactive oxygen species

Introduction

Endothelial dysfunction is caused by decreased levels of nitric oxide (NO) derived from the endothelium. This deleterious condition is strongly associated with hypertension and therefore an important predictor of cardiovascular risk. The amount of biologically active NO, which plays a pivotal role in vascular homeostasis, is determined by the balance between the biosynthesis of NO and its degradation by endogenous reactive oxygen species (ROS) (Cai and Harrison, 2000).

Angiotensin (Ang) II, the major effector molecule of the renin-angiotensin-system (RAS) has an important effect on the genesis of endothelial dysfunction. Ang II, through its actions at the angiotensin II type 1 (AT_1) receptor (nomenclature follows Alexander et al., 2009), increases ROS production which leads subsequently to NO degradation (Mehta and Griendling, 2007). Thus, inhibition of Ang II generation by angiotensin converting enzyme (ACE) inhibitors or blockade of the AT_1 receptor ameliorates endothelial dysfunction and thereby reduces cardiovascular morbidity and mortality. New components and functions of the RAS are still being uncovered. Besides the classical main effector Ang II, other peptides of the RAS, like Ang III, Ang IV and Ang-(1-7) have been shown to have biological actions (Ferrario et al., 1998; Stegbauer et al., 2003). Ang-(1-7) can be formed from Ang I or Ang II by several peptidases including the carboxypetidases ACE and ACE2 (Iusuf et al., 2008) whereas the conversion of Ang II to Ang-(1-7) by ACE2 seems to be the preferred pathway of Ang-(1-7) generation. Ang-(1-7) activates its own GPCR, the Mas receptor and this receptor has been characterized as a physiological antagonist of the AT_1 receptor (Santos et al., 2003; Kostenis et al., 2005). Moreover, Ang-(1-7)-mediated activation of Mas receptors has been shown to inhibit endothelial cell growth, proliferation and cardiac remodelling by influencing MAP kinase signalling (Sampaio et al., 2007a; Mercure et al., 2008), and to improve cardiac function after myocardial infarction (Loot et al., 2002; Grobe et al., 2007). Moreover, activation of Mas receptors located in the endothelium induced vasodilation by generating NO and prostaglandins (Castro et al., 2005; Sampaio et al., 2007b). Also, Ang-(1-7) improved endothelial-dependent vasorelaxation in normotensive rats by increasing NO bioavailability (Faria-Silva et al., 2005). Consequently, Mas receptor-deficient mice showed decreased endothelial NO synthase and increased NAD(P)H oxidase activity, leading to endothelial dysfunction and subsequently to hypertension (Xu et al., 2008).

However, not much is known about the effects of Ang-(1-7) on endothelial dysfunction. To answer that question, we have used apolipoproteinE (–/–) mice, as an experimental model for human atherosclerosis. These animals develop pronounced endothelial dysfunction when fed a lipid- and cholesterol-rich diet (Wassmann et al., 2004). Thus, they provide an ideal model to dissect the consequences of Ang-(1-7)-mediated Mas receptor signalling for endothelial function.

Methods

Animals and osmotic minipump implantation

All animal care and experimental investigations were in accordance with the Guide for Care and Use of Laboratory Animals published by the US National Institutes of Health (NIH Publication no. 85–23, revised 1996) and were approved by the local Animal Care Committee (licence no. 50.8735.1 Nr. 109/6). Six-week-old male apoE (–/–) mice (C57Bl/6 background) and their littermates were obtained from Jackson Labs, Bar Harbor. Mice were fed with 'Western-type' diet (Sniff, Soest, Germany) (42% fat, 0.15% cholesterol) and allowed free access to tap water. After 6 weeks, mice were treated with either saline, Ang-(1-7) or with a combination of Ang-(1-7) and D-Ala-Ang-(1-7), delivered over 6 weeks by osmotic minipumps. The minipumps (Alzet Model 1004) were filled with either saline, Ang-(1-7) (to deliver 82 µg·kg^{-1}·h^{-1}) (Bachem) or D-Ala-Ang-(1-7) (to deliver 125 µg·kg^{-1}·h^{-1}) (Bachem). Osmotic minipumps were inserted subcutaneously during anaesthesia with ketamine (100 mg·kg^{-1}, i.p.) and xylazine (5 mg·kg^{-1}, i.p.) and replaced after 3 weeks. When both Ang-(1-7) and D-Ala-Ang-(1-7) were administered together, two osmotic minipumps were implanted.

Blood pressure measurements

Systolic blood pressure was measured in conscious mice by tail-cuff plethysmography (BP-98A; Softron Co.). For habituation, mice were trained daily for 5 days. After training period, 10 measurements per mouse were recorded daily for 5 days, 1 week before and 6 weeks after minipump implantation respectively.

Preparation of isolated perfused kidneys from mice

Eighteen-week-old apoE (–/–) mice and their wild-type littermates were anesthetized i.p. with ketamine (100 mg·kg^{-1}) and xylazine (5 mg·kg^{-1}). Kidneys were isolated under a microscope (Olympus CO11) and perfused with Krebs–Henseleit buffer according to an amended method described previously (Stegbauer et al., 2005). Changes in perfusion pressure reflected changes in vascular resistance of renal resistance vessels.

Immediately after preparation, a bolus injection of 60 mM KCl was delivered to test the viability of the preparation followed by a stabilization period of 30 min. After the stabilization period, renal vasoconstriction was induced by noradrenaline (1 µM; Sigma-Aldrich) and concentration–response curves of the vasodilators carbachol (Sigma-Aldrich) in the presence or absence of Tempol (1 mM; Sigma-Aldrich) and S-nitrosoglutathione (GSNO, Alexis Corp.) were assessed. Vasodilation induced by GSNO was recorded in the presence of L-N^G-nitro-arginine methyl ester (L-NAME; 0.3 mM; Sigma-Aldrich) and diclofenac (3 µM). Renal relaxation was calculated as percentage of reduction in the precontracted kidneys which was set as 100%.

Measurement of H_2O_2

Isolation of preglomerular vessels does not yield enough tissue for reliable measurement of H_2O_2 production. Thus, H_2O_2 production of renal cortex including preglomerular vessels was measured with the Amplex Red H_2O_2/Peroxidase Assay Kit (Molecular Probes) in triplicates. Kidneys were perfused with cold Krebs–Henseleit buffer. After removing the renal capsule, renal cortex was cut into three 2 mm cubes and placed into warm buffer (37°C) and incubated in the reaction mixture for 1 h at 37°C in the dark. The supernatant was then

read in a fluorescence spectrophotometer (Cary eclipse, Varian Inc.). The fluorescent values were normalized to the protein content measured in the samples.

Determination of cGMP content in renal cortical slices

Renal cortical slices (250 µm) were cut with a vibratome (NVSLM1 from WPI) and equilibrated for 10 min in tempered (37°C), oxygenated (with 95% O_2, 5% CO_2) Krebs–Henseleit buffer. Slices were incubated with the non-specific phosphodiesterase inhibitor 3-isobutyl-1-methylxanthine (IBMX, 300 µM; Sigma Aldrich) for 10 min at 37°C. Subsequently, in the presence of IBMX the slices were incubated either with carbachol (100 µM; Sigma-Aldrich) or with diethylamine nitric oxide (DEA-NO) (100 µM; Alexis) for an additional 3 min. To extract cGMP, slices were frozen in liquid nitrogen, homogenized in 70% (v/v) ice-cold ethanol using a glass/glass homogenizer and then centrifuged (14 000x g, 15 min, 4°C). Supernatants were dried at 95°C and the cGMP content was measured by RIA (Brooker et al., 1979). Preparation of tracer, acetylation of samples and standards and incubation with antibody were performed as described. In order to standardize the different samples, protein pellets were dissolved in 0.1 M NaOH/0.1% SDS and protein content was determined using the bicinchoninic acid method (Uptima).

Measurement of urinary nitrite/nitrate concentrations (Griess assay)

Twenty-four-hour urine samples were collected in metabolic cages at the end of the experimental period. Urinary concentrations of nitrite (NO_2) and nitrate (NO_3) were measured using a colorimetric assay kit (Cayman Chemical Company).

Measurement of urinary 8-isoprostane concentration

Twenty-four-hour urine samples were collected in metabolic cages at the end of the experimental period. Urinary concentrations of 8-isoprostane were measured using a colorimetric assay kit (Cayman Chemical Company) and normalized to urinary creatinine.

Isolation of preglomerular vessels

Preglomerular vessels, containing mainly interlobular arteries and afferent arterioles, were isolated by a modified iron oxide-sieving technique as described previously (Patzak et al., 2008). As minor modifications, the kidneys were perfused via cannulation of the aorta, smaller needles (G20, G23) and pore sieves (100 µm) were used for tissue separation and separation of renal particles respectively.

Quantitative real-time PCR

Preglomerular vessels were used to study the expression of catalase and endothelial NO synthase (eNOS) and of the NAPH proteins, Nox1, gp91phox (Nox2), Nox4, p22pox and p47phox. After homogenization of isolated vessels with a Tissue Ruptor (Qiagen, Germany), total RNA was isolated using a RNA Micro Kit (Qiagen, Germany) according to the manufacturer's instructions. Quantitative real-time PCR was performed with an ABI PRISM 7300 (Applied Biosystem, Germany) and the SYBR Green master mix (Qiagen, Germany). The PCR reaction was performed in a total volume of 20 µL with 1 µL cDNA corresponding to 100 ng RNA as template and 1 pmol·µL^{-1} of each primer [Nox1 NM_172203, Nox2 NM_007807, Nox4 NM_015760, p22phox NM_007806, p47phox NM_010876, catalase NM_009804, eNOS NM_008713, Mas NM_008552; Qiagen, Germany and AT$_{1A}$ receptor (forward 5′-GCTTGGTGGTGATCGTCACC-3′ and reverse 5′-GGGCGAGATTTAGAAGAACG-3′)]. The two-step PCR conditions were 2 min at 50°C, 15 min at 95°C, followed by 40 cycles (denaturation of 94°C for 15 s; annealing 55°C 30 s and extension at 72°C for 34 s). Experiments were performed in triplicate. Glyceraldehyde-3-phosphate dehydrogenase (GAPDH NM_008084) was chosen as the endogenous control (housekeeping gene). The levels of Nox1, Gp91phox, Nox4, p22pox, p47phox, catalase, eNOS, AT$_{1A}$ and Mas cDNA were normalized to GAPDH by the ΔC_T method.

Immunoblotting for eNOS and phospho-eNOS

Renal cortex tissue was placed into ice-cold protein lysis buffer (600 µL EMPIGENE, 10 mL phosphate buffered saline, 44 nM phenylmethanesulphonylfluoride) containing a protease inhibitor cocktail (Sigma Aldrich) and immediately homogenized. Lysates were centrifuged at 4000 g for 10 min at 4°C. Protein concentrations from the supernatant were determined by a Bradford assay (Bioassay Systems). After treatment with dithiothreitol (100 mM) and denaturation (5 min at 95°C), 30 µg of total protein were loaded onto 8% SDS-PAGE gels and then transferred to nitrocellulose membranes according to manufacturer's instructions (X-Cell Blot Module, Invitrogen). Membranes were blocked in blocking buffer (5% BSA, and 0.1% tween 20 in PBS) for 1 h at room temperature and then incubated either with primary monoclonal mouse anti-eNOS antibody (1:3000) (BD Transduction Laboratories, material number 610297) or with primary monoclonal mouse Anti-phospho-eNOS (phospho-Ser[1177]) antibody (1:1000) (BD Transduction Laboratories, material number 612392), and mouse anti-β-actin (1:5000) (Sigma Aldrich, St. Luis, MO, USA) over-night. Bound primary antibody was detected with anti-mouse HRP conjugated secondary antibody (1:10 000) (Dako, Germany) by 60 min incubation at room temperature. Antibody labelling was visualized by the addition of a chemiluminescence reagent. Chemiluminescence was visualized using a FluorChem FC2 Imager (Alpha Innotec, San Leandro, CA, USA). Immunoblots from each tissue were performed in triplicates.

Statistical analysis

Data are expressed as mean ± SEM (n = number of animals). Differences between dose–response curves were analysed by one-way ANOVA for repeated measurements, followed by unpaired Student's t-test. Statistical analyses of data not normally distributed were analysed by the Kruskal–Wallis test followed by Mann–Whitney U-test. Probability levels of $P < 0.05$ were considered statistically significant. The number of experiments indicates the number of mice.

Results

Six-week-old apoE (–/–) and wild-type mice were fed with a lipid-rich Western diet for the present study. After 6 weeks,

Table 1

Systemic blood pressure and circulating lipids in mice

	ApoE (+/+)	ApoE (−/−)	ApoE (−/−) + Ang-(1-7)
Blood pressure (mmHg)	117.8 ± 3.4	114 ± 4.1	113 ± 6.5
Cholesterol (mmol·L^{-1})	1.6 ± 0.3	13.7 ± 4.3**	15.7 ± 4.0**
Triglycerides (mmol·L^{-1})	0.6 ± 0.1	1.3 ± 0.4*	1.4 ± 0.5*
HDL (mmol·L^{-1})	0.4 ± 0.1	0.3 ± 0.1	0.4 ± 0.1
LDL (direct) (mmol·L^{-1})	0.2 ± 0.1	6.3 ± 3.1***	6.4 ± 1.8***

Blood pressure was measured by tail-cuff and serum was collected for lipid analysis from six mice per group at the end of the study. Data are means ± SEM; *$P < 0.05$, **$P < 0.01$, ***$P < 0.001$ different from values for apoE (+/+) mice: Student's t-test.
Ang, angiotensin; apoE, apolipoproteinE; HDL, high-density lipoprotein; LDL, low-density lipoprotein.
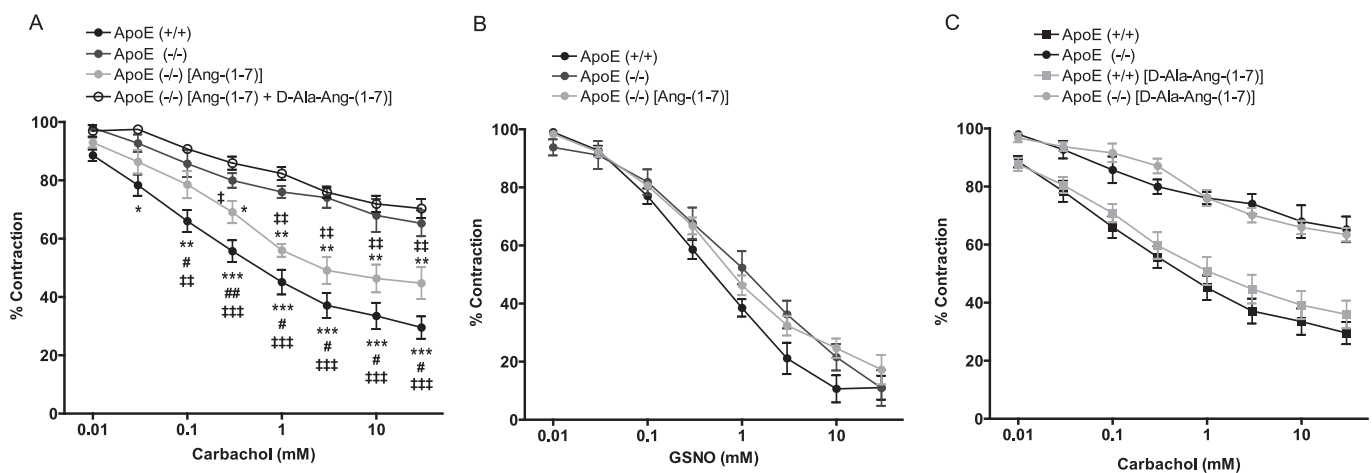
Figure 1

(A) The carbachol-induced endothelial-dependent vasorelaxation was impaired in isolated kidneys of apoE (−/−) mice ($n = 7$), compared with that in kidneys from apoE (+/+) mice ($n = 6$). Chronic Ang-(1-7) treatment (82 mg·kg^{-1}·h^{-1}) improved endothelium-dependent relaxation in kidneys of apoE (−/−) mice ($n = 7$). Combining Ang-(1-7) with D-Ala-Ang-(1-7) (125 mg·kg^{-1}·h^{-1}), a specific Mas receptor antagonist, attenuated the beneficial effects of Ang-(1-7) ($n = 6$). (B) Smooth muscle cell-dependent renal vasorelaxation, tested with the NO donor GSNO, did not differ between apoE (+/+) ($n = 6$), apoE (−/−) ($n = 9$) and Ang-(1-7)-treated apoE (−/−) ($n = 9$) mice. (C) D-Ala-Ang-(1-7) treatment alone showed no effects on carbachol-induced vasorelaxation in apoE (+/+) or apoE (−/−) mice. Data represent means ± SEM; *$P < 0.05$, **$P < 0.01$, ***$P < 0.001$ versus apoE (−/−). #$P < 0.05$, ##$P < 0.01$ versus apoE (−/−) [Ang-(1-7)]. ‡$P < 0.05$, ‡‡$P < 0.01$, ‡‡‡$P < 0.001$ versus apoE (−/−) [Ang-(1-7) + D-Ala-Ang-(1-7)]. One-way ANOVA for repeated measurements followed by Student's t-test. Ang, angiotensin; apoE, apolipoproteinE; GSNO, S-nitrosoglutathione; NO, nitric oxide.

apoE (−/−) mice were divided into three groups and treated with either saline, Ang-(1-7) (82 µg·kg^{-1}·h^{-1}) or a combination of Ang-(1-7) (82 µg·kg^{-1}·h^{-1}) and the specific Mas receptor antagonist D-Ala-Ang-(1-7) (125 µg·kg^{-1}·h^{-1}) via osmotic minipump subcutaneously. Osmotic minipumps were replaced after 3 weeks. No differences were seen in blood pressure and lipid profiles between Ang-(1-7)-treated and untreated apoE (−/−) mice (Table 1).

Ang-(1-7) treatment improves endothelial-dependent renal vasorelaxation in apoE (−/−) mice through activation of Mas receptors

To evaluate the influence of Ang-(1-7) treatment on endothelial- and smooth muscle cell-dependent vasorelax-ation in kidneys of apoE (−/−) mice, isolated kidneys were pre-constricted with noradrenaline (1 µM). Compared with apoE (+/+) mice, kidneys of apoE (−/−) showed a reduced endothelial-dependent vasorelaxation induced by carbachol (Figure 1A). Interestingly, chronic treatment with Ang-(1-7) improved endothelial-dependent renal vasorelaxation. This improved level of response was still less than that in the apoE (+/+) mice. To test whether the effect of chronic Ang-(1-7) treatment is restricted to the endothelium or in addition has an effect on muscle cell-dependent relaxation, the effects of GSNO, a NO donor, were assessed. GSNO-induced renal vasorelaxation did not differ between apoE (+/+), apoE (−/−) and Ang-(1-7)-treated apoE (−/−) mice (Figure 1B).

As Ang-(1-7) mediates its effects through Mas receptors, D-Ala-Ang-(1-7), a specific Mas receptor antagonist, was

tested. In kidneys of apoE (–/–) mice treated simultaneously with Ang-(1-7) and D-Ala-Ang-(1-7), endothelial-dependent vasorelaxation induced by carbachol was significantly reduced compared with apoE (–/–) mice treated only with Ang-(1-7). The dose–response curve was almost identical compared with untreated apoE (–/–) mice (Figure 1A). In contrast, treatment with the Mas receptor antagonist alone did not affect endothelial-dependent vasodilition in kidneys of apoE (+/+) or apoE (–/–) mice (Figure 1C).

In isolated preglomerular vessels, no differences of RNA expression levels of the Mas and AT_{1A} receptor were observed between apoE (+/+), apoE (–/–), Ang-(1-7)-treated apoE (+/+) and Ang-(1-7)-treated apoE (–/–) mice [Mas mRNA expression: apoE (+/+): 1.00 ± 0.10; apoE (–/–): 0.91 ± 0.08; apoE (–/–) + Ang-(1-7): 1.13 ± 0.06; apoE (+/+) + Ang-(1-7): 1.76 ± 0.76 arbitrary units; AT_{1A} mRNA expression apoE (+/+): 1.00 ± 0.15; apoE (–/–): 1.09 ± 0.13; apoE (–/–) + Ang-(1-7): 0.90 ± 0.07; apoE (+/+) + Ang-(1-7): 1.132 ± 0.12 arbitrary units).

Increased NO bioavailability in Ang-(1-7)-treated apoE (–/–) Mice

Endothelial dysfunction correlates closely with decreased NO bioavailability. Thus, we tested whether Ang-(1-7) treatment increased NO levels in apoE (–/–) mice. To prevent cGMP degradation, experiments were performed in the presence of IBMX, a non-specific phosphodiesterase inhibitor. Basal cGMP production was significantly increased in kidney slices from Ang-(1-7)-treated mice compared with those from saline-treated apoE (–/–) mice. In line with the results performed in isolated perfused kidneys, cGMP generation induced by carbachol was markedly increased in Ang-(1-7)-treated mice. Exogenous NO, provided by DEA-NO (100 μM), induced the same increases in cGMP generation in slices from Ang-(1-7)-treated as in slices from untreated mice, showing that the beneficial effects of Ang-(1-7) on renal vasorelaxation was restricted to the endothelium (Figure 2A). In addition, Ang-(1-7)-treated apoE (–/–) mice showed increased 24-hour urinary excretion rates of nitrate and nitrite compared with untreated apoE (–/–) mice (Figure 2B). Moreover, nitrate/nitrite urinary excretion rates were significantly greater in apoE (+/+) mice compared with the rates in Ang-(1-7)-treated and untreated apoE (–/–) mice. Finally, mRNA expression levels of eNOS, the main NO synthase in the renal vasculature, were measured and found to be significantly reduced in preglomerular arterioles of apoE (–/–) mice. Ang-(1-7) treatment slightly but significantly increased eNOS RNA expression (Figure 2C). These results were confirmed by measurement of total eNOS protein levels in the renal cortex of Ang-(1-7)-treated and saline-treated apoE (–/–) mice (Figure 2D). Interestingly, the ratio between expression levels of phospho-Ser[1177]-eNOS, a marker for activated eNOS, and total eNOS were not significantly different between both groups (Figure 2D).

Chronic Ang-(1-7) treatment influences ROS production

It has been reported that production of ROS is increased in apoE (–/–) mice and responsible for endothelial dysfunction. To test if Ang-(1-7) mediated its effect by influencing ROS production, we used the ROS scavenger, tempol. In the pres-

ence of tempol (1 mM), endothelium-dependent vasorelaxation was significantly improved in kidneys of saline-treated apoE (–/–) mice (Figure 3A). This improvement was almost identical to that observed in Ang-(1-7)-treated mice. Interestingly, tempol had no additional effect on endothelial-dependent renal vasorelaxation in Ang-(1-7)-treated apoE (–/–) mice, providing the first evidence that Ang-(1-7) reduces ROS production.

To further support this observation, we measured H_2O_2 production in the renal cortex of apoE (+/+), apoE (–/–) and Ang-(1-7)-treated apoE (–/–) mice and urinary 8-isoprostane levels, a marker for oxidative stress. H_2O_2 production in the renal cortex as well as urinary 8-isoprostane levels were significantly increased in apoE (–/–) mice compared with apoE (+/+) mice and treatment with Ang-(1-7) attenuated H_2O_2 production and 8-isoprostane levels to baseline levels (Figure 3B).

Next, we analysed expression levels of enzymes involved in the metabolism of ROS. Expression levels of the NAD(P)H family differ between large conductance vessels and resistance arteries. Therefore, it was important to isolate preglomerular arterioles of mice kidneys. As the amount of isolated vessels is very limited, RNA instead of protein expression levels of Nox1, gp91phox, Nox 4, p22phox, p47phox and catalase, involved in the generation and catabolism of ROS, were measured by using quantitative real-time PCR. RNA levels of catalase which degrades H_2O_2 to H_2O were decreased in isolated preglomerular arterioles of apoE (–/–) compared with apoE (+/+) mice. However, treatment with Ang-(1-7) did not significantly increase catalase expression in isolated preglomerular arterioles of apoE (–/–) mice (Figure 4A). Next, we investigated whether expression levels of the NAD(P)H family involved in the generation of ROS were influenced by chronic Ang-(1-7) treatment. A significant increase in RNA expression levels was found for gp91phox and p47phox in preglomerular vessels of apoE (–/–) mice. Chronic treatment with Ang-(1-7) significantly reduced gp91phox and p47phox. However, gp91phox and p47phox expression levels were still increased compared with those in apoE (+/+) mice (Figure 4B). In contrast, RNA expression levels of Nox1, Nox4 and p22phox were unaltered in Ang-(1-7)-treated and untreated apoE (–/–) compared with apoE (+/+) mice (Figure 4C).

Discussion

Endothelial dysfunction is defined as decreased levels of NO, caused by either diminished NO generation or increased NO degradation and precedes vascular diseases at several sites of the vasculature, including kidney and heart. ApoE (–/–) mice fed a cholesterol- and lipid-rich diet develop endothelial dysfunction (Osada *et al.*, 2000; d'Uscio *et al.*, 2001; Laursen *et al.*, 2001). Despite the significantly impaired endothelium-dependent vasorelaxation observed in the renovascular bed of apoE (–/–) mice, we could not detect an increase in systemic blood pressure, relative to that of wild-type littermates. This, at first sight surprising finding, is in line with results obtained by others (Hartley *et al.*, 2000; Arruda *et al.*, 2005; Custodis *et al.*, 2008). The underlying compensatory mechanisms are still not fully understood but may be related to the genetic background (Rabelo *et al.*, 2008), the age of the
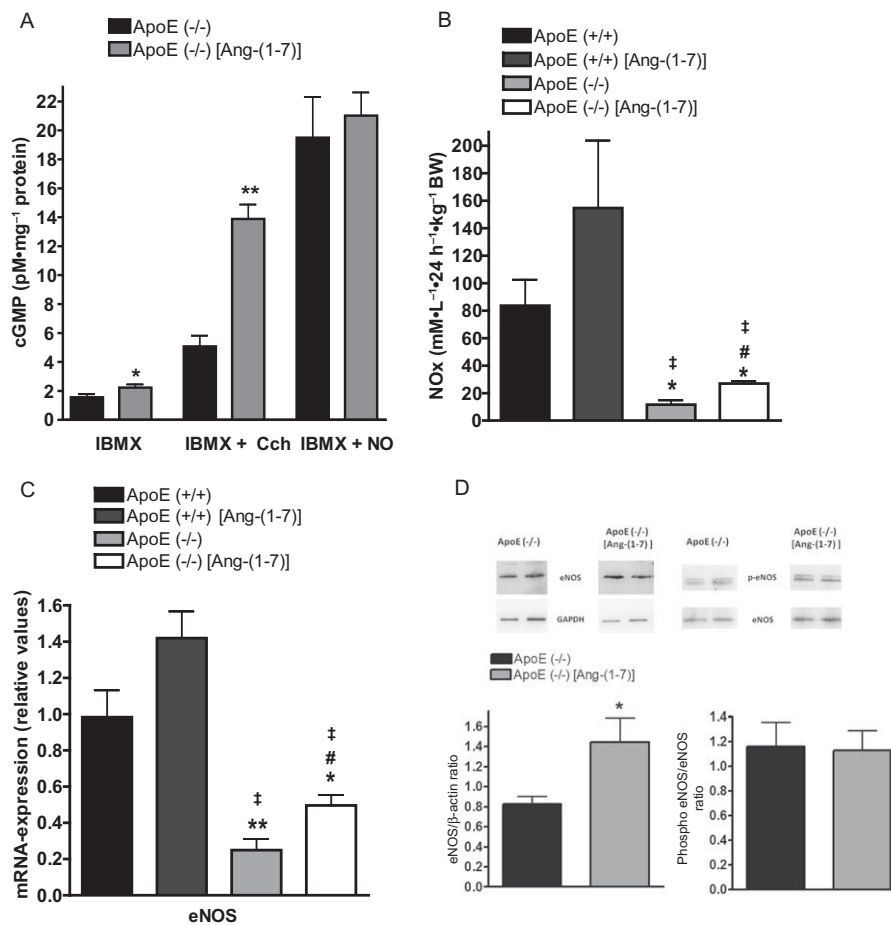
Figure 2

(A) cGMP production was measured, in the presence of IBMX, in cortical renal slices from apoE (−/−) mice, with or without Ang-(1-7) treatment. Basal and carbachol (CCh)-induced cGMP production was significantly increased in Ang-(1-7)-treated apoE (−/−) ($n = 4$) mice, compared with untreated apoE (−/−) mice ($n = 4$). Exogenous NO (IBMX + NO) was provided by DEA-NO (100 μM). Data represent means ± SEM; *$P < 0.05$, **$P < 0.01$ versus apoE (−/−), Student's t-test. (B) Urinary excretion (over 24 h) of nitric/nitrate (NO_x) in apoE (+/+) ($n = 14$), Ang-(1-7)-treated apoE (+/+) ($n = 8$), apoE (−/−) ($n = 7$) and Ang-(1-7)-treated apoE (−/−) ($n = 7$) mice. Ang-(1-7) treatment significantly increased NO_x excretion in apoE (−/−) mice. *$P < 0.05$ versus apoE (+/+), #$P < 0.01$, versus apoE (−/−). ‡$P < 0.05$ versus apoE (+/+) [Ang-(1-7)]. Kruskal–Wallis test followed by Mann–Whitney U-test. (C) Relative expression of eNOS mRNA, respectively, in relation to GAPDH mRNA in isolated preglomerular arteries of apoE (+/+) ($n = 12$), Ang-(1-7)-treated apoE (+/+) ($n = 4$), apoE (−/−) ($n = 9$) and Ang-(1-7)-treated apoE (−/−) ($n = 9$) measured by quantitative real-time PCR. *$P < 0.05$, **$P < 0.01$ versus apoE (+/+), #$P < 0.05$, versus apoE (−/−), ‡$P < 0.01$ versus apoE (+/+) [Ang-(1-7)]. Kruskal–Wallis test followed by Mann–Whitney U-test. (D) representative immunoblots of renal cortical eNOS and phosphorylated eNOS in samples from apo (−/−) and Ang-(1-7)-treated apoE (−/−) mice. Ang-(1-7) treatment significantly increased eNOS protein levels ($n = 4$), expressed as eNOS/β-actin levels, but did not change the ratio between phosphorylated eNOS and total eNOS levels in apoE (−/−) mice ($n = 4$). *$P < 0.05$ versus apoE (−/−). Kruskal–Wallis test followed by Mann–Whitney U-test. Ang, angiotensin; apoE, apolipoproteinE; IBMX, 3-isobutyl-1-methylxanthine; NO, nitric oxide.

animals or the tail-cuff method for measuring blood pressure which has its limitation in detecting small blood pressure differences.

The most striking finding of the present study was that chronic treatment with Ang-(1-7) restored endothelial function in isolated kidneys from apoE (−/−) mice. This effect seems to be exclusively mediated by activation of Mas receptors as D-Ala-Ang-(1-7), a specific Mas receptor antagonist, abolished the beneficial effect of Ang-(1-7) on endothelium-dependent vasorelaxation in kidneys of apoE (−/−) mice. This observation would discount effects of Ang-(1-7) on other possible targets such as ACE and the AT_1 receptor (Stegbauer

$et~al.$, 2003; Stegbauer $et~al.$, 2004). Moreover, effects of Ang-(1-7) treatment on renal AT_{1A} receptor expression levels could also be excluded, although Mas receptor-deficient mice have increased renal AT_1 receptor expression levels (Pinheiro $et~al.$, 2009). Additionally, chronic Ang-(1-7) treatment did not have any effects on blood pressure in apoE (−/−) mice and, in our study, we could not find any difference in blood pressure between any of the experimental groups. This observation is not surprising and might be related to the genetic background (Rabelo $et~al.$, 2008). Furthermore, it should be noted that Ang-(1-7) seems to be effective in reducing blood pressures in animal models of severe hypertension (Rentzsch
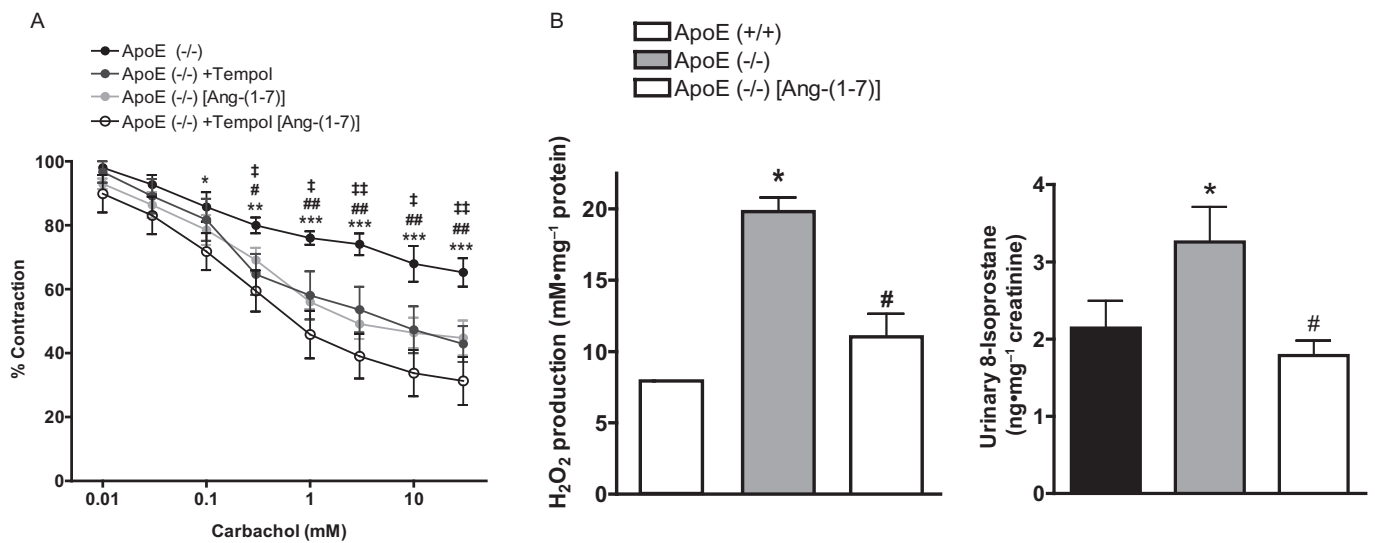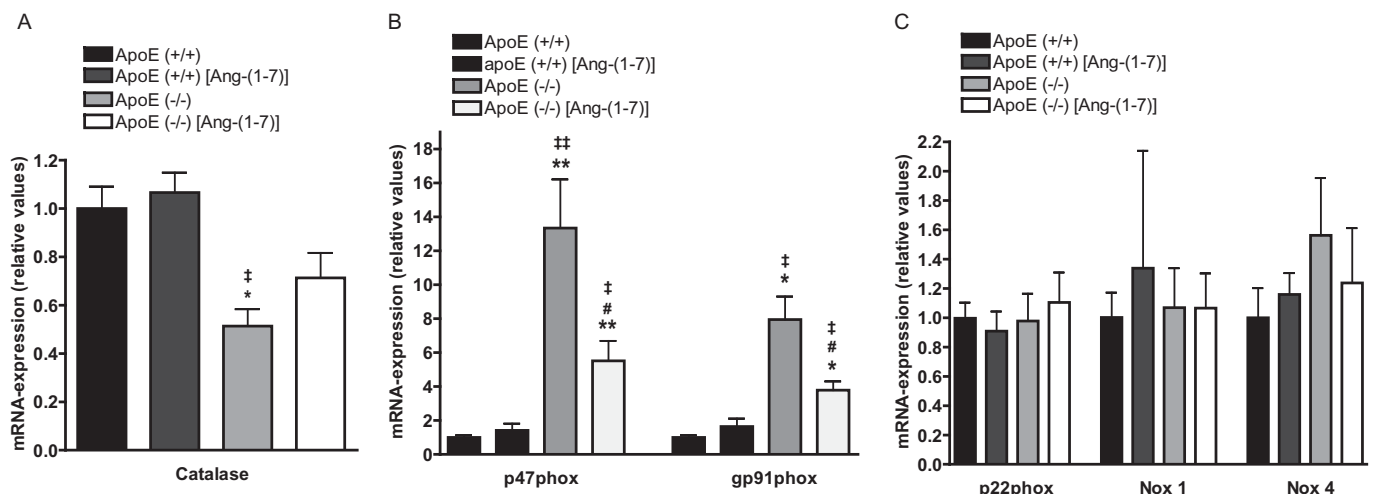
Figure 3

(A) carbachol-induced endothelial-dependent vasorelaxation was impaired in kidneys of apoE (−/−) mice (n = 7). In the presence of tempol (1 mM), endothelial-dependent vasorelaxation improved in kidneys of apoE (−/−) mice (n = 5). No additional effect of tempol on carbachol-induced vasorelaxation was observed in kidneys of Ang-(1-7)-treated apoE (−/−) mice (n = 6). Data represent means $\pm$ SEM; *$P < 0.05$, **$P < 0.01$, ***$P < 0.001$ versus apoE (−/−) + tempol [Ang-(1-7)]. #$P < 0.05$, ##$P < 0.01$ versus apoE (−/−) [Ang-(1-7)]. ‡$P < 0.05$, ‡‡$P < 0.01$ versus apoE (−/−) + tempol. One-way ANOVA for repeated measurements followed by Student's t test. (B) H_2O_2 production in renal cortex of apoE (+/+) (n = 9), apoE (−/−) (n = 7) and Ang-(1-7)-treated apoE (−/−) (n = 9) was measured using the Amplex Red assay. H_2O_2 production was increased in renal cortex of apoE (−/−) compared with apoE (+/+) mice. Ang-(1-7) treatment significantly decreased H_2O_2 production in apoE (−/−) mice. The fluorescence values were normalized to protein content in the tissue probes. Urinary 8-isoprostane levels (over 24 h) were measured in apoE (+/+) (n = 16), apoE (−/−) (n = 10) and Ang-(1-7)-treated apoE (−/−) mice (n = 9). Urinary 8-isoprostane levels were increased in apoE (−/−) mice compared with apoE (+/+). Chronic Ang-(1-7) treatment reduced urinary 8-isoprostane levels significantly. Data represent means $\pm$ SEM; *$P < 0.01$ versus apoE (+/+), #$P < 0.01$ versus apoE (−/−). Kruskal–Wallis test followed by Mann–Whitney U-test. Ang, angiotensin; apoE, apolipoproteinE.

Figure 4

Relative expression of catalase (A), gp91phox (B), p47phox (B), Nox1 (C), Nox4 (C) and p22phox (C) mRNA, respectively, in relation to GAPDH mRNA in isolated preglomerular arteries of apoE (+/+) (n = 12), Ang-(1-7)-treated apoE (+/+) (n = 4), apoE (−/−) (n = 11) and Ang-(1-7)-treated apoE (−/−) (n = 11) measured by quantitative PCR. *$P < 0.05$, **$P < 0.01$ versus apoE (+/+). #$P < 0.05$ versus apoE (−/−), ‡$P < 0.05$, ‡‡$P < 0.01$ versus apoE (+/+) [Ang-(1-7)]. Kruskal–Wallis test followed by Mann–Whitney U-test. Ang, angiotensin; apoE, apolipoproteinE.

et al., 2008) but this effect appears to be limited in normotensive animals (Gomes et al., 2010).

The beneficial effect of Ang-(1-7) treatment in our experiments seems to be restricted to endothelial cells, as a direct vasodilatory effect of Ang-(1-7) on smooth muscle cells could be ruled out as renal vasorelaxation induced by exogenous NO was similar in kidneys of wild type, apoE (−/−) and Ang-(1-7)-treated apoE (−/−) mice. In line with these results,

Lovren *et al*. (2008) demonstrated that ACE2 over-expression leading to increased Ang-(1-7) generation, protects the endothelium in apoE (–/–) mice and therefore attenuates the development of atherosclerosis. Additionally, improved endothelial function in Ang-(1-7)-treated apoE (–/–) seemed to be independent of lipid status, as no changes in the lipid profile were observed after Ang-(1-7) treatment in apoE (–/–) mice. However, Mas receptor-deficient mice on the FVB background do show increased serum triglyceride and cholesterol levels (Santos *et al*., 2008).

Endothelial dysfunction results from decreased levels of NO. Therefore, we investigated whether Ang-(1-7) increased NO production or decreased NO degradation. Renal basal cGMP levels as well as urinary excretion of NO metabolites were increased in Ang-(1-7)-treated mice, showing direct evidence for increased NO bioavailability after Ang-(1-7) treatment in apoE (–/–) mice. Recent studies showed that ROS are increased in the vascular bed of apoE (–/–) mice (Doran *et al*., 2007) and therefore are in part responsible for NO degradation. Tempol, a ROS scavenger, improved endothelium-dependent renal vasorelaxation in these mice. Interestingly, no additional effect of tempol was observed in Ang-(1-7)-treated mice, indicating that Ang-(1-7) administration similarly reduced ROS production (Polizio *et al*., 2007). However, tempol can decrease blood pressure and induce vasorelaxation in an O_2-/NO-independent mechanism (Xu *et al*., 2004). Thus, a direct impact of Ang-(1-7) treatment on ROS production was confirmed by H_2O_2 measurements in renal cortex, revealing a decreased H_2O_2 amount in Ang-(1-7)-treated mice compared with untreated apoE (–/–) mice. In line with these results, aortas of Mas receptor-deficient mice, which are characterized by pronounced endothelial dysfunction, showed increased ROS production (Peiro *et al*., 2007; Xu *et al*., 2008). ROS include superoxide anions, hydrogen peroxide or hydroxyl radicals, and they are generated by NAD(P)H oxidases which are detectable in all vascular layers. Membrane bound gp91phox (Nox2) and cytosolic p47phox NAD(P)H oxidase subunits were markedly increased in preglomerular arteries of apoE (–/–) mice and decreased by Ang-(1-7) treatment. However, there were no changes in Nox1, Nox4 and p22phox, under our conditions. Ang-(1-7)-mediated reduction of NAD(P)H activity and NAD(P)H oxidase expression was recently demonstrated in kidney homogenates of diabetic spontaneous hypertensive rats (Benter *et al*., 2008). Moreover, increased Gp91phox expression was also detected in isolated aortas of Mas receptor-deficient mice (Xu *et al*., 2008).

Beside an increased ROS production, ROS degradation seems to be diminished in apoE (–/–) mice (t Hoen *et al*., 2003). Thus, it has been shown that catalase expression, responsible for the conversion of H_2O_2 to H_2O, was decreased. In our experiments in preglomerular arteries, a reduced catalase expression was also detectable, but chronic Ang-(1-7) treatment did not significantly affect catalase expression levels. Hence, in apoE (–/–) mice, Ang-(1-7) seems to reduce ROS levels by decreasing expression of NAD(P)H subunits but not by increasing ROS clearance.

On the other hand, improved NO bioavailability observed after chronic Ang-(1-7) treatment could result not only from decreased NO degradation but also from increased NO synthesis compared with untreated apoE (–/–) mice. Therefore,

we measured eNOS mRNA expression in preglomerular vessels. Endothelial NOS expression was decreased in apoE (–/–) mice and chronic administration of Ang-(1-7) led to a significant increase of eNOS mRNA expression in preglomerular vessels of apo (–/–) mice (Sampaio *et al*., 2007b). Concordant with mRNA measurements, chronic Ang-(1-7) treatment increased renal protein levels of total eNOS in apoE (–/–) mice. The present findings are consistent with findings in Mas receptor-deficient mice, showing decreased total eNOS expression levels. Moreover, activation of Mas receptors induced by Ang-(1-7) improved endothelial function through the facilitation of NO release *in vitro* (Peiro *et al*., 2007; Sampaio *et al*., 2007a). Interestingly, chronic Ang-(1-7) treatment did not influence the ratio between phosphorylated and total eNOS expression levels. These results indicate that chronic Ang-(1-7) treatment in apoE (–/–) mice increased total eNOS expression and, by the preservation of the ratio between phosphorylated and total eNOS, also increased the absolute amount of phosphorylated eNOS, leading to an increased NO/cGMP production in these mice. In contrast to the present study, Costa *et al*. found that acute Ang-(1-7) infusion increased both cardiac eNOS expression and the phosphorylation of eNOS in spontaneous hypertensive rats (Costa *et al*., 2010).

In summary, the present study clearly demonstrated that Ang-(1-7) application had a major effect on vascular function in a well-established mouse model of human cardiovascular disease. Ang-(1-7) increased NO bioavailability by sustained influence on the balance of NO generation and degradation. This beneficial action seems to be mediated by activation of Mas receptors. Thus, Ang-(1-7) may have the potential to be an effective therapeutic agent to reduce cardiovascular morbidity and mortality. Most likely, these effects are related to long-lasting beneficial effects on the endothelium rather than cute effects of Ang-(1-7) administration. The underlying molecular mechanism(s) of the Ang-(1-7)-mediated effects still remain to be established. Furthermore, it will be very interesting to investigate the effects of chronic Ang-(1-7) treatment on the progression of atherosclerosis in this animal model.

Acknowledgements

Conflict of interest

None.

References

Alexander, SPH, Mathie, A, Peters, JA (2009). Guide to Receptors and Channels (GRAC), 4th Edition. Br J Pharmacol 158 (Suppl. 1): S1–254.

Arruda RM, Peotta VA, Meyrelles SS, Vasquez EC (2005). Evaluation of vascular function in apolipoprotein E knockout mice with angiotensin-dependent renovascular hypertension. Hypertension 46: 932–936.

Benter IF, Yousif MH, Dhaunsi GS, Kaur J, Chappell MC, Diz DI (2008). Angiotensin-(1-7) prevents activation of NADPH oxidase and renal vascular dysfunction in diabetic hypertensive rats. Am J Nephrol 28: 25–33.

Brooker G, Harper JF, Terasaki WL, Moylan RD (1979). Radioimmunoassay of cyclic AMP and cyclic GMP. Adv Cyclic Nucleotide Res 10: 1–33.

Cai H, Harrison DG (2000). Endothelial dysfunction in cardiovascular diseases: the role of oxidant stress. Circ Res 87: 840–844.

Castro CH, Santos RA, Ferreira AJ, Bader M, Alenina N, Almeida AP (2005). Evidence for a functional interaction of the angiotensin-(1-7) receptor Mas with AT1 and AT2 receptors in the mouse heart. Hypertension 46: 937–942.

Costa MA, Lopez Verrilli MA, Gomez KA, Nakagawa P, Pena C, Arranz C et al. (2010). Angiotensin-(1-7) upregulates cardiac nitric oxide synthase in spontaneously hypertensive rats. Am J Physiol Heart Circ Physiol 299: H1205–H1211.

Custodis F, Baumhakel M, Schlimmer N, List F, Gensch C, Bohm M et al. (2008). Heart rate reduction by ivabradine reduces oxidative stress, improves endothelial function, and prevents atherosclerosis in apolipoprotein E-deficient mice. Circulation 117: 2377–2387.

Doran DE, Weiss D, Zhang Y, Griendling KK, Taylor WR (2007). Differential effects of AT1 receptor and Ca2+ channel blockade on atherosclerosis, inflammatory gene expression, and production of reactive oxygen species. Atherosclerosis 195: 39–47.

d'Uscio LV, Baker TA, Mantilla CB, Smith L, Weiler D, Sieck GC et al. (2001). Mechanism of endothelial dysfunction in apolipoprotein E-deficient mice. Arterioscler Thromb Vasc Biol 21: 1017–1022.

Faria-Silva R, Duarte FV, Santos RA (2005). Short-term angiotensin(1-7) receptor MAS stimulation improves endothelial function in normotensive rats. Hypertension 46: 948–952.

Ferrario CM, Chappell MC, Dean RH, Iyer SN (1998). Novel angiotensin peptides regulate blood pressure, endothelial function, and natriuresis. J Am Soc Nephrol 9: 1716–1722.

Gomes ER, Lara AA, Almeida PW, Guimaraes D, Resende RR, Campagnole-Santos MJ et al. (2010). Angiotensin-(1-7) prevents cardiomyocyte pathological remodeling through a nitric oxide/guanosine 3',5'-cyclic monophosphate-dependent pathway. Hypertension 55: 153–160.

Grobe JL, Mecca AP, Lingis M, Shenoy V, Bolton TA, Machado JM et al. (2007). Prevention of angiotensin II-induced cardiac remodeling by angiotensin-(1-7). Am J Physiol Heart Circ Physiol 292: H736–H742.

Hartley CJ, Reddy AK, Madala S, Martin-McNulty B, Vergona R, Sullivan ME et al. (2000). Hemodynamic changes in apolipoprotein E-knockout mice. Am J Physiol Heart Circ Physiol 279: H2326–H2334.

t Hoen PA, Van der Lans CA, Van Eck M, Bijsterbosch MK, Van Berkel TJ, Twisk J (2003). Aorta of ApoE-deficient mice responds to atherogenic stimuli by a prelesional increase and subsequent decrease in the expression of antioxidant enzymes. Circ Res 93: 262–269.

Iusuf D, Henning RH, van Gilst WH, Roks AJ (2008). Angiotensin-(1-7): pharmacological properties and pharmacotherapeutic perspectives. Eur J Pharmacol 585: 303–312.

Kostenis E, Milligan G, Christopoulos A, Sanchez-Ferrer CF, Heringer-Walther S, Sexton PM et al. (2005). G-protein-coupled receptor Mas is a physiological antagonist of the angiotensin II type 1 receptor. Circulation 111: 1806–1813.

Laursen JB, Boesgaard S, Trautner S, Rubin I, Poulsen HE, Aldershvile J (2001). Endothelium-dependent vasorelaxation in inhibited by in vivo depletion of vascular thiol levels: role of endothelial nitric oxide synthase. Free Radic Res 35: 387–394.

Loot AE, Roks AJ, Henning RH, Tio RA, Suurmeijer AJ, Boomsma F et al. (2002). Angiotensin-(1-7) attenuates the development of heart failure after myocardial infarction in rats. Circulation 105: 1548–1550.

Lovren F, Pan Y, Quan A, Teoh H, Wang G, Shukla PC et al. (2008). Angiotensin converting enzyme-2 confers endothelial protection and attenuates atherosclerosis. Am J Physiol Heart Circ Physiol 295: H1377–H1384.

Mehta PK, Griendling KK (2007). Angiotensin II cell signaling: physiological and pathological effects in the cardiovascular system. Am J Physiol Cell Physiol 292: C82–C97.

Mercure C, Yogi A, Callera GE, Aranha AB, Bader M, Ferreira AJ et al. (2008). Angiotensin(1-7) blunts hypertensive cardiac remodeling by a direct effect on the heart. Circ Res 103: 1319–1326.

Osada J, Joven J, Maeda N (2000). The value of apolipoprotein E knockout mice for studying the effects of dietary fat and cholesterol on atherogenesis. Curr Opin Lipidol 11: 25–29.

Patzak A, Steege A, Lai EY, Brinkmann JO, Kupsch E, Spielmann N et al. (2008). Angiotensin II response in afferent arterioles of mice lacking either the endothelial or neuronal isoform of nitric oxide synthase. Am J Physiol Regul Integr Comp Physiol 294: R429–R437.

Peiro C, Vallejo S, Gembardt F, Azcutia V, Heringer-Walther S, Rodriguez-Manas L et al. (2007). Endothelial dysfunction through genetic deletion or inhibition of the G protein-coupled receptor Mas: a new target to improve endothelial function. J Hypertens 25: 2421–2425.

Pinheiro SV, Ferreira AJ, Kitten GT, da Silveira KD, da Silva DA, Santos SH et al. (2009). Genetic deletion of the angiotensin-(1-7) receptor Mas leads to glomerular hyperfiltration and microalbuminuria. Kidney Int 75: 1184–1193.

Polizio AH, Gironacci MM, Tomaro ML, Pena C (2007). Angiotensin-(1-7) blocks the angiotensin II-stimulated superoxide production. Pharmacol Res 56: 86–90.

Rabelo LA, Xu P, Todiras M, Sampaio WO, Buttgereit J, Bader M et al. (2008). Ablation of angiotensin (1-7) receptor Mas in C57Bl/6 mice causes endothelial dysfunction. J Am Soc Hypertens 2: 418–424.

Rentzsch B, Todiras M, Iliescu R, Popova E, Campos LA, Oliveira ML et al. (2008). Transgenic angiotensin-converting enzyme 2 overexpression in vessels of SHRSP rats reduces blood pressure and improves endothelial function. Hypertension 52: 967–973.

Sampaio WO, Henrique de Castro C, Santos RA, Schiffrin EL, Touyz RM (2007a). Angiotensin-(1-7) counterregulates angiotensin II signaling in human endothelial cells. Hypertension 50: 1093–1098.

Sampaio WO, Souza dos Santos RA, Faria-Silva R, da Mata Machado LT, Schiffrin EL, Touyz RM (2007b). Angiotensin-(1-7) through receptor Mas mediates endothelial nitric oxide synthase activation via Akt-dependent pathways. Hypertension 49: 185–192.

Santos RA, Simoes e Silva AC, Maric C, Silva DM, Machado RP, de Buhr I *et al.* (2003). Angiotensin-(1-7) is an endogenous ligand for the G protein-coupled receptor Mas. Proc Natl Acad Sci U S A 100: 8258–8263.

Santos SH, Fernandes LR, Mario EG, Ferreira AV, Porto LC, Alvarez-Leite JI *et al.* (2008). Mas deficiency in FVB/N mice produces marked changes in lipid and glycemic metabolism. Diabetes 57: 340–347.

Stegbauer J, Vonend O, Oberhauser V, Rump LC (2003). Effects of angiotensin-(1-7) and other bioactive components of the renin-angiotensin system on vascular resistance and noradrenaline release in rat kidney. J Hypertens 21: 1391–1399.

Stegbauer J, Oberhauser V, Vonend O, Rump LC (2004). Angiotensin-(1-7) modulates vascular resistance and sympathetic neurotransmission in kidneys of spontaneously hypertensive rats. Cardiovasc Res 61: 352–359.

Stegbauer J, Vonend O, Habbel S, Quack I, Sellin L, Gross V *et al.* (2005). Angiotensin II modulates renal sympathetic neurotransmission through nitric oxide in AT2 receptor knockout mice. J Hypertens 23: 1691–1698.

Wassmann S, Czech T, van Eickels M, Fleming I, Bohm M, Nickenig G (2004). Inhibition of diet-induced atherosclerosis and endothelial dysfunction in apolipoprotein E/angiotensin II type 1A receptor double-knockout mice. Circulation 110: 3062–3067.

Xu H, Fink GD, Galligan JJ (2004). Tempol lowers blood pressure and sympathetic nerve activity but not vascular O2- in DOCA-salt rats. Hypertension 43: 329–334.

Xu P, Costa-Goncalves AC, Todiras M, Rabelo LA, Sampaio WO, Moura MM *et al.* (2008). Endothelial dysfunction and elevated blood pressure in MAS gene-deleted mice. Hypertension 51: 574–580.

Hypertension
JOURNAL OF THE AMERICAN HEART ASSOCIATION

American Heart Association®

Angiotensin-(1−7) Modulates Renal Vascular Resistance Through Inhibition of p38 Mitogen-Activated Protein Kinase in Apolipoprotein E −Deficient Mice
Sebastian A. Potthoff, Michael Fähling, Tilman Clasen, Susanne Mende, Bassam Ishak, Tatsiana Suvorava, Stefanie Stamer, Manuel Thieme, Sema H. Sivritas, Georg Kojda, Andreas Patzak, Lars C. Rump and Johannes Stegbauer

The online version of this article, along with updated information and services, is located on the World Wide Web at:

http://hyper.ahajournals.org/content/early/2013/11/04/HYPERTENSIONAHA.113.02289

Data Supplement (unedited) at:

http://hyper.ahajournals.org/content/suppl/2013/11/04/HYPERTENSIONAHA.113.02289.DC1.html

Original Article

Angiotensin-(1–7) Modulates Renal Vascular Resistance Through Inhibition of p38 Mitogen-Activated Protein Kinase in Apolipoprotein E–Deficient Mice

Sebastian A. Potthoff, Michael Fähling, Tilman Clasen, Susanne Mende, Bassam Ishak, Tatsiana Suvorava, Stefanie Stamer, Manuel Thieme, Sema H. Sivritas, Georg Kojda, Andreas Patzak, Lars C. Rump, Johannes Stegbauer

Abstract—Apolipoprotein E–deficient (apoE(−/−)) mice fed on Western diet are characterized by increased vascular resistance and atherosclerosis. Previously, we have shown that chronic angiotensin (Ang)-(1–7) treatment ameliorates endothelial dysfunction in apoE(−/−) mice. However, the mechanism of Ang-(1–7) on vasoconstrictor response to Ang II is unknown. To examine Ang-(1–7) function, we used apoE(−/−) and wild-type mice fed on Western diet that were treated via osmotic minipumps either with Ang-(1–7) (82 µg/kg per hour) or saline for 6 weeks. We show that Ang II–induced renal pressor response was significantly increased in apoE(−/−) compared with wild-type mice. This apoE(−/−)-specific response is attributed to reactive oxygen species–mediated p38 mitogen–activated protein kinase activation and subsequent phosphorylation of myosin light chain (MLC_{20}), causing renal vasoconstriction. Here, we provide evidence that chronic Ang-(1–7) treatment attenuated the renal pressor response to Ang II in apoE(−/−) mice to wild-type levels. Ang-(1–7) treatment significantly decreased renal inducible nicotinamide adenine dinucleotide phosphate subunit p47phox levels and, thus, reactive oxygen species production that in turn causes decreased p38 mitogen-activated protein kinase activity. The latter has been confirmed by administration of a specific p38 mitogen-activated protein kinase inhibitor SB203580 (5 µmol/L), causing a reduced renal pressor response to Ang II in apoE(−/−) but not in apoE(−/−) mice treated with Ang-(1–7). Moreover, Ang-(1–7) treatment had no effect in Mas(−/−)/apoE(−/−) double-knockout mice confirming the specificity of Ang-(1–7) action through the Mas-receptor. In summary, Ang-(1–7) modulates vascular function via Mas-receptor activation that attenuates pressor response to Ang II in apoE(−/−) mice by reducing reactive oxygen species–mediated p38 mitogen-activated protein kinase activity. (*Hypertension*. 2014;63:00-00.) ● Online Data Supplement

Key Words: angiotensin-(1–7) ■ apolipoprotein E ■ p38 mitogen-activated protein kinase

The increasing prevalence of obesity represents a significant health burden in modern societies. It significantly contributes to the cardiovascular morbidity and mortality.[1] Hypercholesterolemia, atherosclerosis, and hypertension are common in obese subjects. Atherosclerosis and hypertension are characterized by increased reactive oxygen species (ROS) production, affecting vascular smooth muscle cell migration and proliferation, and, therefore, play a pivotal role in their pathogenesis.[2,3]

Apolipoprotein E–deficient mice (apoE(−/−)), an animal model of severe hypercholesterolemia, are prone to atherosclerosis and are characterized by severe vascular dysfunction.[4,5] This is accompanied by increased vasoconstrictor response to angiotensin II (Ang II).[6] This development can be drastically accelerated by a high-fat Western diet.[7]

Angiotensin II, the main effector of the renin–angiotensin system, contributes to the development of impaired vascular function in apoE(−/−) mice.[8] Deficiency of the angiotensin II type 1A receptor (AT1aR) in apoE(−/−) mice ameliorates atherosclerosis and endothelial dysfunction, highlighting the importance of the renin–angiotensin system in the pathogenesis of vascular injury.[9,10]

Recent studies indicate that p38 mitogen-activated protein kinase (MAPK) activation is involved in increased Ang II–dependent vasoconstriction. Inhibition of p38 MAPK has been shown to improve endothelial function and decrease Ang II–dependent vasoconstriction.[11–13] Ang II activates the p38 MAPK through increased ROS generation in vitro.[14,15] p38 MAPK activation is thought to be a calmodulin-/calcium-independent pathway of Ang II–mediated vasoconstriction. Activation of p38 MAPK through phosphorylation enhances Ang II–dependent phosphorylation of the myosin light chain (MLC_{20}), thus increasing contractile response.[16]

© 2013 American Heart Association, Inc.

Besides Ang II as the main classical effector of the renin–angiotensin system, Ang-(1–7) has been shown to play a significant role in physiological and pathological states.[17–19] The heptapeptide Ang-(1–7) is derived from Ang I or Ang II by several peptidases, including the carboxypeptidases angiotensin-converting enzyme (ACE) and ACE2.[20] However, the generation of Ang-(1–7) from Ang II by ACE2 seems to be the preferred pathway. In fact, deletion of ACE2 accentuates atherosclerosis in apoE(−/−) mice, which is contributed to decreased Ang-(1–7) formation.[21] Ang-(1–7) acts through its own receptor called Mas. Previously it has been shown that atherogenesis in apoE(−/−) mice can be inhibited by pharmacological Mas activation.[22] Mas-deficient mice show increased nicotinamide adenine dinucleotide phosphate (NADPH) oxidase activity, leading to endothelial dysfunction and strain-dependent hypertension through an increase in ROS abundance.[23]

Previously, we and others have shown that chronic Ang-(1–7) treatment ameliorates endothelial dysfunction in apoE(−/−) mice on a high-fat diet.[24,25] However, the effect of Ang-(1–7) on vasoconstrictor response to Ang II is yet unknown. Therefore, the aim of the present study was to examine whether chronic Ang-(1–7) treatment affects the renal vasoconstrictor response to Ang II in apoE(−/−). Furthermore, we examined the effect of Ang-(1–7) treatment on p38 MAPK activity and ROS abundance in these animals. To confirm that Ang-(1–7) mediates its effects through the Mas-receptor, we performed additional experiments in Mas(−/−)/apoE(−/−) double-knockout mice.

Methods

Animal Care

Wild-type (WT), apoE(−/−), and Mas(−/−)/apoE(−/−) mice were obtained from an in-house breed at the local animal care facility. Mice were on a C57Bl/6j background. Littermates were used as controls. The animals were housed in type III Makrolon polycarbonate cages at 45% humidity, 20°C to 22°C temperature and a 12-hour day and night cycle with free access to water and food.

The investigations were conducted to the Guide for Care and Use of Laboratory Animals published by the US National Institutes of Health (Publication No. 85-23, revised 1996). Detailed Materials and Methods are available in the online-only Supplement.

Results

Six-week-old WT (group 1), apoE(−/−) (groups 2–4), and Mas(−/−)/apoE(−/−) double-knockout (groups 5 and 6) mice were fed a high fat, cholesterol-enriched diet. After 6 weeks, apoE(−/−) mice (groups 2 and 3) were treated with either saline or Ang-(1–7) (82 µg/kg per hour) via osmotic minipumps subcutaneously, as described previously.[24] Another

group of apoE(−/−) mice was treated with a p38 MAPK inhibitor (BIRB796, 50 mg/kg per day) from the age of 6 weeks (group 4). In addition, Mas(−/−)/apoE(−/−) double-knockout mice (groups 5 and 6) were treated as groups 2 and 3. In all groups, osmotic minipumps were replaced after 3 weeks.

No significant differences were observed in blood pressure and lipid profile between Ang-(1–7)–treated and untreated apoE(−/−) mice after 12 weeks of high-fat diet. Interestingly, in Mas(−/−)/apoE(−/−) double-knockout mice, cholesterol levels were significantly higher when compared with the Ang-(1–7)–treated double-knockout group. Untreated Mas(−/−)/apoE(−/−) double-knockout mice also showed a higher level of triglycerides compared with the WT control group (Table).

Chronic Ang-(1–7) Treatment Ameliorates Increased Pressor Response to Ang II in ApoE(−/−)

To evaluate the influence of Ang-(1–7) treatment on Ang II–induced pressor response in renal resistance vessels of apoE(−/−) mice, kidneys were isolated and perfused as described previously.[26] Renal pressor response to Ang II was significantly increased in apoE(−/−) compared with WT mice. Interestingly, chronic treatment with Ang-(1–7) attenuates renal pressor response significantly (Figure 1A; Emax: WT, 114.2±6.1 mm Hg; apoE(−/−), 149.6±4.7 mm Hg; apoE+Ang-(1–7), 107.6±9.3 mm Hg). In WT mice, chronic Ang-(1–7) treatment had no effect on Ang II–dependent pressor response (Figure S1 in the online-only Data Supplement). Accordingly, MLC_{20} phosphorylation (phospho-MLC_{20}), a marker for smooth muscle cell contraction, was significantly increased in untreated apoE(−/−) mice compared with WT mice. Consecutively, Ang-(1–7) treatment significantly attenuated phospho-MLC_{20} levels in apoE(−/−) mice (Figure 1B and 1C). In contrast to chronic Ang-(1–7) treatment, acute administration of Ang-(1–7) (0.1 µmol/L) had no significant effect on renal pressor response to Ang II (Figure S2). To examine a potential influence of chronic Ang-(1–7) treatment on gene expression, mRNA levels of ACE2, AT1aR, AT2R, and the Mas-receptor were determined by quantitative polymerase chain reaction. As shown in Figure S3, chronic Ang-(1–7) treatment did not influence the expression levels of these candidate genes.

Ang-(1–7) Reduces ROS Generation Through a p47phox-Dependent Mechanism

Recently, it has been reported that ROS production is increased in apoE(−/−) mice.[27] To test whether Ang-(1–7) affects ROS production, renal oxygen radical levels and

Table. Systolic Blood Pressure and Lipid Profile of Groups on High-Fat Diet at Age of 18 weeks (12 Weeks of High-Fat Diet)

Characteristics	WT	apoE(−/−)	apoE(−/−)+Ang-(1–7)	Mas(−/−)/apoE(−/−)	Mas(−/−)/apoE(−/−)+Ang-(1–7)
Systolic blood pressure, mm Hg	110±2	108±2	107±2	113±2	114±2
Cholesterol, mmol/L	4.4±1.0	34.0±2.5†	34.9±2.6†	40.5±3.4†‡	27.6±3.0†
Triglycerides. mmol/L	0.4±0.1	1.4±0.3	0.9±0.2	1.68±0.3*	1.28±0.2

Data are mean±SEM (for lipid profile: WT, n=5; apoE(−/−): n=10; apoE(−/−)+Ang-(1–7): n=9; Mas(−/−)/apoE(−/−): n=8; Mas(−/−)/apoE(−/−)+Ang-(1–7): n=10 and for blood pressure, each group: n=5). Significant differences are marked: *$P<0.05$, †$P<0.001$, group comparison vs WT. ‡$P<0.05$: Mas(−/−)/apoE(−/−) vs Mas(−/−)/apoE(−/−)+Ang-(1–7). One-way ANOVA followed by Bonferroni multiple comparison post hoc test. Ang-(1–7) indicates Angiotensin-(1–7); apoE(−/−), apolipoprotein E–deficient mice; and WT, wild type
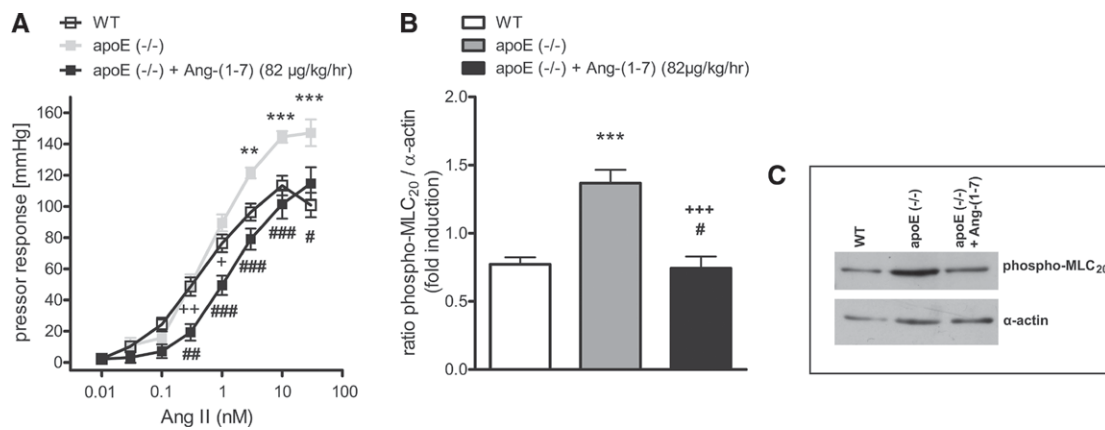
Figure 1. A, Angiotensin (Ang) II–induced pressor response is increased in kidneys of apolipoprotein E–deficient (apoE(−/−)) mice (n=14) compared with wild-type (WT) mice (n=23). Chronic Ang-(1–7) restores Ang II–induced pressor response in kidneys of apoE(−/−) to WT levels (n=9). Data represent mean±SEM. ****$P<0.01$, ***$P<0.001$: WT vs apoE(−/−). +$P<0.05$, ++$P<0.01$ WT vs apoE(−/−)+[Ang-(1–7)], #$P<0.05$, ##$P<0.01$, ###$P<0.001$ apoE(−/−) vs apoE(−/−)+Ang-(1–7). Two-way ANOVA for repeated measurements followed by Bonferroni correction post hoc test. **B**, Western blot analysis of preglomerluar vessel lysates evaluating total abundance of phospho-myosin light chain (MLC$_{20}$). WT vs apoE(−/−): 0.77±0.05 vs 1.37±0.10, ***$P<0.001$; apoE(−/−) vs apoE(−/−)+Ang-(1–7): 1.37±0.10 vs 0.74±0.09, +++$P<0.001$; WT vs apoE(−/−)+Ang-(1–7): 0.77±0.05 vs 0.74±0.09, #$P=NS$; n=8; each group. Data represents mean±SEM. One-way ANOVA followed by Bonferroni multiple comparison post hoc test. **C**, Exemplary Western blot of preglomerular vessel lysates for phospho-MLC$_{20}$.

urinary 8-isoprostane excretion were measured. As shown in Figure 2A and 2B, chronic Ang-(1–7) treatment significantly reduced urinary 8-isoprostane levels and lucigenin-enhanced chemiluminescence in renal cortex samples.

To examine the influence of Ang-(1–7) treatment on ROS production, we analyzed the expression levels of subunits of the NADPH enzyme family in renal cortex lysates. Expression of the NADPH oxidase subunit p47phox, an Ang II inducible NADPH subunit, was significantly increased in apoE(−/−) compared with WT mice.[28] Interestingly, Ang-(1–7) treatment restored p47phox expression to WT levels, suggesting that Ang-(1–7) affects ROS abundance through modulation of NADPH oxidase expression (Figure 2C).

Chronic Ang-(1–7) Treatment Improves Vascular Function by Reducing MAPK p38 Activation

To evaluate whether Ang-(1–7) reduces vascular reactivity through a p38 MAPK-mediated mechanism, we measured p38 MAPK activity in renal cortex and preglomerular resistance vessel samples. Phospho-p38/p38 ratio was increased in apoE(−/−) compared with WT mice (Figure 3A and 3B). Chronic Ang-(1–7) treatment restored the level of phospho-p38 MAPK to WT levels (Figure 3A and 3B). To confirm whether the increased p38 MAPK activation is responsible for the augmented vascular reactivity to Ang II, renal pressor response to Ang II was measured in the presence or in the absence of the specific p38 MAPK inhibitor SB203580 (5 µmol/L). In
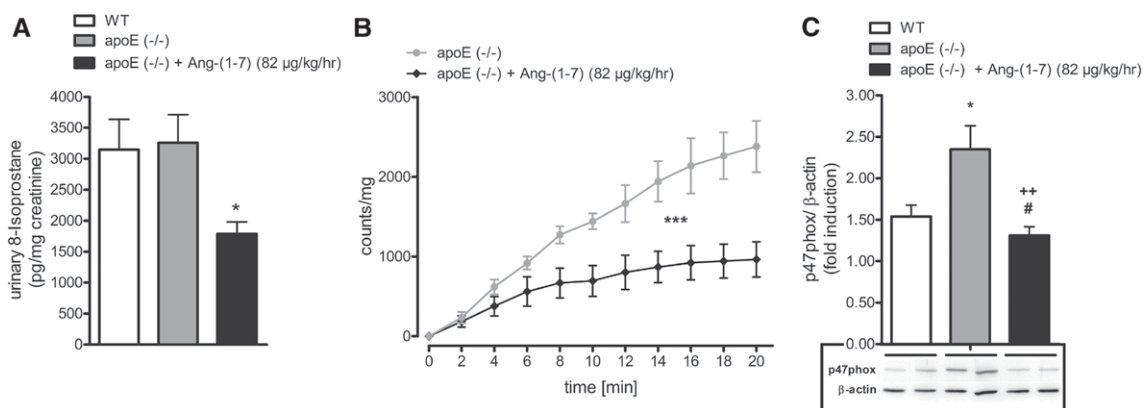

Figure 2. A, Twenty-four–hour urinary 8-isoprostane levels were measured in wild-type (WT; n=9), apolipoprotein E–deficient (apoE(−/−)) mice (n=10) and angiotensin (Ang)-(1–7)–treated apoE(−/−) mice (n=9). Urinary 8-isoprostane levels were not significantly different in apoE(−/−) when compared with WT mice. Chronic Ang-(1–7) treatment reduced urinary 8-isoprostane levels significantly. Data represent mean±SEM (*$P<0.05$). Kruskal–Wallis test followed by Dunn multiple comparison post hoc test. **B**, Lucigenin-enhanced chemiluminescence in kidney cortex tissue from apoE(−/−) mice and Ang-(1–7)–treated apoE(−/−) mice (n=4). Counts per milligram over time were significantly reduced in Ang-(1–7)–treated animals when compared with nontreated apoE(−/−) mice (two-way ANOVA analysis, group effect: *** $P<0.001$). **C**, Representative immunoblots and densitometric analysis of renal cortex lysates evaluating total abundance of nicotinamide adenine dinucleotide phosphate (NADPH) subunit p47phox in WT, apoE(−/−), and Ang-(1–7)–treated apoE(−/−) mice. WT vs apoE(−/−): 1.54±0.14 vs 2.35±0.28, *$P<0.5$; apoE(−/−) vs apoE(−/−)+Ang-(1–7): 2.35±0.28 vs 1.31±0.10, ++$P<0.01$; WT vs apoE(−/−)+Ang-(1–7): 1.54±0.14 vs 1.31±0.10, #$P=NS$; n=4; each group. Data represents mean±SEM. One-way ANOVA followed by Bonferroni multiple comparison post hoc test.

kidneys of WT mice, pressor response induced by Ang II was not significantly different with or without MAPK p38 inhibition (Figure 3C). However, in apoE(−/−) mice, pressor response to Ang II was significantly attenuated in the presence of SB203580 (5 µmol/L; Figure 3D). In contrast, acute p38 MAPK inhibition did not significantly affect Ang II–induced pressor response in apoE(−/−) mice chronically treated with Ang-(1–7), confirming the effect of Ang-(1–7) treatment on p38 MAPK-mediated vascular reactivity (Figure 3E). To evaluate whether the increased renal pressor response to Ang II is solely related to increased p38 activity, we performed additional experiments with the specific extracellular-signal-regulated

kinase (ERK) 1/2 inhibitor PD98059 (5 µmol/L). PD98059 had no effect in WT or apoE(−/−) mice (Figure S4).

Deletion of Mas-Receptor Abolishes Ang-(1–7) Effect in ApoE(−/−)

To test whether the observed effects of Ang-(1–7) were mediated by Mas-receptor activation, we generated Mas(−/−)/apoE(−/−) double-knockout mice. In Mas(−/−)/apoE(−/−) double-knockout mice, chronic Ang-(1–7) treatment did not influence renal pressor response (Figure 4A) and urinary 8-isoprostane excretion (Figure 4B). SB203580 (5 µmol/L) significantly reduced pressor responses to Ang II in kidneys of
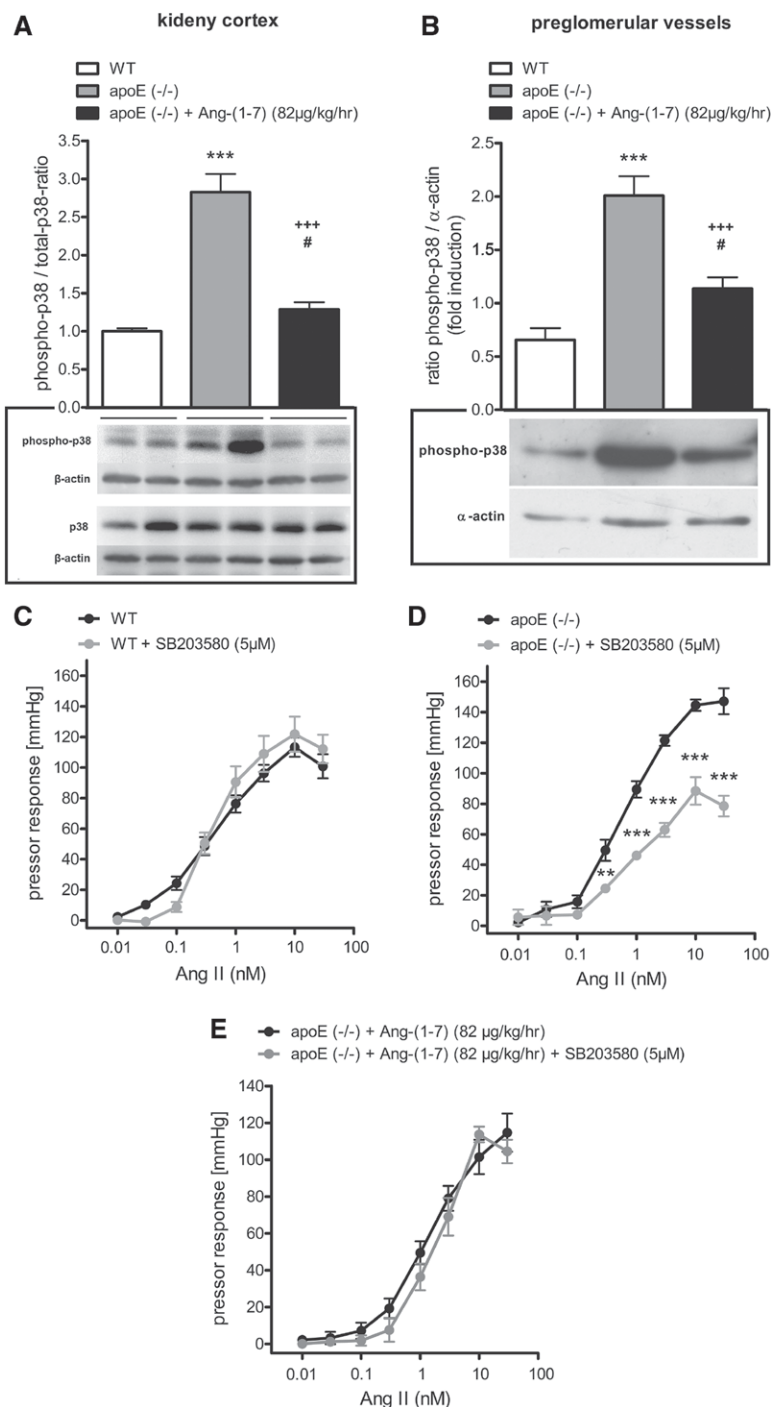

Figure 3. A, Western blot analysis of renal cortex lysates evaluating the phospho-p38/p38 mitogen-activated protein kinase (MAPK) ratio. Ratio was increased in apolipoprotein E–deficient (apoE(−/−)) mice when compared with wild-type (WT) and apoE(−/−) mice treated with angiotensin (Ang)-(1–7). WT vs apoE(−/−): 1.00±0.03 vs 2.83±0.24, *$P<0.5$; apoE(−/−) vs apoE(−/−)+Ang-(1–7): 2.83±0.24 vs 1.29±0.10, ++$P<0.01$; WT vs apoE(−/−)+Ang-(1–7): 1.00±0.03 vs 1.29±0.10, #P=NS; n=4; each group. One-way ANOVA followed by Bonferroni multiple comparison post hoc test. A representative Western blot of p38 and phospho-p38 MAPK expression in renal cortex lysates is shown. **B,** Western blot analysis of preglomerular vessel lysates evaluating total abundance of phospho-p38 MAPK. WT vs apoE(−/−): 0.65±0.11 vs 2.00±0.18, ***$P<0.001$; apoE(−/−) vs apoE(−/−)+Ang-(1–7): 2.00±0.18 vs 1.14±0.10, +++$P<0.001$; WT vs apoE(−/−)+Ang-(1–7): 0.65±0.11 vs 1.14±0.10, #P=NS; n=8; each group. Data represent mean±SEM. One-way ANOVA followed by Bonferroni multiple comparison post hoc test. **C,** Ang II–induced pressor response is not altered in the presence of the p38 MAPK inhibitor SB203580 (5 µmol/L) in kidneys of WT mice. (WT, n=23; WT+SB203580, n=14). **D,** In kidneys of apoE(−/−) mice, p38 MAPK inhibition (SB203580; 5 µmol/L) significantly attenuated Ang II–induced pressor response. (apoE(−/−), n=14; apoE(−/−)+SB203580, n=11). **E,** Pressor response to Ang II in isolated, perfused kidneys of apoE(−/−) mice treated with Ang-(1–7): p38 MAPK inhibition had no significant effect on Ang II–induced vasoconstriction (apoE(−/−)+Ang-(1–7), n=9; apoE(−/−)+Ang-(1–7)+SB203580, n=6). **C–E,** Data represents mean±SEM; (**C**) P=NS WT vs WT+SB203580; (**D**) **$P<0.01$, ***$P<0.001$: apoE(−/−) vs apoE(−/−)+SB203580; and (**E**) P=NS, apoE(−/−)+Ang-(1–7) vs apoE(−/−)+Ang-(1–7)+SB203580. Two-way ANOVA for repeated measurements followed by Bonferroni correction post hoc test.

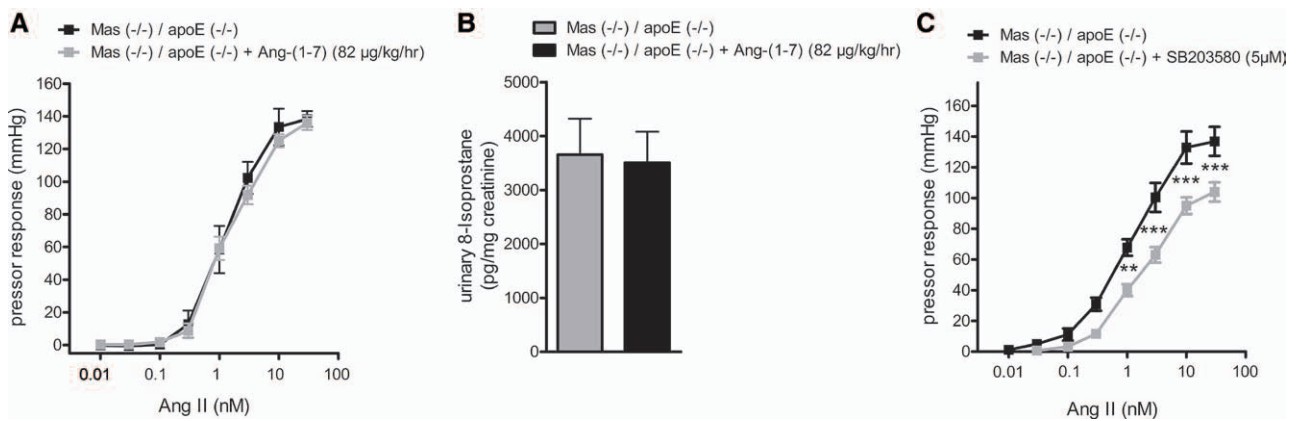**Figure 4. A**, Angiotensin (Ang) II–induced pressor response is similar in kidneys of Mas(–/–)/apoE(–/–) and Mas(–/–)/apoE(–/–)+Ang-(1–7) mice. Mas(–/–)/apoE(–/–): n=6; Mas(–/–)/apoE(–/–)+Ang-(1–7): n=8. Data represents mean±SEM (P=NS). Two-way ANOVA for repeated measurements followed by Bonferroni correction post hoc test. **B**, Twenty-four–hour urinary 8-isoprostane levels were measured in Mas(–/–)/apoE(–/–) mice (n=8) and Mas(–/–)/apoE(–/–) mice treated with Ang-(1–7) (n=10). Urinary 8-isoprostane levels were not significantly different. Data represents mean±SEM; P=NS (Mann–Whitney U test). **C**, Ang II–induced pressor response is significantly reduced in kidneys of Mas(–/–)/apoE(–/–) treated with mitogen-activated protein kinase p38-inhibitor SB203580. Mas(–/–)/apoE(–/–): n=8; Mas(–/–)/apoE(–/–)+SB203580: n=10. Data represents mean±SEM (**$P<0.01$, ***$P<0.001$). Two-way ANOVA for repeated measurements followed by Bonferroni correction post hoc test. apoE(–/–) indicates apolipoprotein E–deficient mice.

Mas(–/–)/apoE(–/–) double-knockout mice (Figure 4C) in a similar manner as seen in single apoE(–/–) mice (Figure 3D).

Chronic Inhibition of p38 MAPK Ameliorates Ang II–Dependent Vasoreactivity and Systemic Pressor Response

To elucidate whether decreased p38 MAPK activity observed in Ang-(1–7)–treated mice is causative for the reduced renal pressor response to Ang II, we tested vascular reactivity in vivo and ex vivo after chronic p38 MAPK inhibition. Therefore, apoE(–/–) mice (group 4) were fed either on an oral p38 MAPK inhibitor (BIRB796, 50 mg/kg per day) or a placebo. In acute infusion experiments (in vivo) and in isolated per-fused kidneys (ex vivo), Ang II–dependent pressor response was significantly attenuated in apoE(–/–) mice chronically treated with BIRB796 compared with placebo-treated animals (Figure 5A and 5B).

Discussion

Hypercholesterolemia is an important risk factor for vascular dysfunction, atherosclerosis, and hypertension. ApoE(–/–) mice subject to high-fat Western diet are characterized by a pronounced vascular dysfunction and rapid progression of atherosclerosis, which is a result of impaired clearance of low-density lipoprotein, leading to downregulation of ROS scavenging mechanisms.[9,24,29] In these mice, mechanisms of proper vasorelaxation and vasoconstriction are compromised because of hypercholesterolemia.[7,27,30] Previously, we showed that apoE(–/–) fed on a high-fat diet exhibit impaired endo-thelial-dependent vasorelaxation.[24] Chronic Ang-(1–7) treatment improved NO bioavailability and, therefore, ameliorated endothelial dysfunction in these mice.

In the present study, we show that pressor response to Ang II is significantly increased in apoE(–/–) renal resistance vessels compared with WT animals and that chronic Ang-(1–7) treatment abolished the elevated pressor response to Ang II. Therefore, Ang-(1–7) does not only ameliorate endothelial

dysfunction but also normalizes vasoconstriction in response to Ang II.

Ang II induces vasoconstriction through the activation of the AT1R.[31] ApoE(–/–) mice are susceptible to Ang II–induced hypertension because chronic Ang II infusion causes increased endothelial dysfunction and accelerated progression of atherosclerosis.[8] This influence is attributed to higher ROS abundance and a sustained inflammatory response in the vasculature.[9,32] Because Ang-(1–7) seems to counteract AT1R–mediated effects, it is coherent that inhibition of Ang-(1–7) generation in ACE2-deficient apoE(–/–) mice accentu-ated vascular inflammation.[21] Hence, Ang-(1–7)–mediated activation of the Mas-receptor attenuated atherogenesis in apoE(–/–) mice.[22,25,33] These studies clearly indicate a ben-eficial role of Ang-(1–7) in atherogenesis. However, little is
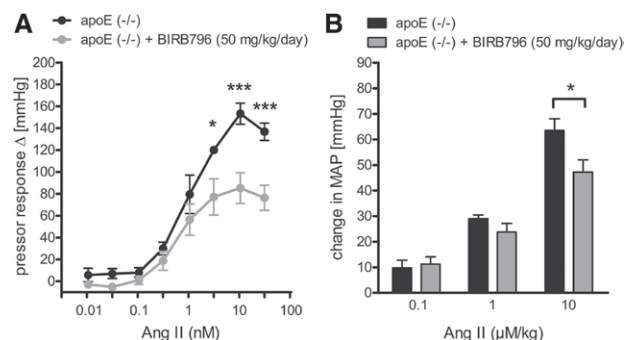

Figure 5. A, Angiotensin (Ang) II–induced pressor response is significantly higher in kidneys of placebo-treated apolipoprotein E–deficient (apoE(–/–)) mice (n=4) when compared with apoE(–/–) on an oral p38 mitogen-activated protein kinase (MAPK)-inhibitor (BIRB796; n=6). Data represent mean±SEM (*$P<0.05$, ***$P<0.001$). Two-way ANOVA for repeated measure-ments followed by Bonferroni correction post hoc test. **B**, Acute Ang II–induced increase in mean arterial pressure in acute infusion experiments is significantly lower in apoE(–/–) mice treated with an oral MAPK p38-inhibitor when compared with placebo-treated animals (n=4). Data represent mean±SEM (*$P<0.05$). Two-way ANOVA for repeated measurements followed by Bonferroni correction post hoc test.

known on changes in vascular function in apoE(−/−) mice and the effect of Ang-(1–7) treatment.

Here, we demonstrate that increased contractility in apoE(−/−) mice is accompanied by an increased phosphorylation of MLC_{20} in preglomerular resistance vessels. Higher basal MLC_{20} phosphorylation increases contraction at a given Ca2+ concentration.[34] Because the p38 MAPK/MK2-pathway causes MLC_{20} phosphorylation, and p38 MAPK is activated by ROS, inflammatory cytokines, and hypertonicity, we hypothesized that ROS-mediated activation of p38 MAPK might have a direct effect on vessel contractility by increased MLC_{20} phosphorylation.[15,16]

We show that p38 MAPK activity is significantly elevated in preglomerular resistance vessels and renal cortex of apoE(−/−) mice. Because the expression of the inducible NADPH subunit p47phox was significantly increased in apoE(−/−) mice compared with WT mice, our data indicate an increase in ROS production capability, which in turn activates p38 MAPK. p47phox is a key component of NADPH oxidase enzyme complex and plays an important role in ROS production in the vasculature.[35] Accordingly, specific markers of ROS are increased in apoE(−/−) compared with WT mice. It has been demonstrated that p47phox contributes significantly to vascular damage in apoE(−/−) mice because it is essential for the development of Ang II–dependent hypertension and atherosclerosis.[36–38] In addition, deletion of p47phox resulted in an attenuated vasoconstrictor response to Ang II and decreased ROS production.[39] In line with these observations, our data confirm that the elevated pressor response to Ang II seen in apoE(−/−) mice is caused by ROS-mediated p38 MAPK activation and subsequent MLC_{20} phosphorylation.

Accordingly, we demonstrate that acute inhibition of p38 MAPK with SB203580, as well as chronic inhibition of p38 MAPK by oral application of BIRB796, reduced pressor response to Ang II (in vivo and ex vivo). This effect was not observed using an ERK 1/2 inhibitor. Our results are in line with previous studies showing that increased p38 MAPK activity enhances vascular contractility in vitro and in vivo.[40,41]

A possible contributor counteracting the exaggerated pressor response to Ang II might be increased Ang-(1–7)–mediated NO bioavailability. However, we previously showed that Ang-(1–7) treatment cannot even closely restore NO bioavailability in apoE(−/−) as found in WT mice.[24] Recently, it has been acknowledged that Ang-(1–7) plays an important role in the control of ROS level in the renal vasculature and affects p38 MAPK signaling in pathophysiological conditions.[24,42–44] For instance, chronic Ang-(1–7) treatment improved endothelial dysfunction and attenuated the progression of atherosclerosis in apoE(−/−) mice by reducing ROS production.[24,25,33] In contrast, ACE2 deficiency causes a marked increase in oxidative stress, which has been attributed to the diminished generation of Ang-(1–7) by ACE2 deficiency as a counter regulatory mechanism to Ang II.[45] In addition, cardiac overexpression of Ang-(1–7) improved Ang II–dependent cardiac hypertrophy by reducing p38 MAPK activity.[46] Therefore, we hypothesized that other mechanisms, independent from NO, might contribute to the attenuated pressor response to Ang II seen in Ang-(1–7)–treated apoE(−/−) mice.

Here, we demonstrate that chronic Ang-(1–7) in apoE(−/−) mice reduced the abundance of phosphorylated MLC_{20} in preglomerular resistance vessels of apoE(−/−) mice. Hence, these mice showed attenuation of renal pressor response to Ang II. This was accompanied by reduced renal p38 MAPK activity in renal cortex and preglomerular resistance vessels and a reduction in ROS generation. In addition, chronic treatment with Ang-(1–7) decreased the expression of the NADPH oxidase subunit p47phox in apoE(−/−) mice and subsequently ROS generation in renal cortex samples. Thus, our study clearly indicates that chronic Ang-(1–7) application attenuated the elevated pressor response to Ang II through a ROS/p38 MAPK-dependent mechanism.

The present study cannot give a clear statement whether the effects of Ang-(1–7) are the result of immediate actions or because of the chronic treatment. However, acute Ang-(1–7) infusion did not affect Ang II–dependent pressor response in apoE(−/−) significantly and, thus, our results suggest no direct effect on p38 MAPK activity. We demonstrate that chronic Ang-(1–7) treatment reduces p47phox-dependent ROS generation and thereby decreases p38 MAPK activation to a basal level seen in WT mice. This is supported by the fact that p38 MAPK inhibition had no effect in WT mice. It has been suggested that Ang-(1–7) exerts its beneficial effects through AT2R activation or AT1R inhibition.[19,47,48] Nevertheless, there is growing evidence that Mas-receptor signaling seems to be the predominant pathway for Ang-(1–7)–mediated beneficial effects on atherosclerosis and vascular function.[25,33] In Mas(−/−)/apoE(−/−) double-knockout mice, chronic Ang-(1–7) treatment neither affected Ang II–induced pressor response nor decreased urinary 8-isoprostane excretion. These results support the importance of Mas-receptor–mediated action of Ang-(1–7) in this model and exclude any nonspecific effect or, for example, the dependency on AT2R signaling. Interestingly, cholesterol levels in untreated double-knockout mice were significantly higher when compared with Ang-(1–7)–treated mice. Because vascular function did not differ between Ang-(1–7)–treated and untreated Mas(−/−)/apoE(−/−) mice, the relevance of this finding remains unclear.

In conclusion, our experiments offer strong evidence that increased ROS-mediated p38 MAPK activity is the underlying cause for the elevated pressor response to Ang II in hypercholesterolemic apoE(−/−) mice. Chronic Ang-(1–7) treatment restores the pressor response to Ang II through a p47phox-dependent reduction of ROS. Because increased ROS is a key mechanism of p38 MAPK activation, Ang-(1–7)–mediated decrease of ROS is one of the underlying mechanisms in restoration of normal vascular function. Deficiency of the Mas-receptor abolishes any action of Ang-(1–7). This indicates the crucial role of Mas-receptor activation in this model and supports the view that the Mas-receptor could be a future target for pharmaceutical treatment in cardiovascular disease.

Perspectives

In the present study, we demonstrated that increased vasoreactivity to Ang II in renal resistance vessels of hypercholesterolemic apoE(−/−) mice is caused by an increased p38 MAPK activity. Acute and chronic inhibition of p38 MAPK inhibition in vivo and ex vivo confirms its pivotal role. In these mice, the

p38 MAPK is activated through a ROS/p47phox mechanism. This mechanism might explain the crucial role of p47phox in Ang II–dependent hypertension seen by others. However, more studies are needed to show a direct effect of tissue-specific deletion of p38 MAPK on blood pressure regulation.

In addition, our study showed that chronic Ang-(1–7) treatment attenuates the increased pressor response to Ang II by a significant reduction in ROS generation and p47phox abundance and hence attenuation of p38 MAPK activity. In this setup, for the first time, using double-knockout mice deficient of the Mas-receptor and apoE, we showed that the beneficial effects of Ang-(1–7) treatment were dependent on Mas-receptor signaling. Hence, any effects on vasoreactivity and ROS were abolished in the double-knockout mice. Therefore, the Mas-receptor seems to be a promising target for intervention in hypercholesterolemia.

Disclosures
None.

References

1. Poirier P, Giles TD, Bray GA, Hong Y, Stern JS, Pi-Sunyer FX, et al. Obesity and cardiovascular disease: pathophysiology, evaluation, and effect of weight loss: an update of the 1997 American Heart Association Scientific Statement on Obesity and Heart Disease from the Obesity Committee of the Council on Nutrition, Physical Activity, and Metabolism. *Circulation*. 2006;113:898–918.
2. Lacolley P, Regnault V, Nicoletti A, Li Z, Michel JB. The vascular smooth muscle cell in arterial pathology: a cell that can take on multiple roles. *Cardiovasc Res*. 2012;95:194–204.
3. Hopkins PN. Molecular biology of atherosclerosis. *Physiol Rev*. 2013;93:1317–1542.
4. Plump AS, Smith JD, Hayek T, Aalto-Setälä K, Walsh A, Verstuyft JG, Rubin EM, Breslow JL. Severe hypercholesterolemia and atherosclerosis in apolipoprotein E-deficient mice created by homologous recombination in ES cells. *Cell*. 1992;71:343–353.
5. Nakashima Y, Plump AS, Raines EW, Breslow JL, Ross R. ApoE-deficient mice develop lesions of all phases of atherosclerosis throughout the arterial tree. *Arterioscler Thromb*. 1994;14:133–140.
6. Arruda RM, Peotta VA, Meyrelles SS, Vasquez EC. Evaluation of vascular function in apolipoprotein E knockout mice with angiotensin-dependent renovascular hypertension. *Hypertension*. 2005;46:932–936.
7. Osada J, Joven J, Maeda N. The value of apolipoprotein E knockout mice for studying the effects of dietary fat and cholesterol on atherogenesis. *Curr Opin Lipidol*. 2000;11:25–29.
8. Weiss D, Kools JJ, Taylor WR. Angiotensin II-induced hypertension accelerates the development of atherosclerosis in apoE-deficient mice. *Circulation*. 2001;103:448–454.
9. Wassmann S, Czech T, van Eickels M, Fleming I, Böhm M, Nickenig G. Inhibition of diet-induced atherosclerosis and endothelial dysfunction in apolipoprotein E/angiotensin II type 1A receptor double-knockout mice. *Circulation*. 2004;110:3062–3067.
10. Rateri DL, Moorleghen JJ, Balakrishnan A, Owens AP 3rd, Howatt DA, Subramanian V, Poduri A, Charnigo R, Cassis LA, Daugherty A. Endothelial cell-specific deficiency of Ang II type 1a receptors attenuates Ang II-induced ascending aortic aneurysms in LDL receptor-/- mice. *Circ Res*. 2011;108:574–581.
11. Taniyama Y, Ushio-Fukai M, Hitomi H, Rocic P, Kingsley MJ, Pfahnl C, Weber DS, Alexander RW, Griendling KK. Role of p38 MAPK and MAPKAPK-2 in angiotensin II-induced Akt activation in vascular smooth muscle cells. *Am J Physiol Cell Physiol*. 2004;287:C494–C499.
12. Meloche S, Landry J, Huot J, Houle F, Marceau F, Giasson E. p38 MAP kinase pathway regulates angiotensin II-induced contraction of rat vascular smooth muscle. *Am J Physiol Heart Circ Physiol*. 2000;279:H741–H751.
13. Kwon S, Fang LH, Kim B, Ha TS, Lee SJ, Ahn HY. p38 Mitogen-activated protein kinase regulates vasoconstriction in spontaneously hypertensive rats. *J Pharmacol Sci*. 2004;95:267–272.
14. Kyaw M, Yoshizumi M, Tsuchiya K, Kirima K, Tamaki T. Antioxidants inhibit JNK and p38 MAPK activation but not ERK ½ activation by angiotensin II in rat aortic smooth muscle cells. *Hypertens Res*. 2001;24:251–261.
15. Ushio-Fukai M, Alexander RW, Akers M, Griendling KK. p38 Mitogen-activated protein kinase is a critical component of the redox-sensitive signaling pathways activated by angiotensin II. Role in vascular smooth muscle cell hypertrophy. *J Biol Chem*. 1998;273:15022–15029.
16. Patzak A, Lai EY, Fähling M, Sendeski M, Martinka P, Persson PB, Persson AE. Adenosine enhances long term the contractile response to angiotensin II in afferent arterioles. *Am J Physiol Regul Integr Comp Physiol*. 2007;293:R2232–R2242.
17. Ferrario CM, Chappell MC, Dean RH, Iyer SN. Novel angiotensin peptides regulate blood pressure, endothelial function, and natriuresis. *J Am Soc Nephrol*. 1998;9:1716–1722.
18. Stegbauer J, Vonend O, Oberhauser V, Rump LC. Effects of angiotensin-(1-7) and other bioactive components of the renin-angiotensin system on vascular resistance and noradrenaline release in rat kidney. *J Hypertens*. 2003;21:1391–1399.
19. Stegbauer J, Oberhauser V, Vonend O, Rump LC. Angiotensin-(1-7) modulates vascular resistance and sympathetic neurotransmission in kidneys of spontaneously hypertensive rats. *Cardiovasc Res*. 2004;61:352–359.
20. Iusuf D, Henning RH, van Gilst WH, Roks AJ. Angiotensin-(1-7): pharmacological properties and pharmacotherapeutic perspectives. *Eur J Pharmacol*. 2008;585:303–312.
21. Thomas MC, Pickering RJ, Tsorotes D, Koitka A, Sheehy K, Bernardi S, Toffoli B, Nguyen-Huu TP, Head GA, Fu Y, Chin-Dusting J, Cooper ME, Tikellis C. Genetic Ace2 deficiency accentuates vascular inflammation and atherosclerosis in the ApoE knockout mouse. *Circ Res*. 2010;107:888–897.
22. Toton-Zuranska J, Gajda M, Pyka-Fosciak G, Kus K, Pawlowska M, Niepsuj A, Wolkow P, Olszanecki R, Jawien J, Korbut R. AVE 0991-angiotensin-(1-7) receptor agonist, inhibits atherogenesis in apoE-knockout mice. *J Physiol Pharmacol*. 2010;61:181–183.
23. Xu P, Costa-Goncalves AC, Todiras M, Rabelo LA, Sampaio WO, Moura MM, Santos SS, Luft FC, Bader M, Gross V, Alenina N, Santos RA. Endothelial dysfunction and elevated blood pressure in MAS gene-deleted mice. *Hypertension*. 2008;51:574–580.
24. Stegbauer J, Potthoff SA, Quack I, Mergia E, Clasen T, Friedrich S, Vonend O, Woznowski M, Königshausen E, Sellin L, Rump LC. Chronic treatment with angiotensin-(1-7) improves renal endothelial dysfunction in apolipoproteinE-deficient mice. *Br J Pharmacol*. 2011;163:974–983.
25. Tesanovic S, Vinh A, Gaspari TA, Casley D, Widdop RE. Vasoprotective and atheroprotective effects of angiotensin (1-7) in apolipoprotein E-deficient mice. *Arterioscler Thromb Vasc Biol*. 2010;30:1606–1613.
26. Stegbauer J, Vonend O, Habbel S, Quack I, Sellin L, Gross V, Rump LC. Angiotensin II modulates renal sympathetic neurotransmission through nitric oxide in AT2 receptor knockout mice. *J Hypertens*. 2005;23:1691–1698.
27. d'Uscio LV, Baker TA, Mantilla CB, Smith L, Weiler D, Sieck GC, Katusic ZS. Mechanism of endothelial dysfunction in apolipoprotein E-deficient mice. *Arterioscler Thromb Vasc Biol*. 2001;21:1017–1022.
28. Ebrahimian T, Li MW, Lemarié CA, Simeone SM, Pagano PJ, Gaestel M, Paradis P, Wassmann S, Schiffrin EL. Mitogen-activated protein kinase-activated protein kinase 2 in angiotensin II-induced inflammation and hypertension: regulation of oxidative stress. *Hypertension*. 2011;57:245–254.
29. t Hoen PA, Van der Lans CA, Van Eck M, Bijsterbosch MK, Van Berkel TJ, Twisk J. Aorta of apoe-deficient mice responds to atherogenic stimuli by a prelesional increase and subsequent decrease in the expression of antioxidant enzymes. *Circ Res*. 2003;93:262–269.
30. Laursen JB, Boesgaard S, Trautner S, Rubin I, Poulsen HE, Aldershvile J. Endothelium-dependent vasorelaxation in inhibited by *in vivo* depletion of vascular thiol levels: role of endothelial nitric oxide synthase. *Free Radic Res*. 2001;35:387–394.
31. Griendling KK, Berk BC, Ganz P, Gimbrone MA Jr, Alexander RW. Angiotensin II stimulation of vascular smooth muscle phosphoinositide

metabolism. State of the art lecture. *Hypertension*. 1987;9(6 Pt 2):III181–III185.

32. Mazzolai L, Duchosal MA, Korber M, Bouzourene K, Aubert JF, Hao H, Vallet V, Brunner HR, Nussberger J, Gabbiani G, Hayoz D. Endogenous angiotensin II induces atherosclerotic plaque vulnerability and elicits a Th1 response in ApoE-/- mice. *Hypertension*. 2004;44:277–282.

33. Yang JM, Dong M, Meng X, Zhao YX, Yang XY, Liu XL, Hao PP, Li JJ, Wang XP, Zhang K, Gao F, Zhao XQ, Zhang MX, Zhang Y, Zhang C. Angiotensin-(1-7) dose-dependently inhibits atherosclerotic lesion formation and enhances plaque stability by targeting vascular cells. *Arterioscler Thromb Vasc Biol*. 2013;33:1978–1985.

34. Kim HR, Appel S, Vetterkind S, Gangopadhyay SS, Morgan KG. Smooth muscle signalling pathways in health and disease. *J Cell Mol Med*. 2008;12(6A):2165–2180.

35. Ago T, Kuroda J, Kamouchi M, Sadoshima J, Kitazono T. Pathophysiological roles of NADPH oxidase/nox family proteins in the vascular system. -Review and perspective-. *Circ J*. 2011;75:1791–1800.

36. Barry-Lane PA, Patterson C, van der Merwe M, Hu Z, Holland SM, Yeh ET, Runge MS. p47phox is required for atherosclerotic lesion progression in ApoE(-/-) mice. *J Clin Invest*. 2001;108:1513–1522.

37. Dikalova A, Clempus R, Lassègue B, Cheng G, McCoy J, Dikalov S, San Martin A, Lyle A, Weber DS, Weiss D, Taylor WR, Schmidt HH, Owens GK, Lambeth JD, Griendling KK. Nox1 overexpression potentiates angiotensin II-induced hypertension and vascular smooth muscle hypertrophy in transgenic mice. *Circulation*. 2005;112:2668–2676.

38. Landmesser U, Cai H, Dikalov S, McCann L, Hwang J, Jo H, Holland SM, Harrison DG. Role of p47(phox) in vascular oxidative stress and hypertension caused by angiotensin II. *Hypertension*. 2002;40:511–515.

39. Lai EY, Solis G, Luo Z, Carlstrom M, Sandberg K, Holland S, Wellstein A, Welch WJ, Wilcox CS. p47(phox) is required for afferent arteriolar contractile responses to angiotensin II and perfusion pressure in mice. *Hypertension*. 2012;59:415–420.

40. Yamboliev IA, Hedges JC, Mutnick JL, Adam LP, Gerthoffer WT. Evidence for modulation of smooth muscle force by the p38 MAP kinase/HSP27 pathway. *Am J Physiol Heart Circ Physiol*. 2000;278:H1899–H1907.

41. Komers R, Schutzer W, Xue H, Oyama TT, Lindsley JN, Anderson S. Effects of p38 mitogen-activated protein kinase inhibition on blood pressure, renal hemodynamics, and renal vascular reactivity in normal and diabetic rats. *Transl Res*. 2007;150:343–349.

42. Su Z, Zimpelmann J, Burns KD. Angiotensin-(1-7) inhibits angiotensin II-stimulated phosphorylation of MAP kinases in proximal tubular cells. *Kidney Int*. 2006;69:2212–2218.

43. Patel VB, Bodiga S, Fan D, Das SK, Wang Z, Wang W, Basu R, Zhong J, Kassiri Z, Oudit GY. Cardioprotective effects mediated by angiotensin II type 1 receptor blockade and enhancing angiotensin 1-7 in experimental heart failure in angiotensin-converting enzyme 2-null mice. *Hypertension*. 2012;59:1195–1203.

44. Beyer AM, Guo DF, Rahmouni K. Prolonged treatment with angiotensin 1-7 improves endothelial function in diet-induced obesity. *J Hypertens*. 2013;31:730–738.

45. Oudit GY, Kassiri Z, Patel MP, Chappell M, Butany J, Backx PH, Tsushima RG, Scholey JW, Khokha R, Penninger JM. Angiotensin II-mediated oxidative stress and inflammation mediate the age-dependent cardiomyopathy in ACE2 null mice. *Cardiovasc Res*. 2007;75:29–39.

46. Mercure C, Yogi A, Callera GE, Aranha AB, Bader M, Ferreira AJ, Santos RA, Walther T, Touyz RM, Reudelhuber TL. Angiotensin(1-7) blunts hypertensive cardiac remodeling by a direct effect on the heart. *Circ Res*. 2008;103:1319–1326.

47. Dilauro M, Burns KD. Angiotensin-(1-7) and its effects in the kidney. *ScientificWorldJournal*. 2009;9:522–535.

48. Bosnyak S, Jones ES, Christopoulos A, Aguilar MI, Thomas WG, Widdop RE. Relative affinity of angiotensin peptides and novel ligands at AT1 and AT2 receptors. *Clin Sci (Lond)*. 2011;121:297–303.

Novelty and Significance

What Is New?

- In apolipoprotein E–deficient mice (apoE(–/–)), vasoreactivity to angiotensin II (Ang II) is increased in renal resistance vessels by reactive oxygen species/p47phox-mediated increase of p38 mitogen-activated protein kinase activity. Chronic Ang-(1–7) treatment restores the Ang II pressor response to levels seen in wild-type animals. Ang-(1–7) exerts its effects via the Mas-receptor, causing decreased oxidative stress and subsequent reduction of p38 mitogen-activated protein kinase activity.

What Is Relevant?

- Ang-(1–7) counteracts increased vasoreactivity to Ang II in apoE(–/–) mice in a Mas-receptor–dependent manner.

Summary

Increased p38 mitogen-activated protein kinase activity is responsible for increased vasoreactivity to Ang II in apoE(–/–). Ang-(1–7) treatment attenuates the increased vasoreactivity by reducing reactive oxygen species and consequently p38 mitogen-activated protein kinase activity.

Angiotensin-(1-7) Modulates Renal Vascular Resistance Through Inhibition Of P38 Mitogen-Activated Protein Kinase In Apolipoprotein E Deficient Mice

Sebastian A. Potthoff[1], Michael Fähling[2], Tilman Clasen[1], Susanne Mende[1], Bassam Ishak[1], Tatsiana Suvorava[3], Stefanie Stamer[1], Manuel Thieme[1], Sema H. Sivritas[1], Georg Kojda[3], Aandreas Patzak[2], Lars C. Rump[1], Johannes Stegbauer[1]

[1]Department of Nephrology, Medical Faculty, Heinrich-Heine University, Düsseldorf, Germany
[2]Institute of Vegetative Physiology, Charité – Universitaetsmedizin Berlin, Berlin, Germany
[3]Institute of Pharmacology and Clinical Pharmacology, Heinrich-Heine-University, Düsseldorf, Germany

Supplement – Materials and Methods

Animal treatment

In this study, apoE (-/-) mice were fed a high fat diet in order to accelerate the progression of endothelial dysfunction due to progressing atherosclerosis. WT animals fed a high fat diet served as healthy controls. Ang-(1-7) treatment was introduced 6 weeks after the start of the high fat diet as an interventional treatment. The rational of this study design was to treat after occurrence of vascular injury.

At age 6 weeks, all groups were set on a high fat "western diet" (Sniff, Soest, Germany) (42 % fat, 0.15 % cholesterol) for 12 weeks.
Group 1: WT untreated for 6 weeks and treated with saline for consecutive 6 weeks (osmotic minipump, Alzet Model 1004)

Group 2: apoE (-/-) untreated for 6 weeks and treated with saline for consecutive 6 weeks (osmotic minipump, Alzet Model 1004)

Group 3: apoE (-/-) untreated for 6 weeks and treated with Ang-(1-7) (82 µg/kg/hr) for consecutive 6 weeks (osmotic minipump, Alzet Model 1004)

Group 4: apoE (-/-) treated for 12 weeks with an oral p38-inhibitor (BIRB796, 50 mg/kg/day, high fat diet preparation containing the inhibitor), after 6 weeks additional treatment with saline for consecutive 6 weeks (osmotic minipump, Alzet Model 1004). 26

Group 5: Mas (-/-) / apoE (-/-) untreated for 6 weeks and treated with saline for consecutive 6 weeks (osmotic minipump, Alzet Model 1004)

Group 6: Mas (-/-) / apoE (-/-) untreated for 6 weeks and treated with Ang-(1-7) (82 µg/kg/hr) for consecutive 6 weeks (osmotic minipump, Alzet Model 1004)

All animals were sacrificed at the age of 18 weeks.

Isolated perfused mouse kidney

Mice were anesthetized by i.p. injection with Ketamin (100 mg/kg) and Xylazin (5 mg/kg). Kidneys were isolated microscopically (Olympus CO11) and perfused with Krebs-Henseleit buffer according to an amended method described previously.[1] Changes in perfusion pressure reflected changes in vascular resistance of renal resistance vessels immediately after preparation, a bolus injection of 60 mM KCl was

delivered to test the viability of the preparation followed by a stabilization period of 30 min. After the stabilization period, renal vasoconstriction was induced by increasing concentrations of Angiotensin II (Sigma-Aldrich) in the presence or absence of the specific p38 MAPK inhibitor SB203580 (5 µM; Sigma-Aldrich), the ERK1/2 inhibitor PD98059 (5 µM; Sigma-Aldrich) or Ang-(1-7) (0.1 µM; Bachem). Increase in pressor response was measured in mmHg.

Acute infusion experiments

18 weeks old apoE (-/-) (group 2 and 4) mice were anesthetized by i.p. injection with Ketamin (100 mg/kg) and Xylazin (5 mg/kg). Mice were placed on a heating plate to ensure constant body temperature at approx. 36 °C. Left carotid artery was cannulated for continuous measurement of mean arterial pressure (MAP). Left jugular vein was cannulated for application of increasing doses of Ang II (bolus of 0.1, 1, 10 µM/kgBW). Change in mean arterial pressure (MAP) was measured for each concentration of Ang II.

Systolic blood pressure measurement

Systolic blood pressure (BP) was measured non-invasively by tail-cuff sphygmomanometer using a BP-98A device (Softron, Japan). Mice were trained for 4 days prior to evaluation of BP. BP was measured for 5 days at the end of the observational period (week 18).

Isolation of preglomerular vessels

Preglomerular vessels, containing mainly interlobular arteries and afferent arterioles, were isolated by a modified iron oxide-sieving technique as described previously.[2] The kidneys were perfused via cannulation of the aorta, smaller needles (G20, G23) and pores sieves (100 µm) were used for tissue separation and separation of renal particles, respectively.

Quantification of urinary 8-isoprostane concentration

24-h urine samples were collected in metabolic cages at the end of the experimental period. Urinary concentrations of 8-isoprostane were measured using a colorimetric-assay kit (*Cayman Chemical Company*) and normalized to urinary creatinine concentration.

Immunoblotting for p38 MAPK and phospho-p38 MAPK

Renal cortex tissue of pre-glomerular vessels were placed into ice-cold 1 % Triton lysis buffer (containing a protease inhibitor cocktail (*Sigma Aldrich*)) and were immediately homogenized. Lysates were centrifuged at 15,000 x g for 10 min at 4 ºC. Protein concentrations from the supernatant were measured using a Bradford assay (*Bioassay Systems*). After dithiothreitol treatment (100 mM) and denaturation (5 min at 95 °C), 30 µg of total protein were loaded onto 10 % SDS-PAGE gels and then transferred to nitrocellulose membranes according to manufacturer's instructions (*X-Cell Blot Module, Invitrogen*). Membranes were treated with blocking buffer (5 % BSA, and 0.1 % tween 20 in PBS) for 1h at room temperature and then incubated either with primary monoclonal rabbit anti-p38 antibody (1:750) (*Cell Signalling Technology*) or primary monoclonal rabbit anti-phospho-p38 antibody (1:1300) (*Cell Signalling Technology*), and rabbit anti-β-actin (1:2000), (*Santa Cruz Biotechnology*) over-night. Bound primary antibody was detected with anti-rabbit HRP conjugated

secondary antibody (1:10000) (*Dako*, Germany) by 60 min incubation at room temperature. Antibody labelling was visualized by the addition of a chemiluminescence reagent. Chemiluminescence was visualized using a *FluorChem FC2 Imager* (*Alpha Innotec*, USA). Immunoblots from each tissue were performed in triplicates.

Immunoblotting for phospho-MLC$_{20}$

Pre-glomerular vessel tissue was lysed and processed as described above. Polyclonal rabbit anti-phospho-MLC$_{20}$ antibody was used as primary antibody (1:500) (*Acris Antibodies GmbH*). Bound primary antibody was detected with anti-rabbit HRP conjugated secondary antibody (1:50000) (*Dako*, Germany) by 60 min incubation at room temperature. Assessment of chemiluminescence was performed as described above. Reference protein was alpha-actin (1:2000).

Immunoblotting for p47phox (renal cortex)

Renal cortex tissue was lysed and processed as described above. Polyclonal rabbit anti-p47phox antibody was used as primary antibody (1:200) (*Santa Cruz Biotechnology*). Bound primary antibody was detected with anti-rabbit HRP conjugated secondary antibody (1:10000) (*Dako*, Germany) by 60 min incubation at room temperature. Assessment of chemiluminescence was performed as described above.

Quantitative real time RT-PCR (qPCR)

Kidney cortex samples were analyzed for relative expression levels (mRNA) of AT1a-receptor (AT1a), AT2-receptor (AT2), angiotensin converting enzyme 2 (ACE2) and Mas-receptor (MasR). After homogenization of tissue with a Tissue Ruptor (Qiagen, Germany), total RNA was isolated using a RNA Micro Kit (Qiagen, Germany) according to the manufacturer's instructions. Quantitative real time RT-PCR was performed with an ABI PRISM 7300 (Applied Biosystem, Germany) and the SYBR Green master mix (Qiagen, Germany). The PCR reaction was performed in a total volume of 20 µl with 1 µl cDNA corresponding to 50 ng RNA as template.

The PCR conditions were 15 min at 95 °C, followed by 40 cycles (denaturation at 95 °C for 15 s, annealing at 58 °C for 30 s, extension at 72 °C for 34 s, detection at 79 °C for 34 s). Experiments were performed in duplicates. 18S ribosomal RNA was chosen as the endogenous control (housekeeping gene). The levels of targeted genes were normalized to 18S rRNA expression. Data was analyzed using the DeltaCT-method. Statistical analysis was performed with a one-way ANOVA for repeated measurements followed by Bonferroni correction post-hoc test.

The following primer sequences were used: 18S ribosomal RNA (*QuantiTect Primer Assays, Qiagene, Cat-N° QT00324940*), MasR: forward: TTGTGGGCAGCAGTAAGAAGA, reverse: ATGGATACAGTGTTGCCGTTG. ACE2: forward: TCTGGGCAAACTCTATGCTGA, reverse: TGATGGGCTGTCAAGAAGTTG. AT2: forward: ACCTGCATGAGTGTCGATAGGT, reverse: CTGACATCCCGGAAATAAAATG. AT1a: forward: GCTTGGTGGTGATCGTCACC, reverse: GGGCGAGATTTAGAAGAACG.

Lucigenin superoxide detection

Lucigenin-enhanced chemiluminescent detection of superoxide production in kidney cortex of apoE (-/-) on western diet treated with or without Ang-(1-7) (group 2 and 3) was performed as described previously.[3] Briefly, freshly cleaned and harvested thoracic aortic and kidney cortex segments were equilibrated in Krebs-HEPES buffer for 30 min at 37 $^\circ$C. Aortic and kidney segments were transferred to vials containing albumin buffer enriched with 5 µM lucigenin, and chemiluminescence was recorded every 2 min for 20 min using *Packard Luminometer Analyzer* (*Picolite A6112, Packard*, Downers Grove, IL, USA). Background readings were subtracted from sample reading and results are expressed as counts/min/mg tissue dry weight (mean ± SEM).

Statistics

Data are expressed as mean ± SEM (n=number of animals). Student's t-test was used to compare means of two groups with Gaussian distribution. Multiple comparison of more than two groups with Gaussian distribution were analysed by one-way ANOVA followed by Bonferroni's multiple comparison post-hoc test. Statistical analyses of data of two groups in which Gaussian distribution was not normal (or could not be assumed) were analysed by the Mann-Whitney-U-Test. Statistical analyses of data of more than two groups in which Gaussian distribution was not normal (or could not be assumed) were analysed by the Kruskal-Wallis-Test followed by Dunn's multiple comparison post-hoc test. Differences between dose-response curves were analysed by two-way ANOVA for repeated measurements followed by Bonferroni correction post-hoc test.

Probability levels of $p < 0.05$ were considered statistically significant. If applicable, a higher level of statistical significance is stated ($p < 0.01$, $p < 0.001$). The number of experiments (n) refers to the number of mice or the number of individual samples.

Supplement – References

1. Stegbauer J, Vonend O, Habbel S, Quack I, Sellin L, Gross V, Rump LC. Angiotensin ii modulates renal sympathetic neurotransmission through nitric oxide in at2 receptor knockout mice. *J Hypertens*. 2005;23:1691-1698
2. Stegbauer J, Potthoff SA, Quack I, Mergia E, Clasen T, Friedrich S, Vonend O, Woznowski M, Konigshausen E, Sellin L, Rump LC. Chronic treatment with angiotensin-(1-7) improves renal endothelial dysfunction in apolipoproteine-deficient mice. *British journal of pharmacology*. 2011;163:974-983
3. Kojda G, Hacker A, Noack E. Effects of nonintermittent treatment of rabbits with pentaerythritol tetranitrate on vascular reactivity and superoxide production. *Eur J Pharmacol*. 1998;355:23-31

Supplement – Figures
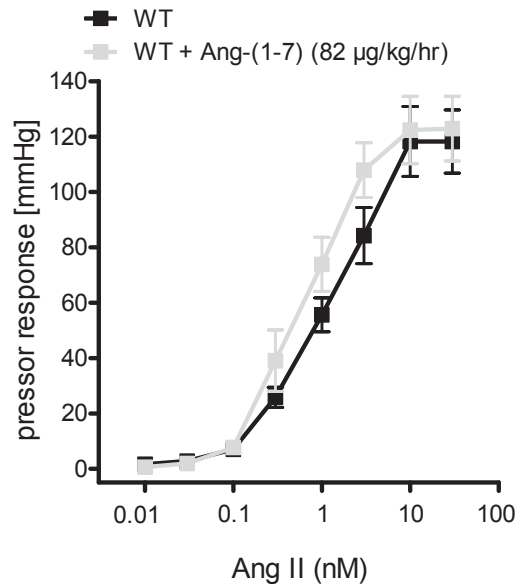
S1: Ang II-induced pressor response in isolated perfused kidney from WT mice was not significantly different if treated chronically with Ang-(1-7) (82µg/kg/hr) (WT: n= 5; WT + Ang-(1-7): n=7) (p=NS). Two-way ANOVA for repeated measurements followed by Bonferroni correction post-hoc test
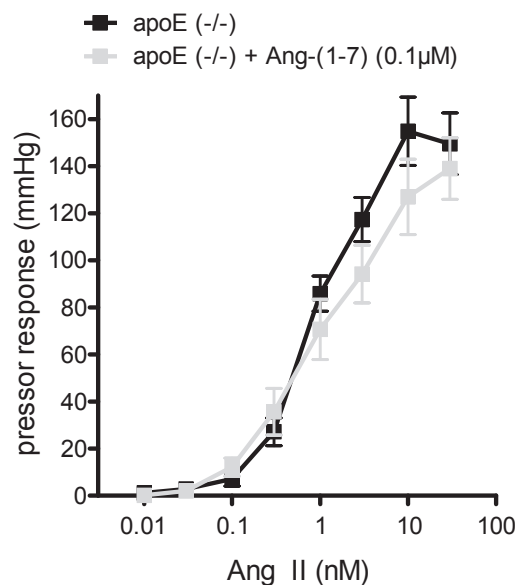
S2: Acute Ang-(1-7) (0.1µM) administration did not influence Ang II-induced pressor response in isolated perfused kidney of non-treated apoE (-/-) mice significantly (n=6; each group) (p=NS). Two-way ANOVA for repeated measurements followed by Bonferroni correction post-hoc test.
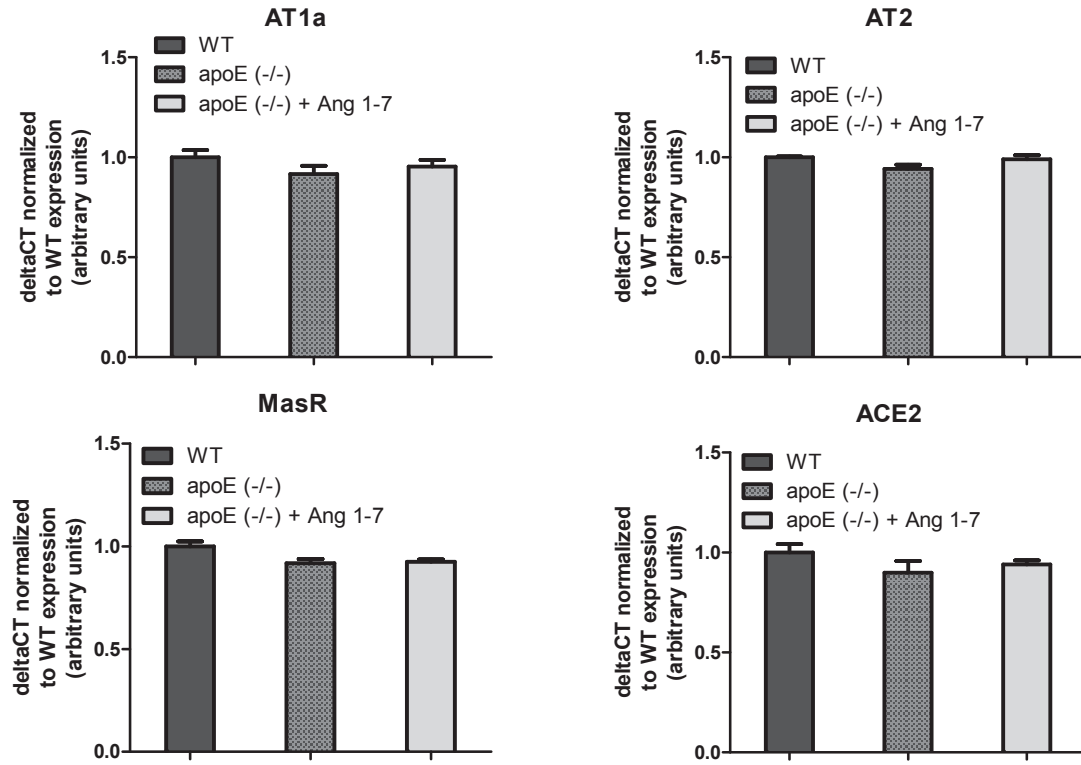
S3: Comparison of relative gene expression (mRNA level) of RAS-related genes in WT vs. apoE (-/-) vs. apoE (-/-) + Ang-(1-7). (n=4; each group) There was no significant difference in gene expression. (real time PCR data for AT1aR, AT2R, ACE2, MasR. deltaCT to 18s expression normalized to WT expression). p=NS. One-way ANOVA for repeated measurements followed by Bonferroni correction post-hoc test.

A
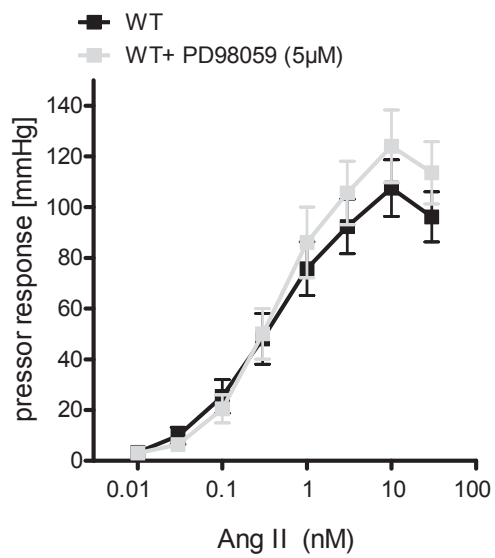
B
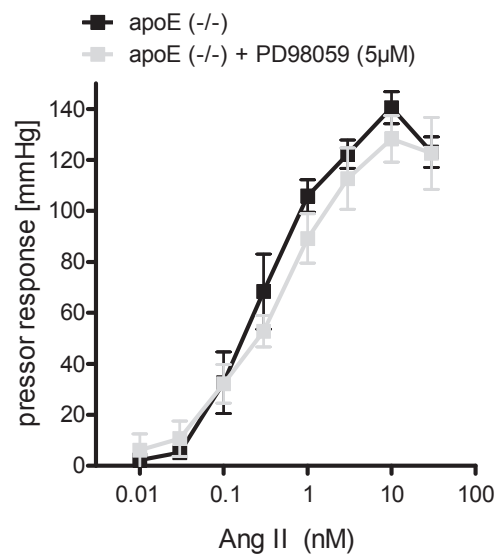
S4: Ang II-induced pressor response is not influenced by MEK 1/2-inhibition neither in kidneys of WT (A; n=11 each group) nor apoE (-/-) (B; n=5 each group) mice. P=NS for apoE (-/-) versus apoE (-/-) + PD98059. P=NS for WT versus WT + PD98059. Two-way ANOVA for repeated measurements followed by Bonferroni correction post-test.

Chronic p38 mitogen-activated protein kinase inhibition improves vascular function and remodeling in angiotensin II-dependent hypertension

SA Potthoff[1], S Stamer[1], K Grave[1], E Königshausen[1], SH Sivritas[1], M Thieme[1], Y Mori[2], M Woznowski[1], LC Rump[1] and J Stegbauer[1]

Abstract

Introduction: An excess of angiotensin II (Ang II) causes hypertension and vascular injury. Activation of mitogen-activated protein kinase p38 (p38-MAPK) plays a substantial role in Ang II-dependent organ damage. Recently, we showed that p38-MAPK activation regulates the pressor response to Ang II. This study evaluates the effect of chronic p38-MAPK inhibition in Ang II-dependent hypertension.

Materials and methods: C57Bl/6J mice were infused with Ang II for 14 days and either treated with the p38-MAPK inhibitor BIRB796 (50 mg/kg/day) or the vehicle as the control. We assessed vascular function in the aorta and isolated perfused kidneys.

Results: Chronic p38-MAPK inhibition did not alter blood pressure at the baseline, but attenuated Ang II-induced hypertension significantly (baseline: 122 ± 2 *versus* 119 ± 4 mmHg; Ang II: 173 ± 3 *versus* 155 ± 3 mmHg; *p* < 0.001). In addition, BIRB796 treatment improved vascular remodeling by reducing the aortic media-to-lumen ratio and decreasing the expression of the membrane metalloproteinases (MMP) MMP-1 and MMP-9. Moreover, renal vascular dysfunction induced by chronic Ang II infusion was significantly ameliorated in the BIRP796-treated mice. Acute p38-MAPK inhibition also improved vascular function in the aorta and kidneys of Ang II-treated mice, highlighting the important role of p38-MAPK activation in the pathogenesis of vascular dysfunction.

Conclusions: Our findings indicated there is an important role for p38-MAPK in regulating blood pressure and vascular injury, and highlighted its potential as a pharmaceutical target.

Introduction

During the past decades, control rates and treatment options for hypertension have improved; however, hypertension is still the leading risk factor of mortality and morbidity in the world.[1] The need for better pharmaceutical treatment options remains high.[2,3] Understanding the mechanisms which lead to hypertension and vascular dysfunction may contribute to the development of new potential targets for drug therapy.

Previously, we and others have shown that p38 mitogen-activated protein kinase (MAPK) is involved in myogenic control of the vascular wall in resistance vessels.[4] In addition, angiotensin II (Ang II)-dependent p38 MAPK activation is involved in vascular smooth muscle cell contraction via p38 MAPK-dependent phosphorylation of the

[1]Department of Nephrology, University Hospital Düsseldorf, Medical Faculty, Heinrich-Heine University, Düsseldorf, Germany
[2]Department of Nuclear Medicine, University Hospital Düsseldorf, Medical Faculty, Heinrich-Heine University, Düsseldorf, Germany

Potthoff and Stamer contributed equally to this work.

Corresponding author:
J Stegbauer, Department of Nephrology, University Hospital Düsseldorf, Medical Faculty, Heinrich-Heine University, Moorenstrasse 5, 40225 Duesseldorf, Germany.
Email: johannes.stegbauer@med.uni-duesseldorf.de

myosin light chain (MLC_{20}).[5–9] Besides increases in contractile response, Ang II-dependent hypertension promotes changes in vascular wall structure and increases stiffening. This process is promoted by vascular inflammation and fibrosis.[10,11] Activation of p38 MAPK through Ang II is attributed to the increased generation of reactive oxygen species (ROS) causing vascular smooth muscle cell hypertrophy.[12,13] In central blood vessels such as the aorta, stiffening of the wall reduces the capacitance properties that usually dampen systolic blood pressure (SBP) elevation. Loss of this function leads to augmentation of the SBP and exaggerates hypertension.[14–16] Augmentation of SBP with increased stiffening is a strong predictor of increase of cardiovascular morbidity and mortality[17,18]; however, whether chronic p38 MAPK directly influences vascular function and reduces blood pressure remains unclear. Therefore, the aim of the present study was to examine whether Ang II-induced hypertension or hypertension-mediated changes in vascular function are dependent on p38 MAPK activation. We hypothesized that p38 MAPK inhibition would ameliorate Ang II-induced hypertension and influence Ang II-mediated changes in the vasculature. To test this hypothesis, we examined the effect of orally available p38 MAPK inhibition through BIRB796, in C57Bl/6 mice.

Materials and methods

Animal care

We obtained 12 week old wild type (WT) mice from an in-house breed at the local animal care facility. The mice were bred on a C57Bl/6J background. Littermates were used as the controls. The animals were housed in Type III Makrolon polycarbonate cages at 45% humidity, 20–22 °C temperature and a 12 h day–night cycle, with free access to water and food. Animal housing and care, and the experiments, took place at the animal care facility of Heinrich-Heine University (Dusseldorf, Germany).

The investigations were conducted according to the US National Institutes of Health (NIH) *Guide for Care and Use of Laboratory Animals* (NIH, 1996), the NIH publication No. 85–23 revised in 1996. Animal treatment and experiments were conducted with approval of the local ethics committee (O68/08 and G216/08).

Animal treatment

In this study, hypertension was induced in all treatment groups via osmotic minipumps (ALZET Osmotic Pumps, model 1002, DURECT Corporation, Cupertino, CA, USA) with Ang II 1000 ng/min per kg of body weight (BW). Treatment and observation time continued throughout 14 days. Mice were divided into two groups prior to insertion of the minipumps, to either treat with the orally available p38 MAPK inhibitor BIRB796 at a dose of 50 mg/kgBW/d (a generous gift of Boehringer Ingelheim Pharma GmbH

& Co. KG, Ingelheim, Germany) or vehicle (the mouse chow, thus oral application) as adopted from previous methods.[19] Treatment started 2 days prior to insertion of the osmotic minipumps and lasted throughout an observation time of 14 days.

For the isolated perfused kidney experiments, mice given a saline infusion only served as the untreated controls.

Treatment groups for chronic p38 MAPK inhibition with BIRB796 were as follows:

1. Untreated mice (C57B/6) (controls);
2. Ang II-treated C57B/6 mice (Ang II 1000 ng/kg BW/min) for 14 days, via vehicle; and
3. Ang II-treated C57B/6 mice (Ang II 1000 ng/kg BW/min) + BIRB796 (50 mg/kg BW/d) for 14 days.

For the ex-vivo inhibition of p38 MAPK (SB203580) in the isolated perfused kidney and thoracic aortic rings experiments, mice were either infused with saline or with Ang II (1000 ng/kg/min) for 14 days.

Isolated perfused mouse kidney

Mice were anesthetized by intraperitoneal injection with ketamine (100 mg/kg) and xylazine (5 mg/kg). Their kidneys were isolated microscopically (Olympus CO11, Olympus Deutschland GmbH, Hamburg, Germany) and perfused with Krebs-Henseleit buffer, according to a method described previously.[20,21] Changes in perfusion pressure reflected the changes in vascular resistance of renal vessels immediately after preparation. A bolus injection of 60 mM of potassium chloride (KCl) was delivered to test the viability of the preparation, followed by a stabilization period of 30 min. After the stabilization period, renal vasoconstriction was induced by increasing concentrations of Ang II (Sigma-Aldrich Chemie GmbH, Munich, Germany). Changes in pressor responses were measured in mmHg. To assess vasorelaxation, renal vasoconstriction was induced by norepinephrine at 1 µM (Sigma-Aldrich Chemie GmbH), and then we assessed the concentration-response curves of the vasodilator S-Nitrosoglutathione (GSNO) (Alexis Corp. / Enzo Life Sciences AG, Lausen, Germany). Renal vascular relaxation was calculated as the percentage of contraction in the pre-contracted kidneys, which was set as 100%.

Assessing the acute effects of p38 MAPK inhibition on renal vascular function, the renal pressor response was induced by Ang II in the presence or absence of the p38 MAPK inhibitor SB203580 at 5 µM (Sigma-Aldrich Chemie GmbH). In addition, we assessed the renal vasodilator response to S-Nitrosoglutathione (GSNO) (Alexis Corp. / Enzo Life Sciences AG) in pre-contracted (with 1 µM norepinephrine (Sigma-Aldrich Chemie GmbH)) isolated perfused kidneys, in the presence or absence of SB203580.

Aortic ring myography

We assessed vasorelaxation of the aortic rings from Ang II-treated mice at 14 days with a multi-wire myograph system, as previously described.[22] In short, in the presence of diclofenac (3 μM), the aortic rings were pre-constricted with norepinephrine 1 μM (Sigma-Aldrich Chemie GmbH). We assessed vasodilation by GSNO in the presence or absence of the p38 MAPK inhibitor SB203580 (Sigma-Aldrich Chemie GmbH) at 5 μM. Aortic vasodilation was calculated as the percentage of contraction in the pre-constricted aorta, which was set as 100%.

Immunoblotting for p38 MAPK and phospho-p38 MAPK

Renal cortex tissue was placed into ice-cold 1% Triton lysis buffer (containing a protease inhibitor cocktail (Sigma-Aldrich Chemie GmbH)) and immediately homogenized. Lysates were centrifuged at 20,500 g for 10 min at 4 ºC. We measured protein concentrations using a Bradford assay (BioAssay Systems, Hayward, USA). After dithiothreitol treatment (100 mM) and denaturation (5 min at 95 °C), 30 μg of total protein were loaded onto 10% SDS-PAGE gels and then transferred to nitrocellulose membranes, according to the manufacturer's instructions (X-Cell Blot Module, Invitrogen / Thermo Fisher Scientific Inc., Oberhausen, Germany). Membranes were treated with blocking buffer (5% bovine serum albumin (BSA) and 0.1% Tween 20 in phosphate buffered saline (PBS)) for 1 h at room temperature, and then incubated either with primary monoclonal rabbit anti-p38 antibody at 1:750 (Cell Signaling Technology, Europe, Leiden, The Netherlands) or primary monoclonal rabbit anti-phospho-p38 antibody at 1:1300 (Cell Signaling Technology), and then mouse anti-β-actin at 1:20,000 (Santa Cruz Biotechnology, Inc., Dallas, USA) overnight. Bound primary antibody was detected with anti-rabbit horseradish peroxidase (HRP)-conjugated secondary antibody at 1:10000 (Dako Deutschland GmbH, Hamburg, Germany) by 60 min incubation at room temperature. Antibody labeling was visualized by the addition of a chemiluminescence reagent (Lumi-LightPLUS Western Blotting Substrate, Sigma-Aldrich Chemie GmbH). Chemiluminescence was visualized using a FluorChem FC2 Imager (alpha innotec / Protein Simple, San Jose, USA). Immunoblots from each tissue were performed in triplicate.

Quantification of urinary 8-isoprostane concentration

We measured 8-isoprostane as previously described.[23] In short, 24-h urine samples were collected in the metabolic cages at the end of the experimental period. We measured the urinary concentrations of 8-isoprostane using a colorimetric assay kit (Cayman Chemical Company, Ann Arbor, USA). This was normalized to the urinary creatinine concentration.

Quantification of urinary norepinephrine concentration

We collected the 24-h urine samples in metabolic cages, at the end of the experimental period. We measured the norepinephrine concentrations using high performance liquid chromatography (HPLC), as previously described.[24]

Histological assessment

At the end of the experimental period, the mice were sacrificed. The mouse aortas were perfused with ice-cold PBS from the left ventricle, embedded in paraffin, and then the abdominal aortas were used for histological assessment.

Ratio of medial area to luminal area in aortas

The aortic rings were embedded in paraffin and cut in 5-μm sections. The slides were stained using a standard PAS (Periodic Acid Schiff) staining protocol. Using the image processing software ImageJ (http://imagej.nih.gov), the lumen and media areas were measured separately, and then the ratio of media to luminal area was calculated.

Quantitative real-time PCR (qPCR)

We used the aorta wall samples to analyze the relative expression of RNA levels for matrix metalloproteinase-1 (MMP-1), matrix metalloproteinase-9 (MMP-9), tissue inhibitor of metalloproteinase 1 (TIMP1), fibronectin and collagen 1. In addition, we analyzed the relative expression levels of the AT1a and AT2 receptor.

After the homogenization of tissue (Tissue Ruptor, QIAGEN GmbH, Hilden, Germany), the total RNA was isolated using a RNA Micro Kit (QIAGEN GmbH, Hilden), according to the manufacturer's instructions. Quantitative real time PCR was performed with an ABI PRISM 7300 (Thermo Fisher Scientific Inc./Applied Biosystems, Oberhausen, Germany) and a SYBR Green master mix (QIAGEN GmbH, Hilden).

Our study experiments were performed in triplicate. We chose the 18S ribosomal RNA as the endogenous control (a housekeeping gene). The levels of targeted genes were normalized to 18S rRNA expression.

The following primer sequences for mouse cDNA were used:

- MMP-1: ACACTCAAATGGTCCCAAACGAA (forward), GGTGTCACATCAGACCAGACC (reverse);

- MMP-9: CACTGGGCTTAGATCATTCCA (forward), GCTTAGAGCCACGACCATACA (reverse);

- TIMP1: ATCTGGCATCCTCTTGTTGCT (forward), GGTGGTCTCGTTGATTTCTGG (reverse);

- Fibronectin 1: CGAGGTGACAGAGACCACAA (forward), CTGGAGTCAAGCCAGACACA (reverse);

- Collagen 1: CTGGTCCACAAGGTTTCCAAG (forward), AGCTTCCCCATCATCTCCATT (reverse);

- AT1a: GCTTGGTGGTGATCGTCACC (forward), GGGCGAGATTTAGAAGAACG (reverse); and

- AT2: ACCTGCATGAGTGTCGATAGGT (forward), CTGACATCCCGGAAATAAAATG (reverse).

Systolic blood pressure measurement

SBP was measured non-invasively by tail-cuff sphygmomanometer using a BP-98A device (Softron, Tokyo, Japan). Mice were trained for 4 consecutive days prior to the start of the experimental period. Blood pressure was measured on a daily basis. We took 10 consecutive measurements from each mouse, each day at the same time, during the whole experiment. We calculated the mean SBP of each week from the mean blood pressure values of each mouse.

Pharmaceutical drugs used

For the present study, we used the p38 MAPK inhibitors BRIB796 (1-(5-tert-butyl-2-p-tolyl-2H-pyrazol-3-yl)-3-[4-(2-morpholin-4-yl-ethoxy)-naphthalen-1-yl] urea) (a generous gift from Boehringer Ingelheim Pharma GmbH & Co. KG) and SB203580 (4-(4-fluorophenyl)-2-(4-methylsulfinylphenyl)-5-(4-pyridyl)1H-imidazole, Sigma-Aldrich Chemie GmbH).

These inhibitors predominantly inhibit p38α; however, they also show inhibition of the β, γ and δ isoforms. BIRB796 has a higher specificity for the α isoform, compared to SB203580. Besides inhibition of p38 MAPK, these compounds can also inhibit c-Jun N-terminal kinases (JNKs) to a certain extent.[25] These small-molecule compounds can be applied orally. In this study, BIRB769 was used for oral treatment, whereas SB203580 was used for the *ex vivo* experiments.

In addition, this study used S-Nitrosoglutathione (GSNO, Alexis Corp. / Enzo Life Sciences AG), angiotensin II (Sigma-Aldrich Chemie GmbH) and norepinephrine (Sigma-Aldrich Chemie GmbH).

Statistics

Data are expressed as the mean ± SEM. Student's *t*-test was used to compare the means of two groups with Gaussian distribution. Multiple comparison of more than two groups with Gaussian distribution were analyzed by 1-way analysis of variance (ANOVA), followed by Bonferroni's multiple comparison *post-hoc* test. Statistical analyses of data from more than two groups in which the Gaussian distribution was not normal (or could not be assumed) were analyzed by the Kruskal-Wallis Test, followed by Dunn's multiple comparison *post-hoc* test. Differences between dose-response curves were analyzed by 2-way ANOVA for repeated measurements, followed by the Bonferroni correction *post-hoc* test.

Probability levels of $P < 0.05$ were considered statistically significant. If applicable, a higher level of statistical significance is stated ($P < 0.01$ or $P < 0.001$). The number of experiments (n) can refer to the number of mice or the number of individual samples.

Results

Chronic p38 MAPK inhibition attenuates SBP in Ang II-induced hypertension

To evaluate the influence of chronic p38 MAPK inhibition on Ang II-induced hypertension, SBP was measured throughout the observation period. SBP was not statistically different at baseline. Chronic treatment with the p38 MAPK inhibitor BIRB796 attenuated the increase of SBP significantly at Week 1 and Week 2 (Figure 1(a)).

In Ang II-induced hypertension, p38 MAPK activation, presented as the ratio of phospho-p38 to total p38 MAPK, was significantly increased compared to controls. Accordingly, chronic treatment with p38 MAPK inhibitor BIRB796 attenuated the increased p38 MAPK activation in Ang II induced hypertension (Figure 1(b)).

This was accompanied by decreased urinary 8-isoprostane excretion in the BIRB796-treated mice, compared to the Ang II-treated controls. Ang II treatment alone significantly increased urinary 8-isoprostane excretion (Figure 1(c)).

Treatment with BIRB796 did not affect urinary norepinephrine excretion, a marker of sympathetic activity (Figure 1(d)).

Chronic p38 MAPK inhibition improves vascular remodeling in Ang II-induced hypertension

Chronic hypertension results in structural changes in aortic wall composition and hypertrophy.[26] Measuring the ratio of media area to luminal area in mice aortas revealed a significantly lower ratio of medial to luminal areas in the BIRB796-treated animals, compared to vehicle-treated animals (0.46 ± 0.02 versus 0.65 ± 0.05; $p < 0.01$) (Figure 2(a)).

We performed qPCR to assess the genes involved in vascular remodeling. Higher expression of MMP-1 and MMP-9 are linked to hypertrophy and stiffening of the aortic vessel wall.[27,28] In the BIRB796-treated animals, the relative expression of MMP-1 and MMP-9 was significantly decreased; for MMP1: 0.424 ± 0.180 *versus* 1.000 ± 0.183 and $p < 0.05$; for MMP-9: 0.508 ± 0.103 *versus* 1.000 ± 0.183 and $p < 0.05$. The stiffening of the aorta is linked to reduced elasticity and increased collagen deposition. These processes are reflected in the reduced matrix turnover and increased collagen and fibronectin expression.[28,29] There was no statistical difference in the relative gene expression of TIMP1, fibronectin nor collagen 1 (Figure 2(b-f)).

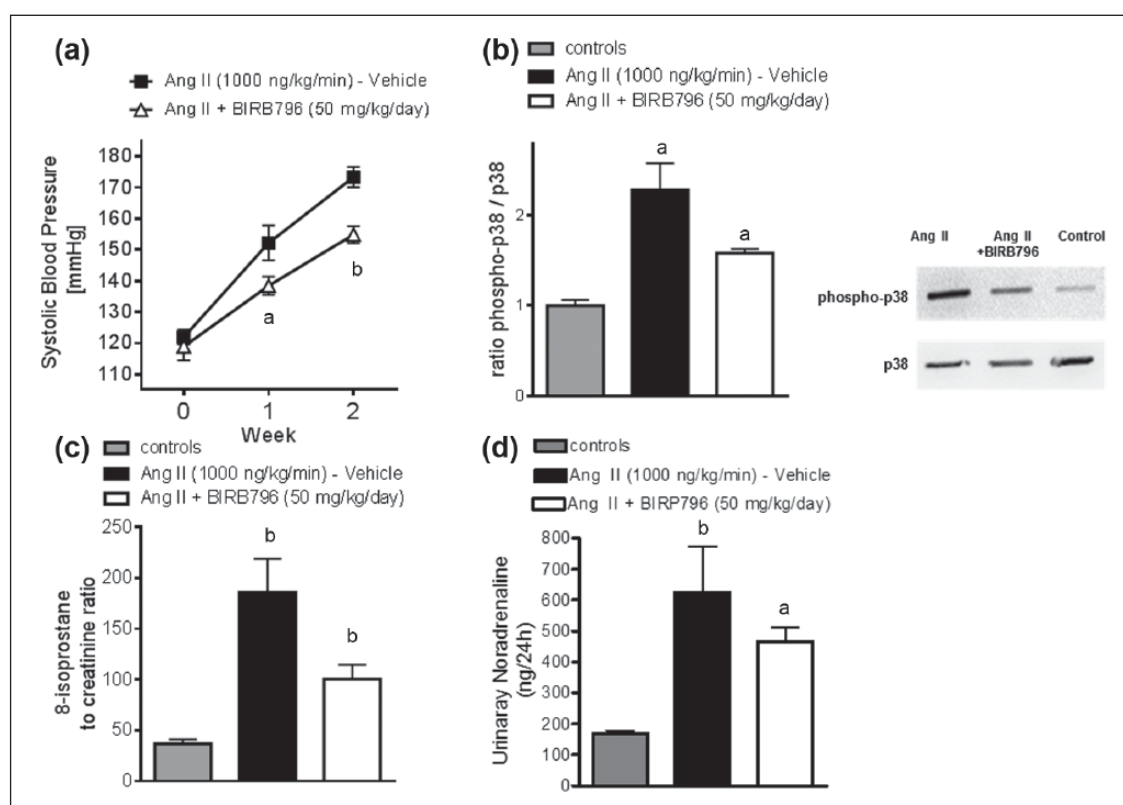In the thoracic aortic lysates, p38 MAPK activation presented as the ratio of phospho-p38 to total p38 MAPK was

Figure 1. Chronic p38 MAPK inhibition attenuates systolic blood pressure in Ang II-induced hypertension. **(a)** SBP in Ang II-induced hypertensive mice treated with either vehicle or BIRB796 at baseline, Week 1 and Week 2 (baseline: 122 ± 2 mmHg (vehicle) *versus* 119 ± 4 mmHg (BIRB796 at 50 mg/kg BW/d); Week 1: 152 ± 6 *versus* 138 ± 3 mmHg, $p < 0.01$; Week 2: 173 ± 3 *versus* 155 ± 3 mmHg, $p < 0.001$). Data are as mean ± SEM (vehicle $n = 8$; BIRB796 $n = 8$); [a]$p < 0.05$, [b]$p < 0.01$. One-way anova followed by Bonferroni's multiple comparison post-hoc test. **(b)** Representative immunoblots and densitometric analysis of renal cortex lysates evaluating p38 MAPK activation measured as the ratio of phospho-p38 to total p38 (vehicle, $n = 6$; BIRB796, $n = 6$; and controls, $n = 6$): [a]$p < 0.05$ vehicle *versus* BIRB796; [a]$p < 0.05$ vehicle *versus* controls. One-way ANOVA followed by Bonferroni's multiple comparison post-hoc test (% change: controls 100%, Ang II 228%, Ang II + BIRB796 158% (mean)). **(c)** Data on 24-hour urinary 8-isoprostane excretion at 2 weeks: Data represents the mean ± SEM for each group ($n = 6$); [b]$p < 0.01$ *versus* controls; [a]$p < 0.05$ Ang II *versus* Ang II + BIRB796. Kruskal-Wallis-Test followed by Dunn's multiple comparison post-hoc test. **(d)** Chronic Ang II infusion significantly increased urinary noradrenaline excretion compared to controls; however, treatment with BIRB796 did not affect urinary noradrenaline excretion, a marker of sympathetic activity (controls, $n = 8$; Ang II (vehicle), $n = 9$; Ang II + BIRB796, $n = 12$) Data are given as a mean ± SEM.
[a]$p < 0.05$.
[b]$p < 0.01$.
p = NS.
Ang II: angiotensin 2; ANOVA: analysis of variance; BIRB796: a MAPK inhibitor; BW: body weight; d: day; kg: kilogram; MAPK: mitogen activated protein kinase; mmHg: millimeters of mercury as units for pressure; N: number of animals; NS: non significant; SBP: systolic blood pressure; SEM: standard error of the mean.

significantly reduced in Ang II-induced hypertensive mice treated with the p38 MAPK inhibitor BIRB796 (Figure 2(g)). Chronic BIRP796 treatment did not affect aortic AT1a and AT2 receptor expression levels (Figure 2(h)).

Improved vascular function by chronic p38 MAPK inhibition in Ang II-induced hypertension

To evaluate whether chronic p38 MAPK inhibition reduces vascular reactivity in Ang II-induced hypertension, the renal pressor response to Ang II was measured *ex vivo*, in kidneys isolated from mice treated with or without BIRB796 in Ang II-induced hypertension. In BIRB796-treated mice,

the pressor response to Ang II significantly decreased, compared to vehicle-treated animals (Figures 3(a) and 3(b)). In contrast, neither the pressor responses to KCl at 60 mM nor to norepinephrine at 1 μM showed any differences (Figure 3(c)). Renal smooth muscle cell-dependent vasorelaxation induced by GSNO was significantly increased in the kidneys of BIRB796-treated mice (Figure 3(b)).

Acute inhibition of p38 MAPK improved vascular function in Ang II-dependent hypertension

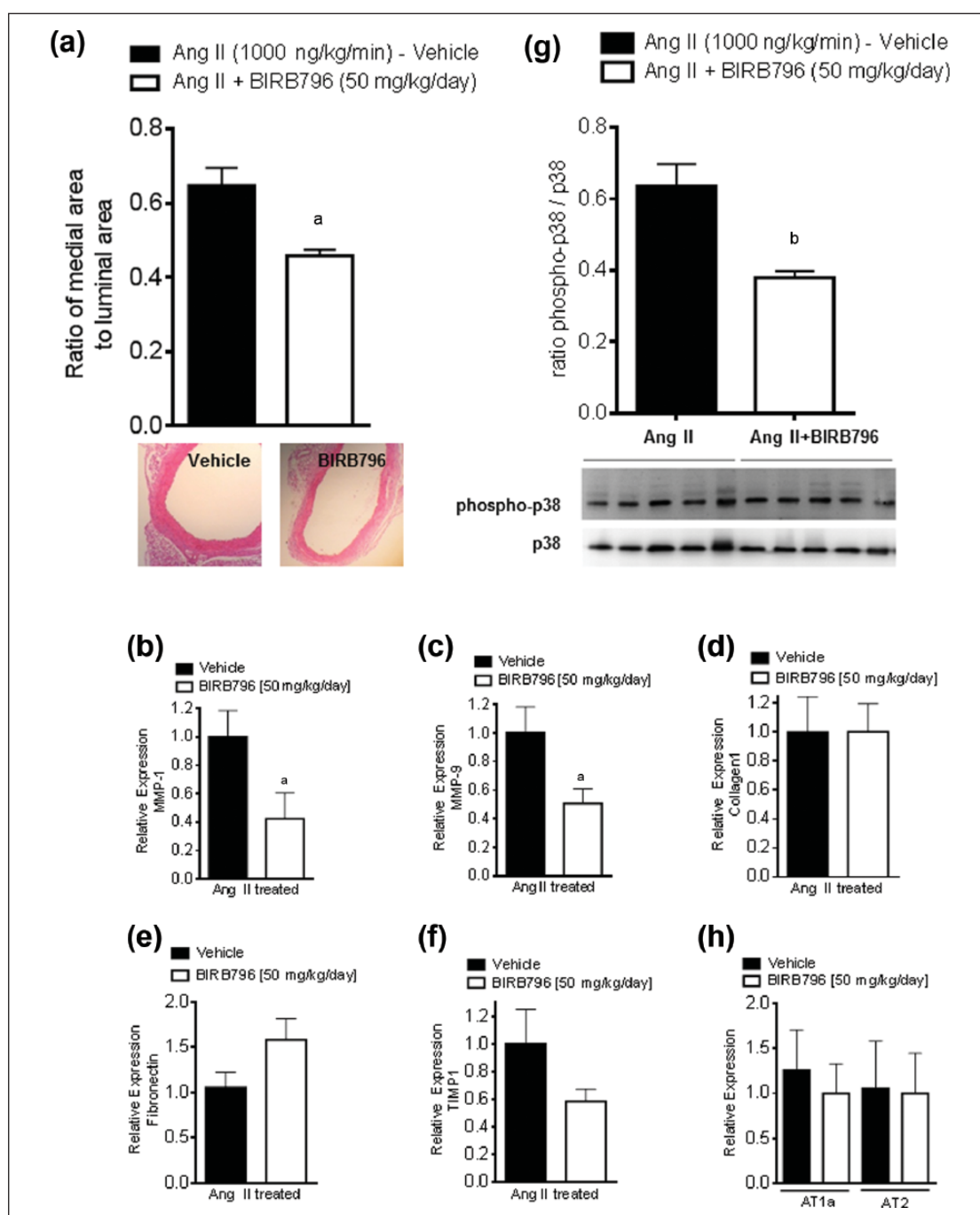In order to test for the acute effect of a p38 MAPK inhibition on the vascular function of resistance and conductance

Figure 2. Chronic p38 MAPK inhibition improves vascular remodeling in Ang II-induced hypertension. **(a)** Ratio of medial to luminal area of the aortic rings at 2 weeks with vehicle *versus* BIRB796. Data are as means ± SEM (vehicle *n* = 16; BIRB796 *n* = 14); [a]*p* < 0.05 vehicle *versus* BIRB796. Student's *t*-test: **(b-f)** The qPCR data from descending thoracic aortic ring lysates evaluating relative RNA expression of MMP-1 **(b)**, MMP-9 **(c)**, TIMP1 **(d)**, fibronectin **(e)** and collagen-1 **(f)**. Data are means ± SEM; [a]*p* < 0.05 *versus* vehicle. Student's *t*-test *n* refers to the number of tissue samples. Each sample is from a single animal. **(g)** Densitometric analysis of aortic lysates evaluating p38 MAPK activation, measured as the ratio of phospho-p38 to total p38. (vehicle *n* = 5; BIRB796 *n* = 5; [b]*p* < 0.01. Student's *t*-test *n* refers to the number of animals. The % change was Ang II, 100%; Ang II + BIRB796, 60% (mean)). **(h)** The qPCR data from descending thoracic aortic ring lysates evaluating relative RNA expression of the AT1a and AT2 receptor. Data are expressed as means ± SEM; [a]*p* < 0.05 *versus* vehicle. In the Student's *t*-test, *n* refers to the number of tissue samples. Each sample is from a single animal.

[a]*p* < 0.05.
[b]*p* < 0.01.
Ang II: angiotensin 2; ANOVA: analysis of variance; BIRB796: a MAPK inhibitor; MAPK: mitogen activated protein kinase; MMP: membrane metalloproteinase; qPCR: quantitative polymerase chain reaction; RNA: ribonucleic acid; SEM: standard error of the mean; TIMP1: tissue inhibitor of metalloproteinase 1.
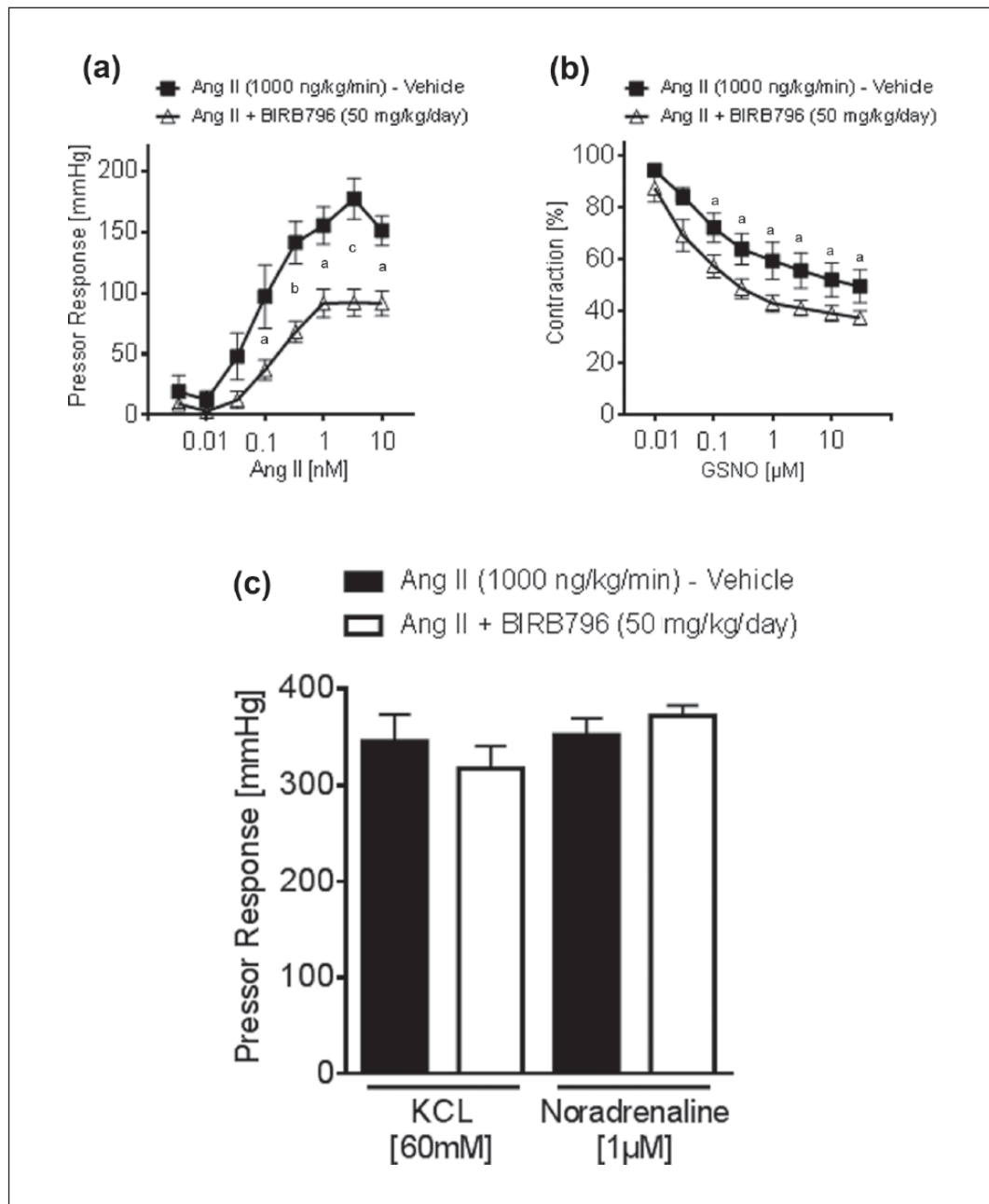
Figure 3. Effects of Ang II and GSNO in the isolated perfused kidney. **(a)** Ang II-induced pressor response increased in kidneys of vehicle-treated mice (*n* = 5), compared to BIRB796-treated mice (*n* = 5). Data represents the mean ± SEM *versus* vehicle. A 2-way ANOVA for repeated measurements, followed by Bonferroni correction *post-hoc* test. **(b)** GSNO-induced vasorelaxation improved in kidneys of BIRB796-treated mice (*n* = 7), compared to vehicle-treated mice (*n* = 6). Data represent the mean ± SEM; [a]$p < 0.05$ *versus* vehicle. A 2-way ANOVA for repeated measurements, followed by Bonferroni correction *post-hoc* test. **(c)** No significant difference could be observed in comparing the maximum pressor response in kidneys from the vehicle and the BIRB796-treated mice, to KCL and to norepinephrine. Data are as mean ± SEM. *p* = NS. Student's *t*-test.
[a]$p < 0.05$.
[b]$p < 0.01$.
[c]$p < 0.001$.
Ang II: angiotensin 2; ANOVA: analysis of variance; BIRB796: a MAPK inhibitor; GSNO: S-Nitrosoglutathione; KCl: potassium chloride; NS: not significant; SEM: standard error of the mean; NS: non significant.

vessels, we performed additional experiments in aortic rings and in isolated perfused kidneys of Ang II-treated mice, in the presence or absence of SB203580 (5 μM). In

kidneys of Ang II-treated mice, pressor responses to Ang II were significantly higher, compared to controls. Acute p38 MAPK-inhibition significantly attenuated Ang II-induced
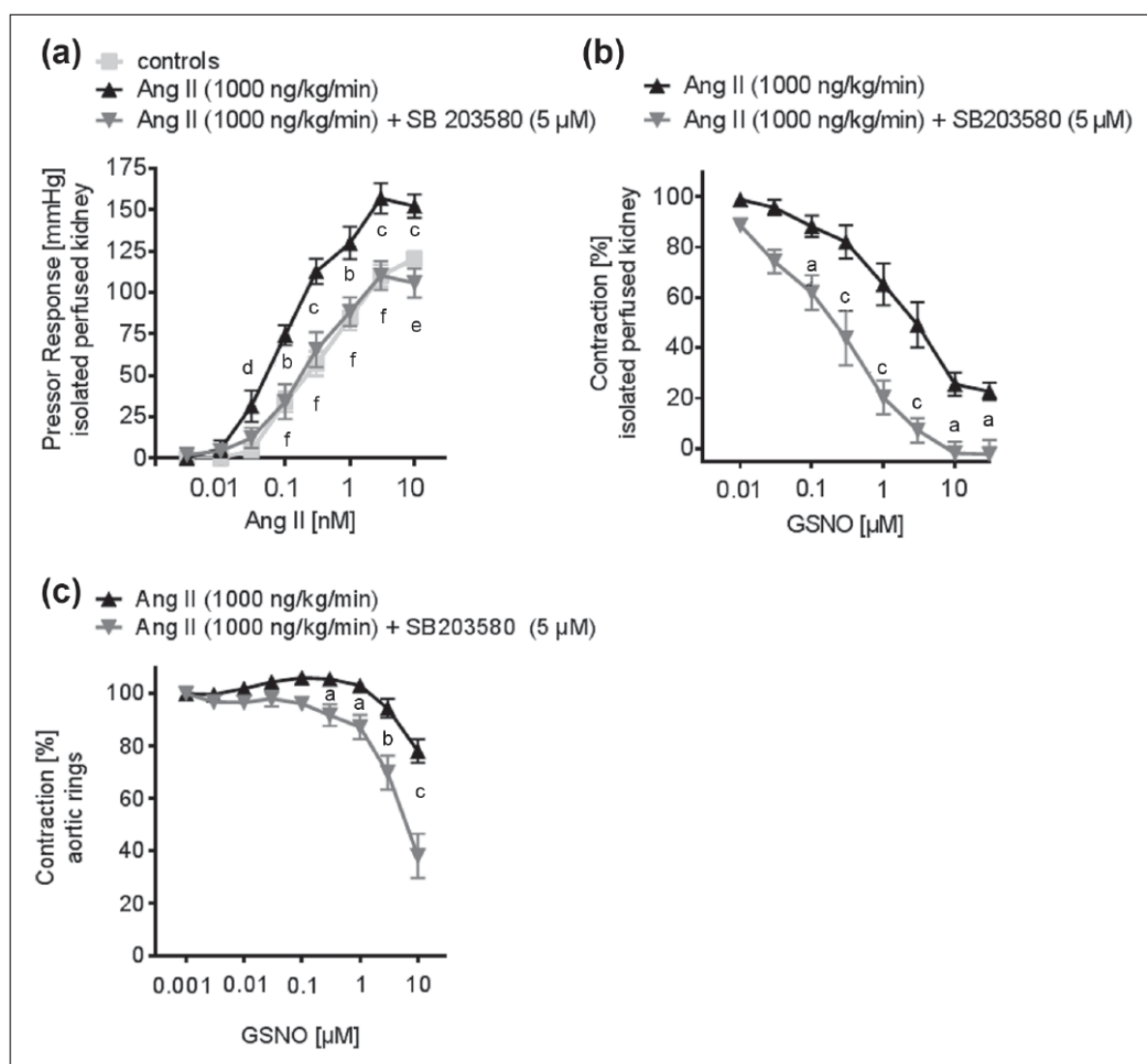
Figure 4. The effect of acute p38 MAPK inhibition on the vascular function of conductance and resistance of vessels was tested in the isolated perfused kidney and thoracic aortic rings. **(a)** The Ang II-induced pressor response was attenuated in the presence of the p38 MAPK inhibitor SB203580 at 5 μM, in the kidneys of hypertensive mice (controls: $n = 11$; Ang II: $n = 8$; Ang II + SB203580: $n = 8$). Data represent the mean ± SEM. [b]$p < 0.01$, [c]$p < 0.001$ controls *versus* Ang II; [d]$p < 0.05$, [e]$p < 0.01$, [f]$p < 0.001$ Ang II versus Ang II + SB203580. **(b)** GSNO induced endothelium-independent vasorelaxation is improved by acute p38 MAPK-inhibition with SB203580 at 5 μM in the kidneys of hypertensive mice (Ang II: $n = 6$; Ang II + SB203580: $n = 6$). Data represent the mean ± SEM. A 2-way ANOVA for repeated measurements was followed by Bonferroni correction *post-hoc* test. [a]$p < 0.05$, [c]$p < 0.001$ Ang II versus Ang II + SB203580. **(c)** GSNO induced endothelium-independent vasorelaxation was improved by acute p38 MAPK inhibition with SB203580 at 5 μM in the aortic rings of hypertensive mice (Ang II: $n = 8$; Ang II + SB203580: $n = 7$). Data represent the mean ± SEM; [a]$p < 0.05$, [b]$p < 0.01$, [c]$p < 0.001$ Ang II versus Ang II + SB203580. A 2-way ANOVA for repeated measurements was followed by Bonferroni correction *post-hoc* test.
[a]$p < 0.05$.
[b]$p < 0.01$.
[c]$p < 0.001$.
[d]$p < 0.05$.
[e]$p < 0.01$.
[f]$p < 0.001$.
Ang II: angiotensin 2; ANOVA: analysis of variance; BIRB796: a MAPK inhibitor; GSNO: S-Nitrosoglutathione; KCl: potassium chloride; NS: not significant; SEM: standard error of the mean

pressor responses in the kidneys of Ang II-treated mice (Figure 4(a)). Renal vasodilator responses to GSNO were

also significantly improved in the presence of SB203580 at 5 μM (Figure 4(b)).

Discussion

In the present study, we evaluated a novel mechanism of pharmacological intervention in Ang II-dependent hypertension. Our data indicates that p38 MAPK activation plays a crucial role in the development of Ang II-induced hypertension and vascular remodeling. Attenuation of Ang II induced hypertension and improved vascular function by BIRB796 was accompanied by changes in gene expression in aorta vessel wall of markers of vascular remodeling. In addition, the vascular function of the renal resistance arteries was ameliorated by inhibition of p38 MAPK.

In the present study, chronic inhibition of p38 MAPK reduced the SBP in Ang II-dependent hypertension significantly; however, blood pressure levels did not normalize in these mice. The p38 MAPK activation is one of a variety of mechanisms that contribute to Ang II-dependent hypertension. Other mechanisms, such as AT1 receptor heterodimerization and the RhoA/Rho kinase pathway that are activated by Ang II are also very important signaling pathways regulating the extent of Ang II-dependent hypertension.[30–32]

Recently, Sparks et al.[33] showed that AT1 receptors in renal vascular smooth muscle cells are essential for the development of Ang II-dependent hypertension; however, the underlying mechanism of how AT1 receptors on vascular smooth muscle cells mediate hypertension is not fully understood. In this regard, p38 MAPK seems to be an important player. Herein, the Ang II treatment led to a significant increase in renal p38 MAPK activation and ROS production. This activation was attenuated by chronic treatment with BIRB796 and accompanied by reduced SBP. Previously, we demonstrated that p38 MAPK activation increases pressor responses to Ang II in renal resistance vessels of hypercholesterolemic mice, through ROS-dependent p38 MAPK activation.[4] In addition, p38 MAPK inhibition increased the vasodilator response to nitric oxide (NO) in humans, and decreased the end organ damage in hypertensive rats, through a reduction of ROS abundance.[34,35] In this study, the reduced phosphorylation of p38 MAPK through BIRB796 treatment was accompanied by a markedly reduced ROS abundance, as measured by urinary 8-isoprostane, emphasizing the importance of ROS in vascular dysfunction.[23]

In this study, chronic inhibition of p38 MAPK not only reduced SBP, but also improved vascular smooth muscle cell-dependent vasodilatation in conductance blood vessels as shown by previous studies.[36] As a significant novelty of the presented study, we could show that chronic inhibition of p38 MAPK attenuated pressor responses to Ang II and improved vasodilatation as a response to GSNO in renal resistance vessels. In contrast to conductance vessels, such as the aorta, resistance vessels play a pivotal role in blood pressure regulation. This finding of the presented study directly links p38 MAPK activation to blood pressure regulation.

Furthermore, the inhibition of p38 MAPK led to a reduction in aortic hypertrophy. These findings are supported by

previous studies, which show that p38 MAPK activation is an important mediator of vascular stiffening.[13,37] Vascular stiffness is a strong predictor of future cardiovascular events and all-cause mortality.[17]

It is well known that p38 MAPK activation mediates hypertrophy of vascular smooth muscle cells *in vitro*.[38] In our present study, we could show that chronic p38 MAPK inhibition reduced vascular hypertrophy *in vivo* and it modulated the genes involved in vascular remodeling. Inhibition of p38 MAPK could significantly reduce the expression of aortic MMP1, which is strongly involved in p38 MAPK-dependent vascular remodeling.[39,40]

In addition, the expression of MMP9, known to be activated by the renin–angiotensin–aldosterone system (RAAS), was also reduced by chronic p38 MAPK inhibition.[41,42] MMP9 is a strong inducer of the TGF-β pathway, leading to an increase in collagen deposition, a crucial mechanism for interstitial fibrosis and aortic stiffness.[43–46] Based on these results, it is feasible that Ang II-mediated p38 MAPK activation led to vascular stiffening, which itself causes augmentation of SBP. In fact, p38 MAPK activation was reduced in the aortas of BIRP796-treated mice. Differences of AT1a or AT2 receptor abundance cannot be considered as a cause of the attenuated vascular injury in BIRP796-treated mice, as both AT1a and AT2 receptor RNA expression levels did not differ between both groups. Therefore, differences in vascular hypertrophy do not appear to be caused by receptor abundance. In this study, in contrast to previous studies, changes in the relative gene expression of collagen1 and fibronectin, markers of interstitial fibrosis and vascular remodeling, were not changed by our inhibition of p38 MAPK.[47] The relatively short observational period of the study could be an explanation for this finding. Moreover, gene expression of the MMP inhibitor TIMP-1 was also not significantly different in the aortic lysates, in this study.

Besides the described effects on vascular stiffening, there is strong evidence that activation of p38 MAPK influences Ang II-dependent signaling in the vasculature.[5,6] Therefore, we examined the acute effect of a p38 MAPK inhibition on vascular function in aortic rings, and in isolated perfused kidneys of Ang II-treated mice, in the presence or absence of SB203580. Control mice were added to these experiments to illustrate the effect of acute p38 MAPK inhibition, compared to subjects of normal blood pressure. Similar to the attenuated renal pressor responses observed in BIRB796-treated hypertensive mice, acute p38 MAPK inhibition reduced renal pressor responses to Ang II to the same extent. Thus, in Ang II-dependent hypertension, the beneficial effect of p38 MAPK inhibition on vascular function is mediated through direct actions on Ang II signaling; and therefore, are at least partially independent from vascular remodeling. Interestingly, p38 MAPK inhibition had no effect on the maximum vasoconstrictive response to KCL nor norepinephrine, in renal resistance

vessels. This implied that the observed changes in vasoreactivity were specific to the actions of Ang II. As Ang II-dependent hypertension is dependent on renal AT1 receptor signaling, p38 MAPK signaling in the renal vasculature might be one essential underlying mechanism for the development of Ang II-dependent hypertension.[33]

Here we found that acute p38 MAPK inhibition in the isolated perfused kidney and aortic rings obtained from Ang II-treated animals showed improved vasodilation when exposed to GSNO. This might be a result of decreased ROS production. Recently, we and others have shown that p38 MAPK inhibition led to reduced expression of different NADPH oxidase subunits, resulting in reduced ROS abundance.[4,34] An increase in ROS abundance contributes to the depletion of NO, a hallmark of endothelial dysfunction.[23] In the presence of increased ROS, the NO scavenging occurs through the formation of peroxynitrite. This mechanism of NO depletion can increase vasoconstriction. Inhibition of p38 MAPK can reduce ROS; and therefore, counteract this mechanism. In addition, p38 MAPK kinase inhibition leads to a reduced MLC(20) phosphorylation in resistance blood vessels.[4] Reduced MLC(20) phosphorylation results in reduced contractility of smooth muscle cells and might potentiate the vasodilatory effect of GSNO in the presence of a p38 inhibitor. Thus, this mechanism might also contribute to the decrease in vasoreactivity and blood pressure through p38 MAPK inhibition, as seen in this study.

In summary, this study elucidated the role of p38 MAPK in Ang II-dependent hypertension. We were able to demonstrate that inhibition of p38-MAPK improves blood pressure and vascular injury through counteracting Ang II-mediated signaling, thus improving vascular remodeling and vascular function. Our findings indicate that p38-MAPK is a potential pharmaceutical target in hypertension.

Note

Authors Potthoff and Stamer contributed equally to this work.

References

1. Lim SS, Vos T, Flaxman AD, et al. A comparative risk assessment of burden of disease and injury attributable to 67 risk factors and risk factor clusters in 21 regions, 1990–2010: A systematic analysis for the Global Burden of Disease Study 2010. *Lancet* 2012; 380: 2224–2260.
2. Schachter M. Changes in the usage of antihypertensive drugs: Implications and prospects. *Brit J Clin Pharmacol* 2005; 60: 231–234.
3. Ikeda N, Sapienza D, Guerrero R, et al. Control of hypertension with medication: A comparative analysis of national surveys in 20 countries. *Bull WHO* 2014; 92: 10–19.
4. Potthoff SA, Fahling M, Clasen T, et al. Angiotensin-(1–7) modulates renal vascular resistance through inhibition of p38 mitogen-activated protein kinase in apolipoprotein E-deficient mice. *Hypertension* 2014; 63: 265–272.
5. Taniyama Y, Ushio-Fukai M, Hitomi H, et al. Role of p38 MAPK and MAPK-APK-2 in angiotensin II-induced Akt activation in vascular smooth muscle cells. *Am J Physiol Cell Physiol* 2004; 287: C494–499.
6. Meloche S, Landry J, Huot J, et al. P38 MAP kinase pathway regulates angiotensin II-induced contraction of rat vascular smooth muscle. *Am J Physiol Heart Circ Physiol* 2000; 279: H741–751.
7. Kwon S, Fang LH, Kim B, et al. P38 Mitogen-activated protein kinase regulates vasoconstriction in spontaneously hypertensive rats. *J Pharmacol Sci* 2004; 95: 267–272.
8. Patzak A, Lai EY, Fahling M, et al. Adenosine enhances long-term contractile response to angiotensin II in afferent arterioles. *Am J Regul Integrat Comparat Physiol* 2007; 293: R2232–2242.
9. Wei C, Cardarelli MG, Downing SW, et al. The effect of angiotensin II on mitogen-activated protein kinase in human cardiomyocytes. *J Renin–Angiotensin–Aldosterone Syst* 2000; 1: 379–384.
10. Wang M, Monticone RE and Lakatta EG. Proinflammation of aging central arteries: A mini-review. *Gerontology* 2014; 60: 519–529.
11. Tsioufis C, Dimitriadis K, Selima M, et al. Low-grade inflammation and hypoadiponectinaemia have an additive detrimental effect on aortic stiffness in essential hypertensive patients. *Eur Heart J* 2007; 28: 1162–1169.
12. Kyaw M, Yoshizumi M, Tsuchiya K, et al. Antioxidants inhibit JNK and p38 MAPK activation but not ERK 1/2 activation by angiotensin II in rat aortic smooth muscle cells. *Hypertens Res* 2001; 24: 251–261.
13. Ushio-Fukai M, Alexander RW, Akers M, et al. P38 Mitogen-activated protein kinase is a critical component of the redox-sensitive signaling pathways activated by angiotensin II. Role in vascular smooth muscle cell hypertrophy. *J Biol Chem* 1998; 273: 15022–15029.
14. Mattace-Raso FU, Van der Cammen TJ, Hofman A, et al. Arterial stiffness and risk of coronary heart disease and stroke: The Rotterdam Study. *Circulation* 2006; 113: 657–663.
15. Laurent S, Katsahian S, Fassot C, et al. Aortic stiffness is an independent predictor of fatal stroke in essential hypertension. *Stroke* 2003; 34: 1203–1206.
16. Palatini P, Casiglia E, Gasowski J, et al. Arterial stiffness, central hemodynamics and cardiovascular risk in hypertension. *Vasc Health Risk Manag* 2011; 7: 725–739.

17. Vlachopoulos C, Aznaouridis K and Stefanadis C. Prediction of cardiovascular events and all-cause mortality with arterial stiffness: A systematic review and meta-analysis. *J Am Coll Cardiol* 2010; 55: 1318–1327.

18. Laurent S, Boutouyrie P, Asmar R, et al. Aortic stiffness is an independent predictor of all-cause and cardiovascular mortality in hypertensive patients. *Hypertension* 2001; 37: 1236–1241.

19. Park JK, Fischer R, Dechend R, et al. P38 mitogen-activated protein kinase inhibition ameliorates angiotensin II-induced target organ damage. *Hypertension* 2007; 49: 481–489.

20. Stegbauer J, Vonend O, Habbel S, et al. Angiotensin II modulates renal sympathetic neurotransmission through nitric oxide in AT2 receptor knockout mice. *J Hypertens* 2005; 23: 1691–1698.

21. Stegbauer J, Kuczka Y, Vonend O, et al. Endothelial nitric oxide synthase is predominantly involved in angiotensin II modulation of renal vascular resistance and norepinephrine release. *Am J Physiol* 2008; 294: R421–428.

22. Broekmans K, Stegbauer J, Potthoff SA, et al. Angiotensin II-induced hypertension is attenuated by reduction of sympathetic output in NO-sensitive guanylyl cyclase 1 knockout mice. *J Pharmacol Exp Therapeut* 2016; 356: 191–199.

23. Stegbauer J, Potthoff SA, Quack I, et al. Chronic treatment with angiotensin-(1–7) improves renal endothelial dysfunction in apolipoprotein E-deficient mice. *Br J Pharmacol* 2011; 163: 974–983.

24. Stegbauer J, Oberhauser V, Vonend O, et al. Angiotensin-(1–7) modulates vascular resistance and sympathetic neurotransmission in kidneys of spontaneously hypertensive rats. *Cardiovasc Res* 2004; 61: 352–359.

25. Joos H, Albrecht W, Laufer S, et al. Differential effects of p38 MAP kinase inhibitors on the expression of inflammation-associated genes in primary, interleukin-1beta-stimulated human chondrocytes. *Brit J Pharmacol* 2010; 160: 1252–1262.

26. Owens AP III, Subramanian V, Moorleghen JJ, et al. Angiotensin II induces a region-specific hyperplasia of the ascending aorta through regulation of the inhibitor of differentiation 3. *Circulat Res* 2010; 106: 611–619.

27. McNulty M, Mahmud A, Spiers P, et al. Collagen type I degradation is related to arterial stiffness in hypertensive and normotensive subjects. *J Hum Hypertens* 2006; 20: 867–873.

28. Castro MM, Rizzi E, Prado CM, et al. Imbalance between matrix metalloproteinases and tissue inhibitor of metalloproteinases in hypertensive vascular remodeling. *Matrix Biol* 2010; 29: 194–201.

29. Koffi I, Lacolley P, Kirchengaast M, et al. Prevention of arterial structural alterations with verapamil and trandolapril; and consequences for mechanical properties in spontaneously hypertensive rats. *Eur J Pharmacol* 1998; 361: 51–60.

30. Nishimura A, Sunggip C, Tozaki-Saitoh H, et al. Purinergic P2Y6 receptors heterodimerize with angiotensin AT1 receptors to promote angiotensin II-induced hypertension. *Sci Signal* 2016; 9: 7.

31. Carbone ML, Bregeon J, Devos N, et al. Angiotensin II activates the RhoA exchange factor Arhgef 1 in humans. *Hypertension* 2015; 65: 1273–1278.

32. Ravarotto V, Pagnin E, Maiolino G, et al. The blocking of angiotensin II Type 1 receptor and RhoA/Rho kinase activity in hypertensive patients: Effect of olmesartan medoxomil and implication with cardiovascular-renal remodeling. *J Renin–Angiotensin–Aldosterone Syst* 2015; 16: 1245–1250.

33. Sparks MA, Stegbauer J, Chen D, et al. Vascular Type 1A angiotensin II receptors control BP by regulating renal blood flow and urinary sodium excretion. *J Am Soc Nephrol* 2015; 26: 2953–2962.

34. Bao W, Behm DJ, Nerurkar SS, et al. Effects of p38 MAPK inhibitor on angiotensin II-dependent hypertension, organ damage and superoxide anion production. *J Cardiovasc Pharmacol* 2007; 49: 362–368.

35. Cheriyan J, Webb AJ, Sarov-Blat L, et al. Inhibition of p38 mitogen-activated protein kinase improves nitric oxide-mediated vasodilatation and reduces inflammation in hypercholesterolemia. *Circulation* 2011; 123: 515–523.

36. Ju H, Behm DJ, Nerurkar S, et al. P38 MAPK inhibitors ameliorate target organ damage in hypertension: Part 1. P38 MAPK-dependent endothelial dysfunction and hypertension. *J Pharmacol Exp Therapeut* 2003; 307: 932–938.

37. Wu J, Thabet SR, Kirabo A, et al. Inflammation and mechanical stretch promote aortic stiffening in hypertension through activation of p38 mitogen-activated protein kinase. *Circulat Res* 2014; 114: 616–625.

38. Griendling KK, Berk BC, Ganz P, et al. Angiotensin II stimulation of vascular smooth muscle phosphoinositide metabolism. State of the art lecture. *Hypertension* 1987; 9: III181–185.

39. Cortez DM, Feldman MD, Mummidi S, et al. IL-17 stimulates MMP-1 expression in primary human cardiac fibroblasts via p38 MAPK-dependent and ERK1/2-dependent C/EBP-beta, NF-kappaB and AP-1 activation. *Am J Physiol Heart Circulat Physiol* 2007; 293: H3356–3365.

40. Wu Y, Zhu L, Liu L, et al. Interleukin-17A stimulates migration of periodontal ligament fibroblasts via p38 MAPK/NF-kappaB-dependent MMP-1 expression. *J Cellul Physiol* 2014; 229: 292–299.

41. Dange MC, Agarwal AK and Kalraiya RD. Extracellular galectin-3 induces MMP9 expression by activating p38 MAPK pathway via lysosome-associated membrane protein-1 (LAMP1). *Molec Cellul Biochem* 2015; 404: 79–86.

42. Gilet A, Zou F, Boumenir M, et al. Aldosterone up-regulates MMP-9 and MMP-9/NGAL expression in human neutrophils through p38, ERK1/2 and PI3K pathways. *Exp Cell Res* 2015; 331: 152–163.

43. Chiao YA, Ramirez TA, Zamilpa R, et al. Matrix metalloproteinase-9 deletion attenuates myocardial fibrosis and diastolic dysfunction in ageing mice. *Cardiovasc Res* 2012; 96: 444–455.

44. Dayer C and Stamenkovic I. Recruitment of matrix metalloproteinase-9 (MMP-9) to the fibroblast cell surface by lysyl hydroxylase-3 (LH3) triggers TGF-beta activation and fibroblast differentiation. *J Biolog Chem* 2015; 290: 13763–13778.

45. Yao J, Xiong M, Tang B, et al. Simvastatin attenuates pulmonary vascular remodelling by down-regulating matrix metalloproteinase-1 and -9 expression in a carotid artery-jugular vein shunt pulmonary hypertension model in rats. *Eur J Cardio-thoracic Surg* 2012; 42: e121–7.

46. Thomas AC and Newby AC. Effect of matrix metalloproteinase-9 knockout on vein graft remodelling in mice. *J Vascular Res* 2010; 47: 299–308.

47. Li Z, Froehlich J, Galis ZS, et al. Increased expression of matrix metalloproteinase-2 in the thickened intima of aged rats. *Hypertension* 1999; 33: 116–123.

Angiotensin II-Induced Hypertension Is Attenuated by Reduction of Sympathetic Output in NO-Sensitive Guanylyl Cyclase 1 Knockout Mice

Kathrin Broekmans, Johannes Stegbauer, Sebastian A. Potthoff, Michael Russwurm, Doris Koesling, and Evanthia Mergia

Institut für Pharmakologie, Ruhr-Universität Bochum, Bochum, Germany (K.B., M.R., D.K., E.M.) and Klinik für Nephrologie, Universitätsklinikum Düsseldorf, Heinrich-Heine-Universität Düsseldorf, Germany (J.S., S.A.P.)

ABSTRACT

In the regulation of vascular tone, the dilatory nitric oxide (NO)/ cGMP pathway balances vasoconstriction induced by the renin-angiotensin and sympathetic nervous systems. NO-induced cGMP formation is catalyzed by two guanylyl cyclases (GC), NO-sensitive guanylyl cyclase 1 (NO-GC1) and NO-GC2, with indistinguishable enzymatic properties. In vascular smooth muscle cells, NO-GC1 is the major isoform and is responsible for more than 90% of cGMP formation. Despite reduced vaso-relaxation, NO-GC1–deficient mice are not hypertensive. Here, the role of NO-GC1 in hypertension provoked by contractile agonists angiotensin II (Ang II) and norepinephrine (NE) was evaluated in NO-GC1–deficient mice. Hypertension induced by chronic Ang II treatment did not differ between wild-type (WT) and NO-GC1 knockout mice (KO). Also, attenuation of NO-dependent aortic relaxation induced by the Ang II treatment was similar in both genotypes and was most probably attributable to an increase of phosphodiesterase 1 expression. Analysis of plasma NE content—known to be influenced by Ang II—revealed lower NE in the NO-GC1 KO under Ang II-treated- and non-treated conditions. The finding indicates reduced sympathetic output and is underlined by the lower heart rate in the NO-GC1 KO. To find out whether the lack of higher blood pressure in the NO-GC1 KO is a result of reduced sympathetic activity counter-balancing the reduced vascular relaxation, mice were challenged with chronic NE application. As the resulting blood pressure was higher in the NO-GC1 KO than in WT, we conclude that the reduced sympathetic activity in the NO-GC1 KO prevents hypertension and postulate a possible sympatho-excitatory action of NO-GC1 counteracting NO-GC1's dilatory effect in the vasculature.

Introduction

Hypertension, a major risk factor for cardiovascular diseases, is associated with increased vascular tone. Within the regulation of the vascular tone, the dilatory nitric oxide (NO)/ cGMP pathway balances the contractile action of: angiotensin II, the major biologically active metabolite of the renin-angiotensin system (RAS); and norepinephrine (NE) released from sympathetic nerve terminals. The cGMP-forming NO-sensitive guanylyl cyclase (NO-GC) holds the key position in the NO/cGMP pathway; in addition, cGMP is formed by the membrane guanylyl cyclase receptors (Kuhn, 2003). The NO-GC is a heterodimeric enzyme composed of an α and a β subunit and contains a prosthetic heme group that binds NO and causes an up to 200-fold stimulation of the cGMP production (Friebe and Koesling, 2003). Two isoforms of the NO-GC exist, NO-GC1 and NO-GC2, which contain the same beta1 subunit but different alpha subunits (α_1 or α_2)

(Russwurm and Koesling, 2002). Although they differ in subcellular localization, the isoforms do not differ in regulatory or catalytic properties (Russwurm et al., 2001). To unravel their physiologic function, we generated knockout mice lacking either the NO-GC1 or NO-GC2 isoform (Mergia et al., 2006). First characterization revealed NO-GC1 as the major isoform in the vascular system, as shown by the pronounced reduction of cGMP-forming activity (>90%) and vascular relaxation. Yet, despite the reduced vascular relaxation, blood pressure of NO-GC1 knockout (KO) mice was not increased.

In addition to cGMP formation, cGMP signals are controlled by cGMP-hydrolyzing phosphodiesterases (PDEs). In vascular smooth muscle cells, PDE1 and PDE5 play important roles in regulation of the intracellular cGMP concentration (Rybalkin et al., 2003). PDE1 degrades cAMP and cGMP, whereas PDE5 is specific for cGMP degradation. PDE1 is activated by Ca^{2+} and calmodulin (CaM); thus, in the presence of a contractile agonist increasing intracellular Ca^{2+}, PDE1 is activated and facilitates contraction by lowering cyclic nucleotide levels (Sonnenburg et al., 1995). An important contractile agonist that acts via a rise of Ca^{2+} is angiotensin II (Ang II) with an established role in the regulation of blood pressure (Stegbauer

ABBREVIATIONS: Ang II, Angiotensin II; CaM, calmodulin; DEA-NO, 2-(*N,N*-diethylamino)-diazenolate-2-oxide; KO, knockout; NE, norepinephrine; NO, nitric oxide; NO-GC, NO-sensitive guanylyl cyclase; PDE, phosphodiesterase; WT, wild-type.

and Coffman, 2011). Ang II is targeted by the antihypertensive ACE inhibitors and AT1 receptor antagonists (Yusuf et al., 2008), and its effects are counteracted by NO/cGMP (Yan et al., 2003).

In the present study, NO-GC1 KO mice with greatly reduced vascular cGMP content were challenged with Ang II (high dose, 1.44 mg/kg per day, 2 weeks) to find out if the resulting hypertension is aggravated. Yet, Ang II-induced hypertension was not exacerbated by the NO-GC1 deficiency. Also, relaxation of aortic rings was likewise reduced by the Ang II treatment in wild-type (WT) and NO-GC1 KO and shown to result from an increased expression of PDE1. Further analysis revealed a reduced sympathetic activity in NO-GC1 KO. Thus, we hypothesized that normotension in the NO-GC1 KO is a balance between the lower sympathetic output and the reduced vascular cGMP. Consistent with this, hypertension induced by NE treatment was higher in NO-GC1 KO than in WT.

Materials and Methods

Animal Models. Experiments were performed with male NO-GC1 KO mice lacking the α_1 subunit of the heterodimeric NO-GC1 ($\alpha_1\beta_1$) and WT littermates backcrossed to C57Bl/6Rj background for more than 12 times (>N12 generation). The KO mice were generated and genotyped as described previously (Mergia et al., 2006). Two- to three-month-old mice were used. All animal experiments were performed according to the *Guide for the Care and Use of Laboratory Animal* published by the US National Institutes of Health (NIH Publication, 8th ed., 2011) and were also approved by the local animal care committee (license no. 87-51.04.2010.A039 and 8.87-50.10.34.08.216).

Angiotensin II, Norepinephrine, and Sildenafil Administration. osmotic minipump (model 1002; ALZET/DURECT Corporation, Cupertino, CA) was implanted subcutaneously in the interscapular region to deliver Ang II or NE at a constant rate of 0.25 μl/hour in saline solution. For implantation, mice were anesthetized (100 mg/kg ketamine, 10 mg/kg xylazine) and thereafter treated with analgesics (0.2 mg/kg meloxicam) for three days. Ang II was infused at a dose of 1.44 mg/kg per day for 2 weeks, NE at a dose of 2.88 mg/kg per day for 2 weeks. Sildenafil citrate (Viagra; Pfizer, New York, NY) was dissolved in drinking water acidified with citric acid (pH ~3) to a final concentration of 800 mg/l and given ad libitum resulting in a free plasma concentration of 21 ± 5 nmol/l sildenafil determined as described by Stegbauer et al. (2013); on the basis of an average water consumption of about 3 ml per day and a body weight of ~25 g for an adult mouse, the daily sildenafil dose corresponded to 100 mg/kg. Mice were treated with sildenafil during the second week of Ang II treatment.

Two weeks after the minipump implantation, the mice were anesthetized by CO_2 inhalation and decapitated. Blood was collected and hearts and aortas were harvested, weighed, and subjected to further analysis.

Blood Pressure Measurement. Systolic blood pressure and heart rate were measured in conscious mice by noninvasive tail-cuff photoplethysmography (BP-98A; Softron Co., Tokyo, Japan). Because this device does not directly measure diastolic pressure but rather supplies an estimation calculated by a software algorithm, we do not report diastolic blood pressure values here.

For habituation the mice were measured daily for 7 days. After training, 10 measurements per mouse were taken daily for at least 5 days. Mice were measured before and during the second week after implantation of the osmotic minipumps.

Chronic Measurement of Intra-Arterial Pressure by Radiotelemetry. Blood pressures were measured in conscious, unrestrained WT and NO-GC1 KO mice using radiotelemetry (PA-C10) as described previously (Butz and Davisson, 2001). In brief, for implantation of the telemetry catheters, the left carotid artery was

cannulated and the catheter was advanced to the point where the small notch on the tubing resided at the vessel opening. Inserting the catheter up to this landmark notch assures the critical placement of the pressure-sensing tip just inside of the thoracic aorta. For the implantation of the telemetry catheters, mice were anesthetized with a single intraperitoneal injection of ketamine and xylazine (100 and 10 mg/kg, respectively). The adequacy of anesthesia was determined by the loss of a pedal withdrawal reflex. For analgesia, all mice received meloxicam (0.2 mg/kg). After transmitter implantation, mice were allowed to recover for 7 days to reestablished normal circadian rhythms. Blood pressure levels were recorded continuously with sampling every 5 minutes for 10-second intervals. Baseline measurements were recorded for 5 consecutive days. On day 6, osmotic minipumps (model 1002; ALZET) were implanted to infuse Ang II (1.44 mg/kg per day) for 14 days.

Organ Bath Experiments with Isolated Aortic Rings. Thoracic aorta placed in Krebs-Henseleit buffer (118 mmol/l NaCl, 4.7 mmol/l KCl, 1.2 mmol/l $MgSO_4$, 1.2 mmol/l KH_2PO_4, 25 mmol/l $NaHCO_3$, 2.55 mmol/l $CaCl_2$, and 7.5 mmol/l D-glucose, oxygenated with 5% CO_2 in O_2) were cut in four rings of similar size. The aortic rings were mounted on fixed segment support pins in two four-chamber myographs (Multi Wire Myograph 610 M; DMT, Aarhus, Denmark) containing 5 ml Krebs-Henseleit buffer. Resting tension was set to 5 mN. After equilibration in the presence of diclofenac (3 μmol/l), aortic rings were contracted (1 μmol/l phenylephrin), and subsequently vasodilation to carbachol, DEA-NO, or forskolin was recorded. Reponses to DEA-NO and forskolin were determined in the presence of the NO synthase inhibitor L-NAME (200 μmol/l).

Aortic rings derived from nontreated and Ang II-treated WT or NO-GC1 KO mice were examined in parallel. Effects of sildenafil were examined in parallel with aortic rings derived from Ang II-treated and Ang II + sildenafil-treated WT mice, and nontreated animals.

Western Blot Analysis. To obtain aortic homogenates, aortas (from aortic arch to abdominal bifurcation) were homogenized in 300 μl of buffer (50 mmol/l TEA/HCl, 50 mmol/l NaCl, 2 mmol/l dithiothreitol, 0.2 mmol/l benzamidine, 0.5 mmol/l phenylmethylsulfonyl fluoride, 1 μmol/l pepstatin A; pH 7.4, 4°C) using a glass/glass homogenizer (900 rpm). After centrifugation (800g, 5 minutes, 4°C), supernatants were removed and subjected to further analysis. Protein concentrations were determined using a Bradford assay (Bio-Rad, Munich, Germany). The following Western blot analyses were performed as described previously (Mergia et al., 2003). Anti-PDE1A (Santa Cruz Biotechnology, Heidelberg, Germany) was used in a 1:500 and anti-PDE5 (New England Biolabs, Frankfurt, Germany) in a 1:1,000 dilution. The PDE signals were normalized to the alpha smooth muscle actin signal in the same lane (1:5000; ab5694; Abcam, Cambridge, UK).

Determination of cGMP Content in Intact Aortic Rings. Aortic rings (eight per aorta) were allowed to equilibrate for 15 minutes in Krebs-Henseleit buffer (37°C, oxygenated with 5% CO_2 in O_2) and were then stimulated by carbachol (30 μmol/l, 5 minutes) or DEA-NO (100 μmol/l, 2.5 minutes). The equilibrated, nonstimulated, aortic rings were used as controls. After the reaction, aortic rings were snap frozen in liquid nitrogen and homogenized in 70% (v/v) ice-cold ethanol using a glass/glass homogenizer (900 rpm). After centrifugation (20,000g, 15 minutes, 4°C), supernatants were dried at 95°C and cGMP contents were measured by radioimmunoassay (Mergia et al., 2006). To standardize the different samples, protein pellets were dissolved (0.1 M NaOH/0.1% SDS) and protein content was determined using the bicinchoninic acid method (Thermo Scientific, Sunnyvale, CA).

Measurement of cGMP-Hydrolyzing PDE Activity. PDE activity was measured by the conversion of [^{32}P]cGMP (synthesized from [α-^{32}P]GTP using purified NO-GC) to guanosine and [^{32}P]phosphate in the presence of alkaline phosphatase (Sigma-Aldrich, St. Louis, MO) at 37°C for 5 minutes.

Reaction mixtures (0.1 ml) contained aortic homogenate (2 μl, ~5 μg protein), [^{32}P]cGMP (~2 kBq), 1 μmol/l cGMP, 12 mmol/l $MgCl_2$,

3 mmol/l dithiothreitol, 0.5 mg/ml bovine serum albumin, 2 IU of alkaline phosphatase, and 50 mmol/l TEA/HCl, pH 7.4. Reactions were stopped by the addition of 900 μl ice-cold charcoal suspension (30% activated charcoal in 50 mmol/l KH_2PO_4, pH 2.3). After pelleting of the charcoal by centrifugation (12,000g, 4 minutes), [^{32}P]phosphate was measured in supernatant.

Sildenafil at 100 nmol/l was added to the measurements to determine the PDE activity ascribed to PDE5. EGTA (2 mmol/l; Sigma-Aldrich) or calcium (1 mmol/l $CaCl_2$) and calmodulin (10 μmol/l; Merck, Darmstadt, Germany) was added to inhibit or stimulate PDE1, respectively. PDE assays were carried out in triplicates.

As the Ang II treatment yielded higher protein concentrations in the aortas, which can mostly be attributed to extracellular matrix proteins, enzyme activities (PDE, GC) were normalized to milliliters, with each aorta homogenized in 300 μl homogenization buffer.

Determination of NO-Stimulated GC activity. The NO-stimulated GC activity (100 μmol/l DEA-NO, 10 minutes, 37°C) was determined in aortic homogenates of WT mice (3 μg) in the presence of GTP. The forming cGMP was quantified by radioimmunoassay as described previously (Mergia et al., 2006).

Determination of Norepinephrine in Plasma and Urine Samples. To obtain plasma, blood from decapitated mice was collected in vials containing 0.3 mol/l EDTA, pH 8.0, and centrifuged (10,000g, 15 minutes, 4°C). Urine was collected from mice housed for 24 hours in metabolic cages (Tecniplast Deutschland, GmbH, Hohenpeißenberg Germany). Norepinephrine and 3,4-dihydoxybenzylamine hydrobromide (added as an internal standard; Chromsystems, München, Germany) were adsorbed onto alumina from EDTA plasma (100 μl) or urine (50 μl) and subsequently eluted with 0.1 mol/l $HClO_4$ (250 μl). The eluate (100 μl) was injected into a high-performance liquid chromatography system equipped with a reverse-phase column (Guard-Pak Resolve C18; Waters Corporation, Milford, MA) in 15 mmol/l Na_2HPO_4, 30 mmol/l citric acid, 2 mmol/l Na_2EDTA, 2.77 mmol/l (−)-octanesulfonic acid, and 12% methanol (v/v) (pH 6.5). Norepinephrine was detected with an electrochemical detector (Waters 460).

Statistics. All data were expressed as means ± S.E.M. (n = number of mice). The experiments were compared statistically by unpaired Students' t test. Concentration-response curves were evaluated by analysis of variance (ANOVA) for repeated measurements. Experiments were regarded as significant at a P value of less then 0.05. Blood pressure control values of all WT and NO-GC1–deficient mice used in the current study were averaged to circumvent minor differences owing to the small number of animals in a given group.

Results

Deletion of the major NO-GC isoform, NO-GC1, resulted in a pronounced reduction of NO-induced cGMP formation and attenuated vascular relaxation. Yet, blood pressure in these mice was not increased (WT 107 ± 1 versus KO 108 ± 1 mmHg, on a C57BL/6 background). Normotension of the NO-GC1–deficient mice did not result from an upregulation of NO-GC2, as the expression NO-GC2 in the KO mice was found to be unaltered (Mergia et al., 2006).

In this study, we challenged mice with a high dose of Ang II (1.44 mg/kg per day, 2 weeks) to examine whether the NO-GC1 deficiency, and thus the reduced cGMP, exacerbates hypertension.

Ang II-Induced Hypertension and Hypertrophy Did Not Differ between WT and NO-GC1 KO Mice. Chronic Ang II infusion is known to induce hypertension and heart hypertrophy in mice. Here, the systolic blood pressure was measured in conscious mice by noninvasive tail-cuff plethysmography. The two-week Ang II treatment led to an increase
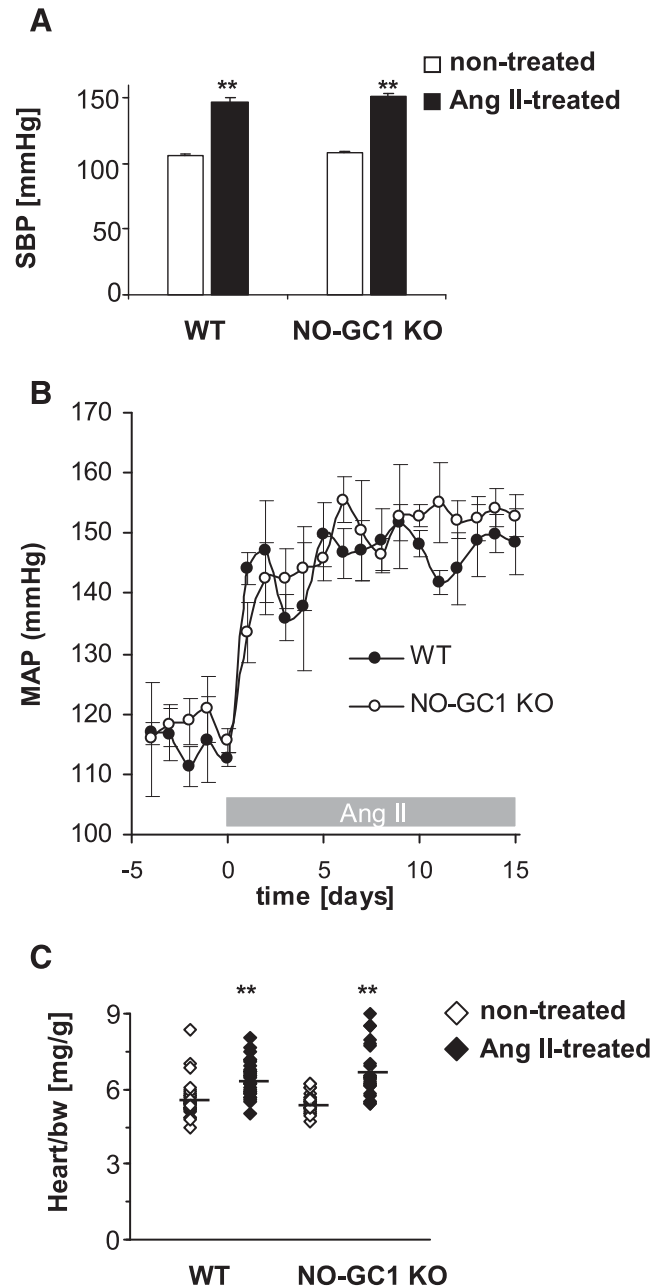

Fig. 1. Ang II-induced hypertension and heart hypertrophy do not differ between WT and NO-GC1 KO mice. (A) Systolic blood pressure (SBP) values of conscious WT and NO-GC1 KO mice without and with Ang II treatment (1.44 mg/kg per day, 2 weeks) measured by noninvasive tail-cuff plethysmography (nontreated n = 38 WT, 29 KO; Ang II-treated n = 26 WT, 21 KO). (B) Mean arterial pressures (MAP) recorded by radiotelemetry of WT (n = 3) and NO-GC1 KO (n = 3) mice before and after Ang II treatment. (C) Ratios of total heart weight to body weight of nontreated and Ang II-treated WT (n = 30) and NO-GC1 KO (n = 25) mice. Shown are means ± S.E.M. **P < 0.01 compared with nontreated group, unpaired Student's t test.

in systolic blood pressure by 42 ± 2 mmHg, which was similar in WT and NO-GC1 KO mice (Fig. 1A). The result indicates that the NO-GC1 deficiency with the reduced cGMP did not aggravate hypertension induced by this treatment. In support, blood pressure responses induced by lower, acute Ang II doses (10- and 100-fold, corresponding to 0.144 and 0.0144 mg/kg, i.p.) were comparable (30 and 10 mmHg,
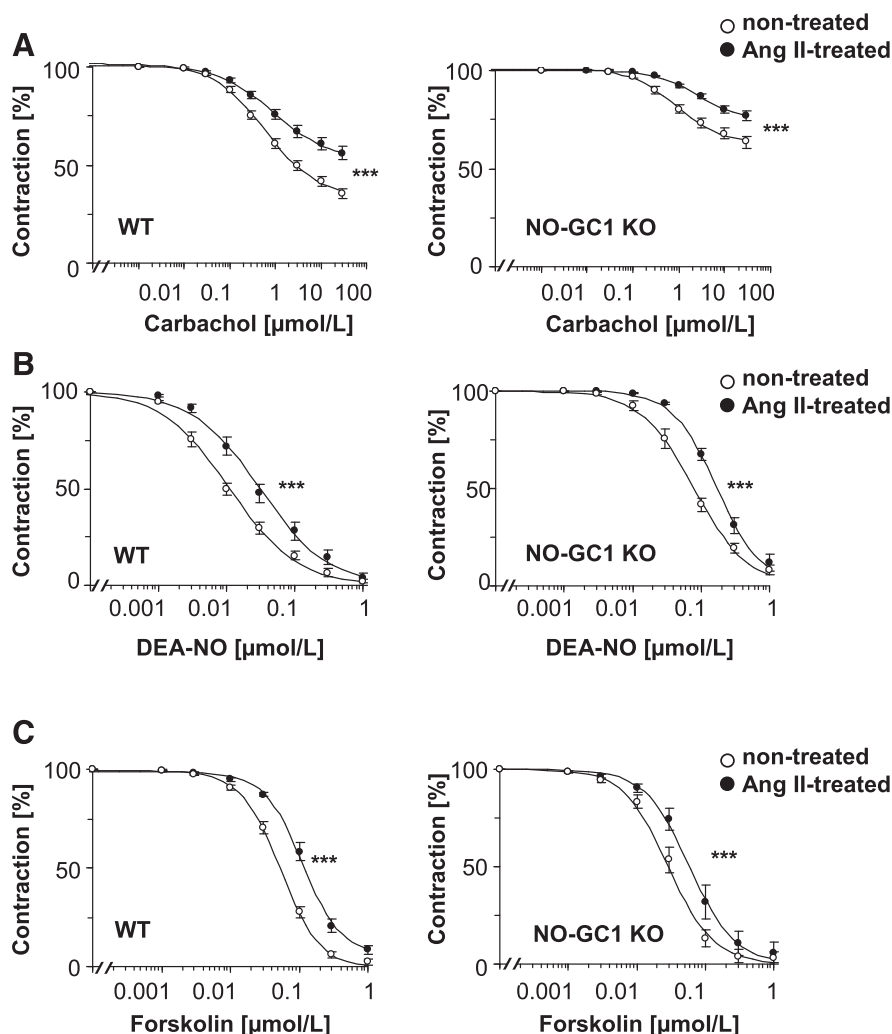
Fig. 2. Ang II-induced reduction of aortic relaxation is similar in WT and NO-GC1 KO mice. Cumulative concentration-response curves for relaxation of aortic rings (precontracted with 1 μmol/l phenylephrine) induced by carbachol (A), DEA-NO (B), and forskolin (C) from nontreated and Ang II-treated WT and NO-GC1 KO mice measured in organ bath experiments (carbachol n = 17 per group; DEA-NO n = 9 per group; forskolin n > 5 per group). EC$_{50}$ Ang II-treated versus nontreated: KO 0.2 $\pm$ 0.03 versus 0.09 $\pm$ 0.01 μM DEA-NO; WT 0.03 $\pm$ 0.01 versus 0.01 $\pm$ 0.002 μM DEA-NO and KO 0.08 $\pm$ 0.02 versus 0.03 $\pm$ 0.01 μM forskolin; WT 0.13 $\pm$ 0.016 versus 0.05 $\pm$ 0.005 μM forskolin. Shown are means $\pm$ S.E.M. ***P < 0.001 compared with nontreated group, analysis of variance for repeated measurements.

respectively), underlining that responsiveness of NO-GC1 KO toward Ang II is as in WT.

To validate the finding of the noninvasive blood pressure measurements, blood pressure was also measured directly using radiotelemetry. As shown in Fig. 1B, recordings of mean arterial pressure (MAP) were similar in WT and NO-GC1 KO

mice under basal conditions and increased to the similar levels after Ang II infusion.

In WT, the Ang II treatment induced a significant heart hypertrophy as measured by heart-to–body-weight ratio. Again, Ang II-induced heart hypertrophy did not differ between WT and NO-GC1–deficient mice (Fig. 1C).
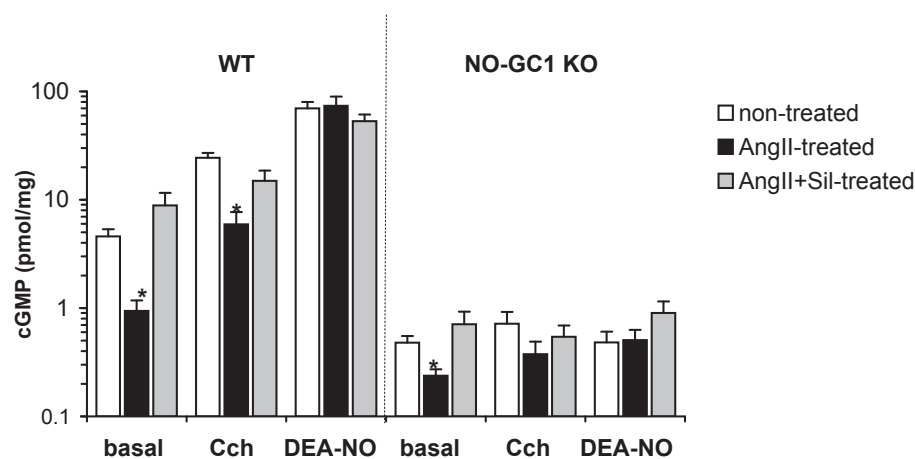

Fig. 3. Ang II-induced reduction of cGMP levels in aortic rings of WT and NO-GC1 KO mice. cGMP content of aortic rings of non-treated, Ang II-treated, and Ang II + sildenafil–treated WT and NO-GC1 KO mice (nontreated n = 12 WT, 9 KO; Ang II-treated n = 7 WT, 6 KO; Ang II + sildenafil-treated n = 2 WT, 3 KO). The aortic rings were nontreated (basal) or incubated with carbachol (30 μmol/l, 5 minutes) or DEA-NO (100 μmol/l, 2.5 minutes). For each condition, two to three aortic rings of each mouse were used. Shown are means $\pm$ S.E.M. *P < 0.05 compared with nontreated mice, unpaired Student's t test. Please note the logarithmic scale of the y-axis.
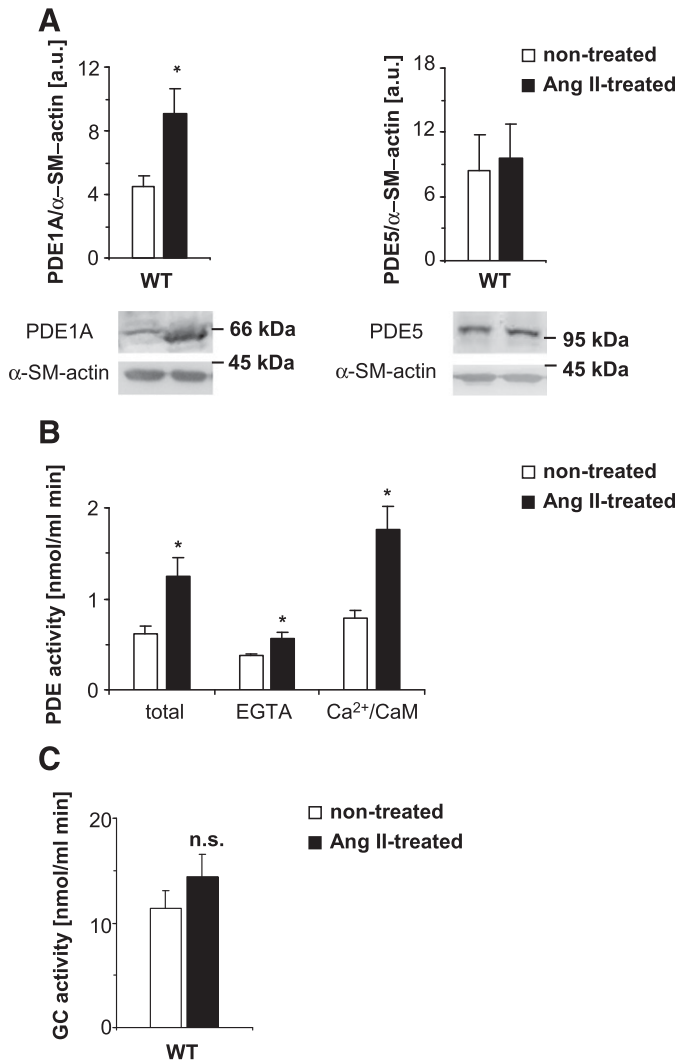
Fig. 4. Ang II treatment increases expression of PDE1. (A) Western blot analysis of PDE1A and PDE5 in aorta homogenates (50 μg) of nontreated and Ang II-treated WT mice (n = 4 per group). PDE1A expression is shown in bars summarizing densitometry analysis normalized to alpha smooth muscle actin in arbitrary units. A representative Western blot is shown underneath. (B) cGMP-degrading activity measured in aortic homogenates (2 μl, 1 μmol/l cGMP as substrate) of nontreated and Ang II-treated WT mice without further addition (total), upon addition of 2 mmol/l EGTA to inhibit PDE1, or 1 mmol/l Ca^{2+}/10 μmol/l CaM to activate PDE1 (n = 6 per group). (C) NO-stimulated GC activity (100 μmol/l DEA-NO) in aortic homogenates of nontreated and Ang II-treated WT mice (n = 4 per group). Shown are means $\pm$ S.E.M. *P < 0.05 compared with nontreated mice, unpaired Student's t test (n.s., not significant).

The Ang II Treatment Reduced Vascular Relaxation. The functional consequences of long term Ang II treatment on blood vessel properties were analyzed by measuring relaxation of aortic rings in organ bath experiments. In line with previous results, endothelium-dependent relaxation in response to carbachol was reduced in nontreated NO-GC1 KO mice (54 $\pm$ 4% of WT maximal response). Ang II treatment attenuated endothelium-dependent relaxation in both WT and NO-GC1 KO mice with the extent of reduction being similar (WT 21 $\pm$ 3% and KO 17 $\pm$ 3%; Fig. 2A).

Next, aortic relaxation induced by an NO donor (DEA-NO) was studied. As shown by the rightward shift of the DEA-NO concentration-response curves, the Ang II treatment caused a reduction of NO-induced relaxation in both WT and

NO-GC1–deficient mice; again the reduction was similar in WT and NO-GC1 KO as reflected by the 2-fold higher EC$_{50}$ values (Fig. 2B). Thus, the Ang II treatment comparably affected NO/cGMP-dependent vascular relaxation in WT and NO-GC1 KO mice.

In addition to cGMP, cAMP also causes smooth muscle relaxation using similar cellular mechanisms. So, we asked whether cAMP-mediated relaxation is also affected by the Ang II treatment and studied aortic relaxation induced by the adenylyl cyclase (AC) stimulator forskolin (Fig. 2C). As with the NO-response, Ang II treatment caused a rightward shift of the forskolin concentration-response curve in both WT and NO-GC1–deficient aortic rings, reflected by 2-fold higher EC$_{50}$ values for forskolin (see Fig. 2C).

Together, these results demonstrate: 1) alterations in vascular relaxation induced by Ang II treatment, which 2) were not aggravated by deletion of NO-GC1, the major vascular NO-GC.

Ang II Reduced the cGMP Content in Aortic Rings. To test whether the Ang II treatment affected the aortic cGMP content, cGMP was measured in aortas in the absence or presence of a stimulator (carbachol, 30 μmol/l, 5 minutes; DEA-NO, 100 μmol/l, 2.5 minutes) by radioimmunoassay. In WT, the aortic cGMP content and the cGMP increased by carbachol was found to be reduced in the rings of the Ang II-treated mice (Fig. 3). Yet, aortic cGMP increases induced by high NO concentrations were unaffected by the Ang II-treatment (see Fig. 3).

In the aortas of NO-GC1–deficient mice, cGMP levels under nonstimulated conditions were only 10% of WT, which is in accord with a 90% reduction of the cGMP-forming activity. Also here, aortas of Ang II-treated mice showed reduced cGMP levels (see Fig. 3). Neither carbachol nor DEA-NO caused measurable cGMP increases in the NO-GC1 KO rings and the Ang II treatment had no effect (see Fig. 3).

The finding of decreased cGMP levels under Ang II treatment is in accord with the reduction of aortic relaxation and points to alterations of either cGMP-forming or -degrading activities.

Ang II Treatment Increased Aortic cGMP–Degrading Activity by Enhancing PDE1 Expression. The intracellular cGMP concentration depends on the cGMP-degrading phosphodiesterases and the cGMP-forming guanylyl cyclases. Changes in expression and/or activity of one of these enzymes affect intracellular cGMP levels.

At first, the expression of PDE1A and PDE5, the major PDEs responsible for cGMP degradation in smooth muscle cells, was measured in aortic homogenates of nontreated and Ang II-treated WT mice. Quantitative analysis of Western blot results normalized to smooth muscle α-actin shows a 2-fold increase in expression of the PDE1A isoform in the Ang II-treated group, whereas the PDE5 content was unaffected by the Ang II treatment (Fig. 4A).

To verify enhanced expression of PDE1, PDE activity was determined in the respective aortic homogenates (1 μmol/l cGMP as substrate). Total PDE activity, as well as the PDE activity in the presence of Ca^{2+}/CaM known to stimulate PDE1, was increased in Ang II-treated animals (Fig. 4B). Compared with nonstimulated conditions (EGTA), the Ca^{2+}/CaM-induced increase in PDE activity was 3-fold in the Ang II-treated versus only 2-fold in the nontreated group, which is in accord with the enhanced expression of PDE1A in Western blot analysis. In
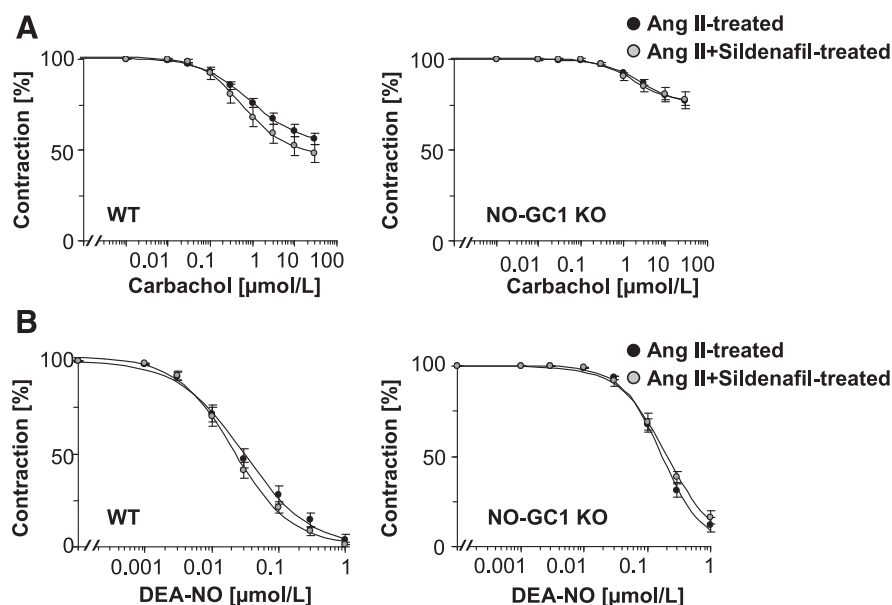
A

Contraction [%] (WT) vs Carbachol [μmol/L]

● Ang II-treated
○ Ang II+Sildenafil-treated

Contraction [%] (NO-GC1 KO) vs Carbachol [μmol/L]

B

Contraction [%] (WT) vs DEA-NO [μmol/L]

● Ang II-treated
○ Ang II+Sildenafil-treated

Contraction [%] (NO-GC1 KO) vs DEA-NO [μmol/L]

Fig. 5. Vascular relaxation reduced by the Ang II-treatment is not improved by the sildenafil treatment. Cumulative concentration-response curves of carbachol- (A) and DEA-NO- (B) induced relaxation of precontracted (1 μmol/l phenylephrine) aortic rings of Ang II- and sildenafil-treated WT and NO-GC1 KO mice measured in organ-bath experiments ($n = 9$ per group). Concentration-response curves of Ang II-treated mice (Fig. 2) are shown for comparison. Shown are means ± S.E.M.

contrast, PDE5 activity as measured in the absence and presence of 100 nmol/l sildenafil was not altered by the Ang II treatment.

To see whether the Ang II treatment also altered cGMP-forming activity, NO-stimulated GC activity was measured in aortic homogenate of nontreated and Ang II-treated WT mice. Yet, NO-stimulated cGMP-forming activities (100 μmol/l DEA-NO, 10 minutes) were not altered by the Ang II treatment.

A

Norepinephrine [pg/ml plasma]

□ non-treated
■ Ang II-treated

WT   NO-GC1 KO

B

Norepinephrine [μg/24 h urine]

WT   NO-GC1 KO

Fig. 6. NO-GC1 KO mice exert reduced noradrenalin levels in plasma and urine. Shown are the norepinephrine content measured in plasma (A) and 24-hour urine (B) of nontreated and Ang II-treated WT and NO-GC1 KO mice. Shown are means ± S.E.M. (plasma $n = 7$ WT, 10 KO nontreated, and 3 WT, 4 KO Ang II-treated; urine $n = 16$ WT, 12 KO). ***$P < 0.001$, *$P < 0.05$, compared with nontreated mice; +++$P < 0.001$, +$P < 0.05$, compared with WT group, unpaired Student's t test.

In sum, Ang II treatment increased expression of PDE1, which most likely accounts for the Ang II-induced decrease of cGMP levels.

Sildenafil Treatment Reversed Ang II-Induced Reduction of the cGMP Content but Did Not Cause Functional Improvement. To study whether inhibition of PDE1 is able to reverse the Ang II effects, the mice were treated with high sildenafil doses—considered to inhibit PDE1 in addition to PDE5—in the second week of Ang II treatment (800 mg of sildenafil per liter of drinking water).

Sildenafil was able to reverse the reductions in the cGMP content of aortic rings caused by the Ang II treatment in WT and NO-GC1 KO mice (see Fig. 3). Yet, despite the increased cGMP content in the aortic rings, the Ang II-induced impairment of endothelium-dependent and NO-induced aortic relaxation was unaffected (Fig. 5). Additionally, the sildenafil treatment did not affect the Ang II-induced hypertension in WT and NO-GC1 KO mice (WT: 142 ± 4 versus 147 ± 1 mmHg; KO: 155 ± 2 versus 152 ± 2 mmHg, sildenafil+ Ang II- and Ang II-treated mice, respectively).

In sum, although sildenafil increased the cGMP content, the functional impairment caused by the Ang II treatment was not improved.

Norepinephrine Content Is Lower in the NO-GC1 KO Mice. Ang II is known to increase activity of the sympathetic nervous system by increasing norepinephrine (NE) release. Thus, the activity status of the sympathetic system was monitored by determining NE in plasma and urine of WT and NO-GC1 KO mice. It is noteworthy that plasma NE of the NO-GC1 KO was found to be lower than in WT (Fig. 6A); a result further substantiated by the reduced NE content in the urine (Fig. 6B). As expected, Ang II treatment increased plasma NE levels in both NO-GC1 KO and WT mice (KO 1.4 ± 0.1-fold and WT 1.9 ± 0.05-fold). However, Ang II-induced plasma NE was still lower in NO-GC1 KO than in WT mice, indicating a reduction of sympathetic activity (see Fig. 6A). This finding prompted us to take a closer look at the heart rate, an important parameter regulated by the vegetative nervous system, and we found the heart rate in the NO-GC1 KO to be reduced (584 ± 10 versus 625 ± 7 beats/min, KO and WT,
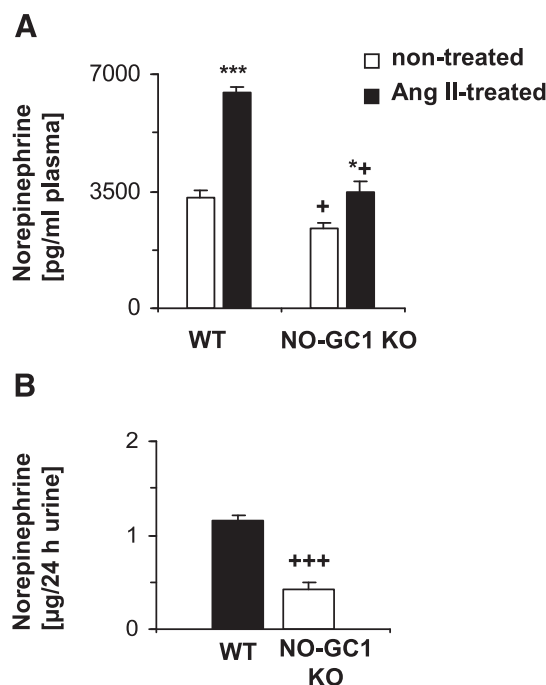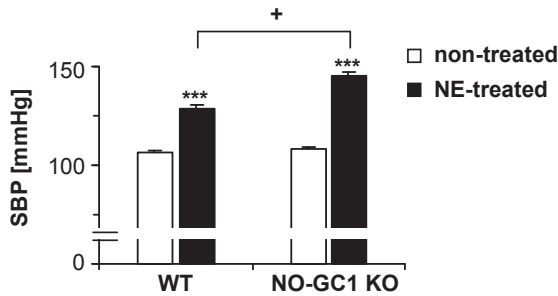
Fig. 7. Norepinephrine-treated NO-GC1 KO mice develop hypertension. Systolic blood pressure (SBP) values of conscious WT and NO-GC1 KO mice with and without norepinephrine treatment (2 weeks, 2.88 mg/kg per day) measured by noninvasive tail-cuff plethysmography (nontreated n = 38 WT, 29 KO; NE-treated n = 4 WT, 5 KO). Shown are means ± S.E.M. ***P < 0.001 compared with nontreated mice, ^{+}P < 0.05 compared with WT group, unpaired Student's t test.

respectively; P < 0.001). In line with a reduced sympathetic activity, the ganglion blocker hexamethonium (30 mg/kg, i.p.) only increased the heart rate in the NO-GC1 KO to WT level (672 to 740 bpm in NO-GC1 KO, P < 0.05; 707 to 728 bpm in WT, n = 12 WT and 12 NO-GC1 KO) indicating that the parasympathetic control of the heart rate in the NO-GC1 KO is higher than in WT.

These results reveal a reduced sympathetic activity in the NO-GC1 KO mice that may be able to counterbalance the reduced cGMP in the vasculature, thereby explaining why Ang II-induced blood pressure increases are similar in WT and NO-GC1 KO mice.

NE-Induced Blood Pressure Increase Is Higher in the NO-GC1 KO Mice. To verify the assumption that a reduced sympathetic activity is required for normotension in the NO-GC1 KO, the mice were treated with NE (2.88 mg/kg per day, 2 weeks).

As anticipated, NE treatment increased blood pressure in WT and NO-GC1 KO mice (Fig. 7). Yet, the NE-induced blood pressure increase in NO-GC1 KO mice was far more pronounced than in WT mice (ΔSBP: WT 22 ± 2 versus KO 37 ± 2 mmHg; P < 0.002). This finding supports our hypothesis that reduced sympathetic activity in the NO-GC1–deficient mice counteracts the reduced vascular cGMP content, thereby preventing hypertension. Thus, upon application of NE, the blood pressure increase in the NO-GC1 KO is higher than in WT. The results demonstrate for the first time the relevance of the NO-GC1–formed cGMP for the sympathetic tone in a KO model.

Discussion

In the present study, we analyzed the role of the major NO-GC isoform (NO-GC1) in the vascular system and development of hypertension with the help of NO-GC1–deficient mice. In these mice, the NO-induced cGMP content in the vascular system is greatly reduced (by about 90%) as is vascular relaxation. Yet, these mice do not show any increase in blood pressure (on a C57BL/6 background; Buys et al., 2012; Stegbauer et al., 2013). Deletion of the β subunit, causing deficiency in both NO-GC isoforms, NO-GC1 and NO-GC2, is known to cause hypertension, suggesting that minor cGMP generation catalyzed by the NO-GC2 is able to prevent the increase of blood pressure (Friebe at al., 2007).

Chronic Ang II Treatment Impairs Vascular Relaxation. In our study, chronic Ang II infusion was used to evaluate whether the resulting hypertension is exacerbated by the greatly reduced cGMP response caused by deletion of the NO-GC1. Ang II as a contractile agonist increases Ca^{2+} influx in the vascular smooth muscle cell causing smooth muscle contraction (Wynne et al., 2009). As expected, the treatment with Ang II caused a pronounced increase in blood pressure (∼40 mmHg) and heart weight. However, both parameters did not differ between WT and NO-GC1 KO mice.

Vascular relaxation analyzed in isolated aortic rings revealed that the Ang II treatment caused a reduction of endothelium-dependent relaxation, which is in accord with the results of others (Rajagopalan et al., 1996; Mollnau et al., 2002). Notably, WT and NO-GC1–deficient aortic rings were likewise affected by the Ang II treatment. A reduction of endothelium-dependent vascular relaxation has also been reported in the 2-kidney 1-clip model, another method known to increase the renin-angiotensin-system (Heitzer et al., 1999; Jung et al., 2003, 2004; Stegbauer et al., 2013). Increased superoxide production reducing bioavailability of NO is postulated to be responsible for the reduced endothelium-dependent vascular relaxation and is summarized in the term endothelial dysfunction (Förstermann and Sessa, 2012).
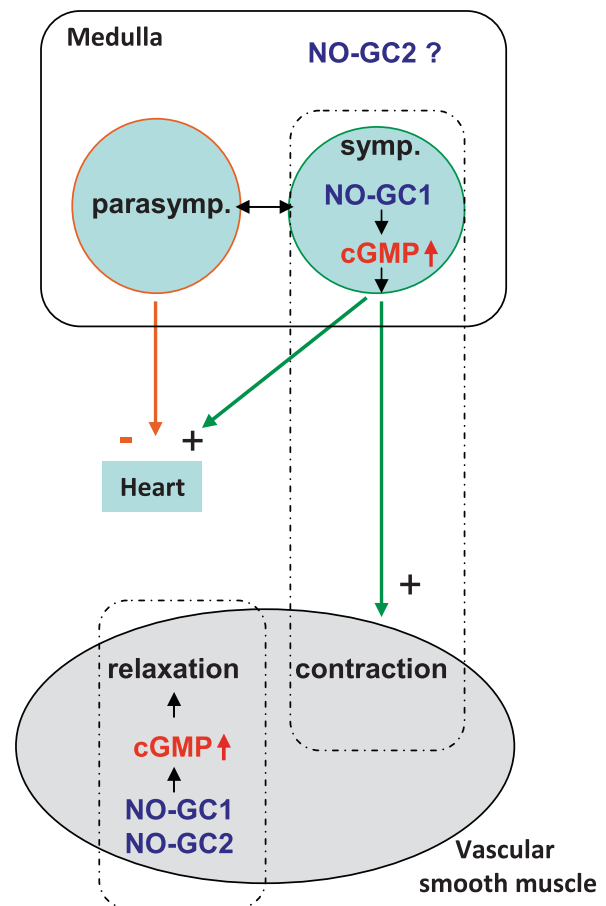

Fig. 8. Proposed roles of NO-GC1 in smooth muscle tone. Both isoforms of NO-GCs (NO-GC1, NO-GC2) have an established role in smooth muscle relaxation. Results of the present study indicate a possible additional sympatho-stimulatory action of NO-GC1 in the medulla oblongata. NO-GC2 is also expressed in the medulla oblongata, but its role remains elusive. parasymp., symp.: parasympathetic and sympathetic nervous systems.

In addition to its effect on endothelium-dependent relaxation, Ang II treatment also reduced NO-induced relaxation in WT and NO-GC1 KO mice. The impairment of NO-mediated relaxation demonstrates that the effects of Ang II on the NO/cGMP cascade are not limited to the endothelium but also occur in smooth muscle cells, most likely on the level of the cGMP-forming/degrading enzymes. Respective Ang II-induced alterations like reduced expression of NO-GC (Mollnau et al., 2002), *S*-nitrosation of sGC (Crassous et al., 2012), or enhanced expression of PDEs (Giachini et al., 2011) have been reported.

Chronic Ang II Treatment Enhances PDE1 Expression. In line with a reduced NO responsiveness, cGMP-levels of aortic rings of Ang II-treated WT and NO-GC1 KO mice were reduced under nonstimulated and carbachol-stimulated conditions. Our analysis of cGMP-forming and -degrading activities showed unaltered activity of NO-GCs, whereas cGMP degradation was enhanced in Ang II-treated WT mice. Closer analysis revealed an increase in Ca^{2+}/CaM-stimulated cGMP-degrading activity, which can be ascribed to PDE1, the Ca^{2+}-sensitive PDE. Increased expression of PDE1 was verified in Western blots. As PDE1 is known to also degrade cAMP, the enhanced PDE1 expression is in accord with the decreased vascular relaxation toward forskolin, the AC stimulator found in the present study.

Our results are in agreement with the study of Giachini et al. (2011), who also showed increased PDE1 expression in rat arteries induced by Ang II treatment. On the other hand, increased expression of PDE1 has been reported in vessels of rats treated with nitroglycerin to induce nitrate tolerance (Kim et al., 2001). Apparently, expression of PDE1 is an important mechanism in the control of cellular cGMP levels under quite diverse pathophysiological conditions (Miller et al., 2009). Yet, high Ang II doses are required for the pronounced increase of PDE1 expression, as a moderate increase of the renin-angiotensin-system induced in the 2K1C model was not paralleled by an increase of PDE1 expression (Stegbauer et al., 2013).

Increasing cGMP Levels Does Not Improve Ang II-Induced Dysfunctions. The increased PDE1 most probably accounts for the Ang II-mediated reduction of NO/cGMP-signaling. To find out whether inhibition of PDEs and the subsequent cGMP increase can attenuate Ang II-induced effects, sildenafil in a high concentration (100 mg/kg per day) was applied during the second week of the Ang II treatment. Although cGMP levels were restored or even increased by the sildenafil treatment, confirming the effectiveness of the drug, vascular relaxation remained reduced and the Ang II-induced hypertension was not reversed.

We conclude that alterations already induced by Ang II (first week) are not susceptible to further increases by cGMP. For closer analysis of the contractility of the NO-GC1 KO mice, we plan to challenge the mice in the hypertensive state with relaxing agents that exert the dilatory function outside the NO/cGMP signaling cascade, e.g., calcium channel blockers.

Sympathetic Activity Is Reduced in the NO-GC1 KO. In the vasculature, contractile agonists like Ang II and NE balance vasodilators like NO to maintain smooth muscle tone. By treating NO-GC1 KO mice with Ang II, we expected to see a blood pressure increase higher than in WT. Intriguingly, neither the blood pressure increase nor the impairment of vascular relaxation was aggravated by the NO-GC1 deficiency.

The lack of an effect of the NO-GC1 deficiency can be explained by the Ang II-induced increase of PDE1 that reduces cGMP and thereby transforms WT into a NO-GC1–deficient–like phenotype. Still, why does NO-GC1 deficiency with an almost complete loss of vascular cGMP (90%) not cause hypertension?

Our analysis of the NE content revealed that sympathetic activity is reduced by the NO-GC1 deficiency as indicated by lower plasma and urine NE levels. NE levels, although increased by the Ang II treatment, still remained lower in the KO than in the Ang II-treated WT. In support of a reduction of sympathetic activity, the heart rate, a cardiovascular parameter highly regulated by the sympathetic tone, was found to be reduced in the NO-GC1 KO. The results underline that the sympathetic activity is reduced in the NO-GC1 KO and suggest that the reduction of sympathetic activity counterbalances the reduced vascular cGMP in the NO-GC1 KO mice. In support of the thesis, hypertension induced by NE treatment was more severe in NO-GC1 KO than in WT. The findings show that: 1) the reduced sympathetic activity has an important impact in the control of the blood pressure in the NO-GC1 KO; and 2) assign a sympatho-stimulatory role to NO-GC1. Indeed, stimulatory and inhibitory effects of NO/cGMP in the regulation of sympathetic activity in the blood pressure-controlling areas of brain stem have been shown before (Harada et al., 1993; Hirooka et al., 1996; Martins-Pinge et al., 1997; Sander and Victor, 1999; Morimoto et al., 2000; Mayorov DN 2005; Wang et al., 2007), and occurrence of NO-GC1 and NO-GC2 in the medulla oblongata has been reported (Mergia et al., 2003). Yet, although our data provide evidence for the notion that NO via NO-GC1 increases sympathetic tone, more direct measurements such as recordings of renal sympathetic activity are necessary to definitely establish this relationship.

Moreover, the relative impact of NO-GC1's direct vasodilatory effect versus its sympatho-excitatory blood pressure–increasing effect has to be unraveled with the help of genetically modified mice with distinct neuronal or vascular NO-GC1 deficiency (Fig. 8).

References

Butz GM and Davisson RL (2001) Long-term telemetric measurement of cardiovascular parameters in awake mice: a physiological genomics tool. *Physiol Genomics* **5**: 89–97.

Buys ES, Raher MJ, Kirby A, Shahid M, Baron DM, Hayton SR, Tainsh LT, Sips PY, Rauwerdink KM, and Yan Q, et al. (2012) Genetic modifiers of hypertension in soluble guanylate cyclase α1-deficient mice. *J Clin Invest* **122**:2316–2325.

Crassous PA, Couloubaly S, Huang C, Zhou Z, Baskaran P, Kim DD, Papapetropoulos A, Fioramonti X, Durán WN, and Beuve A (2012) Soluble guanylyl cyclase is a target of angiotensin II-induced nitrosative stress in a hypertensive rat model. *Am J Physiol Heart Circ Physiol* **303**:H597–H604.

Förstermann U and Sessa WC (2012) Nitric oxide synthases: regulation and function. *Eur Heart J* **33**:829–837, 837a–837d.

Friebe A and Koesling D (2003) Regulation of nitric oxide-sensitive guanylyl cyclase. *Circ Res* **93**:96–105.

Friebe A, Mergia E, Dangel O, Lange A, and Koesling D (2007) Fatal gastrointestinal obstruction and hypertension in mice lacking nitric oxide-sensitive guanylyl cyclase. *Proc Natl Acad Sci USA* **104**:7699–7704.

Giachini FR, Lima VV, Carneiro FS, Tostes RC, and Webb RC (2011) Decreased cGMP level contributes to increased contraction in arteries from hypertensive rats: role of phosphodiesterase 1. *Hypertension* **57**:655–663.

Harada S, Tokunaga S, Momohara M, Masaki H, Tagawa T, Imaizumi T, and Takeshita A (1993) Inhibition of nitric oxide formation in the nucleus tractus solitarius increases renal sympathetic nerve activity in rabbits. *Circ Res* **72**: 511–516.

Heitzer T, Wenzel U, Hink U, Krollner D, Skatchkov M, Stahl RA, MacHarzina R, Bräsen JH, Meinertz T, and Münzel T (1999) Increased NAD(P)H oxidase-mediated superoxide production in renovascular hypertension: evidence for an involvement of protein kinase C. *Kidney Int* **55**:252–260.

Hirooka Y, Polson JW, and Dampney RA (1996) Pressor and sympathoexcitatory effects of nitric oxide in the rostral ventrolateral medulla. *J Hypertens* **14**: 1317–1324.

Jung O, Marklund SL, Geiger H, Pedrazzini T, Busse R, and Brandes RP (2003) Extracellular superoxide dismutase is a major determinant of nitric oxide bioavailability: in vivo and ex vivo evidence from ecSOD-deficient mice. *Circ Res* **93**: 622–629.

Jung O, Schreiber JG, Geiger H, Pedrazzini T, Busse R, and Brandes RP (2004) gp91phox-containing NADPH oxidase mediates endothelial dysfunction in renovascular hypertension. *Circulation* **109**:1795–1801.

Kim D, Rybalkin SD, Pi X, Wang Y, Zhang C, Munzel T, Beavo JA, Berk BC, and Yan C (2001) Upregulation of phosphodiesterase 1A1 expression is associated with the development of nitrate tolerance. *Circulation* **104**:2338–2343.

Kuhn M (2003) Structure, regulation, and function of mammalian membrane guanylyl cyclase receptors, with a focus on guanylyl cyclase-A. *Circ Res* **93**:700–709.

Martins-Pinge MC, Baraldi-Passy I, and Lopes OU (1997) Excitatory effects of nitric oxide within the rostral ventrolateral medulla of freely moving rats. *Hypertension* **30**:704–707.

Mayorov DN (2005) Selective sensitization by nitric oxide of sympathetic baroreflex in rostral ventrolateral medulla of conscious rabbits. *Hypertension* **45**:901–906.

Mergia E, Friebe A, Dangel O, Russwurm M, and Koesling D (2006) Spare guanylyl cyclase NO receptors ensure high NO sensitivity in the vascular system. *J Clin Invest* **116**:1731–1737.

Mergia E, Russwurm M, Zoidl G, and Koesling D (2003) Major occurrence of the new α2β1 isoform of NO-sensitive guanylyl cyclase in brain. *Cell Signal* **15**:189–195.

Miller CL, Oikawa M, Cai Y, Wojtovich AP, Nagel DJ, Xu X, Xu H, Florio V, Rybalkin SD, and Beavo JA, et al. (2009) Role of Ca2+/calmodulin-stimulated cyclic nucleotide phosphodiesterase 1 in mediating cardiomyocyte hypertrophy. *Circ Res* **105**: 956–964.

Mollnau H, Wendt M, Szöcs K, Lassègue B, Schulz E, Oelze M, Li H, Bodenschatz M, August M, and Kleschyov AL, et al. (2002) Effects of angiotensin II infusion on the expression and function of NAD(P)H oxidase and components of nitric oxide/cGMP signaling. *Circ Res* **90**:E58–E65.

Morimoto S, Sasaki S, Miki S, Kawa T, Nakamura K, Itoh H, Nakata T, Takeda K, Nakagawa M, and Fushiki S (2000) Nitric oxide is an excitatory modulator in the rostral ventrolateral medulla in rats. *Am J Hypertens* **13**:1125–1134.

Rajagopalan S, Kurz S, Münzel T, Tarpey M, Freeman BA, Griendling KK, and Harrison DG (1996) Angiotensin II-mediated hypertension in the rat increases vascular superoxide production via membrane NADH/NADPH oxidase activation. Contribution to alterations of vasomotor tone. *J Clin Invest* **97**:1916–1923.

Russwurm M and Koesling D (2002) Isoforms of NO-sensitive guanylyl cyclase. *Mol Cell Biochem* **230**:159–164.

Russwurm M, Wittau N, and Koesling D (2001) Guanylyl cyclase/PSD-95 interaction: targeting of the nitric oxide-sensitive alpha2beta1 guanylyl cyclase to synaptic membranes. *J Biol Chem* **276**:44647–44652.

Rybalkin SD, Yan C, Bornfeldt KE, and Beavo JA (2003) Cyclic GMP phosphodiesterases and regulation of smooth muscle function. *Circ Res* **93**:280–291.

Sander M and Victor RG (1999) Neural mechanisms in nitric-oxide-deficient hypertension. *Curr Opin Nephrol Hypertens* **8**:61–73.

Sonnenburg WK, Seger D, Kwak KS, Huang J, Charbonneau H, and Beavo JA (1995) Identification of inhibitory and calmodulin-binding domains of the PDE1A1 and PDE1A2 calmodulin-stimulated cyclic nucleotide phosphodiesterases. *J Biol Chem* **270**:30989–31000.

Stegbauer J and Coffman TM (2011) New insights into angiotensin receptor actions: from blood pressure to aging. *Curr Opin Nephrol Hypertens* **20**:84–88.

Stegbauer J, Friedrich S, Potthoff SA, Broekmans K, Cortese-Krott MM, Quack I, Rump LC, Koesling D, and Mergia E (2013) Phosphodiesterase 5 attenuates the vasodilatory response in renovascular hypertension. *PLoS One* **8**:e80674 DOI: 10.1371/journal.pone.0080674.

Yan C, Kim D, Aizawa H, and Berk BC (2003) Functional interplay between angiotensin II and nitric oxide: cyclic GMP as a key mediator. *Arterioscler Thromb Vasc Biol* **23**:26–36.

Yusuf S, Teo KK, Pogue J, Dyal L, Copland I, Schumacher H, Dagenais G, Sleight P, and Anderson C; ONTARGET Investigators (2008) Telmisartan, ramipril, or both in patients at high risk for vascular events. *N Engl J Med* **358**:1547–1559.

Wang S, Paton JF, and Kasparov S (2007) Differential sensitivity of excitatory and inhibitory synaptic transmission to modulation by nitric oxide in rat nucleus tractus solitarii. *Exp Physiol* **92**:371–382.

Wynne BM, Chiao CW, and Webb RC (2009) Vascular Smooth Muscle Cell Signaling Mechanisms for Contraction to Angiotensin II and Endothelin-1. *J Am Soc Hypertens* **3**:84–95.

Address correspondence to: Dr. Evanthia Mergia, Institut für Pharmakologie und Toxikologie, Medizinische Fakultät MA N1, Ruhr-Universität Bochum, 44780 Bochum, Germany. E-mail: mergia@evanthia.de

RESEARCH ARTICLE | *Renal Hemodynamics*

Phosphodiesterase 5 inhibition ameliorates angiotensin II-dependent hypertension and renal vascular dysfunction

Manuel Thieme,[1]* Sema H. Sivritas,[1]* Evanthia Mergia,[2] Sebastian A. Potthoff,[1] Guang Yang,[1] Lydia Hering,[1] Katharina Grave,[1] Henning Hoch,[1] Lars C. Rump,[1] and Johannes Stegbauer[1]

[1]*Department of Nephrology, Medical Faculty, University Hospital Düsseldorf, Heinrich-Heine-University Düsseldorf, Düsseldorf, Germany; and* [2]*Department of Pharmacology and Toxicology, Ruhr-University Bochum, Bochum, Germany*

Thieme M, Sivritas SH, Mergia E, Potthoff SA, Yang G, Hering L, Grave K, Hoch H, Rump LC, Stegbauer J. Phosphodiesterase 5 inhibition ameliorates angiotensin II-dependent hypertension and renal vascular dysfunction. *Am J Physiol Renal Physiol* 312: F474–F481, 2017. First published January 4, 2017; doi:10.1152/ajprenal.00376.2016.—Changes in renal hemodynamics have a major impact on blood pressure (BP). Angiotensin (Ang) II has been shown to induce vascular dysfunction by interacting with phosphodiesterase (PDE)1 and PDE5. The predominant PDE isoform responsible for renal vascular dysfunction in hypertension is unknown. Here, we measured the effects of PDE5 (sildenafil) or PDE1 (vinpocetine) inhibition on renal blood flow (RBF), BP, and renal vascular function in normotensive and hypertensive mice. During acute short-term Ang II infusion, sildenafil decreased BP and increased RBF in C57BL/6 (WT) mice. In contrast, vinpocetine showed no effect on RBF and BP. Additionally, renal cGMP levels were significantly increased after acute sildenafil but not after vinpocetine infusion, indicating a predominant role of PDE5 in renal vasculature. Furthermore, chronic Ang II infusion (500 ng·kg^{-1}·min^{-1}) increased BP and led to impaired NO-dependent vasodilation in kidneys of WT mice. Additional treatment with sildenafil (100 mg·kg^{-1}·day^{-1}) attenuated Ang II-dependent hypertension and improved NO-mediated vasodilation. During chronic Ang II infusion, urinary nitrite excretion, a marker for renal NO generation, was increased in WT mice, whereas renal cGMP generation was decreased and restored after sildenafil treatment, suggesting a preserved cGMP signaling after PDE5 inhibition. To investigate the dependency of PDE5 effects on NO/cGMP signaling, we next analyzed eNOS-KO mice, a mouse model characterized by low vascular NO/cGMP levels. In eNOS-KO mice, chronic Ang II infusion increased BP but did not impair NO-mediated vasodilation. Moreover, sildenafil did not influence BP or vascular function in eNOS-KO mice. These results highlight PDE5 as a key regulator of renal hemodynamics in hypertension.

phosphodiesterase; renal blood flow; angiotensin; cGMP; hypertension

HYPERTENSION IS THE LEADING RISK FACTOR for cardiovascular morbidity and mortality. Increase in blood pressure is characterized by an increase in vascular resistance. In this regard, renal arteries are playing an important role in blood pressure control. Changes in vascular function, including increased vasocontractility and impaired vasorelaxation, result in vascular dysfunction, leading to hypertension (8).

The renin-angiotensin system (RAS) and the NO/cGMP signaling cascade are key players in the regulation of vascular function. In this regard, angiotensin (Ang) II promotes vascular injury by inducing vasoconstriction, vascular smooth muscle cell proliferation and hypertrophy, and vascular inflammation as well as extracellular matrix degradation (21, 33). Furthermore, angiotensin II (Ang II) infusion has been shown to decrease NO bioavailabilty, leading to vascular dysfunction (2, 12, 14, 15, 34). Besides the impact of Ang II on NO bioavailability, several studies have highlighted the role of Ang II in modulating cGMP degradation by influencing the activity of cGMP-degrading phosphodiesterases (PDE) in vascular smooth muscle cells. Ang II has been shown to increase the expression of PDE1 and PDE5, both of which are PDEs of particular importance for vasorelaxation of resistance arteries (10, 16, 17). In general, PDE1 is activated by increased intracellular Ca^{2+} concentrations, which are observed during Ang II mediated vasoconstriction (13, 30, 31). PDE5 is activated by allosteric binding of cGMP to the noncatalytic GAF domain of PDE5 (29). Thus, PDE5 limits cGMP induced vasorelaxation through a cGMP-mediated negative feedback mechanism. Until now, there has been conflicting data about the predominant PDE regulating vascular function in resistance arteries during Ang II-dependent hypertension. Giachini et al. (10) reported that chronic Ang II infusion reduces cGMP bioavailability through a PDE1-dependent mechanism. In contrast, we and others have shown that vascular dysfunction in renovascular hypertension was mediated initially by an increased NO/cGMP signaling, which resulted in an exaggerated PDE5 activation and finally in reduced NO/cGMP mediated relaxation (34). The aim of the present study was to identify the predominant PDE regulating renal vascular function. Based on these results, we examined whether acute and chronic inhibiton of a specific PDE protects from hypertension and vascular dysfunction.

MATERIALS AND METHODS

Animal care. All animal experiments were approved by the responsible federal state authority (Landesamt fuer Natur-, Umwelt-, und Verbraucherschutz Nordrhein-Westfalen; reference: AZ. 8.87-50.10.34.08.216) and performed according to the guidelines from Directive 2010/63/EU of the European Parliament on the protection of animals used for scientific purposes. Twelve- to 14-week-old male C57BL/6J wild-type (WT) mice and endothelial nitric oxide synthase-

* M. Thieme and S. H. Sivritas contributed equally to this work.

Address for reprint requests and other correspondence: J. Stegbauer, Dept. of Nephrology, Medical Faculty, Univ. Hospital Düsseldorf Heinrich-Heine-University Düsseldorf Moorenstrasse 5, 40225 Düsseldorf, Germany (e-mail: johannes.stegbauer@med.uni-duesseldorf.de).

knockout (eNOS-KO) mice (generous gift from Dr. A. Gödecke, Cardiovascular Physiology, Dusseldorf, Germany) were bred and housed in the local animal care facility of the University Hospital Düsseldorf, as described previously (11).

Acute vasoconstrictor responses and changes in renal blood flow. Acute pressor responses and renal blood flow to vinpocetine and sildenafil were measured in anesthetized mic,e as described previously (32). In brief, mice were anesthetized intraperitoneally with ketamine (100 mg/kg) and xylazine (5 mg/kg) and decapitated at the end of the experiment. Arterial BP was monitored continuously through a catheter placed in the carotid artery. Basal fluids, Ang II, and PDE inhibitors were administered through the right jugular vein. For measuring renal blood flow (RBF), a small incision was made on the left flank to expose the kidney, and an ultrasonic flowmeter interfaced with a 5-mm V-shaped probe was placed around the left renal artery (MA0.5PSB and TS420 Flowmeter; Transonic Systems, Ithaca, NY). Mice were allowed to stabilize for 30 min before measurements were started. The effects of PDE1 or PDE5 on BP and RBF were tested under normotensive and hypertensive conditions. Therefore, either the PDE5 inhibitor sildenafil or the PDE1 inhibitor vinpocetine was administered in increasing doses (0.0008, 0.008, 0.08, and 0.8 mg/kg body wt) at 5-min intervals. To test the effect of PDE inhibition under hypertensive conditions, Ang II (200 ng·min^{-1}·kg^{-1}) was applied continuously throughout the experiment. After a stabilization period, sildenafil or vinpocetine was injected in increasing doses, as described above. Intra-arterial pressure and renal blood flow were monitored continuously using the PowerLab data acquisition system and LabChart software (ADInstruments, Colorado Springs, CO). Changes in BP or RBF were recorded as the delta of BP or RBF increase or decrease in relation to their baseline values determined before the application of the first PDE inhibitor dose.

Renal cGMP levels in cortical slices. Immediately after application of either sildenafil (800 μg/kg BW) or vinpocetine (800 μg/kg body wt) in acute experiments, or after the termination of chronic experiments, renal cortex was cut into small pieces and snap-frozen in liquid nitrogen. The samples were homogenized in 70% ice-cold ethanol using a glass/glass homogenizer and finally centrifuged (14,000 *g*, 15 min, 4°C) and dried at 95°C, and the cGMP content was measured in duplicate by RIA. Protein pallets were dissolved in 0.1 M NaOH-0.1% SDS, and protein content was determined using the bicinchoninic acid method (Uptima).

Isolated perfused kidneys. At baseline or 14 days after the induction of Ang II-dependent hypertension, the kidneys of each group were isolated and perfused with Krebs-Henseleit buffer, as described previously (36). Kidneys were isolated from mice anesthetized intraperiteoneally (ip) with ketamine (100 mg/kg and xylazine (5 mg/kg\). Changes in perfusion pressure reflected changes in vascular resistance of renal vessels. Immediately after preparation, a bolus of 60 mM KCl was injected to test the viability of the preparation, followed by a stabilization period of 30 min. To assess renal vasodilation, kidneys were preconstricted with norepinephrine (1 μM; Sigma-Aldrich). Concentration-response curves induced by carbachol (Sigma-Aldrich) and *S*-nitrosgluthathione (GSNO; Alexis) were recorded in the presence of either diclofenac (3 μM) or L-NAME (300 μM; Sigma-Aldrich) and diclofenac (3 μM), respectively. To test the influence of vinpocetine (Calbiochem) and sildenafil (a generous gift from Pfizer) on NO-mediated vasodilation, we used a sildenafil (300 nM) and vinpocetine (10 μM) concentration known to reduce vasocontraction by ~20-30% and added the respective substances to the perfusion solution 10 min before GSNO or carbachol administration. Renal relaxation is expressed as a percentage pressor response of the preconstricted kidney, which was set as 100%.

Isometric force in aortic rings. Aortic rings from Ang II-infused WT mice (500 ng·kg^{-1}·min^{-1} for 14 days) were mounted in a wire myography (Multi Myograph Model 610 M; Danish Myo Technology), as described previously (4). After equilibration, aortic rings were contracted with norepinephrine (1 μM; Sigma-Aldrich), and dose-response curves to GSNO were recorded in the presence or absence of either sildenafil (300 nM) or vinpocetine (1 μM). Isometric forces are expressed as a percentage of the maximal response to norepinehrine.

Model of Ang II-induced hypertension. WT and eNOS-KO mice were infused continuously with Ang II (500 ng·kg^{-1}·min^{-1}; Sigma-Aldrich) via osmotic minipumps (model 1002; Alzet, Cupertino, CA) for 14 days. Osmotic minipumps were implanted in anesthetized mice [intraperitoneal anesthesia with ketamine (100 mg/kg) and xylazine (5 mg/kg)]. Four days before Ang II infusion, WT and eNOS-KO mice were divided into a sildenafil (100 mg·kg^{-1}·day^{-1}) and vehicle-treated group. Sildenafil was dissolved in tap water acidified to pH 3 at a concentration of 400mg/l, resulting in the ingestion of ~100 mg·kg^{-1}·day^{-1} and in sufficient sildenafil plasma levels (1, 34). The vehicle group received only tap water acidified to pH 3.

Blood pressure measurements. Systolic blood pressure (BP) was measured in conscious mice by tail-cuff plethysmography (BP-98A; Softron). For habituation, before the experiment, mice were trained daily for 5 consecutive days. Thereafter, 10 measurements per mouse were recorded daily, starting on the day when the mice were assigned into sildenafil or vehicle-treated groups.

Metabolic cages. Mouse metabolic cages (Tecniplast, Gams, Switzerland) were utilized, allowing the collection of urine for further analysis. During the 24-h collection period, mice were supplied with chaw and vehicle or sildenafil dissolved in tap water (acidified to pH3).

Quantification of sodium balance and urinary nitrate/nitrite excretion. Urine samples were collected daily in metabolic cages for 24 h. Mice were fed a gel diet (Diet-Gel; Sniff, Soest, Germany) containing nutrients and water (0.15% NaCl). Cumulative urinary sodium excretion was determined by flame photometry (Beckman Coulter), utilizing an internal lithium standard. Cumulative sodium balance was determined by subtracting sodium intake from urinary sodium excretion, as described previously. Cumulative nitrate/nitrite was measured by using a colorimetric assay kit (780001; Cayman Chemical) and normalized to urinary creatinine (50070; Cayman Chemical).

Statistical analysis. All data are expressed as means ± SE (*n* = no. of animals). Student's *t*-test was used to compare means of two groups with Gaussian distribution. Differences between dose-response curves were analyzed by one-way or two-way ANOVA for repeated measurements, followed by Bonferroni's multiple comparison post hoc test. Statistical analyses of data of two groups in which Gaussian distribution was not (or could not be assumed to be) normal were analyzed by the Mann-Whitney *U*-test. Probability levels of $P < 0.05$ were considered statistically significant.

RESULTS

Phosphodiesterase 5 regulates blood pressure and renal blood flow. To identify the predominant PDE subunit regulating renal blood flow (RBF) in vivo, we tested the acute effects of sildenafil, a selective PDE5 inhibitor, and vinpocetine, a selective PDE1 inhibitor on RBF and blood pressure, under baseline conditions or during acute Ang II infusion (200 ng·kg^{-1}·min^{-1}). As shown in Fig, 1, *A* and *B*, sildenafil decreased blood pressure dose dependently. Due to hypotensive blood pressure values induced by sildenafil (80 μg/kg body wt: 54 ± 9 mmHg; 800 μg/kg body wt: 56 ± 8 mmHg), renal blood flow was decreased in the two highest sildenafil concentrations (Fig. 1, *A–C*). During Ang II infusion, PDE5 inhibition reduced blood pressure even more potently than in the absence of Ang II infusion (39 ± 4 vs. 12 ± 1 ΔmmHg; *n* = 4–5, *P* < 0.001; Fig. 1, *D–F*). Moreover, sildenafil
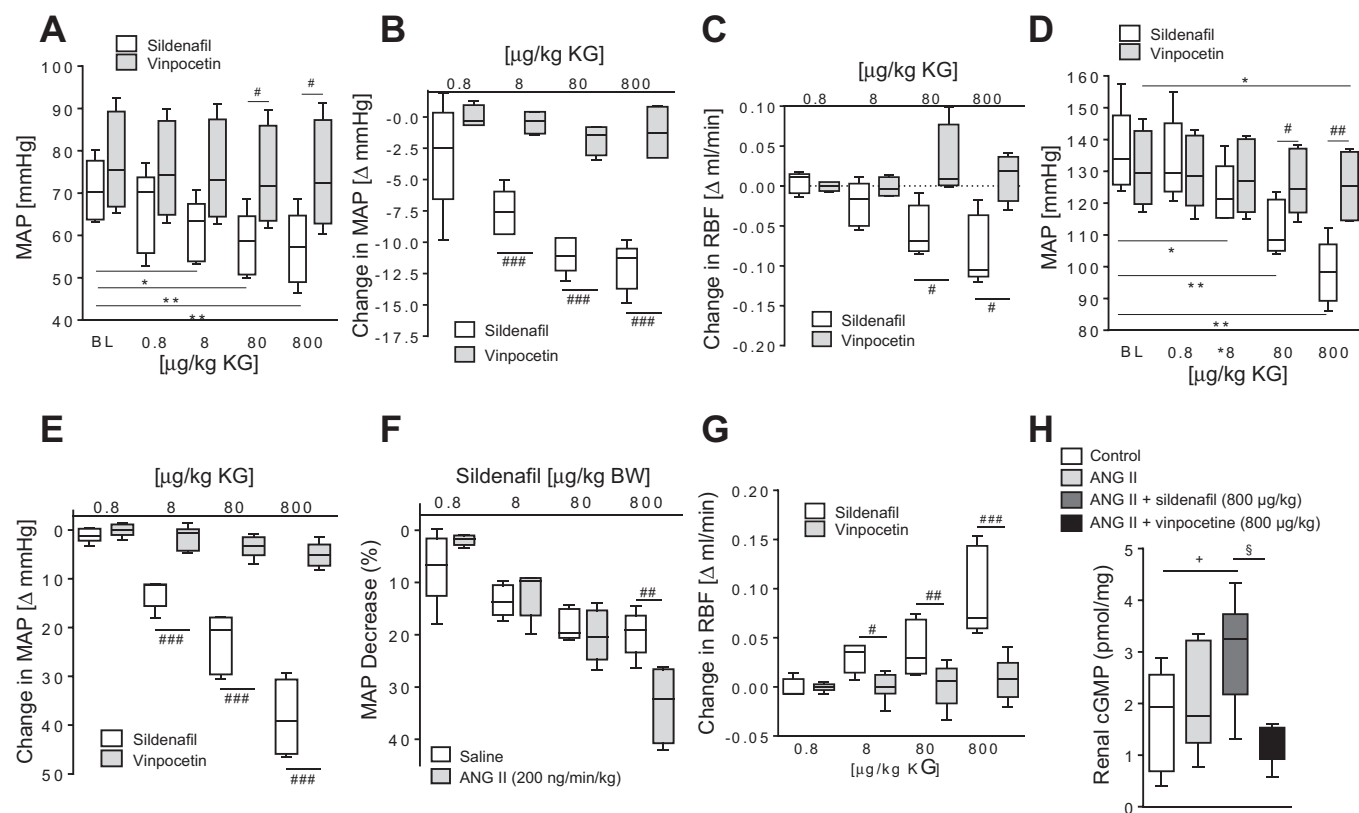
Fig. 1. Sildenafil decreased blood pressure (BP) and increased renal blood flow (RBF) in wild-type (WT) mice during angiotensin II (Ang II)-induced hypertension. *A* (absolute values) and *B* [change in mean arterial pressure (MAP)]: acute administration of sildenafil ($n = 5$) but not vinpocetine ($n = 4$) reduced BP significantly in normotensive mice. *C*: acute administration of sildenafil ($n = 5$) but not vinpocetine ($n = 4$) decreased RBF significantly in normotensive mice. *D* (absolute values) and *E* (change in MAP): during acute Ang II infusion (200 ng·kg^{-1}·min^{-1}), administration of sildenafil ($n = 5$) reduced BP significantly. Vinpocetine ($n = 6$) reduced BP only in the highest concentration. *G*: blood pressure-lowering effect of sildenafil was more potent in Ang II-infused mice compared with normotensive mice. *F:* during acute Ang II infusion (200 ng·kg^{-1}·min^{-1}), administration of sildenafil ($n = 5$) increased RBF significantly. *H*: renal cGMP levels were increased significantly after sildenafil application ($n = 6$–9). Data represent means ± SE. *$P < 0.01$ and **$P < 0.001$ vs. baseline; #$P < 0,05$, ##$P < 0.01$, and ###$P < 0.001$ vs. equivalent dose of vinpocetine; +$P < 0.05$ vs. control; §$P < 0.01$ vs Ang II + vinpocetine. One-way ANOVA followed by Bonferroni's multiple comparison post hoc test (*A*, *D*, and *H*) and Student's unpaired *t*-test (*B*, *C*, *E*, *F*, and *G*).

induced a significant increase in renal blood flow in acute Ang II-infused mice (Fig. 1*G*).

In contrast, vinpocetine reduced blood pressure only in the highest concentration of Ang II-infused mice but did not show any effect on RBF, suggesting that BP and RBF are regulated predominantly by PDE5 (Fig. 1, *A*–*G*). In line with these results, renal cGMP content was significantly increased after acute sildenafil (0.8μ g/kg) compared with both vinpocetine (0.8 μg/kg) or vehicle application (Fig. 1*H*).

Acute treatment with sildenafil but not vinpocetine restores impaired vasodilator responses in isolated perfused kidneys of hypertensive WT mice. To exclude a substantial influence of systemic blood pressure changes on renal hemodynamics induced by acute PDE5 or PDE1 inhibition in vivo, we examined renal vasorelaxation ex vivo by using the model of isolated perfused kidneys. Interestingly, the inhibition of neither PDE1 nor PDE5 affects smooth muscle cell-dependent vasorelaxation induced by exogenous NO [(*S*-nitrosgluthathione (GSNO)] in preconstricted kidneys of normotensive WT mice (Fig. 2*A*). However, sildenafil (0.3 μM) significantly improved the impaired GSNO-mediated vascular relaxation in kidneys of chronically Ang II-infused WT mice (Fig. 2*B*). In contrast, vinpocetine (10 uM) used in a 33-fold higher concentration

compared with sildenafil did not show any effect on the vasodilator responses in kidneys of hypertensive mice (Fig. 2*B*). Interestingly, in aortic rings of Ang II-treated mice, vinpocetine improved GSNO-dependent vasodilation in the same manner as sildenafil, suggesting that PDE1 is playing a different role in conductance arteries and the vascular bed of the kidney (Fig. 2*C*).

To examine the impact of PDE5 inhibition in a mouse model, which is characterized by decreased NO/cGMP levels, we tested renal vasodilator responses in isolated perfused kidneys of Ang II-treated hypertensive eNOS-KO mice. As shown in Fig. 2*D*, sildenafil did not affect NO-mediated renal vasorelaxation in kidneys of chronically Ang II-infused eNOS-KO mice

Chronic sildenafil treatment attenuates Ang II-dependent hypertension in WT but not in eNOS-KO mice. Next, we tested the effect of chronic PDE5 inhibition (sildenafil 100 mg·kg^{-1}·day^{-1}) on Ang II-dependent hypertension in WT and eNOS-KO mice. After 4 days of sildenafil treatment, mice were additionally infused with Ang II (500 ng·kg^{-1}·min^{-1}) for 14 days. In vehicle-treated mice, baseline systolic blood pressure was significantly higher in eNOS-KO compared with WT mice (131 ± 3 mmHg, $n = 9$, vs. 110 ± 3 mmHg, $n = 9$, $P <$
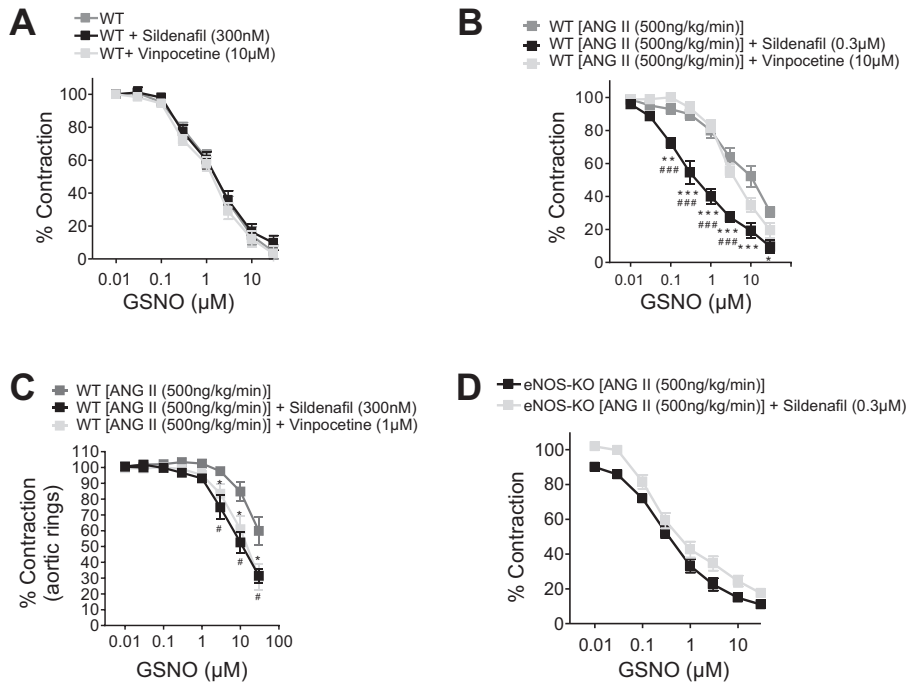
Fig. 2. Acute sildenafil administration improved smooth muscle cell-dependent vasorelaxation in kidneys of Ang II-treated WT but not endothelial nitric oxide synthase-knockout (eNOS-KO) mice. *A*: administration of sildenafil or vinpocetine did not improve smooth muscle cell-dependent vasorelaxation induced by the NO donor *S*-nitrosglutathione (GSNO) in the isolated perfused kidney of untreated WT mice ($n = 5$–9). *B:* acute administration of sildenafil but not vinpocetine improved GSNO-induced vasorelaxation in isolated perfused kidneys of chronically Ang II-infused WT mice ($n = 5$–6). *C*: acute vasodilator response to GSNO in the presence or absence of either sildenafil or vinpocetine in an aortic ring preparation of Ang II-infused mice. *D*: acute administration of sildenafil did not affect GSNO-induced renal vasorelaxation in kidneys of eNOS-KO mice ($n = 9$–19). Data represent means $\pm$ SE. *$P < 0.001$, Ang II (500 ng·kg^{-1}·min^{-1}) vs. Ang II (500 ng·kg^{-1}·min^{-1}) + vinpocetine; #$P < 0.001$, Ang II (500 ng·kg^{-1}·min^{-1}) vs. Ang II (500 ng·kg^{-1}·min^{-1}) + sildenafil; **$P < 0.01$ and ***$P < 0.001$ vs. WT [Ang II (500 ng·kg^{-1}·min^{-1})]; ###$P < 0.001$ vs. WT Ang II (500 ng·kg^{-1}·min^{-1}) + vinpocetine. Two-way ANOVA followed by Bonferroni's multiple comparison post-hoc test.

0.001). During chronic Ang II infusion, blood pressures were significantly higher in eNOS-KO mice compared with WT mice (172 $\pm$ 4 mmHg, $n = 9$, vs.157 $\pm$ 2 mmHg, $n = 9$, $P < 0.001$; Fig. 3*A*). Interestingly, the increase in blood pressure induced by Ang II did not differ between either group (50 $\pm$ 3 vs. 45 $\pm$ 7 mmHg, $P = 0.47$).

Under baseline conditions, treatment with sildenafil did not affect blood pressures significantly in any strain (vehicle-treated vs. treated; WT mice: 110 $\pm$ 3 mmHg, $n = 9$, vs. 106 $\pm$ 2 mmHg, $n = 9$, $P = 0.27$; eNOS-KO mice: 132 $\pm$ 2 mmHg, $n = 9$, $vs.$ 131 $\pm$ 3 mmHg, $n = 9$, $P = 0.652$). Chronic sildenafil treatment reduced Ang II-dependent hypertension in WT (140 $\pm$ 2 mmHg, $n = 9$, vs. 157 $\pm$ 2 mmHg, $n = 9$, $P < 0.01$) but not in eNOS-KO mice (166 $\pm$ 4 mmHg, $n = 9$, vs. 172 $\pm$ 4 mmHg, $n = 9$, $P = 0.2753$; Fig. 3*A*). In addition, cumulative sodium balance over 7 days was significantly increased in sildenafil-treated hypertensive WT mice compared

with vehicle-treated hypertensive WT mice (0.46 $\pm$ 0.02 mmol/7 days vs. 0.33 $\pm$ 0.3 mmol/7 days; $n = 8$, $P < 0.01$). In eNOS-KO mice, sildenafil treatment did not affect sodium balance significantly (0.30 $\pm$ 0.05 vs. 0.24 $\pm$ 0.04 mmol/7 days, $n = 8$, $P = 0.5203$; Fig. 3*B*).

Chronic sildenafil treatment restores impaired renal vasodilator response in Ang II-dependent hypertensive WT but not in eNOS-KO mice. To evaluate the impact of chronic sildenafil treatment on renal vasodilator response ex vivo, we tested renal endothelium-dependent relaxation in response to carbachol and smooth muscle cell-dependent relaxation in response to GSNO in isolated perfused kidneys. As expected, under baseline conditions, endothelium-dependent renal vasorelaxation was significantly impaired in eNOS-KO compared with WT mice (Fig. 4*A*). Accordingly, urinary nitrate/nitrite, a marker for renal nitric oxide generation, was significantly higher in WT compared with eNOS-KO mice (3.5 $\pm$ 0.4 mg/dl creatinine vs.
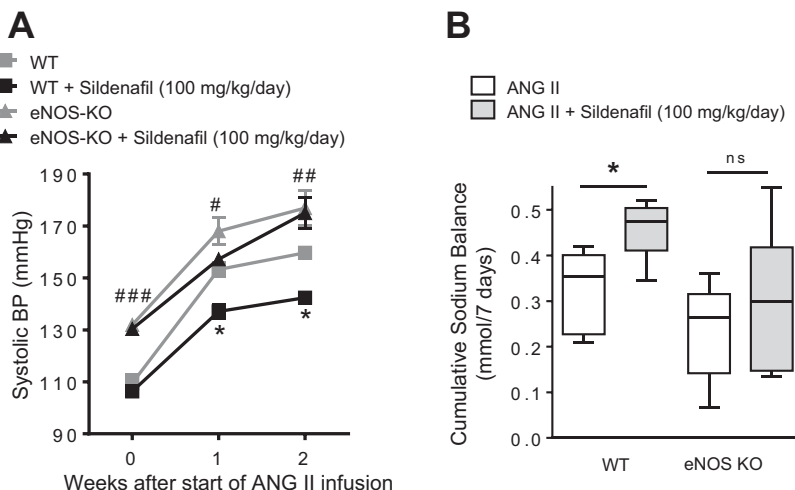

Fig. 3. Chronic sildenafil treatment attenuated Ang II-dependent hypertension and increased sodium balance in WT but not in eNOS-KO mice. *A:* BP was significantly higher in eNOS-KO ($n = 9$) than in WT ($n = 9$) before and during Ang II treatment. Chronic treatment with sildenafil significantly reduced BP during Ang II-dependent hypertension in WT ($n = 9$) but not in eNOS-KO ($n = 9$). *B*: during Ang II-induced hypertension, sildenafil significantly increased sodium balance in WT ($n = 8$) but not in eNOS-KO ($n = 8$). Data represent means $\pm$ SE. *$P < 0.01$, WT + sildenafil vs. WT; #$P < 0.05$, ##$P < 0.01$, and ###$P < 0.001$, eNOS-KO vs. WT. Two-way ANOVA followed by Bonferroni's multiple comparison post hoc test (*A*) and Student's unpaired *t*-test (*B*). NS, not significant.
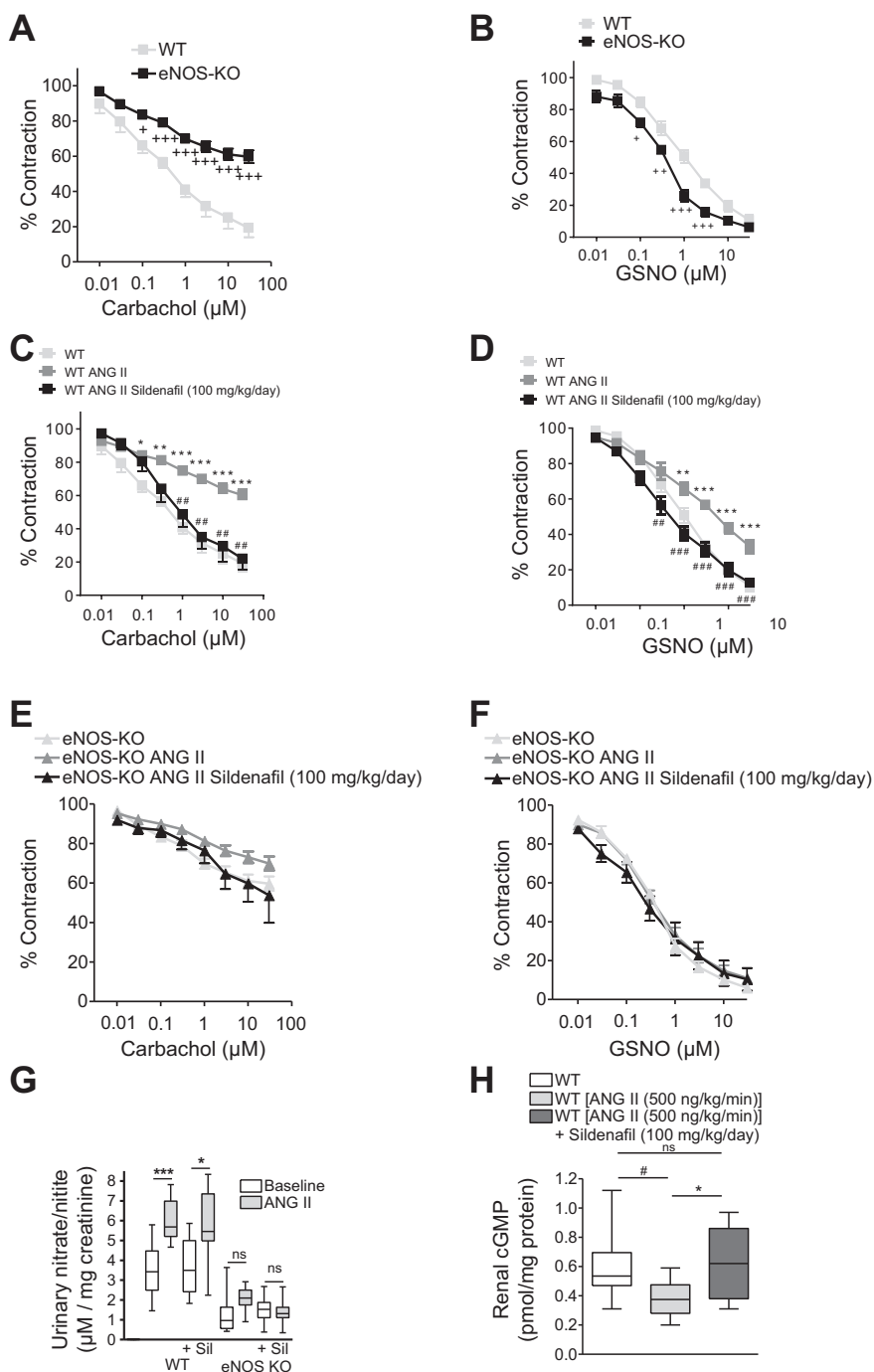
Fig. 4. Chronic sildenafil administration improved endothelium- and smooth muscle cell-dependent vascular dysfunction in Ang II-infused WT but not in eNOS-KO mice. *A:* endothelium-dependent vasorelaxation induced by carbachol was significantly reduced in isolated perfused kidneys of eNOS-KO compared with WT mice ($n = 5–6$). *B:* vascular smooth muscle cell-dependent vasorelaxation induced by GSNO was significantly increased in kidneys of eNOS-KO compared with WT mice ($n = 9–12$). *C–F:* vasorelaxation to carbachol and GSNO was significantly impaired in isolateed perfused kidneys of Ang II-infused WT ($n = 5–12$) but not eNOS-KO mice ($n = 6$). Chronic sildenafil treatment significantly improved the impaired vasorelaxation to carbachol and GSNO in kidneys of Ang II-infused WT but not eNOS-KO mice. *G:* urinary nitrate levels were increased after Ang II infusion in WT but not eNOS-KO mice ($n = 9$). WT mice showed increased nitrate excretion compared with eNOS-KO. *H:* renal cGMP levels were significantly decreased in Ang II treated WT mice compared with untreated WT mice. Chronic sildenafil treatment restored renal cGMP levels in Ang II-treated mice ($n = 12$). Data represent means ± SE. $+P < 0.05$, $++P < 0.01$, and $+++P < 0.001$, eNOS-KO vs. WT; $\#P < 0.05$, $\#\#P < 0.01$ WT, and $\#\#\#P < 0.001$ (Ang II) vs. WT. $*P < 0.05$, $**P < 0.01$, and $***P < 0.001$ WT (Ang II) + sildenafil vs. WT (Ang II). Two-way ANOVA followed by Bonferroni's multiple comparison post hoc test (*A–F* and *H*) and Student's unpaired *t*-test (*G*).

1.3 ± 0.3 mg/dl creatinine; $n = 9$, $P < 0.001$). In contrast, NO-induced renal vasorelaxation was increased in eNOS-KO mice, suggesting an increased sensitivity to exogenous NO in eNOS-KO compared with WT mice (Fig. 4B).

Chronic Ang II infusion significantly impaired the vasodilator response to carbachol and GSNO in isolated perfused kidneys of WT (Fig. 4, *C* and *D*). In contrast, chronic Ang II infusion did not impair the vasodilator response to GSNO and carbachol in eNOS-KO mice (Fig. 4, *E* and *F*). In addition, nitrate/nitrite levels increased during chronic Ang II infusion in WT but not in eNOS-KO mice, suggesting that

the impaired renal vasodilator response is not due to decreased NO production (WT mice: 6.0 ± 0.3 vs. 3.5 ± 0.4 mg/dl creatinine, $P < 0.01$; and eNOS-KO mice: 2.0 ± 0.2 vs. 1.3 ± 0.2 $\mu M \cdot mg^{-1} \cdot dl^{-1}$ creatinine, $P = 0.087$; Fig. 4G). Similar to acute PDE5 inhibition, chronic sildenafil treatment significantly restored the impaired vasodilator responses to carbachol and GSNO in WT mice but did not influence endothelial or smooth muscle cell-dependent vasodilator responses to carbachol or GSNO in eNOS-KO mice, suggesting that Ang II-induced vascular dysfunction is mediated by increased cGMP degradation (Fig. 4, *C–F*). Indeed, renal cGMP content

was significantly reduced in Ang II-treated mice and restored in those mice additionally treated with sildenafil (Fig. 4*H*).

DISCUSSION

The PDEs, which are the rate-limiting enzymes for cGMP-induced vasodilation, are important targets of pharmacological therapy in cardiovascular diseases and erectile dysfunction (6, 19, 22, 39). In addition, studies have shown that selective inhibition of both PDE5 and PDE1 improved vascular dysfunction in experimental hypertension (10, 16, 17, 34). However, it is unknown which PDE controls renal vascular resistance and blood flow and thereby influences systemic blood pressure in hypertension.

In the present study we showed that, under baseline conditions, sildenafil, a selective PDE5 inhibitor, decreased blood pressure dose dependently. Furthermore, sildenafil applied in the two highest concentrations induced a decrease in renal blood flow. This renal hypoperfusion was more likely due to hypotensive blood pressure values than to a direct effect of sildenafil on renal vascular resistance. On the other hand, PDE1 inhibition showed no effect on renal blood flow or blood pressure during baseline conditions.

Ang II plays a major role in the pathogenesis of hypertension by inducing vasoconstriction and impairing vascular function (7, 18, 26, 38). Recent studies suggested that those effects are mediated partly by activation of PDEs. Thus, it has been shown that PDE1, activated by increased intracellular Ca^{2+} levels, plays a dominant role in Ang II-mediated vascular dysfunction or vascular aging (3, 10, 13, 17, 31). Surprisingly, we observed only minor in vivo effects of PDE1 inhibition on blood pressure and no effect on renal blood flow during acute Ang II infusion. Moreover, vinpocetine did not affect the vasodilator response in isolated perfused kidneys of normotensive or hypertensive mice. These results are in contrast to observations performed in aortic and mesenteric arteries of rats where PDE1 inhibition decreased vascular contractility from Ang II-treated rats (10). The discrepancy might be explained by differences in vascular bed and species as well as different methods testing vascular function. And indeed, the present study provides evidence for this hypothesis, as we could show that vinpocetine improved NO-induced vasodilation in aortic rings but not in renal resistance arteries of Ang II-treated mice.

Besides PDE1, recent data emphasized the PDE5 as a key regulator in vascular function (16, 28, 34). In the present study, selective PDE5 inhibition increased renal blood flow and decreased blood pressure during acute Ang II infusion in vivo. In addition, renal cGMP levels were increased after sildenafil but not after vinpocetine application, highlighting the role of the PDE5 in the regulation of renal vascular tone in Ang II-dependent hypertension. To rule out the possibility that the increase in renal blood flow is in part mediated by sildenafil-induced blood pressure changes, we performed additional ex vivo experiments in the isolated perfused kidney. Here, we clearly showed that acute sildenafil administration significantly improves the impaired renal vasodilator response to exogenous NO in kidneys of Ang II-induced hypertensive mice. Together with the observation that PDE1 inhibition affected neither renal blood flow nor renal vascular function under normotensive conditions and was only very mild under hypertensive conditions, our results suggest that PDE5, and not PDE1, seems to be the major PDE regulating renal vascular resistance in experimental hypertension.

The mechanism through which Ang II interacts with PDE5 is still not fully understood. PDE5, activated by an allosteric binding of cGMP to the noncatalytic GAF domain of the PDE5, limits cGMP-induced vasorelaxation through a cGMP-mediated negative feedback mechanism (20, 23, 29). It has been suggested that Ang II-induced PDE5 activation is a result of an initially enhanced NO/cGMP signaling during Ang II infusion (34). To test this hypothesis and to see whether chronic sildenafil treatment affects blood pressure and renal vascular function, we treated WT and eNOS-KO mice with sildenafil and infused them with Ang II for 14 days.

First, we could show that chronic PDE5 inhibition ameliorated Ang II-dependent hypertension and attenuated renal sodium balance. Beside the investigated vasodilatory effect, we could not exclude that inhibition of PDE5 also reduced blood pressure and increased sodium excretion in part by directly affecting renal tubular sodium and water channels, as described previously (20, 24, 27, 37). However, Sparks et al. (32) could show that Ang II-induced sodium handling was directly affected by renal vascular function. Second, to elucidate the underlying mechanism of how PDE5 inhibition attenuated Ang II-dependent hypertension, we could demonstrate and confirm that chronic Ang II infusion increased urinary nitrate production, a marker for renal NO generation, and that PDE5 inhibition attenuated Ang II-dependent hypertension. In line with these observations, recent studies confirmed Ang II-mediated NO generation and the blood pressure-lowering effect of chronic PDE5 inhibition in several models of cardiovascular diseases (5, 9, 25, 28, 34, 35). Based on these results, it seems plausible that the initial increase in NO generation activates PDE5-mediated cGMP degradation, leading to vascular dysfunction and hypertension. Accordingly, renal cGMP levels were reduced in Ang II-treated WT mice and restored in those mice treated additionally with sildenafil. Moreover, we showed that the beneficial effect of PDE5 inhibition was abrogated in eNOS-KO mice, a mouse model characterized by low NO/cGMP levels. Chronic PDE5 inhibition had no effect on Ang II-dependent hypertension in eNOS-KO mice, suggesting that the efficacy of a PDE5 inhibition is dependent on the amount of produced cGMP (23). In line with this assumption, PDE5 inhibition improved the vasodilator response in kidneys of Ang II-infused WT mice but failed to modulate the renal vasodilator response to NO in kidneys of Ang II-infused eNOS-KO mice, indicating that vascular dysfunction in Ang II-dependent hypertension is mediated by increased cGMP degradation. Finally, we showed that both acute and chronic sildenafil inhibition improved vascular function in isolated perfused kidneys of Ang II-infused WT mice, suggesting that the effect of PDE5 inhibition is rather a result of increased cGMP availability than an indirect effect of sildenafil-induced blood pressure reduction or attenuated renal vascular injury.

In summary, the present study identifies the PDE5 as the relevant PDE regulating renal blood flow and renal vasodilator response during Ang II-dependent hypertension. Moreover, these data suggest that activation of PDE5 depends on the amount of produced NO/cGMP, as selective inhibition of PDE5 did not show any effects in eNOS-KO mice. Further studies are required to investigate the exact molecular mechanism by which PDE5 is activated during Ang II infusion.

REFERENCES

1. **Adamo CM, Dai DF, Percival JM, Minami E, Willis MS, Patrucco E, Froehner SC, Beavo JA.** Sildenafil reverses cardiac dysfunction in the mdx mouse model of Duchenne muscular dystrophy. *Proc Natl Acad Sci U S A* 107: 19079–19083, 2010. doi:10.1073/pnas.1013077107.

2. **Arruda RM, Peotta VA, Meyrelles SS, Vasquez EC.** Evaluation of vascular function in apolipoprotein E knockout mice with angiotensin-dependent renovascular hypertension. *Hypertension* 46: 932–936, 2005. doi:10.1161/01.HYP.0000182154.61862.52.

3. **Bautista Niño PK, Durik M, Danser AH, de Vries R, Musterd-Bhaggoe UM, Meima ME, Kavousi M, Ghanbari M, Hoeijmakers JH, O'Donnell CJ, Franceschini N, Janssen GM, De Mey JG, Liu Y, Shanahan CM, Franco OH, Dehghan A, Roks AJ.** Phosphodiesterase 1 regulation is a key mechanism in vascular aging. *Clin Sci (Lond)* 129: 1061–1075, 2015. doi:10.1042/CS20140753.

4. **Broekmans K, Stegbauer J, Potthoff SA, Russwurm M, Koesling D, Mergia E.** Angiotensin II-Induced Hypertension Is Attenuated by Reduction of Sympathetic Output in NO-Sensitive Guanylyl Cyclase 1 Knockout Mice. *J Pharmacol Exp Ther* 356: 191–199, 2016. doi:10.1124/jpet.115.227728.

5. **Brown KE, Dhaun N, Goddard J, Webb DJ.** Potential therapeutic role of phosphodiesterase type 5 inhibition in hypertension and chronic kidney disease. *Hypertension* 63: 5–11, 2014. doi:10.1161/HYPERTENSIONAHA.113.01774.

6. **Carson CC, Lue TF.** Phosphodiesterase type 5 inhibitors for erectile dysfunction. *BJU Int* 96: 257–280, 2005. doi:10.1111/j.1464-410X.2005.05614.x.

7. **Diep QN, Amiri F, Touyz RM, Cohn JS, Endemann D, Neves MF, Schiffrin EL.** PPARalpha activator effects on Ang II-induced vascular oxidative stress and inflammation. *Hypertension* 40: 866–871, 2002. doi:10.1161/01.HYP.0000037969.41360.CC.

8. **Endemann DH, Schiffrin EL.** Endothelial dysfunction. *J Am Soc Nephrol* 15: 1983–1992, 2004. doi:10.1097/01.ASN.0000132474.50966.DA.

9. **George EM, Palei AC, Dent EA, Granger JP.** Sildenafil attenuates placental ischemia-induced hypertension. *Am J Physiol Regul Integr Comp Physiol* 305: R397–R403, 2013. doi:10.1152/ajpregu.00216.2013.

10. **Giachini FR, Lima VV, Carneiro FS, Tostes RC, Webb RC.** Decreased cGMP level contributes to increased contraction in arteries from hypertensive rats: role of phosphodiesterase 1. *Hypertension* 57: 655–663, 2011. doi:10.1161/HYPERTENSIONAHA.110.164327.

11. **Gödecke A, Decking UK, Ding Z, Hirchenhain J, Bidmon HJ, Gödecke S, Schrader J.** Coronary hemodynamics in endothelial NO synthase knockout mice. *Circ Res* 82: 186–194, 1998. doi:10.1161/01.RES.82.2.186.

12. **Heitzer T, Wenzel U, Hink U, Krollner D, Skatchkov M, Stahl RA, MacHarzina R, Bräsen JH, Meinertz T, Münzel T.** Increased NAD(P)H oxidase-mediated superoxide production in renovascular hypertension: evidence for an involvement of protein kinase C. *Kidney Int* 55: 252–260, 1999. doi:10.1046/j.1523-1755.1999.00229.x.

13. **Huang CY, Chau V, Chock PB, Wang JH, Sharma RK.** Mechanism of activation of cyclic nucleotide phosphodiesterase: requirement of the binding of four Ca2+ to calmodulin for activation. *Proc Natl Acad Sci U S A* 78: 871–874, 1981. doi:10.1073/pnas.78.2.871.

14. **Jung O, Marklund SL, Geiger H, Pedrazzini T, Busse R, Brandes RP.** Extracellular superoxide dismutase is a major determinant of nitric oxide bioavailability: in vivo and ex vivo evidence from ecSOD-deficient mice. *Circ Res* 93: 622–629, 2003. doi:10.1161/01.RES.0000092140.81594.A8.

15. **Jung O, Schreiber JG, Geiger H, Pedrazzini T, Busse R, Brandes RP.** gp91phox-containing NADPH oxidase mediates endothelial dysfunction in renovascular hypertension. *Circulation* 109: 1795–1801, 2004. doi:10.1161/01.CIR.0000124223.00113.A4.

16. **Kim D, Aizawa T, Wei H, Pi X, Rybalkin SD, Berk BC, Yan C.** Angiotensin II increases phosphodiesterase 5A expression in vascular smooth muscle cells: a mechanism by which angiotensin II antagonizes cGMP signaling. *J Mol Cell Cardiol* 38: 175–184, 2005. doi:10.1016/j.yjmcc.2004.10.013.

17. **Kim D, Rybalkin SD, Pi X, Wang Y, Zhang C, Munzel T, Beavo JA, Berk BC, Yan C.** Upregulation of phosphodiesterase 1A1 expression is associated with the development of nitrate tolerance. *Circulation* 104: 2338–2343, 2001. doi:10.1161/hc4401.098432.

18. **Kim S, Iwao H.** Molecular and cellular mechanisms of angiotensin II-mediated cardiovascular and renal diseases. *Pharmacol Rev* 52: 11–34, 2000.

19. **Kukreja RC, Salloum FN, Das A, Koka S, Ockaili RA, Xi L.** Emerging new uses of phosphodiesterase-5 inhibitors in cardiovascular diseases. *Exp Clin Cardiol* 16: e30–e35, 2011.

20. **Mergia E, Stegbauer J.** Role of Phosphodiesterase 5 and Cyclic GMP in Hypertension. *Curr Hypertens Rep* 18: 39, 2016. doi:10.1007/s11906-016-0646-5.

21. **Montezano AC, Nguyen Dinh Cat A, Rios FJ, Touyz RM.** Angiotensin II and vascular injury. *Curr Hypertens Rep* 16: 431, 2014. doi:10.1007/s11906-014-0431-2.

22. **Mostafa T.** Oral phosphodiesterase type 5 inhibitors: nonerectogenic beneficial uses. *J Sex Med* 5: 2502–2518, 2008. doi:10.1111/j.1743-6109.2008.00983.x.

23. **Mullershausen F, Friebe A, Feil R, Thompson WJ, Hofmann F, Koesling D.** Direct activation of PDE5 by cGMP: long-term effects within NO/cGMP signaling. *J Cell Biol* 160: 719–727, 2003. doi:10.1083/jcb.200211041.

24. **Ortiz PA, Garvin JL.** Role of nitric oxide in the regulation of nephron transport. *Am J Physiol Renal Physiol* 282: F777–F784, 2002. doi:10.1152/ajprenal.00334.2001.

25. **Patzak A, Mrowka R, Storch E, Hocher B, Persson PB.** Interaction of angiotensin II and nitric oxide in isolated perfused afferent arterioles of mice. *J Am Soc Nephrol* 12: 1122–1127, 2001.

26. **Rajagopalan S, Kurz S, Münzel T, Tarpey M, Freeman BA, Griendling KK, Harrison DG.** Angiotensin II-mediated hypertension in the rat increases vascular superoxide production via membrane NADH/NADPH oxidase activation. Contribution to alterations of vasomotor tone. *J Clin Invest* 97: 1916–1923, 1996. doi:10.1172/JCI118623.

27. **Ramseyer VD, Ortiz PA, Carretero OA, Garvin JL.** Angiotensin II-mediated hypertension impairs nitric oxide-induced NKCC2 inhibition in thick ascending limbs. *Am J Physiol Renal Physiol* 310: F748–F754, 2016. doi:10.1152/ajprenal.00473.2015.

28. **Rodríguez-Iturbe B, Ferrebuz A, Vanegas V, Quiroz Y, Espinoza F, Pons H, Vaziri ND.** Early treatment with cGMP phosphodiesterase inhibitor ameliorates progression of renal damage. *Kidney Int* 68: 2131–2142, 2005. doi:10.1111/j.1523-1755.2005.00669.x.

29. **Rybalkin SD, Rybalkina IG, Shimizu-Albergine M, Tang XB, Beavo JA.** PDE5 is converted to an activated state upon cGMP binding to the GAF A domain. *EMBO J* 22: 469–478, 2003. doi:10.1093/emboj/cdg051.

30. **Rybalkin SD, Yan C, Bornfeldt KE, Beavo JA.** Cyclic GMP phosphodiesterases and regulation of smooth muscle function. *Circ Res* 93: 280–291, 2003. doi:10.1161/01.RES.0000087541.15600.2B.

31. **Sonnenburg WK, Rybalkin SD, Bornfeldt KE, Kwak KS, Rybalkina IG, Beavo JA.** Identification, quantitation, and cellular localization of PDE1 calmodulin-stimulated cyclic nucleotide phosphodiesterases. *Methods* 14: 3–19, 1998. doi:10.1006/meth.1997.0561.

32. **Sparks MA, Stegbauer J, Chen D, Gomez JA, Griffiths RC, Azad HA, Herrera M, Gurley SB, Coffman TM.** Vascular Type 1A Angiotensin II Receptors Control BP by Regulating Renal Blood Flow and Urinary Sodium Excretion. *J Am Soc Nephrol* 26: 2953–2962, 2015. doi:10.1681/ASN.2014080816.

33. **Stegbauer J, Coffman TM.** New insights into angiotensin receptor actions: from blood pressure to aging. *Curr Opin Nephrol Hypertens* 20: 84–88, 2011. doi:10.1097/MNH.0b013e3283414d40.

34. **Stegbauer J, Friedrich S, Potthoff SA, Broekmans K, Cortese-Krott MM, Quack I, Rump LC, Koesling D, Mergia E.** Phosphodiesterase 5 attenuates the vasodilatory response in renovascular hypertension. *PLoS One* 8: e80674, 2013. doi:10.1371/journal.pone.0080674.

35. **Stegbauer J, Kuczka Y, Vonend O, Quack I, Sellin L, Patzak A, Steege A, Langnaese K, Rump LC.** Endothelial nitric oxide synthase is predominantly involved in angiotensin II modulation of renal vascular resistance and norepinephrine release. *Am J Physiol Regul Integr Comp Physiol* 294: R421–R428, 2008. doi:10.1152/ajpregu.00481.2007.

36. **Stegbauer J, Vonend O, Habbel S, Quack I, Sellin L, Gross V, Rump LC.** Angiotensin II modulates renal sympathetic neurotransmission through nitric oxide in AT2 receptor knockout mice. *J Hypertens* 23: 1691–1698, 2005. doi:10.1097/01.hjh.0000179763.02583.8e.

37. **Stoos BA, Garvin JL.** Actions of nitric oxide on renal epithelial transport. *Clin Exp Pharmacol Physiol* 24: 591–594, 1997. doi:10.1111/j.1440-1681.1997.tb02097.x.

38. **Touyz RM, Chen X, Tabet F, Yao G, He G, Quinn MT, Pagano PJ, Schiffrin EL.** Expression of a functionally active gp91phox-containing neutrophil-type NAD(P)H oxidase in smooth muscle cells from human resistance arteries: regulation by angiotensin II. *Circ Res* 90: 1205–1213, 2002. doi:10.1161/01.RES.0000020404.01971.2F.

39. **Trigo-Rocha F, Hsu GL, Donatucci CF, Martinez-Piñeiro L, Lue TF, Tanagho EA.** Intracellular mechanism of penile erection in monkeys. *Neurourol Urodyn* 13: 71–80, 1994. doi:10.1002/nau.1930130110.
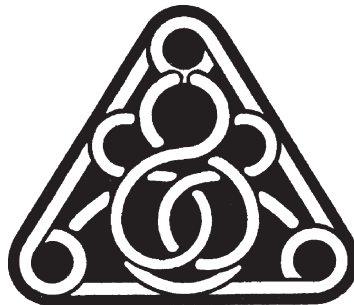
Phosphodiesterase 5 Attenuates the Vasodilatory Response in Renovascular Hypertension

Johannes Stegbauer[1], Sebastian Friedrich[1], Sebastian A. Potthoff[1], Kathrin Broekmans[3], Miriam M. Cortese-Krott[2], Ivo Quack[1], Lars Christian Rump[1], Doris Koesling[3], Evanthia Mergia[3*]

1 Klinik für Nephrologie, Universitätsklinikum Heinrich-Heine-Universität Düsseldorf, Düsseldorf, Germany, 2 Klinik für Kardiologie, Universitätsklinikum Heinrich-Heine-Universität Düsseldorf, Düsseldorf, Germany, 3 Institut für Pharmakologie Ruhr-Universität Bochum, Bochum, Germany

Abstract

NO/cGMP signaling plays an important role in vascular relaxation and regulation of blood pressure. The key enzyme in the cascade, the NO-stimulated cGMP-forming guanylyl cyclase exists in two enzymatically indistinguishable isoforms (NO-GC1, NO-GC2) with NO-GC1 being the major NO-GC in the vasculature. Here, we studied the NO/cGMP pathway in renal resistance arteries of NO-GC1 KO mice and its role in renovascular hypertension induced by the 2-kidney-1-clip-operation (2K1C). In the NO-GC1 KOs, relaxation of renal vasculature as determined in isolated perfused kidneys was reduced in accordance with the marked reduction of cGMP-forming activity (80%). Noteworthy, increased eNOS-catalyzed NO formation was detected in kidneys of NO-GC1 KOs. Upon the 2K1C operation, NO-GC1 KO mice developed hypertension but the increase in blood pressures was not any higher than in WT. Conversely, operated WT mice showed a reduction of cGMP-dependent relaxation of renal vessels, which was not found in the NO-GC1 KOs. The reduced relaxation in operated WT mice was restored by sildenafil indicating that enhanced PDE5-catalyzed cGMP degradation most likely accounts for the attenuated vascular responsiveness. PDE5 activation depends on allosteric binding of cGMP. Because cGMP levels are lower, the 2K1C-induced vascular changes do not occur in the NO-GC1 KOs. In support of a higher PDE5 activity, sildenafil reduced blood pressure more efficiently in operated WT than NO-GC1 KO mice. All together our data suggest that within renovascular hypertension, cGMP-based PDE5 activation terminates NO/cGMP signaling thereby providing a new molecular basis for further pharmacological interventions.

Introduction

Hypertension is the leading risk factor for cardiovascular mortality and has been associated with alterations in vascular relaxation. One of the major pathways that mediate vascular relaxation is the NO/cGMP signaling cascade, in which the NO-stimulated guanylyl cyclase (NO-GC) holds a key position by translating the NO signal into cGMP formation [1–3]. The NO-GC contains a prosthetic heme group as a specific NO binding site and exhibits enhanced rates of cGMP formation in response to NO activation [4]. Two isoforms of the NO receptor GC exist; NO-GC1 and NO-GC2 which consist of an identical β subunit dimerized to an α_1 or α_2 subunit, respectively [5]. Knock-out (KO) mice deficient in either one of the NO-GCs, NO-GC1 or NO-GC2, revealed that both NO-GCs participate in vascular relaxation [6]. Outside the central nervous system,

NO-GC1 is the major isoform, particularly in aorta, where NO-GC1 represents approximately 90% of the WT NO-GC content. Although deletion of the NO-GC1 resulted in reduced vascular relaxation, the NO-GC1 KO mice develop hypertension only on the 129S6 background which displays higher activity of the renin-angiotensin-aldosterone system (RAAS) than other inbred mouse strains [7].

In the vasculature, the cGMP-mediated relaxation is transduced by the cGMP-dependent protein kinase I (PKGI) [8]. The cGMP effects are controlled by the activity of cGMP-hydrolysing phosphodiesterases (PDEs) with PDE1 and PDE5 being of particular importance for cGMP degradation in vascular smooth muscle [9]. PDE1 is stimulated by Ca^{2+}/calmodulin and has been suggested to play a more dominant role under conditions of higher calcium (Ca^{2+}), e.g., in the presence of vasoconstrictors. Under conditions of low calcium,

PDE5 is considered to be the major cGMP-degrading PDE. NO-induced cGMP increase does not only activate PKGI but also cause allosteric activation of PDE5 by cGMP binding to the regulatory GAF-A domain of PDE5 which is paralleled by PKGI-mediated phosphorylation [10,11]. Hence, by activating PDE5 the NO/cGMP signal initiates a negative feedback loop to limit its own action [12].

It is widely accepted that the vasodilatory NO/cGMP pathway counteracts the vasoconstriction induced by the renin-angiotensin system (RAS) to maintain normal circulatory homeostasis. Thus, an activated RAS as in the 2-kidney 1-clip (2K1C) Goldblatt model of human renovascular hypertension causes hypertension and a reduction of endothelium-dependent relaxation [13–16].

In the present study, we characterized the NO/cGMP pathway in kidneys of NO-GC1 KO mice, in which the major NO-GC isoform of the kidney, NO-GC1, is deleted. Despite a pronounced reduction of cGMP forming activity (80%), the decrease of the renal cGMP content was moderate (50%) as was the decrease of relaxation of the renal vasculature determined in the isolated perfused kidneys. Comparison of endothel- and smooth muscle-dependent relaxation indicated increased NO formation in the NO-GC1 KO that partially compensates for the deficiency of NO-GC1.

We challenged NO-GC1 KO mice by the 2K1C operation to investigate the impact of the NO/cGMP pathway on renovascular hypertension. Unexpectedly, 2K1C-operated NO-GC1 KO mice did not develop a higher degree of hypertension than WT and the reduction of endothelium-dependent relaxation found in operated WT kidney and aortas was not observed in operated NO-GC1 KO mice. Furthermore, a reduction of responsiveness towards exogenous NO was detected in 2K1C WT that was not based on decreased NO-GC content or altered sensitivity towards cGMP. As the reduced NO sensitivity in operated WT kidneys was restored by the inhibitor of PDE5, sildenafil, PDE5 emerges as the key vascular component responsible for the reduction of endothelium-dependent relaxation in renovascular hypertension.

Materials and Methods

KO mice

Studies were performed with NO-GC1 KO mice lacking the α_1 subunit of the heterodimeric NO-GC1 receptor and wild-type (WT) littermates backcrossed to C57Bl/6Rj background for 5-7 times (N5-N7 generation). Generation and genotyping of the NO-GC1 KO mice have been described by Mergia et al., 2006 [6]. Two- to 4-month-old males (~30 g) were used in all studies. Mice were fed a low salt diet containing 0.12% NaCl (Sniff, Soest, Germany) and allowed free access to tap water. All animal investigations conformed to the Guide for the care and Use of laboratory Animals published by the US national Institutes of Health (NIH Publication No. 85-23, revised 1996) and were also approved by the local animal care committee (Landesamt für Natur, Umwelt und Verbraucherschutz Nordrhein-Westfalen, Recklinghausen, licence no. AZ. 8.87-50.10.34.08.216).

2K1C operation

In the 2K1C model, partial occlusion of one renal artery reduces renal blood flow causing activation of the RAS. The 2K1C operation was performed in 8 week old male mice according to the reported method [17] with some modifications. In brief, mice were anesthetized with Ketamine (100 mg/kg, i.p.) and Xylazin (5 mg/kg, i.p.). The depth of anaesthesia was confirmed by lack of toe pinch response. After a latero-abdominal incision, the left renal artery dissected from renal vein and nerves over a short segment close to the abdominal aorta was partially occluded (silver clip, 0.12mm internal gap, Klaus Effenberger, Med. Tech. Gerätebau, Pfaffing, Germany). Mice with an 80 to 90% reduction of renal blood flow after clipping measured with a laser Doppler blood flow probe (ADI Instruments) were used. Sham-operated mice, which underwent the same surgical procedure except for placement of the renal artery clip, served as controls.

Isolated perfused murine kidneys

Experiments with isolated perfused kidneys were performed using the non-clipped kidney 4 weeks after 2K1C or sham operation according to the method described previously [18]. Perfusion pressure was monitored continuously with a Statham P23 Db pressure transducer (Gould, Oxnard, CA) coupled to a Watanabe pen recorder (Graphtec Corp., Tokyo, Japan). Changes in perfusion pressure reflected changes in vascular resistance with an increase indicating vasoconstriction. Renal vasoconstriction was induced by norepinephrine (NA 1 µM; Sigma-Aldrich). Vasorelaxation induced by carbachol (30 µM; Sigma-Aldrich) was recorded in presence of diclofenac (3 µM). Concentration-response curves of the vasodilators GSNO (Alexis Corp.) and 8-pCPT-cGMP (8-(p-chlorophenylthio)-cGMP; Biolog Inc.) were assessed in the presence of L-NAME (300 µM; Sigma-Aldrich) and diclofenac (3 µM). To test the influence of vinpocetine (10 µM; Calbiochem) and sildenafil (300 nM; a generous gift from Pfizer) on vasodilative properties of GSNO, the respective PDE inhibitors were added to the perfusion solution 10 minutes before GSNO administration. Renal relaxation is expressed as pressure reduction with the pressure of the precontracted kidney set as 100%.

Preparation of murine homogenates

Mice were anesthetized by CO_2 inhalation and decapitated, non-clipped kidneys or aortas (free of surrounding tissue) were removed and homogenized immediately with a glass/glass homogenizer (700 rpm) in buffer (50 mmol/L triethanolamine (TEA)/HCl, 50 mmol/L NaCl, 1 mmol/L EDTA, 2 mmol/L DTT, 0.2 mmol/L benzamidine, 0.5 mmol/L phenylmethylsulfonylfluoride (PMSF), and 1 µmol/L pepstatin A; pH 7.4, 4°C). After centrifugation (800 x g, 5 min, 4°C), homogenates were used in experiments as described. The protein concentration was determined in triplicates and repeated three times (Bradford, Bio-Rad).

Determination of NO-stimulated GC activity

NO-stimulated GC activity was measured for 10 min (37°C) in kidney and aorta homogenates (2 µg and 3 µg protein,

respectively), in the presence of 100 µM DEA-NO (2-(N,N-diethylamino)-diazenolate-2-oxide, Alexis) as described previously [6].

Measurement of cGMP-hydrolyzing PDE activity

PDE activity in homogenates was measured by the conversion of [32P]cGMP (synthesized from [α-32P]GTP using purified NO-GC) to guanosine and [32P]phosphate in the presence of alkaline phosphatase (Sigma) at 37 °C for 7 min. Reactions mixtures (0.1 ml) contained 0.5-15 µl of the homogenates (~1-15 µg protein), [32P]cGMP (~2 kBq), 1 µM or 30 nM cGMP, 12 mM $MgCl_2$, 3 mM DTT, 0.5 mg/ml BSA, 2 U of alkaline phosphatase, and 50 mM TEA/HCl, pH 7.4. Reactions were stopped by adding 900 µl ice cold charcoal suspension (30% activated charcoal in 50 mM KH_2PO_4, pH 2.3). After pelleting the charcoal by centrifugation, [32P] phosphate was measured in supernatant. Sildenafil 100 nM was used to inhibit PDE5. PDE assays were carried out in triplicates and repeated two or three times.

Western blot analysis

Separation of proteins (homogenates 50 µg/lane), blotting, detection and quantification of the chemiluminescence signals were performed as described [19]. The signals of the $α_2$ and $β_1$ subunit of the NO-GCs, eNOS and PDE5 were standardized relative to the amount of the respective protein in the WT sample on the same blot. eNOS phosphorylation was assessed as the ratio of phospho-eNOS and eNOS signals standardized to the one of the WT sample on the same blot. eNOS and phospho-eNOS (Ser1177) antibodies used in a 1:1000 dilution were from BD Biosciences. Antibodies against the $α_1$, $α_2$ and $β_1$ subunits were raised and purified as described [6]. PDE5 antibody used in a 1:1000 dilution was from Cell Signaling Danvers, USA. Beta tubulin antibody used in 1:500 dilution was from Abcam, Cambridge, UK.

Determination of cGMP content in renal cortical slices

Cortical slices (250 µm) of kidneys were cut with a vibratome (NVSLM1 from WPI), equilibrated for 30 min in temperate (37 °C), oxygenated (in 95% O_2, 5% CO_2) Krebs-Henseleit buffer and thereafter were incubated with ODQ (20 µM, 15 min), or Cch (30 µM, 3 min), or DEA-NO (100 µM, 3 min), or sildenafil (100 µM, 10 min). The cGMP levels of equilibrated untreated slices were taken as controls. After incubation, slices were snap frozen in liquid nitrogen, homogenized in 70% (v/v) ice-cold ethanol using a glass/glass homogenizer, and then centrifuged (14,000 x g, 15 min, 4°C). Supernatants were dried at 95°C and the cGMP content was measured in duplicate by RIA. To standardize the different samples, protein pellets were dissolved in 0.1 M NaOH/0.1% SDS, and protein content was determined using the bicinchoninic acid method (Uptima).

Determination of NOS activity

Renal homogenates were prepared with a glass/glass homogenizer (1500 rpm, 4°C) in 1 ml buffer (25 mmol/L TRIS-HCl, 10 mmol/L EDTA at pH 7.4, 4°C) supplemented with a commercial cocktail of protease/phosphatase inhibitors (Pierce,

Thermo Scientific, Bonn, Germany) and centrifugated at 1000 x g, 15 min, 4°C. NOS activity of 1 µg total protein was assayed by detecting NO produced by the conversion of L-arginine to citrulline using a NO-specific fluorescent probe 4-Amino-5-Methylamino-2',7'-Difluorofluorescein (DAF-FM) diacetate. Briefly, the reaction was conducted in the dark in a buffer containing 1 µM DAF-FM diacetate, 3 mM L-arginine, 2 µM FAD, 2 µM FMN, 1 mM NADPH, 6 µM tetrahydrobiopterine, 0.04 µg/µl calmodulin, and 20 mM $CaCl_2$ for 10 min at RT and green fluorescence (ex 485 nm, em 520 nm) due to the nitrosation of DAF-FM [20] was measured in a FluoStar Omega (BMG Labtech, Ortenberg, Germany). NOS-independent background signal was assessed in all samples by adding the specific NOS inhibitor L-NAME (1 mM). Fluorescence-background was taken as index for NOS-dependent NO production.

Organ bath experiments with aortic rings

Thoracic aortic rings were mounted isometrically on fixed segment support pins in two four-chamber myographs (Multi Myograph Model 610 M, Danish Myo Technology, Denmark) containing 5 ml of Krebs-Henseleit buffer (118 mmol/L NaCl, 4.7 mmol/L KCl, 1.2 mmol/L MgSO4, 1.2 mmol/L KH_2PO_4, 25 mmol/L $NaHCO_3$, 2.55 mmol/L $CaCl_2$, 7.5 mmol/L D-glucose) in the presence of diclofenac (3 µmol/L) and gassed with 5% CO_2 in O_2. Resting tension was set to 5 mN. After equilibration, rings were contracted (1 µmol/L NA) and vasodilation to carbachol (30 µmol/L) was recorded. Each experiment was performed in parallel with four aortic rings each derived from sham- and 2K1C-operated WT or NO-GC1 KO mice, respectively.

Isolation of preglomerular vessels

Preglomerular vessels containing mainly interlobular arteries and afferent arterioles were isolated by a modified iron oxide-sieving technique as described [21]. As minor modifications, the kidneys were perfused via cannulation of the aorta, and smaller needles (20G, 23G) and pore sieves (100 and 80 µm) were used for separation of tissue and renal particles, respectively.

Analysis of PDE5 mRNA content

Preglomerular vessels of the non-clipped kidneys were used to study the PDE5 mRNA content. After homogenization of isolated vessels with a Tissue Ruptor (Qiagen, Germany), total RNA was isolated using a RNA Micro Kit (Qiagen, Germany) according to the manufacturer's instructions. Quantitative PCR was performed with an ABI PRISM 7300 (Applied Biosystem, Germany) and the SYBR Green master mix (Qiagen, Germany). The PCR reaction was performed in a total volume of 20 µl with 1 µl cDNA corresponding to 100 ng RNA as template and 1 pmol of each PDE5 primer (NM_153422; Qiagen, Germany). The two-step PCR conditions were 2 min at 50°C, 15 min at 95°C, followed by 40 cycles (denaturation of 94°C for 15 s; annealing 55 °C 30 s and extension at 72°C for 34 s). Experiments were performed in triplicate. Glyceraldehyde-3-phosphate dehydrogenase (GAPDH) was chosen as the endogenous control (housekeeping gene). The

levels of PDE5 cDNA were normalized to GAPDH by the ΔC_T method.

Blood pressure measurements

Systolic blood pressures were measured in conscious mice by tail-cuff plethysmography (BP-98A; Softron Co.). For habituation, mice were trained daily for five days. After the training period, 10 measurements per mouse were recorded daily for 5 days, 1 week before and 4 weeks after 2K1C-operation.

Oral administration of sildenafil

Sildenafil citrate (100-mg tablets; Viagra; Pfizer) was dissolved in acidified water (pH ~ 3) to a final concentration of 800 mg/L, and given ad libidum, resulting in the ingestion of approximately 100 mg/kg d of sildenafil [22]. The free plasma concentration of sildenafil determined by measuring inhibition of recombinant PDE5 at 1 μM cGMP amounted to 21 ± 5 nM which is around the IC_{50} for PDE5 inhibition (10 nM sildenafil). Mice were treated with sildenafil in the fourth week after the 2K1C-operation.

Statistical analysis

Data are expressed as mean ± SEM (n=number of animals). Statistical analysis was carried out by the unpaired or paired 2-tailed Student's t test. Concentration-response curves were compared by ANOVA for repeated measurements. Differences were considered significant at a P value of less than 0.05.

Results

Cyclic GMP in kidneys of NO-GC1 KO mice

Deletion of the NO-GC1 isoform resulted in 80% reduction of NO-stimulated GC activity (DEA-NO, 100 μM) in renal homogenates with the residual NO-GC activity reflecting the content of the NO-GC2 isoform (0.5 ± 0.1 nmol/mg min versus 2.3 ± 0.3 nmol cGMP/mg min in WT; Figure 1A). The results indicate that NO-GC1 amounts to 80% and the NO-GC2 to 20% of the total NO-GC content in kidney. Measurements of cGMP hydrolysis revealed that PDE activity (1μM cGMP) is unaltered in NO-GC1-deficient kidneys (KO 527 ± 47 versus WT 517 ± 87 pmol GMP/mg min).

Analysis of the protein content in Western blot revealed that the loss of the α_1 subunit in kidney was accompanied by a decrease of the β_1 subunit content (60 ± 16%; Figure 1B). The observed reduction of the β_1 subunit confirms the NO-GC1 ($\alpha_1\beta_1$ heterodimer) as the major NO-GC isoform in kidney. In addition, similar amounts of the α_2 subunit were determined in WT and NO-GC1 KO kidneys excluding upregulation of the NO-GC2 isoform ($\alpha_2\beta_1$ heterodimer).

Compared to NO-GC activity, the cGMP content in renal cortical slices of NO-GC1 KO mice was reduced by only 45% compared to WT under untreated conditions (KO 0.27 ± 0.04 pmol cGMP/mg protein, versus WT 0.5 ± 0.07 pmol cGMP/mg protein; Figure 1C). In WT slices, the inhibitor of NO-stimulated GC activity, ODQ (20 μM, 15 min), reduced the cGMP content by 56% indicating continuous eNOS activation in renal slices

under basal i.e. untreated conditions. In NO-GC1 KO slices, ODQ treatment did not lower the cGMP content showing that in the absence of NO-GC1, cGMP formation in response to basically produced NO is too low to yield measurable cGMP increases.

To determine the capacity for renal cGMP formation, we incubated the renal cortical slices with exogenous NO (DEA-NO 100 μM, 3 min) or carbachol (100 μM, 3 min) which stimulates endogenous NO formation by eNOS. DEA-NO caused a 20-fold increase of the cGMP content in WT (10 ± 1.4 pmol cGMP/mg protein). The cGMP content in the NO-GC1 KO was also increased 20-fold by DEA-NO but was 50% lower than in WT (5 ± 0.7 pmol cGMP/mg protein). Carbachol caused a 7-fold and 2-fold cGMP increase in WT and NO-GC1 KO, respectively (WT 3.6 ± 0.4 versus KO 0.6 ± 0.2 pmol cGMP/mg protein). In sum, the decrease of the renal cGMP content was less than expected by the 80% reduction of the cGMP-forming enzyme.

Renal vascular relaxation of NO-GC1 KO mice

Next, we wanted to know whether the reduced cGMP content in NO-GC1 KO mice affects renal hemodynamics. Therefore, renal vascular relaxation was measured in the isolated perfused kidneys. In NO-GC1 KO kidneys, endothelium-dependent relaxation (30 μM carbachol) was reduced by 36% compared to WT (Figure 1D). In accordance, maximal renal vascular relaxation of the NO-GC1 KO kidneys by GSNO (S-nitrosoglutathione) was reduced to 56% of WT and the concentration-response curve was shifted to the right yielding about 17-fold higher EC_{50} values (KO 10.16 ± 0.51 μM GSNO versus WT 0.60 ± 0.1 μM GSNO; Figure 1E).

To determine the amount of NO formed in response to carbachol in the renal vasculature, the carbachol response (35% in NO-GC1 KO and 54% in WT) was plotted to the respective GSNO concentration-response curve and corresponded to 7 μM GSNO in NO-GC1 KO kidneys and 0.6 μM GSNO in WT kidneys (see Figure 1E). These data show that relaxation in the NO-GC1 KO requires 10 times more NO than in WT kidneys and indicate that carbachol elicits a higher NO production in NO-GC1 KO kidneys than in WT to achieve the observed relaxation.

To support the finding of an enhanced renal NO production in response to carbachol in NO-GC1 KO mice, expression of endothelial NO synthase (eNOS) was quantified by Western blot analysis. As shown in Figure 1F, expression of eNOS was 1.3-fold increased in NO-GC1 KO kidneys substantiating the notion of enhanced NO production in the NO-GC1 KO kidneys. To quantify NO production in the NO-GC1 KO kidneys more directly, NOS activity in renal homogenates was assessed in an enzymatic assay and monitored as NOS-dependent nitrosation of the NO-specific fluorescent probe DAF-FM diacetate [20]. NOS activity was found to be 4-fold higher in the NO-GC1 KO than in WT kidneys (KO 384 ± 116% versus WT 100 ± 20%; Figure S1). Specificity of the signal was controlled by adding the NOS inhibitor L-NAME. The data suggest that NO-GC1 deficiency in the renal vasculature is partially compensated by increased NO generation.
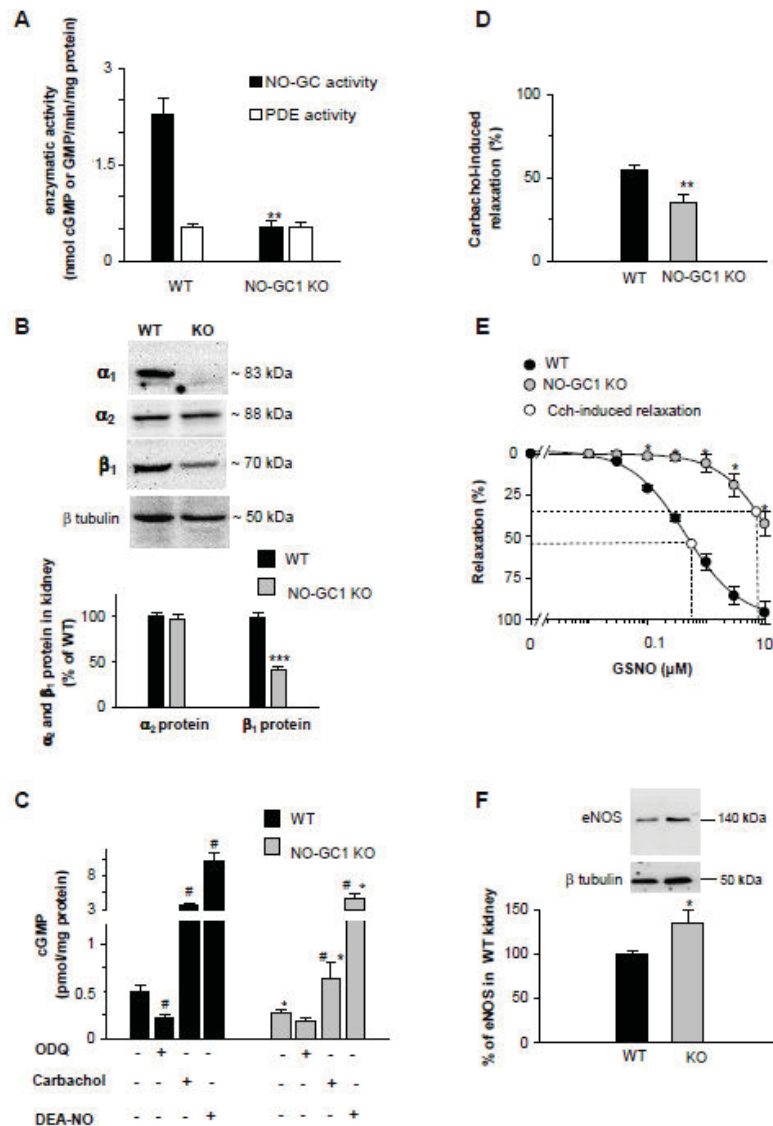
Figure 1. Reduced cGMP response in kidneys of NO-GC1 KO mice. A, NO-stimulated cGMP-forming activity (100 µM DEA-NO) determined in kidney homogenates of WT and NO-GC1 KO mice (n=19 and 6 mice, respectively). PDE activity in WT and KO kidneys measured with 1 µM cGMP as substrate (n=11 and 7 mice, respectively). ** P< 0.01 versus WT, unpaired Student's t test. B, absent of the α1 subunit in NO-GC1 KO kidney homogenates and quantification of the α2 and β1 subunit content with respect to the subunit amount in WT using subunit specific antibodies (n=8 mice per genotype). Representative strips with α1, α2, β1 and the respective β tubulin bands of the same lanes are shown above. *** P< 0.001 versus WT, unpaired Student's t test. C, cyclic GMP content determined in renal cortical slices of WT and KO mice without any addition (n=20 and 10 mice, respectively), or in the presence of ODQ (20 µM, 15 min; n=5 and 4 mice, respectively) or carbachol (30 µM, 3 min; n=10 and 6 mice, respectively) or DEA-NO (100 µM 3 min; n=10 and 7 mice, respectively). # P< 0.01 versus untreated slices in the same group; *P< 0.01 versus WT, unpaired Student's t test. D, carbachol-induced relaxation of NA-contracted isolated perfused kidneys of NO-GC1 KO (n=12) and WT mice (n=21). ** P< 0.01 versus WT, unpaired Student's t test. E, concentration-response curves for GSNO-induced relaxation of NA-contracted isolated perfused kidneys in the presence of L-NAME (n=5 WT and 7 KO mice). The white dots indicate the Cch-induced relaxation plotted on the curves to determine the corresponding GSNO concentration. F, Western blot detection of eNOS in 50 µg kidney homogenates of NO-GC1 KO (n=8) and WT mice (n=5) and quantification with respect to the eNOS amount in WT kidneys. A representative strip with eNOS and the respective β tubulin bands of the same lanes is shown above. * P< 0.05 versus WT, unpaired Student's t test.

Table 1. Effects of 2K1C operation on WT and NO-GC1 KO mice.

| | WT mice | | NO-GC1 KO mice | |
	Sham	2K1C	Sham	2K1C
SBP (mmHg)	116 ± 2	128 ± 2[*]	116 ± 1	128 ± 2[*]
Kidney left (mg/g BW)	7.73 ± 0.29	4.03 ± 0.66[*]	7.50 ± 0.37	3.37 ± 0.59[*]
Kidney right (mg/g BW)	7.66 ± 0.33	8.54 ± 0.38	8.00 ± 0.41	8.81 ± 0.41

Data are means ± SEM (Blood pressure was measured in 10 WT and 11 KO mice; kidney weights were averaged over 18 WT and 11 KO mice per treated group). Body weight and heart weight were not affected by the 2K1C operation (data not shown). BW indicates body weight; * P<0.001 2K1C- vs. sham-operated mice of both groups

doi: 10.1371/journal.pone.0080674.t001

Comparable blood pressures increase in NO-GC1 KO and WT mice in the 2K1C model

To study the NO/cGMP signaling under pathophysiological conditions, we challenged the NO-GC1 KO mice by the 2K1C operation which provokes renovascular hypertension by activation of the renin-angiotensin system.

Four weeks after clipping the left renal artery (2K1C operation) in NO-GC1 KO and WT mice, the clipped kidneys exhibited a similar degree of atrophy, while right kidneys of both groups showed comparable compensatory hypertrophy (Table 1). The similar changes in renal weights observed in both groups indicated that the 2K1C-induced ischemic stress was comparable. Systolic blood pressures (SBP) measured by the tail-cuff method were elevated in 2K1C-operated NO-GC1 KO and WT mice (see Table 1). Interestingly, despite the absence of NO-GC1, blood pressures increases did not differ between KO and WT mice indicating that reduced cGMP levels did not aggravate hypertension in this model.

The 2K1C operation reduces renal vascular relaxation in WT but not in NO-GC1 KO mice

The 2K1C operation has been published to reduce endothelium-dependent relaxation of aortic rings [13–16]. In accordance to these studies, we observed a reduction in endothelium-dependent relaxation of aortic rings in 2K1C-operated WT mice (14% of sham; Figure 2A). This reduction was found to be even more pronounced in the vasculature of the 2K1C WT kidneys (41% of sham; see Figure 2A). In order to differentiate between endothelium- and smooth muscle-dependent relaxations, we also used the NO donor GSNO. Compared to sham-operated WT mice, GSNO shifted the concentration-response curve to higher EC_{50} values in the kidneys of the 2K1C WT (EC_{50} 2K1C 1 ± 0.3 μM versus sham 0.5 ± 0.07 μM; Figure 2B) demonstrating a reduced NO sensitivity rather than a reduced NO generation in kidneys of 2K1C WT mice.

In the NO-GC1 KO mice, the 2K1C operation did neither affect relaxation of aortic rings nor did it alter relaxation of isolated perfused kidneys (Figure 2C, D). NO-GC1 KOs have lower cGMP formation which found to be partially compensated by higher NO levels than in WT. Thus, the lack of difference between sham and 2K1C NO-GC1 KO further supports the notion that the reduced vascular relaxation in 2K1C WT mice depends on cGMP levels and not on the amount of NO.

The 2K1C operation does neither alter cGMP synthesis nor cGMP sensitivity

To assess whether impaired cGMP synthesis accounts for the impaired vasodilator response to GSNO in 2K1C-operated WT mice, NO-stimulated cGMP-forming activities were determined in kidney homogenates. As shown in Figure 3A, NO-stimulated cGMP-forming activities did not differ between 2K1C-operated and control WT mice (2K1C, 2 ± 0.3 versus sham, 1.8 ± 0.3 nmol/mg min). In addition western blot quantification of the $β_1$ subunit which is present equally in the NO-GC1 ($α_1β_1$) and NO-GC2 ($α_2β_1$) heterodimer did not reveal any differences between both groups (Figure 3B). Thus, we conclude that the 2K1C operation did not alter the expression of NO-GCs. Next, sensitivity towards cGMP was studied with the direct PKGI activator, 8-(p-chlorophenylthio)-cGMP (8-pCPT-cGMP). Renal relaxation in 2K1C-operated WT mice induced by the membrane-permeable cGMP analogue did not differ from that in control kidneys demonstrating that sensitivity towards cGMP was unchanged (Figure 3C).

The 2K1C-induced reduction of vascular NO sensitivity is restored by PDE5 inhibition

Subsequently, we asked whether enhanced cGMP degradation accounts for the reduction of NO sensitivity in 2K1C WT mice and used vinpocetine (10 μM) and sildenafil (0.3 μM) to inhibit PDE1 and PDE5, the main cGMP-hydrolyzing enzymes in smooth muscle. The PDE inhibitors were administered in concentrations which alone did not affect vascular reactivity in WT. Under PDE1 inhibiting conditions, the NO response in the non-clipped kidneys of 2K1C WT mice remained significantly reduced (Figure 4A). In contrast, inhibition of PDE5 restored the reduced NO sensitivity in 2K1C WT kidneys as sildenafil shifted the GSNO concentration-response curve to that determined in control kidneys in the presence of sildenafil (Figure 4B). These findings indicate a role of PDE5 in the reduction of vascular relaxation caused by the 2K1C operation.

PDE5 is not up-regulated by the 2K1C operation

To detect a possible PDE5 up-regulation induced by the 2K1C operation, we examined PDE5 mRNA and protein expression by quantitative real-time PCR and Western blot analysis in renal tissues. As shown in Figure 5A, levels of PDE5 mRNA were comparable in isolated preglomerular arterioles of 2K1C- compared to sham-operated mice. In accordance, PDE5 protein levels determined in kidney homogenates did not show any difference (Figure 5B). Together these results argue against an up-regulation of PDE5 as the reason for the reduced vascular relaxation in the 2K1C model.
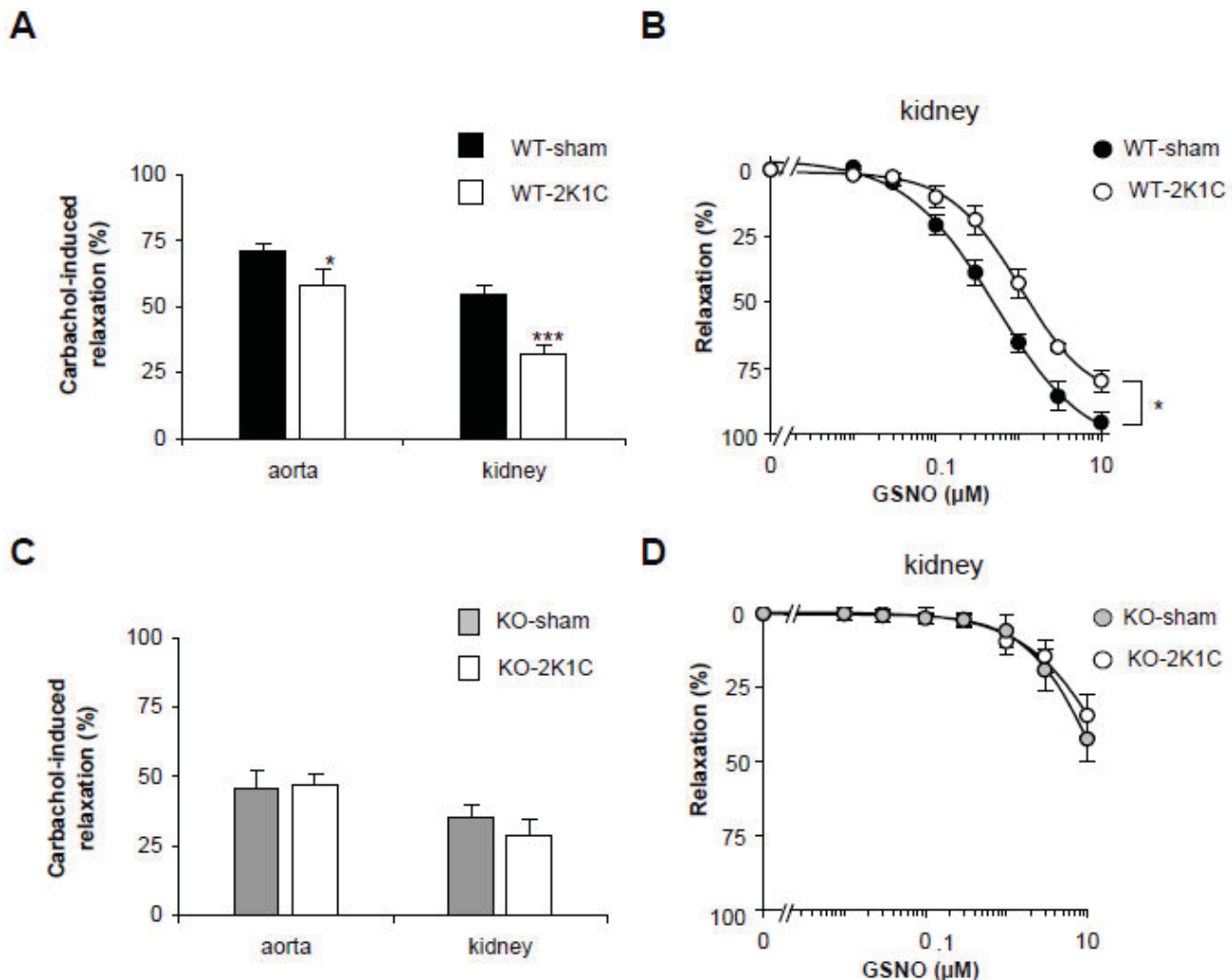
Figure 2. 2K1C operation did not reduce vascular relaxation in NO-GC1 KOs but in WT mice. A, endothelium-dependent relaxation induced by carbachol (30 µM) in NA-contracted aortic rings and isolated perfused kidneys of sham- and 2K1C-operated WT mice (36 aortic rings of n=9 mice per group; kidneys of n=21 and 8 mice, respectively). * P< 0.05 versus aorta of WT-sham, paired 2-tailed Student's t test; ** P<0.001 versus kidney of WT-sham, unpaired 2-tailed Student's t test. **B**, concentration-response curves for GSNO-induced relaxation determined in NA-contracted isolated perfused kidneys of sham- and 2K1C-operated WT mice in the presence of L-NAME (n=5 and 7 mice, respectively). P=0.037, ANOVA for repeated measurements. **C**, endothelium-dependent relaxation induced by carbachol (30 µM) in NA-contracted aortic rings and isolated perfused kidneys of sham- and 2K1C-operated NO-GC1 KO mice (28 aortic rings of n=7 mice per group; kidneys n=12 and 7 mice, respectively). **D**, concentration-response curves for GSNO-induced relaxation determined in NA-contracted isolated perfused kidneys of sham- and 2K1C-operated NO-GC1 KO mice in the presence of L-NAME (n=8 and 6 mice, respectively). Experiments were performed using the non-clipped kidney of 2K1C mice and the respective kidney of sham mice.
doi: 10.1371/journal.pone.0080674.g002

Greater effect of sildenafil in 2K1C WT mice points to an activated PDE5 state

PDE5 is known to exist in two different states, a non-activated and an activated state with an increased catalytic rate due to allosteric binding of cGMP to PDE5's GAF domains. To directly address activated PDE5 in 2K1C WT mice, we determined PDE activity which should be enhanced in the case of PDE5 activation. PDE activity was measured as cGMP

hydrolysis in the presence and absence of sildenafil (100 nM) in kidneys and preglomerular arterioles of sham- and 2K1C-operated WT mice. Hence, we did not detect enhanced PDE5 or total PDE activity in kidneys or preglomerular arterioles of 2K1C-operated WT mice (Figure 5C and 5D). However, measurements revealed that PDE5 represents only a fractional amount of total PDEs (20% using 1 µM cGMP or 40% with 30 nM cGMP as substrate) and that PDE activity varies ~30%
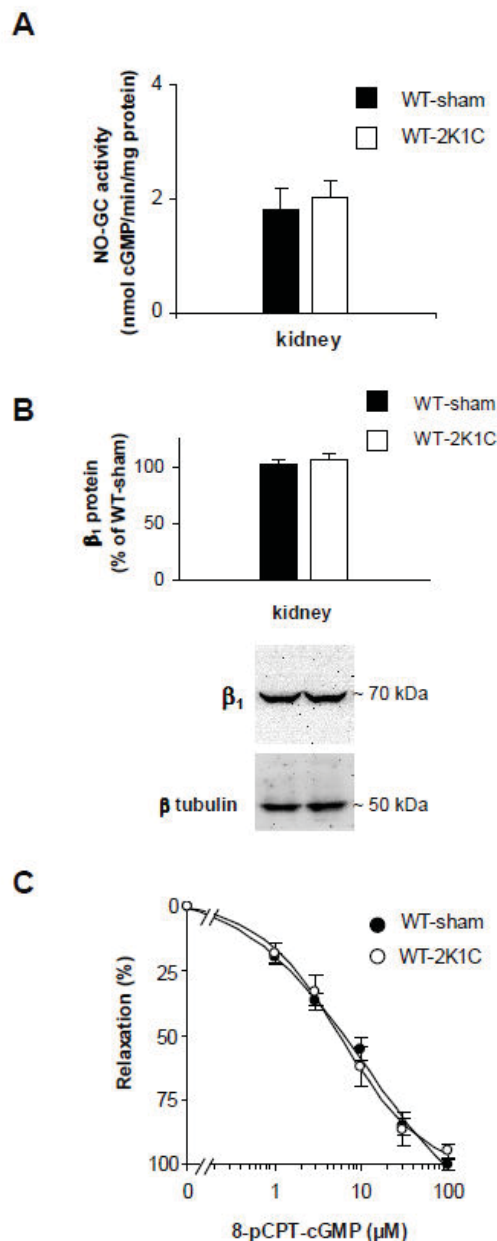
Figure 3. 2K1C operation does not alter cGMP synthesis or cGMP sensitivity in WT kidneys. **A**, NO-stimulated cGMP-forming activity (DEA-NO 100 µM) determined in kidney homogenates of sham- and 2K1C-operated WT mice (n=6 mice per group). **B**, quantification of the β_1 subunit content with respect to the subunit amount in sham-operated WT mice using subunit specific antibodies (n=12 mice per group). **C**, concentration-response curves for 8-pCPT-cGMP of NA-contracted isolated perfused kidneys of sham- and 2K1C-operated WT mice in the presence of L-NAME (n=13 and 7 mice, respectively). Experiments were performed using the non-clipped kidney of 2K1C mice and the respective kidney of sham mice.
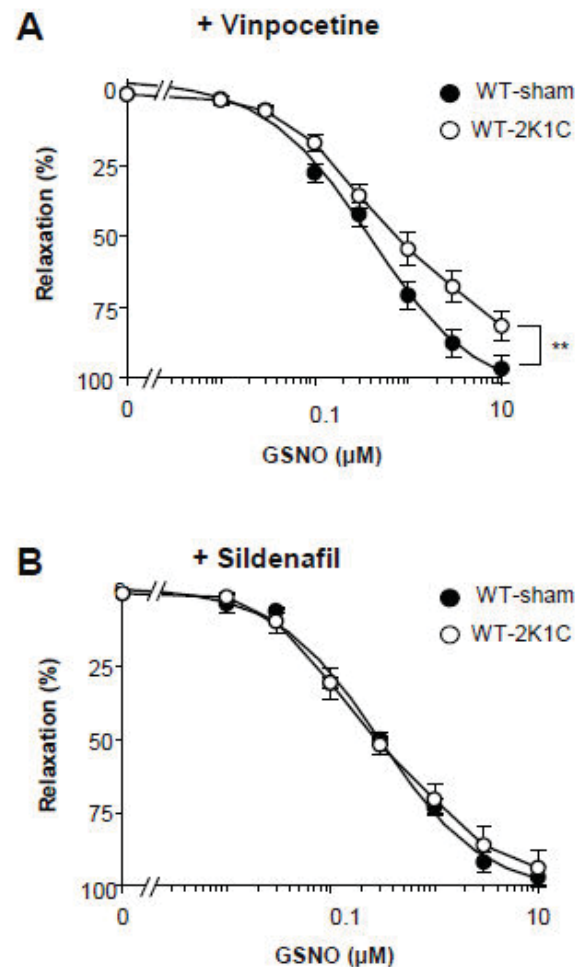
Figure 4. PDE5 inhibitor, sildenafil, restores reduced NO sensitivity of renal vessels from operated WT. Concentration-response curves for GSNO-induced relaxation determined in NA-contracted isolated perfused kidneys of sham- and 2K1C-operated WT mice in the presence of (**A**) the PDE1 inhibitor vinpocetine (10 µM; n=6 and 5 mice, respectively) or (**B**) the PDE5 inhibitor sildenafil (300 nM; n=5 mice per group). ****P< 0.01**, ANOVA for repeated measurements. Experiments were performed using the non-clipped kidney of 2K1C mice and the respective kidney of sham mice.

among mice. Thus, PDE5 activation may not be detectable in tissues with various PDE isoforms like the kidney.

In an attempt to demonstrate the impact of putative higher PDE5 activity in the 2K1C WT mice *in vivo*, we treated 2K1C- and sham-operated WT and KO mice with sildenafil (100 mg/kg d for 1 week, three weeks after the 2K1C operation) and subsequently, monitored blood pressures in conscious mice by tail-cuff. As shown in Figure 6, sildenafil reduced blood pressures more efficiently in 2K1C-operated WT compared to
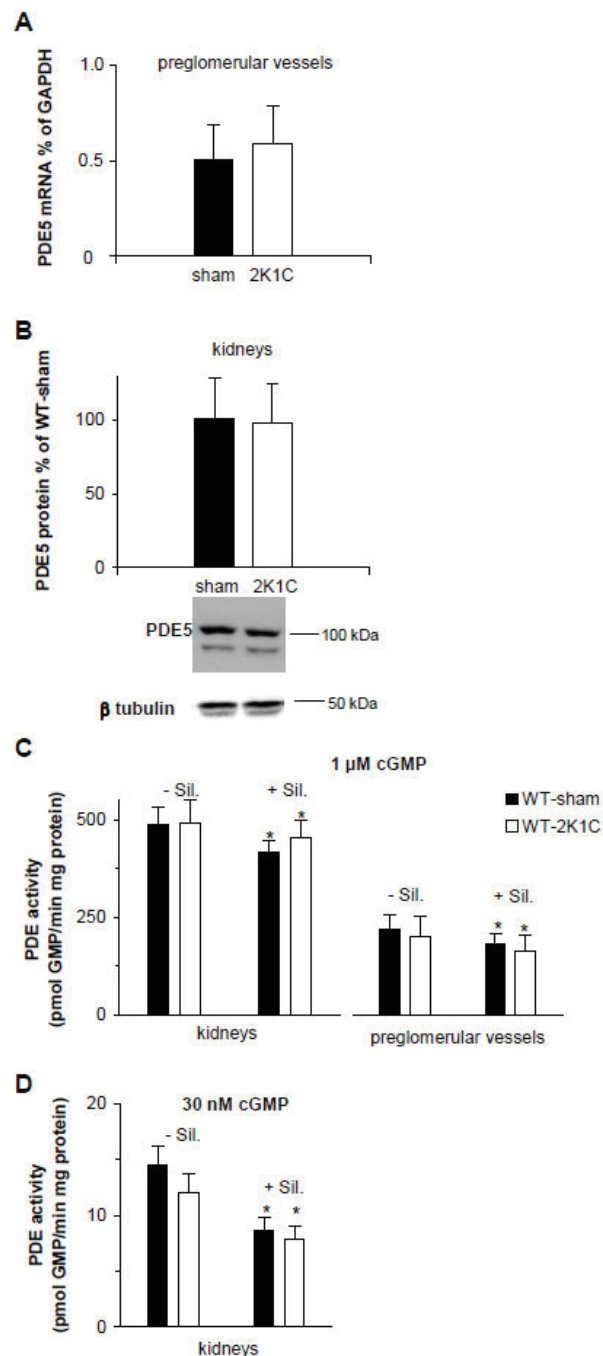
Figure 5. 2K1C operation did not up-regulate PDE5. A, PDE5 mRNA in preglomerular vessels of sham- and 2K1C-operated WT mice detected by quantitative real-time PCR and quantified relative to GAPDH with the ΔC_T method (n=8 and 9 mice, respectively). **B**, PDE5 protein detected by Western blot in 50 μg kidney homogenates of sham- and 2K1C-operated WT mice and expressed as % of PDE5 content in kidneys of sham-WT mice (n=7 mice per group). A representative strip with PDE5 and the respective β tubulin bands of the same lanes is shown below. PDE activities in homogenates of kidneys and preglomerular vessels of sham- and 2K1C-operated WT mice in the absence and presence of sildenafil (100 nM) measured by 1 μM (**C**) or 30 nM cGMP (**D**). PDE activities were obtained of 3 mice per group in kidneys by 1 μM cGMP; n=13 and 10 mice per group, preglomerular vessels; n=6 per group kidneys by 30 nM. * P< 0.001 versus corresponding PDE activity without sildenafil, paired 2-tailed Student's t test. Experiments were performed using the non-clipped kidney of 2K1C mice and the respective kidney of sham mice.
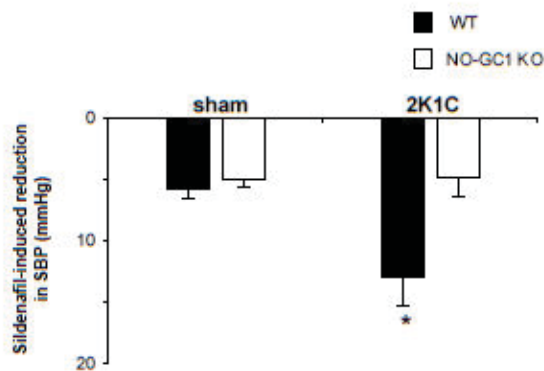
doi: 10.1371/journal.pone.0080674.g005

Figure 6. Sildenafil effects on blood pressures. Sildenafil (100 mg/kg d) effects on systolic blood pressures measured in conscious sham- and 2K1C-operated WT (WT-sham 118 ± 1 mmHg without, and 112 ± 1 mmHg with sildenafil; WT-2K1C 130 ± 4 mmHg without, and 118 ± 2 mmHg with sildenafil) and NO-GC1 KO mice (KO-sham 118 ± 1 mmHg without, and 113 ± 2 mmHg with sildenafil; KO-2K1C 125 ± 2 mmHg without, and 121 ± 2 mmHg with sildenafil) using tail-cuff manometer (n=4 WT-sham, 5 WT-2K1C, 6 KO-sham, and 10 KO-2K1C mice). Sildenafil administration and SBP measurements were performed during the 4th week after operation. *P< 0.05 2K1C WT compared to sham WT, unpaired Student's t test. SBP indicates systolic blood pressure.

doi: 10.1371/journal.pone.0080674.g006

sham WT mice (2K1C WT 13 ± 2 mmHg versus sham WT 6 ± 1 mmHg; p= 0.026) indicating a higher impact for sildenafil inhibition in the 2K1C model. In the NO-GC1 KOs, the sildenafil effect on blood pressure was comparable in operated and non-operated mice (2K1C KO 5 ± 2 mmHg versus sham KO 5 ± 1 mmHg) indicating that the cGMP-dependent activation of PDE5 does not occur in the NO-GC1 KO.

Enhanced eNOS-catalyzed NO formation induced by the 2K1C operation

An activated state of PDE5 implies enhanced NO/cGMP formation in the 2K1C model. Thus, we used Western-blot analysis to determine the eNOS content in the 2K1C WT kidneys. While eNOS expression was unaltered, increased phosphorylation of eNOS on Ser-1177, a marker for increased eNOS activity was detected (Figure 7A). Phosphorylation of eNOS depends on shear stress which is provoked by vasoconstriction. In accordance, we found an increased contractile response towards Angiotensin II in 2K1C WT mice explaining the enhanced eNOS activation (Figure 7B).

To confirm our assumption of an increased biologically active NO in 2K1C WT mice, we measured cGMP levels in renal cortical slices of sham- and 2K1C-operated WT mice (Figure 7C). Indeed, basal levels of cGMP were found to be 2.7-fold higher in kidneys of 2K1C WT mice than in the control group (2K1C, 0.84 ± 0.08 versus sham, 0.31 ± 0.06 pmol cGMP/mg protein; p< 0.001). Furthermore, cGMP accumulation in the
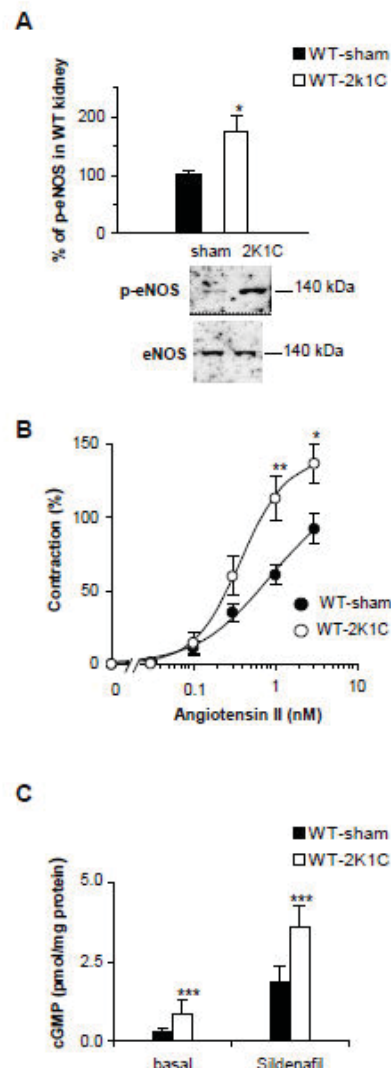

Figure 7. Evidence of enhanced eNOS-catalyzed NO formation induced by the 2K1C operation. A, Western blot detection of p-eNOS (serine 1177) and eNOS in 50 µg kidney homogenates of sham- and 2K1C-operated WT mice and quantification with respect to the ratio of p-eNOS to eNOS in kidneys of sham-operated WT (n=8 and 7 mice, respectively). * P< 0.05 versus WT-sham, unpaired Student's t test. **B**, concentration-response curves for angiotensin II-induced vasoconstriction of isolated perfused kidneys of sham- and 2K1C-operated WT mice in the presence of L-NAME (n=9 and 6 mice, respectively). * P< 0.05, and ** P< 0.01 versus WT-sham, unpaired Student's t test. **C**, cyclic GMP content determined in renal cortical slices of sham- and 2K1C-operated WT mice without any addition (15 slices of 5 mice per group) or in the presence of sildenafil (100 µM, 10 min; 15 slices of 5 mice per group). ***P< 0.001 versus WT-sham, unpaired Student's t test. Experiments were performed using the non-clipped kidney of 2K1C mice and the respective kidney of sham mice.

doi: 10.1371/journal.pone.0080674.g007

presence of sildenafil (100 µM, 10 min) was higher in kidneys of 2K1C WT mice. In sum, our results indicate enhanced eNOS-catalyzed NO formation in 2K1C WT mice and support our hypothesis that enhanced NO/cGMP causing PDE5 activation finally results in a decrease of NO sensitivity.

Discussion

The NO/cGMP signaling has an established role in vascular relaxation and regulation of blood pressure. Genetic or pharmacological inhibition of the cascade decreases relaxation and increases blood pressure [23,24]. In the vasculature, two different forms of the cGMP forming NO-GCs, NO-GC1 and NO-GC2, exist which correspond to the earlier described $\alpha_1\beta_1$ and $\alpha_2\beta_1$ heterodimer, respectively. We previously reported that deletion of the NO-GC1 resulted in 90% reduction of the total NO-GC content in aortic tissues, and an attenuated endothelium- und smooth muscle-dependent relaxation.

Here we describe that in kidneys of NO-GC1 KO mice, NO-stimulated cGMP formation is also markedly reduced (80% of WT) with the amount of the remaining NO-GC2 being higher in kidney (0.5 ± 0.1 nmol cGMP/mg min) than in aorta (0.2 ± 0.1 nmol cGMP/mg min). A particular role for NO-GC2 in the renal vasculature is supported by the ability of NO to increase cGMP levels in the NO-GC1 KO renal cortical slices while in aorta NO stimulation did not yield measurable cGMP increases. On the other hand it should be kept in mind that the PDE isoforms expressed in a certain tissue have a great impact on the cGMP response.

Relaxation of renal vasculature was determined in isolated perfused kidneys, a model for examining the function of resistance arteries. In accordance with the reduced cGMP formation, relaxation was attenuated in NO-GC1 KO mice. The residual NO/cGMP effects are mediated by NO-GC2 demonstrating that cGMP produced by this isoform regulates physiological processes. Hence, analysis of the carbachol- and GSNO-induced relaxation revealed an increase in NO production in responses to carbachol in the NO-GC1 KO. In line with this observation, up-regulation of eNOS expression was found in Western blot analysis. Thus; we conclude that enhanced NO formation supports NO-GC2-catalyzed cGMP formation in the NO-GC1 KO mice to ensure an adequate renal perfusion.

Despite the reduction of the cGMP-forming enzyme, the NO-GC1 KO mice are not hypertensive. To provoke hypertension, we challenged NO-GC1 KO mice with the 2K1C operation, which activates the renin-angiotensin-aldosterone system (RAAS). The 2K1C operation increased blood pressures to a similar extend in NO-GC1 KO and WT mice showing that the degree of hypertension in the 2K1C model is not influenced by the level of NO/cGMP. This is surprising at first, but in line with the finding that the 80-90% reduction of the cGMP forming enzyme in the NO-GC1 KO does not affects blood pressure (on the C57Bl/6 background) whereas additional deletion of the remaining enzyme (NO-GC2) results in pronounced hypertension [24]. The results indicate that only minor amounts of cGMP (as supplied by the NO-GC2) are sufficient to prevent blood pressure increases. Hypertension of the NO-GC1 KO

mice described by Buys and colleagues was found to be strain-specific and dependent on higher activity of the RAAS in the 129S6 background [7].

The 2K1C operation has been reported to reduce endothelium-dependent relaxation of aortic rings [13–16]. Accordingly, 2K1C-operated WT mice showed a reduction of carbachol-induced relaxation which was more pronounced in kidneys than in aortas. In contrast, carbachol-induced relaxation was not reduced in the 2K1C-operated NO-GC1 KO mice. Kidneys of operated WT mice also exhibited a reduced sensitivity to exogenous NO, thus, the attenuated responsiveness towards NO most likely accounts for the reduction of endothelium-dependent relaxation. This result is in conflict with reports by others who propose endothelial dysfunction i.e. decreased NO bioavailability as the major reason for the reduction of endothelium-dependent relaxation in renovascular hypertension [13–16]. On the other hand, the discrepancy may be explained by different vessels used: whereas in our study renal resistance arteries responsible for blood pressure regulation were analyzed, large conductance vessels were studied by the colleagues.

In search for the reason of the reduced NO sensitivity in 2K1C-operated WT mice NO-stimulated GC activity was measured in kidney homogenates. Similar rates of cGMP synthesis in control and 2K1C-operated mice ruled out differences in NO-GC expression. Also relaxation induced by the cGMP analogue 8-pCPT-cGMP was unaltered in the 2K1C-operated WT mice and we conclude that sensitivity or activity of the cGMP-dependent protein kinases is unchanged.

Next, we addressed a possible increase of cGMP degradation in vascular smooth muscle by analyzing NO-induced relaxation in the presence of PDE1 or PDE5 inhibitors. As PDE1 is stimulated by Ca^{2+}, the enzyme was a tempting candidate to mediate an AngII-induced decrease of relaxation [25,26]. However, inhibition of PDE1 did not improve sensitivity to exogenous NO. Unexpectedly, PDE5 inhibition restored the reduced NO sensitivity observed in 2K1C WT pointing to PDE5 as the responsible component for the reduction of vascular relaxation in renovascular hypertension. The mechanism through which PDE5 is affected in renovascular hypertension is not clear. Although, it has been reported that Ang II upregulates PDE5 in VSMCs [27], we did not detect any changes in PDE5 protein or mRNA levels in kidneys from 2K1C WT mice.

Within NO/cGMP signaling, a negative feedback regulation depending on PDE5 activation has been reported [10,12]. In this context, cGMP does not only bind to the catalytic center but also binds to PDE5's regulatory GAF-A domains thereby enhancing catalytic rate [10,11]. Thus, increased NO/cGMP signaling finally leads to its desensitization. However, the detection of an activated cGMP-bound PDE5 state ex vivo is difficult as the cGMP used as substrate in PDE activity measurements will also shift non-activated PDE5 to the activated state. The fact, that the 2K1C-operation did not reduce vascular relaxation in the NO-GC1 KO mice, indicates that here NO/cGMP signaling is too low to initiate internal feedback regulation.

In order to confirm the impact of activated PDE5 in renovascular hypertension we used an in vivo approach, where we treated mice with sildenafil. As expected for an activated PDE5, sildenafil reduced blood pressure more efficiently in 2K1C- than in sham-operated WT mice. In line, the sildenafil effect on blood pressure was not increased by the operation in the NO-GC1 KOs. PDE5 activation requires enhanced NO/cGMP signaling. In support of this notion, increased renal contractility, eNOS phosphorylation at serine1177 and cGMP levels were found in the operated WT mice. Increased NO production in the 2K1C model has also been postulated by others [28–30].

Our results support the following scenario: renovascular hypertension induced by the 2K1C operation enhances NO/cGMP signaling in the kidney finally resulting in long-lasting PDE5 activation which in turn is responsible for the reduced NO/cGMP-mediated relaxation. In line, reduction in vascular relaxation does not occur in NO-GC1-deficient mice as cGMP forming activity is lower and long-lasting PDE5 activation does not happen.

According to our concept, low doses of PDE5 inhibitors reported to preferentially inhibit the cGMP-bound, activated state of the enzyme, appear to be indicated as a possible rational pharmacological intervention in the treatment of renovascular hypertension.

Supporting Information

Figure S1. Enhanced NOS activity in kidneys of NO-GC1 KO mice. NOS activity in kidney homogenates of WT and NO-GC1 KO mice determined as NOS-dependent nitrosation of the NO-specific fluorescent probe DAF-FM diacetate (n=5 and 4 mice, respectively). * P< 0.05 versus WT, unpaired Student's t test.
(TIF)

Acknowledgements

Author Contributions

Conceived and designed the experiments: JS EM LCR. Performed the experiments: JS EM SF SAP KB MCK. Analyzed the data: JS EM SF. Contributed reagents/materials/analysis tools: MCK IQ. Wrote the manuscript: JS EM DK.

References

1. Waldman SA, Murad F (1987) Cyclic GMP synthesis and function. Pharmacol Rev 39: 163-196. PubMed: 2827195.
2. Moncada S, Higgs EA (1995) Molecular mechanisms and therapeutic strategies related to nitric oxide. FASEB J 9: 1319-1330. PubMed: 7557022.
3. Ignarro LJ (2002) Nitric oxide as a unique signaling molecule in the vascular system: a historical overview. J Physiol Pharmacol 53: 503-514. PubMed: 12512688.
4. Friebe A, Koesling D (2003) Regulation of nitric oxide-sensitive guanylyl cyclase. Circ Res 93: 96-105. doi:10.1161/01.RES.0000082524.34487.31. PubMed: 12881475.
5. Russwurm M, Koesling D (2002) Isoforms of NO-sensitive guanylyl cyclase. Mol Cell Biochem 230: 159-164. doi:10.1023/A:1014252309493. PubMed: 11952091.
6. Mergia E, Friebe A, Dangel O, Russwurm M, Koesling D (2006) Spare guanylyl cyclase NO receptors ensure high NO sensitivity in the vascular system. J Clin Invest 116: 1731-1737. doi:10.1172/JCI27657. PubMed: 16614755.
7. Buys ES, Raher MJ, Kirby A, Shahid M, Baron DM et al. (2012) Genetic modifiers of hypertension in soluble guanylate cyclase α1-deficient mice. J Clin Invest 122: 2316-2325. doi:10.1172/JCI60119. PubMed: 22565307.
8. Feil R, Lohmann SM, de Jonge H, Walter U, Hofmann F (2003) Cyclic GMP-dependent protein kinases and the cardiovascular system: insights from genetically modified mice. Circ Res 93: 907-916. doi:10.1161/01.RES.0000100390.68771.CC. PubMed: 14615494.
9. Rybalkin SD, Yan C, Bornfeldt KE, Beavo JA (2003) Cyclic GMP phosphodiesterases and regulation of smooth muscle function. Circ Res 93: 280-291. doi:10.1161/01.RES.0000087541.15600.2B. PubMed: 12933699.
10. Rybalkin SD, Rybalkina IG, Shimizu-Albergine M, Tang XB, Beavo JA (2003) PDE5 is converted to an activated state upon cGMP binding to the GAF A domain. EMBO J 22: 469-478. doi:10.1093/emboj/cdg051. PubMed: 12554648.
11. Mullershausen F, Friebe A, Feil R, Thompson WJ, Hofmann F et al. (2003) Direct activation of PDE5 by cGMP: long-term effects within NO/cGMP signaling. J Cell Biol 160: 719-727. doi:10.1083/jcb.200211041. PubMed: 12604588.
12. Mullershausen F, Russwurm M, Koesling D, Friebe A (2004) In vivo reconstitution of the negative feedback in nitric oxide/cGMP signaling:

13. role of phosphodiesterase type 5 phosphorylation. Mol Biol Cell 15: 4023-4030. doi:10.1091/mbc.E03-12-0890. PubMed: 15240816.
13. Arruda RM, Peotta VA, Meyrelles SS, Vasquez EC (2005) Evaluation of vascular function in apolipoprotein E knockout mice with angiotensin-dependent renovascular hypertension. Hypertension 46: 932-936. doi:10.1161/01.HYP.0000182154.61862.52. PubMed: 16087779.
14. Jung O, Marklund SL, Geiger H, Pedrazzini T, Busse R et al. (2003) Extracellular superoxide dismutase is a major determinant of nitric oxide bioavailability: in vivo and ex vivo evidence from ecSOD-deficient mice. Circ Res 93: 622-629. doi:10.1161/01.RES.0000092140.81594.A8. PubMed: 12933702.
15. Jung O, Schreiber JG, Geiger H, Pedrazzini T, Busse R et al. (2004) gp91phox-containing NADPH oxidase mediates endothelial dysfunction in renovascular hypertension. Circulation 109: 1795-1801. doi:10.1161/01.CIR.0000124223.00113.A4. PubMed: 15037533.
16. Heitzer T, Wenzel U, Hink U, Krollner D, Skatchkov M et al. (1999) Increased NAD(P)H oxidase-mediated superoxide production in renovascular hypertension: evidence for an involvement of protein kinase C. Kidney Int 55: 252-260. doi:10.1046/j.1523-1755.1999.00229.x. PubMed: 9893134.
17. Wiesel P, Mazzolai L, Nussberger J, Pedrazzini T (1997) Two-kidney, one clip and one-kidney, one clip hypertension in mice. Hypertension 29: 1025-1030. doi:10.1161/01.HYP.29.4.1025. PubMed: 9095094.
18. Stegbauer J, Vonend O, Habbel S, Quack I, Sellin L et al. (2005) Angiotensin II modulates renal sympathetic neurotransmission through nitric oxide in AT2 receptor knockout mice. J Hypertens 23: 1691-1698. doi:10.1097/01.hjh.0000179763.02583.8e. PubMed: 16093914.
19. Mergia E, Russwurm M, Zoidl G, Koesling D (2003) Major occurrence of the new α2β1 isoform of NO-sensitive guanylyl cyclase in brain. Cell Signal 15: 189-195. doi:10.1016/S0898-6568(02)00078-5. PubMed: 12464390.
20. Cortese-Krott MM, Rodriguez-Mateos A, Kuhnle GG, Brown G, Feelisch M et al. (2012) A multilevel analytical approach for detection and visualization of intracellular NO production and nitrosation events using diaminofluoresceins. Free Radic Biol Med 53: 2146-2158. doi:10.1016/j.freeradbiomed.2012.09.008. PubMed: 23026413.
21. Chaudhari A, Kirschenbaum MA (1988) A rapid method for isolating rabbit renal microvessels. Am J Physiol 254: F291-F296. PubMed: 3125749.
22. Takimoto E, Champion HC, Li M, Belardi D, Ren S et al. (2005) Chronic inhibition of cyclic GMP phosphodiesterase 5A prevents and reverses

cardiac hypertrophy. Nat Med 11: 214-222. doi:10.1038/nm1175. PubMed: 15665834.

23. Huang PL, Huang Z, Mashimo H, Bloch KD, Moskowitz MA et al. (1995) Hypertension in mice lacking the gene for endothelial nitric oxide synthase. Nature 377: 239-242. doi:10.1038/377239a0. PubMed: 7545787.

24. Friebe A, Mergia E, Dangel O, Lange A, Koesling D (2007) Fatal gastrointestinal obstruction and hypertension in mice lacking nitric oxide-sensitive guanylyl cyclase. Proc Natl Acad Sci U S A 104: 7699-7704. doi:10.1073/pnas.0609778104. PubMed: 17452643.

25. Kim D, Rybalkin SD, Pi X, Wang Y, Zhang C et al. (2001) Upregulation of phosphodiesterase 1A1 expression is associated with the development of nitrate tolerance. Circulation 104: 2338-2343. doi:10.1161/hc4401.098432. PubMed: 11696475.

26. Giachini FR, Lima VV, Carneiro FS, Tostes RC, Webb RC (2011) Decreased cGMP level contributes to increased contraction in arteries from hypertensive rats: role of phosphodiesterase 1. Hypertension 57:

655-663. doi:10.1161/HYPERTENSIONAHA.110.164327. PubMed: 21282562.

27. Kim D, Aizawa T, Wei H, Pi X, Rybalkin SD et al. (2005) Angiotensin II increases phosphodiesterase 5A expression in vascular smooth muscle cells: a mechanism by which angiotensin II antagonizes cGMP signaling. J Mol Cell Cardiol 38: 175-184. doi:10.1016/j.yjmcc.2004.10.013. PubMed: 15623434.

28. Sigmon DH, Beierwaltes WH (1998) Influence of nitric oxide in the chronic phase of two-kidney, one clip renovascular hypertension. Hypertension 31: 649-656. doi:10.1161/01.HYP.31.2.649. PubMed: 9461236.

29. Turkstra E, Braam B, Koomans HA (2000) Impaired renal blood flow autoregulation in two-kidney, one-clip hypertensive rats is caused by enhanced activity of nitric oxide. J Am Soc Nephrol 11: 847-855. PubMed: 10770962.

30. Hiyoshi H, Yayama K, Takano M, Okamoto H (2005) Angiotensin type 2 receptor-mediated phosphorylation of eNOS in the aortas of mice with 2-kidney, 1-clip hypertension. Hypertension 45: 967-973. doi:10.1161/01.HYP.0000164571.77710.19. PubMed: 15837834.

SCIENTIFIC REP⚙RTS

OPEN

Angiotensin II increases glomerular permeability by β-arrestin mediated nephrin endocytosis

Eva Königshausen, Ulf M. Zierhut, Martin Ruetze, Sebastian A. Potthoff, Johannes Stegbauer, Magdalena Woznowski, Ivo Quack, Lars C. Rump & Lorenz Sellin

Glomerular permeability and subsequent albuminuria are early clinical markers for glomerular injury in hypertensive nephropathy. Albuminuria predicts mortality and cardiovascular morbidity. AT1 receptor blockers protect from albuminuria, cardiovascular morbidity and mortality. A blood pressure independent, molecular mechanism for angiotensin II (Ang II) dependent albuminuria has long been postulated. Albuminuria results from a defective glomerular filter. Nephrin is a major structural component of the glomerular slit diaphragm and its endocytosis is mediated by β-arrestin2. Ang II stimulation increases nephrin-β-arrestin2 binding, nephrin endocytosis and glomerular permeability in mice. This Ang II effect is mediated by AT1-receptors. AT1-receptor mutants identified G-protein signaling to be essential for this Ang II effect. Gαq knockdown and phospholipase C inhibition block Ang II mediated enhanced nephrin endocytosis. Nephrin Y1217 is the critical residue controlling nephrin binding to β-arrestin under Ang II stimulation. Nephrin Y1217 also mediates cytoskeletal anchoring to actin via nck2. Ang II stimulation decreases nephrin nck2 binding. We conclude that Ang II weakens the structural integrity of the slit diaphragm by increased nephrin endocytosis and decreased nephrin binding to nck2, which leads to increased glomerular permeability. This novel molecular mechanism of Ang II supports the use of AT1-receptor blockers to prevent albuminuria even in normotensives.

Albuminuria is a strong and independent predictor of cardiovascular mortality in the general population[1,2]. In patients with non-diabetic and diabetic kidney disease albuminuria is not only associated with cardiovascular mortality but also with progression to end-stage renal disease[3]. Inhibition of the renin angiotensin system (RAS) with angiotensin converting enzyme (ACE)-inhibitors or angiotensin-receptor blockers (ARB) effectively reduces and delays albuminuria[4–6]. Studies revealed that the anti-albuminuric effect of ACE-inhibitors and ARBs exceeded the benefit of blood pressure control alone[4,7–10]. ACE-inhibitors were shown to have the strongest anti-albuminuric effect under comparable blood pressure control when compared to calcium antagonists, diuretics and beta-blockers[10]. Therefore blood-pressure independent mechanisms for ACE-inhibitors and ARBs have been postulated to explain the renoprotective effects[5,11].

Angiotensin II (Ang II) infusion in a non-blood pressure effective dose induces a significant transient increase in glomerular permeability[12]. The increased transient glomerular permeability under Ang II infusion without a significant rise of systemic blood pressure points to a blood pressure independent effect on the glomerular filtration barrier[13,14].

The glomerular filtration barrier is composed of the three layers: the fenestrated endothelium, the glomerular basement membrane and the glomerular slit diaphragm formed in between the secondary podocyte foot processes. An essential component of the glomerular slit diaphragm is nephrin which is subjected to endocytosis by binding to β-arrestin2[15]. We and others have shown that endocytosis is crucial to podocyte integrity in development, health and disease[16,17].

Previous studies have investigated the influence of Ang II on aspects of podocyte biology. Macconi *et al.* showed that Ang II stimulation in podocyte cell culture leads to an increased albumin permeability across podocyte monolayers and an Ang II mediated reorganization of the actin cytoskeleton[18]. Hsu *et al.* demonstrated the role of the activated Rac-1 on the remodeling of the F-actin cytoskeleton under Ang II stimulation of podocytes with stable AT1-receptor expression[19]. Greka and Mundel summarized their work on the influence of Ang II on the cytoarchitecture of the podocyte[20], Yu *et al.* observed a significantly reduced nephrin phosphorylation *in vitro*

Nephrology, Medical School Duesseldorf, Heinrich Heine University, Moorenstr. 5, 40225 Duesseldorf, Germany. Correspondence and requests for materials should be addressed to L.S. (email: lorenz.sellin@med.uni-duesseldorf.de)
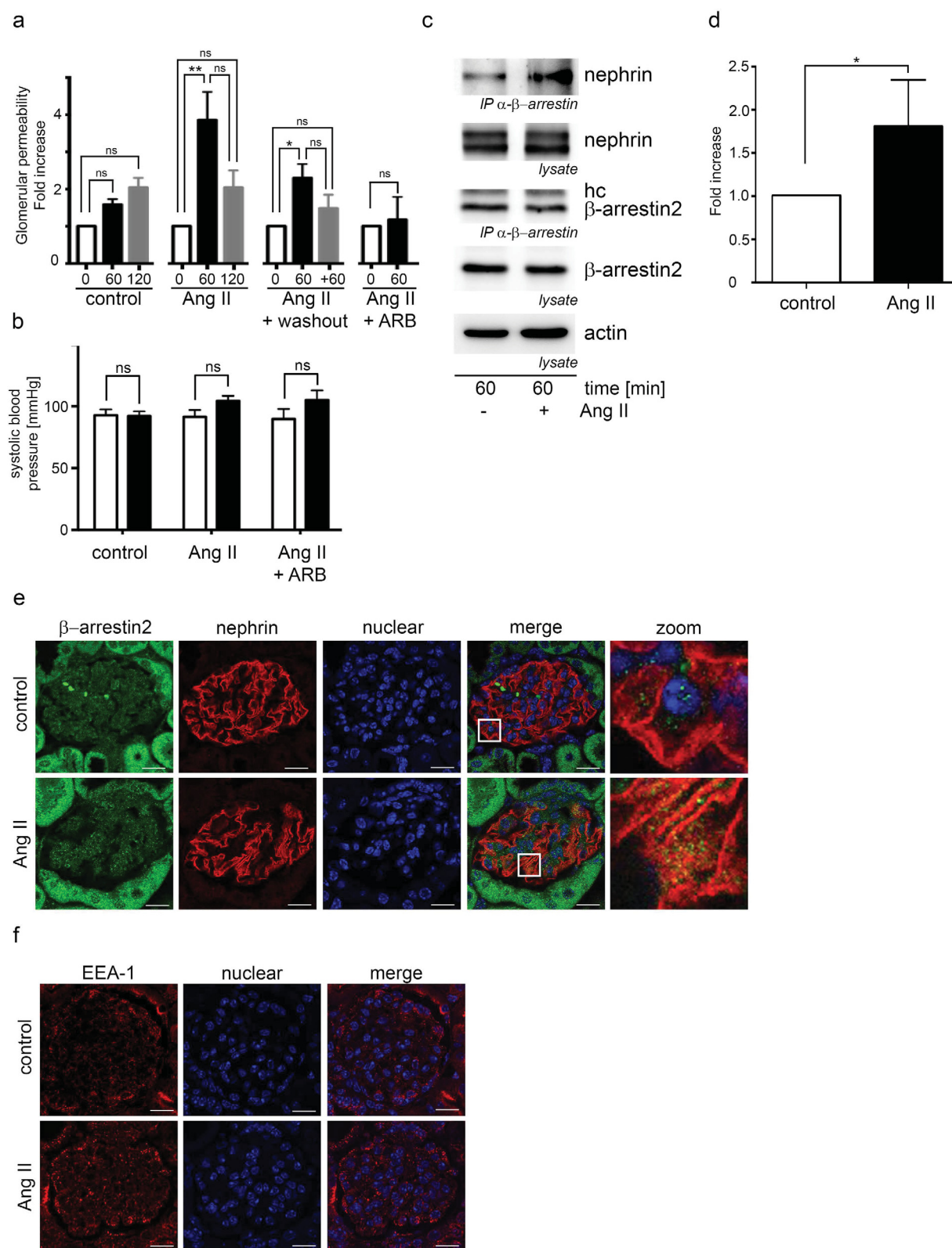
Figure 1. Ang II increases the glomerular permeability and enhances the interaction of β-arrestin to nephrin. (**a**) Ang II increases the glomerular permeability significantly in FVB mice (n = 5 per data point, p < 0.004 tested by Kruskal-Wallis test). The glomerular permeability was measured by FITC-Ficoll 70 appearance in the urine before (white columns, 0 min), 60 minutes after the begin of Ang II stimulation (black columns, 60 min) and after additional 60 minutes of Ang II stimulation or 60 minutes of Ang II discontinuation washout (grey columns, 120 min or +60 min). The measured FITC-Ficoll 70 concentrations in the urine were referenced to the urine creatinine concentration. Pretreatment with candesartan blocks the Ang II mediated increased glomerular permeability (control n = 9, 0 min vs 60 min p = 0.35, 60 min vs 120 min p = 0.87; Ang II

n = 9, 0 min vs 60 min p = 0.0036, 60 min vs 120 min p = 0.18, 0 min vs 120 min p = 0.16; Ang II + washout
n = 5, 0 min vs 60 min p = 0.038, 60 min vs 120 min p = 0.25, 0 min vs 120 min p = 0.58; Ang II + ARB n = 3,
0 min vs 60 min p = 0.99). (**b**) Systolic blood pressure was controlled by tail cuff measurement. No significant
systolic blood pressure differences between the Ang II treated mice and the controls were found. (**c**) Mouse
glomeruli were isolated from kidneys and stimulated with Ang II. Thereafter β-arrestin was immunoprecipitated
from glomerular lysates and nephrin was shown to coimmunoprecipitate with β-arrestin. Ang II enhances the
interaction of β-arrestin to nephrin significantly (n = 4, p = 0.03). Comparable protein amounts for β-arrestin,
nephrin and actin were ensured by Western blotting. (hc – IgG heavy chain). (**d**) Densitometry of the by
β-arrestin2 coimmunoprecitated nephrin. (**e**) Kidneys from mice treated with Ang II were stained for nephrin
and β-arrestin2. The merged images from Ang II treated animals showed a pronounced colocalization of
nephrin with β-arrestin2 after Ang II stimulation in comparison to the control. The scale bar represents 20 μm.
(**f**) Kidneys from mice treated with Ang II were stained for EEA-1. Under Ang II stimulation an enhanced
EEA-1 expression is noted. The scale bar represents 20 μm.

---

after Ang II stimulation[21]. Ang II is also linked to proinflammatory states. Ayoub *et al.* described a functional
interaction between the AT1-receptor and the chemokine receptor CCR2 which could be an interesting link
between glomerular inflammation and proteinuria[22].

In this study, we examined the influence of Ang II on nephrin endocytosis in order to identify the underlying
signaling mechanisms that potentially contribute to blood pressure independent effects of ACE-inhibitors and
ARBs on podocytes.

Results

Here we show enhanced nephrin endocytosis by Ang II stimulation of podocytes. Nephrin endocytosis is responsible for the systemic blood pressure independent increase of glomerular permeability.

Ang II increases glomerular permeability, enhances nephrin binding to β-arrestin2 and nephrin endocytosis.

In mice the administration of Ang II for 60 minutes significantly increases the glomerular permeability in doses which do not influence blood pressure effectively (Fig. 1a + b). This effect is prevented by
administration of an AT1 receptor blocker (Fig. 1a). After additional 60 minutes of Ang II washout the glomerular
permeability decreases (Fig. 1a). The blood pressure was monitored by tail cuff measurements. No significant
blood pressure changes were observed between the groups (Fig. 1b). Ang II mediated AT1 receptor signaling was
controlled by increased phosphorylation of ERK (p42/p44) (Fig. 1Sa).

In isolated mouse glomeruli the stimulation with Ang II for 60 minutes enhances the β-arrestin binding to
nephrin (Fig. 1c + d).

Ang II stimulation increases nephrin β-arrestin colocalization in mouse glomeruli (Fig. 1e). Due to previous
data describing β-arrestin binding to nephrin as a mediator of nephrin endocytosis[15] we looked for increased
appearance of early endosomes in mouse glomeruli after stimulation with Ang II by EEA-1 staining. EEA-1 is
a marker for early endosomes[23]. Ang II stimulation enhances endocytosis with increased appearance of EEA-1
positive vesicles (Fig. 1f).

In line with this, biotinylation assays show a significantly enhanced nephrin disappearance from the cell surface under Ang II stimulation in HEK293T cells and mouse podocytes (Fig. 2a + b). In mice the *in vivo* biotinylation of nephrin from glomerular extracts was shown to be reduced after 60 minutes of Ang II stimulation
(Fig. 2c). This effect was blocked by the AT1 receptor blocker candesartan (Fig. 2c).

AT1 receptor is essential for the Ang II mediated nephrin binding to β-arrestin2.

In HEK
293 T cells expressing the nephrin c-terminus, β-arrestin2 and AT1 receptor, an enhanced β-arrestin2 binding
to nephrin is observed under Ang II stimulation. Ang II stimulation increases β-arrestin2 binding to nephrin
c-terminus already after 5 minutes. This binding is time dependent and was the strongest at 60 min Ang II stimulation (Fig. 3a). The AT1 receptor is mandatory to enhance the β-arrestin2 binding to nephrin c-terminus under
Ang II stimulation (Fig. 3b). In experiments with cells lacking the AT1 receptor the Ang II stimulation fails
to induce the enhanced β-arrestin2 binding to the nephrin c-terminus. AT1 receptor antagonist candesartan
blocked the enhanced β-arrestin2 binding to the nephrin c-terminus under Ang II stimulation (Fig. 3c).

The expression of the transfected nephrin fusion proteins and its control is shown in the supplemental Fig. 1Sb–d. The Ang II mediated activation of ERK is shown in the supplemental Fig. 3Sa.

G-protein coupled signaling of the AT1 receptor and PLC enhance nephrin binding to β-arrestin2.

To get more insights into the relevant AT1 receptor mediated signaling in this context we used an AT1 receptor
mutant (AT1-R D125A R126L) deficient for G-protein signaling. This mutant AT1 receptor failed to enhance the
β-arrestin2 binding to nephrin under Ang II stimulation (Fig. 4a). The expression of the AT1 receptor mutants
were ensured by RT-PCR (supplement Fig. 3Sb). We used inhibitors and siRNA to unravel the G-protein signaling responsible in conveying the signal from the activated AT1 receptor to the enhanced β-arrestin2 binding to
nephrin. The use of PTX as an inhibitor of Gαi did not block the Ang II mediated enhanced β-arrestin2 binding
to nephrin (Fig. 4b). The use of Ly294002 as a PI3 kinase inhibitor downstream of Gβγ failed to block the Ang
II mediated enhanced β-arrestin2 binding to nephrin (Fig. 4c). As no suitable pharmacological inhibitors of Gα
q are available we chose a siRNA knockdown approach. The efficient siRNA knockdown of Gαq inhibited the
Ang II mediated enhancement of the β-arrestin2 binding to nephrin (Fig. 4d). PLC is downstream of Gαq in the
signaling cascade. To further confirm the Gαq pathway of the activated AT1 receptor we used the PLC inhibitor
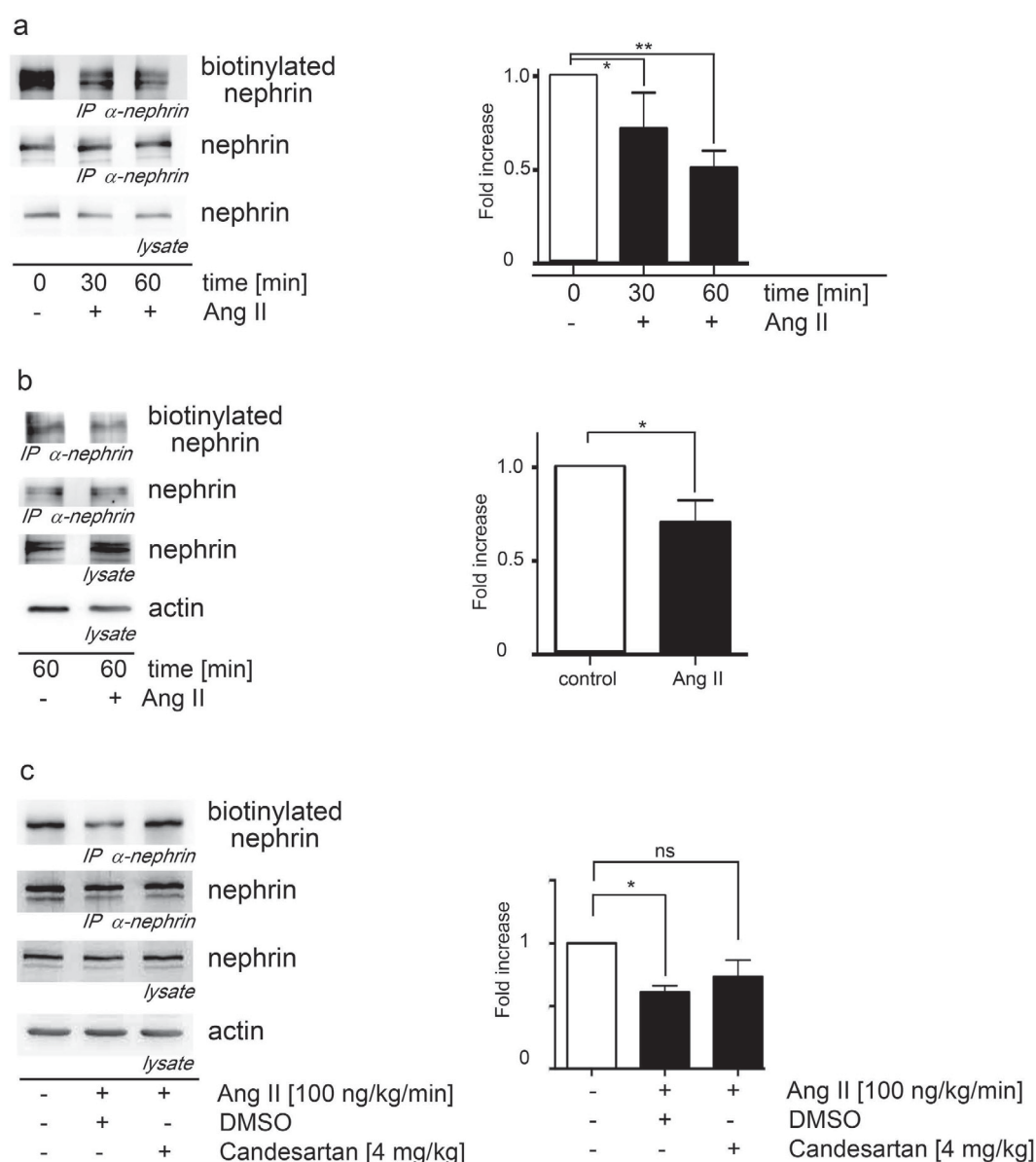U73122. The PLC inhibitor prevented the Ang II mediated enhancement of the β-arrestin2 binding to nephrin

Figure 2. Ang II promotes nephrin endocytosis. (**a**) Ang II induces the endocytosis of nephrin in HEK293T cells significantly in a time dependent fashion. The biotinylated nephrin fraction decreases the longer the Ang II exposure lasts (Kruskal-Wallis test: *n = 5, p = 0.04; **n = 5, p = 0.009). The AT1-receptor plasmid was cotransfected in all conditions to the AT1-receptor deficient HEK293T cells. (**b**) Nephrin endocytosis in murine podocytes is significantly enhanced by Ang II (*n = 5, p = 0.03). Biotinylated nephrin is significantly decreased in mouse podocytes when they are stimulated with Ang II. (**c**) Nephrin endocytosis in mice without and with Ang II stimulation and additional candesartan treatment. Biotinylated nephrin is significantly decreased in Ang II treated animals compared to control mice and restored to nearly control levels by additional candesartan treatment. (*Kruskal-Wallis test: n = 5, p = 0.02).

(Fig. 4f) and blocked the enhanced nephrin endocytosis under Ang II stimulation (Fig. 4e) confirming the Ang II mediated activations of the AT1-receptor and the signaling through Gαq and PLC. The use of the PLC inhibitor U73122 causes a reduced protein expression compared to conditions without U73122. The expression of the transfected nephrin fusion proteins and its control is shown in the supplemental Fig. 1Se–g. The expression of equivalent amounts of the AT1-receptors and its mutants was ensured by RT-PCR (supplemental Fig. 3Sb).

Nephrin Y1217 is mandatory for the Ang II mediated enhanced binding of nephrin to β-arrestin2. We further investigated the molecular mechanism within the nephrin c-terminus to elucidate how the Ang II treatment modifies nephrin's capability to bind to β-arrestin2. Previous experiments showed that the β-arrestin2 binding site within nephrin is the T-GERD-T motif at nephrin 1120-1125[15,16]. Point mutations of nephrin T1120 and nephrin T1125 demonstrate the importance of both threonines for the nephrin–β-arrestin binding (Fig. 5a + b). The Ang II mediated enhanced nephrin-β-arrestin binding is not affected by the nephrin

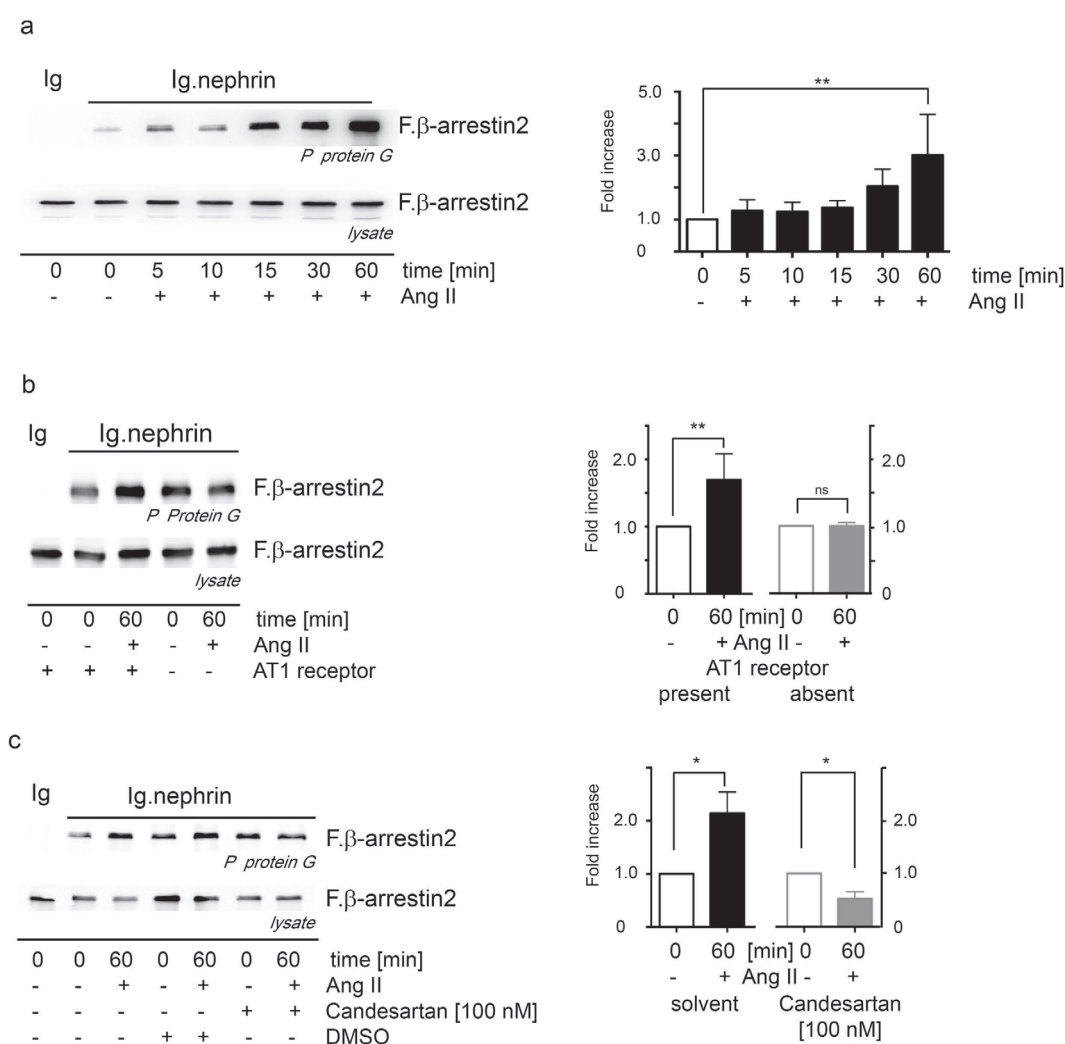**Figure 3. Ang II enhances the interaction of nephrin with β-arrestin2 through AT1 receptor activation.**
(**a**) HEK293T cells expressing nephrin, β-arrestin2 and the AT1-receptor were stimulated with Ang II. Ang II stimulation enhances the binding of β-arrestin2 to nephrin in a time dependent fashion. The maximum enhancement of 3-fold is seen after 60 min of Ang II stimulation (**Kruskal-Wallis test n = 12, p = 0.026). (**b**) HEK293T cells lacking the AT1 receptor do not show enhanced binding of nephrin to β-arrestin2 under stimulation with Ang II (**n = 9, p = 0.0019). The Ang II mediated enhanced binding of β-arrestin2 to nephrin is blocked by the AT1 receptor antagonist (**c**) Candesartan [100 nM] (*n = 3, p = 0.03, ns = 0.314). Comparable amounts of nephrin fusion protein expression and its control were controlled by western blot (experiments were conducted in HEK293T cells). The expression of the transfected nephrin fusion proteins and its control is shown in the supplemental Fig. 1Sb–d. The Ang II mediated activation of ERK is shown in the supplemental Fig. 3Sa.

T1120A mutation (Fig. 5a). Only the double mutation of both threonines abolishes the nephrin-β-arrestin binding as the β-arrestin2-binding site is destroyed (Fig. 5b). The phosphorylation of nephrin T1120/T1125 by PKC is a mandatory prerequisite to mediate binding between nephrin and β-arrestin2. Truncation mapping of the nephrin c-terminus (Fig. 5c + d) helped to narrow the regulatory region for the Ang II mediated enhanced binding of β-arrestin2 to nephrin down to the six nephrin amino acids 1216–1221 (IYDQVA). This region contains also one of the three known nck binding sites. A point mutation of the relevant Y1217 to an alanine or aspartic acid allowed the binding of β-arrestin2 to nephrin but inhibited the Ang II mediated enhanced binding of β-arrestin2 to nephrin (Fig. 5e). Interestingly for nephrin Y1217 is a non-synonymous SNP (db SNP number: rs114879227) causing the tyrosine to aspartate mutation known.

The expression of the transfected nephrin fusion proteins and its control is shown in the supplemental Fig. 2Sa–d.

Ang II attenuates nephrin binding to nck2. Being aware of the tyrosine kinases's role for β-arrestin2 binding to nephrin, the treatment with the tyrosine kinase inhibitor PP2 inhibits the Ang II mediated β-arrestin2 binding to nephrin (Fig. 6a). Knowing that Ang II promotes the nephrin endocytosis through an enhanced
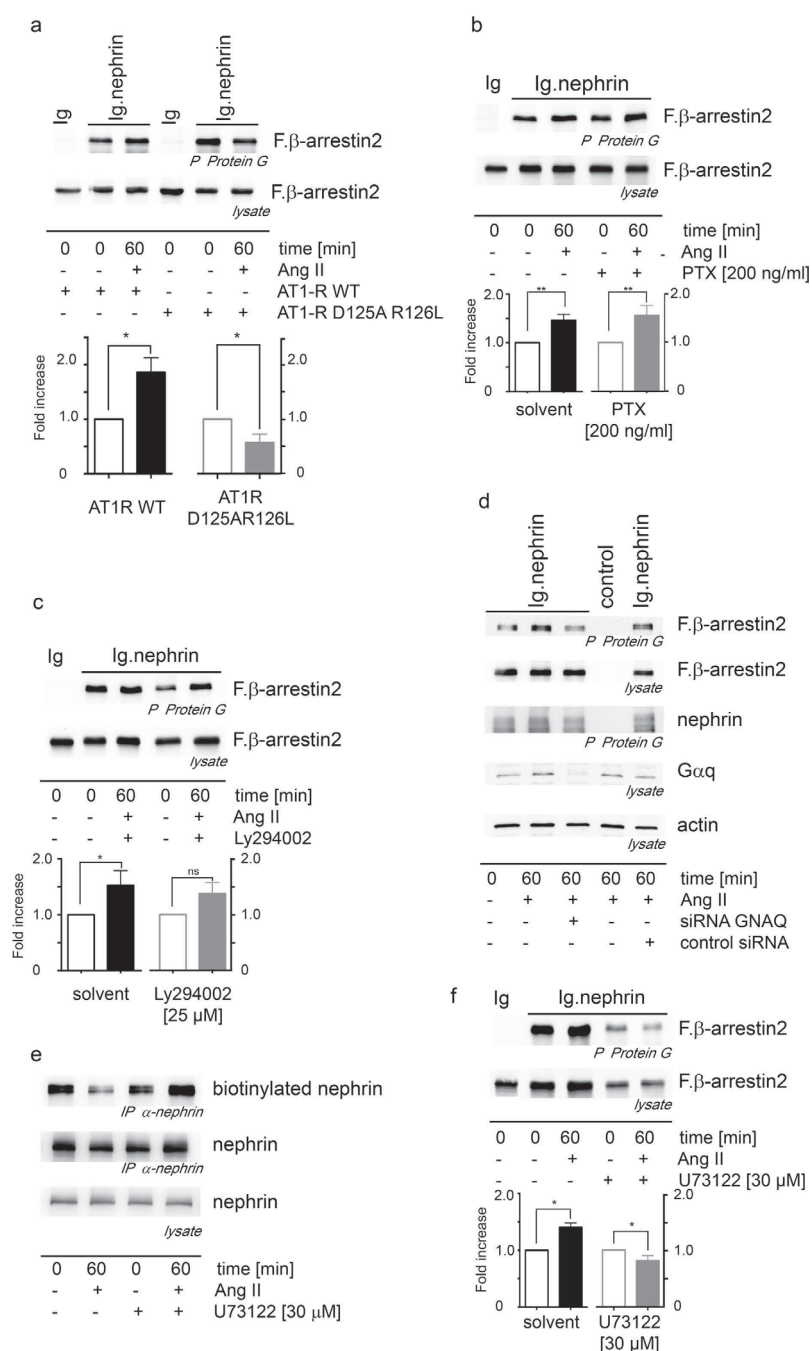
Figure 4. The Gα$_i$ signaling is essential in conveying the Ang II mediated, enhanced β-arrestin2 binding to the nephrin-c-terminus and nephrin endocytosis. (**a**) The AT1 receptor D125AR126L mutant abolishes G-protein signaling and disables the Ang II induced enhanced β-arrestin2 binding to the nephrin-c-terminus (*n = 4, p = 0.014). (**b**) The inhibition of Gα$_i$ by pertussis toxin (PTX) does not prevent the Ang II mediated enhanced β-arrestin2 binding to the nephrin-c-terminus (**n = 5, p = 0.0079). (**c**) The inhibition of the PI3kinase with Ly294002 does not influence the Ang II enhanced interaction of the nephrin-c-terminus-β-arrestin2 excluding the Gβγ pathway (*n = 4, p = 0.0143, p = 0.15 for Ly294002). (**d**) Gα$_q$ mediates the AT1 receptor activation resulting in enhanced β-arrestin2 binding to the nephrin-c-terminus. The expression of GNAQ siRNA blocks the Ang II mediated enhancement of the β-arrestin2 binding to the nephrin-c-terminus. (**e**) The PLC inhibitor U73122 reduces the Ang II mediated nephrin endocytosis in HEK293T cells. (**f**) The PLC inhibitor U73122 abolishes the Ang II mediated enhanced β-arrestin2 binding to the nephrin-c-terminus in HEK293T (*n = 3, p = 0.0318). The use of the PLC inhibitor U73122 causes a reduced protein expression compared to conditions without U73122. All experiments were conducted in HEK293T cells. Comparable amounts of the nephrin-c-terminus fusion protein expression and its control were controlled by western blot. The expression of equivalent amounts of the AT1-receptors and its mutants was ensured by RT-PCR. The expression of the transfected nephrin fusion proteins and its control is shown in the supplemental Fig. 1Se–g. The expression of equivalent amounts of the AT1-receptors and its mutants was ensured by RT-PCR (supplemental Fig. 3Sb).
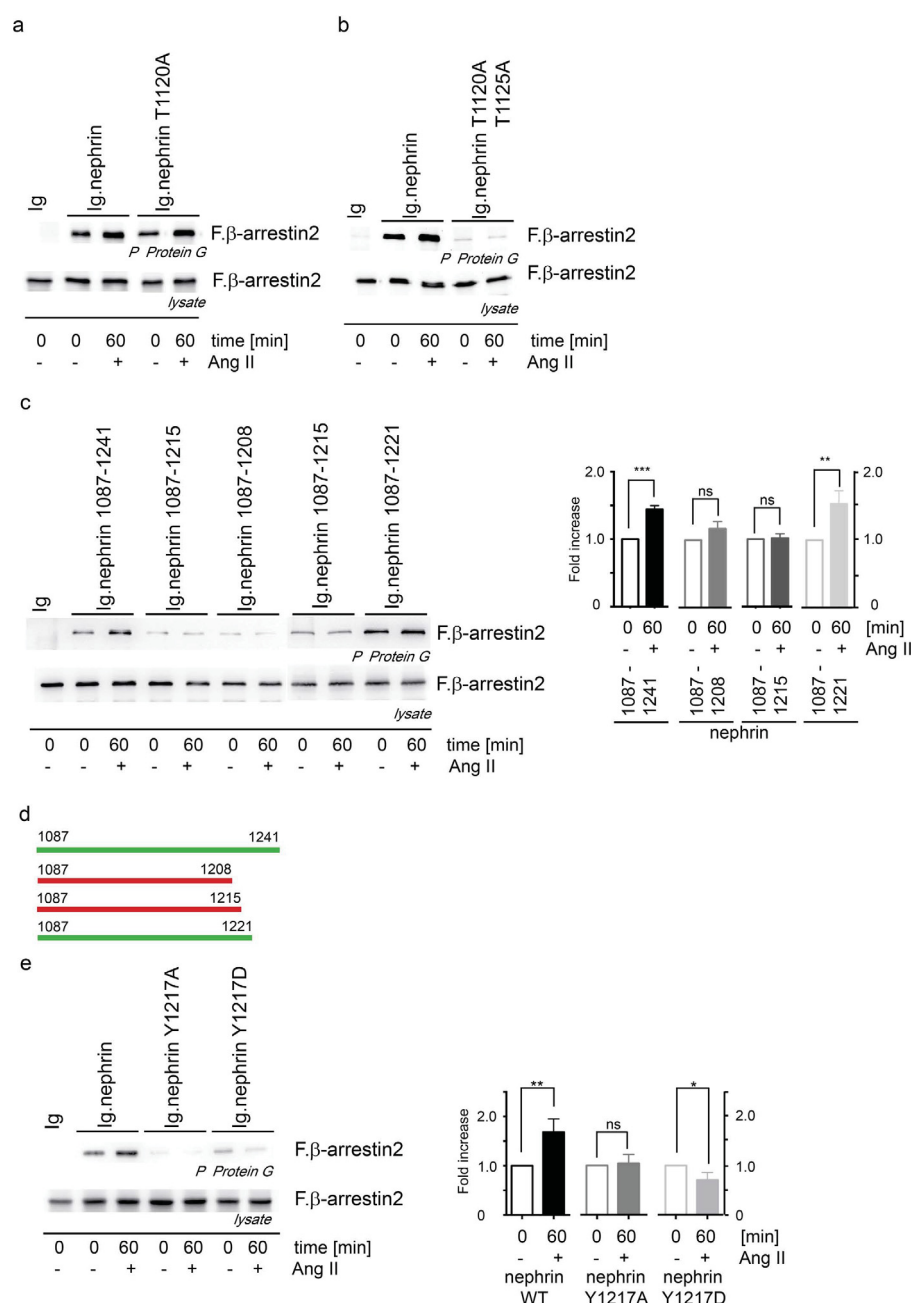
Figure 5. Nephrin Y1217 is critical for the Ang II mediated enhancement of the β-arrestin2 binding to nephrin. Several distinct nephrin residues have influence on the nephrin β-arrestin2 binding and the regulatory sensitivity to Ang II stimulation. The nephrin motif T-GERD-T at nephrin T1120/T1125 forms the β-arrestin2 binding site. (**a**) The nephrin T1120A mutant does not impair the binding of β-arrestin2 to nephrin and is still susceptible to Ang II. (**b**) The nephrin double mutant T1120A/T1125A impairs binding of β-arrestin2 completely. (**c**) The truncation mapping of the nephrin c-terminus unravels the nephrin aminoacid residues 1215–1221 to harbor the region that mediates the Ang II dependent enhanced β-arrestin2 binding to nephrin. The c-terminal nephrin truncations nephrin 1087–1221 show the Ang II mediated enhanced β-arrestin2 binding to nephrin whereas the nephrin truncations nephrin 1087–1208 and nephrin 1087–1215 lack the Ang II mediated enhanced β-arrestin2 binding to nephrin. P-values β-arrestin binding to nephrin for the comparison of Ang II stimulation versus without Ang II stimulation: Nephrin 1087–1241 n = 8, p = 0.0006; Nephrin 1087–1208 n = 4, p = 0.27; Nephrin 1087–1215 n = 6, p < 0.9; Nephrin 1087–1221 n = 5, p = 0,01 (**d**) Graphical summary of the nephrin c-terminal truncation mapping locating the transmission site of the Ang II mediated enhanced β-arrestin2 binding to nephrin. Green bars symbolize truncations which harbor the Ang II effect, red bars symbolize truncations that lack the Ang II effect. (**e**) The point mutations of nephrin Y1217 to an alanine or aspartatic acid allow the β-arrestin2 binding to nephrin but lack the Ang II mediated enhanced β-arrestin2 binding to nephrin (**n = 5, p = 0.004; *n = 5, p = 0.0476). All experiments were conducted in HEK293T cells. Comparable amounts of nephrin fusion protein expression and its control were controlled by western blot. The expression of the transfected nephrin fusion proteins and its control is shown in the supplemental Fig. 2Sa–d.
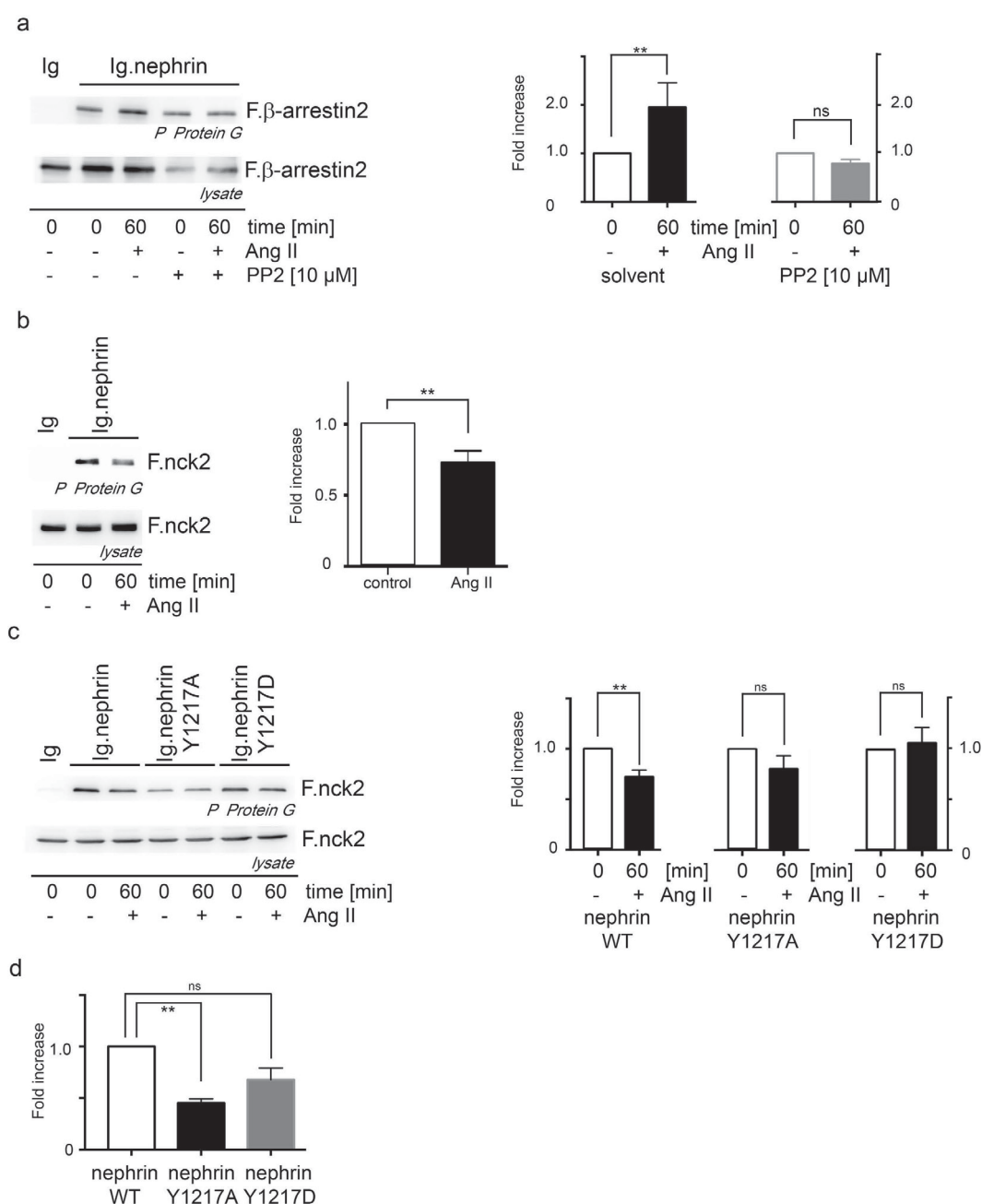
Figure 6. **Ang II decreases nck2 binding to nephrin.** (**a**) The tyrosine kinase inhibitor PP2 enhances the β-arrestin2 binding to nephrin under Ang II stimulation. PP2 alone without Ang II stimulation does not influence the β-arrestin2 binding to nephrin (**DMSO: n = 5, p = 0.004; PP2: n = 5, p = 0.0079). The use of the tyrosine kinase inhibitor PP2 causes a reduced protein expression compared to conditions without PP2. (**b**) Ang II stimulation attenuates nephrin nck2 binding (**n = 5, p = 0.0079). (**c**) Nephrin Y1217WT demonstrates under Ang II stimulation a significantly decreased binding to nck2 Y1217WT (n = 6, p < 0.008). The nephrin mutants Y1217A and Y1217D failed to demonstrate an effect to the nck2 binding to nephrin under Ang II stimulation. But the nephrin Y1217A mutant showed a significantly decreased binding to nck2 whereas the Y1217D mutant presented no different binding to nck2 than the nephrin. (**d**) Densitometry of nck2 binding to nephrin and its mutants without Ang II stimulation (n = 6, **p = 0.0023, ns p = 0.17). All experiments were performed in HEK293T cells. Comparable amounts of nephrin fusion protein expression and its control were controlled by western blot. The expression of the transfected nephrin fusion proteins and its control is shown in the supplemental Fig. 2Se–g.

β-arrestin2 binding to nephrin we were curious what happens to known cytoskeletal anchoring structures of nephrin. Nck is a prominent and well described adaptor molecule of tyrosine phosphorylated nephrin that builds the link to the actin cytoskeleton and uses nephrin Y1217 as one interaction site[24]. The typical nck binding
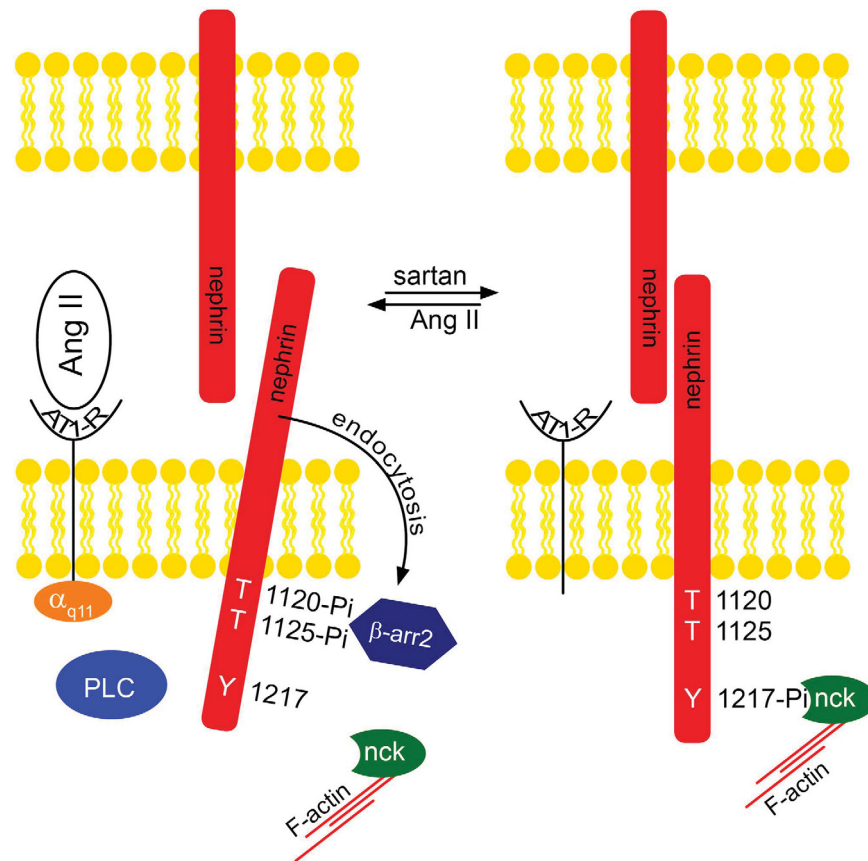
Figure 7. This scheme of function depicts how Ang II promotes glomerular permeability by nephrin endocytosis. Ang II activates the AT1-receptor (AT1-R). The activated AT1-receptor transfers the signal through $G_{\alpha q/11}$ and PLC. In turn nephrin gets phosphorylated at T1120/T1125 forming a β-arrestin2 binding site[16]. The binding of β-arrestin2 leads to increased nephrin endocytosis. This could be the mode of action how the glomerular permeability is increased beyond hemodynamic effects. In contrast, inhibition of the AT1-receptor by sartans promotes less β-arrestin2 nephrin interaction and less nephrin endocytosis leading to decreased glomerular permeability.

motif within nephrin is the aminoacid sequence LYDEV which appears three times within the human nephrin c-terminus. Only the mutation of all these three tyrosines within nephrin LYDEV motifs abolishes the nck binding to nephrin[24,25]. Interestingly the Ang II stimulation attenuates the nck2 binding to nephrin (Fig. 6b). By the use of nephrin Y1217 mutants the importance of this residue for nck2 binding is underlined. The nephrin WT shows a decreased interaction with nck2 under Ang II stimulation. The nephrin point mutants Y1217A and Y1217D lost the Ang II sensitivity (Fig. 6c). Independent of Ang II stimulation the nephrin Y1217A mutant shows significantly reduced binding to nck2, whereas the nephrin Y1217D mutant mimicking a constantly phosphorylated Y1217 residue binds at normal levels to nck2 without sensitivity to Ang II stimulation (Fig. 6c + d). This observation stresses the importance of the nephrin Y1217 residue for the nck2 interaction and underlines that the Ang II influence on the nephrin nck2 binding is conveyed by the phosphorylation change of the nephrin Y1217 (Fig. 6c). The expression of the transfected nephrin fusion proteins and its control is shown in the supplemental Fig. 2Se–g.

In summary we found an Ang II enhanced nephrin endocytosis mediated by β-arrestin2. At the same time the known interaction of nephrin to nck2 is alleviated under Ang II stimulation. One could speculate that Ang II functionally switches nephrin from its stabilizing nck interaction to the destabilizing interaction to β-arrestin2 (Fig. 7).

Discussion

Previously Buter *et al.*[26] showed that initiation of losartan treatment in diabetic patients reduces urine albumin excretion within 3 days without a significant blood pressure reduction. After discontinuation of losartan the anti-albuminuric effect disappeared. Furthermore, Axelsson *et al.* demonstrated a significant rise of glomerular permeability within minutes after Ang II stimulation. This Ang II infusion showed no significant change of the systemic blood pressure[12]. The Ang II mediated rapid increase in glomerular permeability is reversible within several minutes after Ang II stimulation[12]. We also observed a rapid response to Ang II stimulation leading to enhanced β-arrestin2 binding to nephrin within minutes and subsequent nephrin endocytosis. In our animal model we also observed a decrease of the Ang II mediated glomerular permeability after 60 minutes of Ang II

washout. However, the permeability decrease was not significantly different versus the control nor the Ang II treatment. It is debatable whether 60 minutes of washout are sufficient to fully reverse the Ang II mediated increase of the glomerular permeability. This is a novel molecular mechanism to describe the rapid increase of glomerular permeability by Ang II stimulation. It is without question that significant decrease in systemic blood pressure and influence on the intraglomerular hemodynamics will decrease albuminuria[27]. Independent of the systemic blood pressure ARB treatment significantly reduced albuminuria whereas a calcium antagonist was potent to control the blood pressure but failed to reduce the albuminuria[28]. Despite possible different effects on intraglomerular hemodynamics one might attribute something unique to Ang II inhibition conveying an additional anti-albuminuric effect. The Ang II enhanced binding to nephrin and subsequent nephrin endocytosis provides a novel molecular mechanism to explain the anti-albuminuric moiety of Ang II inhibition beyond hemodynamic effects. This novel mechanism supports the clinical observation that the pharmacologic inhibition of Ang II reduces albuminuria in normotensive albuminuric patients. From previous work we know that nephrin tyrosine phosphorylation regulates the nephrin binding to β-arrestin2[15,17] as well as to nck[24]. For the nephrin β-arrestin2 interaction the nephrin tyrosine 1193 dephosphorylation was critical. This previous work also showed the β-arrestin2 interaction to nephrin being attenuated in presence of enhanced tyrosine kinase activity (Yes)[15]. The additional use of the tyrosine kinase inhibitor PP2 neutralized the effect of the tyrosine kinase (Yes) on the nephrin β-arrestin2 interaction[15]. Here the use of PP2 inhibits the tyrosine phosphorylation of nephrin and thereby enhances the binding of β-arrestin2 to nephrin and diminishes the binding of nck to nephrin. The PP2 effect of diminished nephrin binding to β-arrestin2 can be in part functionally antagonized by Ang II stimulation.

For the nephrin nck binding the nephrin tyrosine phosphorylation of Y1176, 1193, 1217 was essential[24]. Here our results underline the stabilizing effect of nephrin tyrosine 1217 phosphorylation favoring the binding to nck and at the same time reducing the binding to β-arrestin2.

In the human 1000 genome population the nephrin tyrosine 1217 is a non-synonymous SNP (rs 114879227, Y1217D) with a heterozygosity frequency of 0.009[29]. It would be interesting to know if the carriers of this SNP are protected against Ang II mediated albuminuria. Interestingly in clinical situations the use of the tyrosine kinase inihibitors ramucirunab, sorafinib and sunitinib could cause reversible albuminuria as a side effect[30–33] underlining the clinical relevance of tyrosine dephosphorylation for albuminuria.

One might ask whether the nephrin endocytosis causes the increased glomerular permeability or the nephrin endocytosis is the consequence of increased glomerular permeability. Further work will be needed to answer this question.

It needs to be mentioned that cell surface disappearance of biotinylated nephrin could also be caused by extracellular nephrin shedding as it has been observed in a podocyte cell culture based study[34]. If nephrin shedding does occur a truncated nephrin can be detected. In our study we could not detect truncated nephrin. Therefore we expect the nephrin endocytosis to be the cause of the nephrin cell surface disappearance.

In summary, we could demonstrate a molecular mechanism for Ang II increasing glomerular permeability and paving the track for albuminuria beyond hemodynamic effects. The relevant AT1-receptor signaling and its downstream messengers were unraveled. Within nephrin the critical residue controlling between endocytosis and the stabilizing linkage to the actin cytoskeleton was identified. This opened the perspective for a regulatory model: AT1 receptor activation by Ang II promotes glomerular permeability and mediates nephrin endocytosis. On the other hand AT1 receptor blockade favors nephrin binding to nck linking nephrin to the actin cytoskeleton.

Materials and Methods

All of the reagents were purchased from Sigma Aldrich (Munich, Germany) unless stated otherwise. Candesartan (CV 11974) was a kind gift of Astra Zeneca (Wedel, Germany). PP2 (tyrosine kinase inhibitor), U73122 (PLC inhibitor) and Ly294002 (PI3 kinase inhibitor) were purchased from Calbiochem (Merck, Darmstadt, Germany). PTX was obtained from List Biological Laboratories (Campbell, CA, USA) and N-hydroxysulfosuccinimydyl-SS-biotin was purchased from Pierce (Bonn, Germany); siRNA and transfection reagents (SMARTpool: ON-TARGETplus GNAQ siRNA L-008562-00-0005 and ON-TARGETplus Non-targeting Pool D-001810-10-05 as control, Dharmacon, Cologne, Germany) were obtained from Thermo Scientific and Dynabeads from Invitrogen (Darmstadt, Germany). Gamma bind plus sepharose was purchased from GE healthcare (Muenchen, Germany).

Plasmids. Human nephrin cDNA was a gift from Dr. Gerd Walz (University of Freiburg, Germany). Membrane-bound fusion proteins of the C-terminal cytoplasmic domains of nephrin (AA 1087–1241, 1087–1215, 1158–1215, 1158–1241, 1087–1208, 1087–1221, 1087–1228) were generated by PCR and using a pCDM8 cassette that contained the leader sequence of CD5 fused to the CH2 and CH3 domains of human IgG1, followed by the transmembrane region of CD7 (Ig.nephrin)[35]. In brief, PCR was performed with the primers mentioned. The PCR product was purified by phenol extraction and further treated with restriction enzyme *Dpn I* and thereafter transformed into competent bacterial cells[36]. The Y1217A nephrin mutant (forward primer 5′cgcgggacgcgtcgcgggacgcgtcagcggagactcagg3′, reverse primer 5′gcggggcggccgccgcgggggcggccgccttacacc agatgtcccctcagctcgaagggcagagaatcgggttccagagtgtccaagtctccggccacctggtccgcgattcctcttggatcc-3′) and the Y1217D nephrin mutant (5′gcggggccgccttacaccagatgtcccctcagctcgaagggcagagaatc gggttccagagtgtcc-aagtctccggccacctggtcatcgattcctcttggatc-3′) were generated by PCR and cloned *MluI*/*NotI* into pCDM8 vector (see C-terminal cytoplasmic domain above). Clones were verified by sequencing.

FLAG-tagged β-arrestin2 (F.β-arrestin2) was a generous gift from Dr. Robert Lefkowitz[3] while GFP-tagged AT1-receptor was provided by Dr. László Hunyady (Semmelweis University, Budapest, Hungary). Dr. Ying-Hong Feng (Uniformed Services University of the Health Sciences, Bethesda, MD) provided the AT1-receptor mutant (D125AR126L) which lacks G-protein coupled receptor signaling[37]. PCR from FLAG-tagged Nck2, which was a

generous gift from Dr. Nina Jones (University of Guelph, Guelph, Canada), was performed and cloned *MluI/NotI* into the pCDM8 vector[24].

Cell Culture.
Immortalized murine podocytes were generously provided by Dr. Peter Mundel (Massachusetts General Hospital, Boston, MA). The podocytes were grown on type I collagen under permissive temperature (33 °C) in the presence of 10 units/ml IFN-γ. To induce differentiation, the cells were maintained at 37 °C without IFN-γ for 10–14 days[38].

AT1-receptor expressing murine podocytes were generated by retroviral transduction. The AT1-receptor was cloned into the pLEGFP-C1 vector *HindIII/NotI* via PCR with the following primers: 5′cgcgggaagcttatggccct-taactcttc and 5′ gcggggcggccgcctcactccacctcaaaac. Briefly, infectious viral supernatants - containing the sequence verified AT1-receptor cDNA or the GFP control - were produced by transient transfection of HEK293T cells. Immortalized murine podocytes were infected with viral supernatants containing either the AT1-receptor or a GFP control for 48 h. Selection of transduced cells was performed by G418 (200 μg/ml). The expression of the AT1-receptor was confirmed by *q*-PCR and activation of the AT1-receptor signaling pathway p42/44 by Angiotensin II (Ang II) was confirmed by Western blot.

HEK293T cells were grown in DMEM/F-12 medium supplemented with FCS.

Antibodies.
The following antibodies were used: mouse anti-M2 and mouse anti-actin (Sigma Aldrich, Taufkirchen, Germany), mouse anti-V5 (Invitrogen, Karlsruhe, Germany), sheep anti-human IgG (GE Healthcare, Freiburg, Germany), rabbit anti-GNAQ (Santa Cruz Biotechnology, Santa Cruz, CA), guinea pig anti-Nephrin (Progen Biotechnik, Heidelberg, Germany), rabbit β-arrestin1/2 (Cell Signaling Technology, Frankfurt, Germany), rabbit anti-p42/44 und rabbit anti-phospho p42/44 (Cell Signaling, Leiden, Netherlands), streptavidin-HRP (Thermo Scientific, Darmstadt, Germany), protein A and G sepharose (GE, Freiburg, Germany). As secondary antibodies for Western blotting anti-mouse-HRP (Dako, Hamburg, Germany), anti-guinea pig-HRP (Millipore, Darmstadt, Germany) and anti-rabbit-HRP (GE, Freiburg, Germany) were used. Antibodies used for immunofluorescence are indicated below.

Coimmunoprecipitation.
Coimmunoprecipitation experiments were carried out as described before[35]. Briefly, HEK293T cells were transiently transfected by using the calcium phosphate method. After incubation for 24 h, the cells were stimulated with Ang II (1 μM) for the time indicated and harvested thereafter. For inhibitor experiments, cells were pretreated with the inhibitor or its control (Candesartan 100 nM, PP2 10 μM, PTX 200 ng/ml, Ly294002 25 μM, U73122 30 μM) for 60 min and stimulated with Ang II 1 μM thereafter. After cell lysis in 1% Triton X-100 lysis buffer, centrifugation (20000 × g, 15 min, 4 °C) was performed. Cell lysates containing equal amounts of total protein were incubated 1 h at 4 °C with protein G sepharose and extensively washed afterwards with lysis buffer. The precipitated proteins were resolved by 10% SDS-PAGE and visualized by Western blotting.

siRNA knockdown.
Cotransfection of HEK293T cells with specific siRNA and cDNA plasmids was performed according the manufacturer's protocol. In brief, the cells were seeded into 6 cm tissue culture dishes in low glucose (5.5 mM) cell culture media. The next day cells were transfected with 2 μg DNA and 0.4 nmol of (control or target) siRNA in 4 ml transfection medium. After 24 h, the cells were equally divided into several dishes. HEK293T cells were treated with Ang II (1 μM, 60 min) or H₂O 72 h after transfection before coimmunoprecipitation was performed. If an inhibitor was used, cells were pretreated with the inhibitor 60 min before stimulation with Ang II (1 μM).

Biotinylation Assay.
HEK293T cells were transfected with human nephrin cDNA. Before the cells were harvested in ice-cold PBS buffer containing 0.1 mM CaCl₂ and 1 mM MgCl₂ (PBSCM – phosphate buffered saline with CaCl₂ and MgCl₂), pH 8.0, cells were incubated with Ang II (1 μM, 60 min) or H₂O. For inhibitor experiments, cells were pretreated with the inhibitor 60 min before stimulation with Ang II. Plasma membrane proteins were labeled with N-hydroxysulfosuccinimydyl-SS-biotin (0.5 mg/ml; Pierce) for 30 min at 4 °C. Unbound biotin was quenched twice with ice-cold PBSCM containing 100 mM glycine. Cells were lysed in 1% Triton X100 lysis buffer and nephrin was precipitated with GP-N2 antibody from Progen Biotechnik, Heidelberg, Germany. After extensive washing, cell lysates and bound proteins were resolved in 10% SDS and visualized via Western blotting.

For endogenous immunoprecipitation differentiated AT-1 receptor murine podocytes ($8 \times 19 \times 10^5$ cells/data point) were incubated with Vitamin D3 (100 nM) as described elsewhere[39]. Before the process of biotin labelling (as indicated above) and cell lysis in Triton 1% lysis buffer podocytes were stimulated with Ang II or H₂O (1 μM, 60 min), centrifuged (20.000 × g, 30 min, 4 °C) and equal amounts of protein were incubated with an anti-nephrin antibody over night at 4 °C. Afterwards cell lysates were incubated with protein A sepharose for 3 h at 4 °C followed by extensive washing and protein denaturation by SDS.

For immunfluorescence of mouse kidneys, mice were treated with a continuous infusion of Nacl 0,9% or Ang II (100ng/kg/min) via a central venous catheter. After 60 min, mice were sacrificed and their kidneys perfused with ice-cold PBS. Kidneys were fixed in paraformaldeyd. Slides were deparaffinized, pretreated with citrate buffer (pH 6.1) for 15 min at 98 °C and blocked with biotin block and protein block (Dako, Hamburg, Germany). Anti-β-arrestin 2 (Cell Signaling technology, Frankfurt, Germany 1:50) and anti-nephrin (Progen Biotechnik, Heidelberg, Germany 1:100) antibodies were incubated at 4 °C over night. For β-arrestin2 staining, enhancement with a biotinylated anti-rabbit antibody (Dianova, Hamburg, Germany 1:1000) was followed by incubation with streptavidin-Cy2 (Dianova, Hamburg, Germany 1:500). Nephrin was visualized via anti-guinea pig Alexa Flour 647 (Dianova, Hamburg, Germany 1:1000). Anti-EEA-1 (Santa Cruz Biotechnology, Santa Cruz, CA, USA 1:100) was stained with a biotinylated secondary rabbit antibody (Dianova, Hamburg, Germany 1:1000) and visualized with Streptavidin Cy3 (Dianova, Hamburg, Germany 1:1000). Mounting medium with Dapi was used (Dianova, Hamburg, Germany).

Samples were analyzed on a Leica TCS SP2 confocal laser-scanning microscope using a 63x HCX PL Apo water immersion objective (Leica, Wetzlar, Germany).

Animal care.   Mice were obtained from the local animal care facility. The investigations were conducted according the guidelines outlined in the Guide for Care and Use of Laboratory Animals (US National Institutes of Health Publication No. 85–23, revised 1996). All animal experiments were performed in accordance and compliance with the relevant institutional approvals (state government LANUV reference number: 84-02.04.2012. A397).

Glomerular permeability measurement in mice.   Female FVB mice at the age of 6–8 weeks were anesthetized. A central venous catheter was placed while urine was collected continuously. A bolus of FITC-Ficoll 70 (40 μg) was applied intravenously followed by a continuous infusion of 8 μl/min of FITC-Ficoll 70 (20 μg/ml in 0.9% NaCl). DMSO or CV11974 (4 mg/kg) were administered i.p. at this point. After 60 minutes of equilibration, continuous infusion of Ang II (100 ng/kg/min) (Ang II or Ang II + washout) or NaCl 0.9% (control) was started additionally. Urine collection was performed at 60 and 120 minutes thereafter. For the AngII washout experiment, continuous infusion of Ang II (Ang II) or Nacl 0,9% (control and Ang II + washout) was continued for another 60 minutes. Blood pressure measurement was performed every 60 minutes via the tail cuff method (Softron BP-98A, Japan). Urine was subjected to fluorescence measurement at 490 nm and creatinine was analyzed via an enzymatic assay following the manufactures instructions (Sigma Aldrich, Taufkirchen, Germany). Data were displayed as FITC/creatinine ratios at the end of the equilibration time (0 min) vs. the end of the experiment (60 min). Statistics were performed using 2-way ANOVA.

For *in vivo* endocytosis, mice were sacrificed and perfused with PBSCM, followed by biotin and glycine. Glomeruli were isolated and lysed as described below. Cell lysates were adjusted using the BCA method. Nephrin was precipitated with an anti-nephrin (Progen) antibody (5 μl) at 4 °C over night followed by 30 μl of protein A sepharose. After extensive washing of the precipitates, Western blot was performed under reducing conditions.

Glomeruli isolation.   Balb/c mice (male, 6–8 weeks of age) were sacrificed and their kidneys perfused with ice-cold PBS via the abdominal aorta. Thereafter the kidneys were perfused with Dynabeads (diameter: 4.5 μM; Invitrogen) at a concentration of 1.2×10^7 beads/ml in PBS. The kidneys were removed, minced, and digested with collagenase A (Roche Applied Science, Mannheim, Germany) for 30 min at 37 °C. The digested kidney tissue was sieved through a 100 μM cell mesh with intermittent PBS flushing. After centrifugation (620 × g, 5 min, 4 °C) the cell pellet was dissolved in 2 ml of PBS and transferred into a 2 ml tube. By using a magnet catcher and subsequent washing procedure, the Dynabeads containing glomeruli were washed until an appropriate purity of 95% was achieved. Isolated glomeruli were stimulated with Ang II (1 μM) for 60 min and lysed on ice in CHAPS buffer (20 mM CHAPS, 20 mM Tris pH 7,5, 50 mM NaCl, 50 mM NaF, 15 mM $Na_4P_2O_7$, 0,1 mM EDTA pH 8,0, 2 mM sodiumorthovanadate, 2 mM ATP) by using a TissueRuptor (Quiagen, Hilden, Germany). Insoluble cellular material was removed by centrifugation (20.000 × g, 4 °C, 30 min). The resulting cell lysates were adjusted to ensure equal total protein content using the BCA method. After addition of an anti-β-arrestin antibody (1:50) the cell lysates were incubated over night at 4 °C followed by the incubation with 30 μl of Gamma bind plus sepharose for 3 h. The immunoprecipitates were washed extensively with lysis buffer, and the precipitated proteins were resolved by 10% SDS-PAGE under non-reducing conditions and visualized by Western blotting.

Statistics
If not otherwise stated Mann-U-Whitney test was used (Graph Pad, Prism, Version 6a).

References

1. Matsushita, K. *et al.* Association of estimated glomerular filtration rate and albuminuria with all-cause and cardiovascular mortality in general population cohorts: a collaborative meta-analysis. *Lancet* **375,** 2073–2081 (2010).
2. Nitsch, D. *et al.* Associations of estimated glomerular filtration rate and albuminuria with mortality and renal failure by sex: a meta-analysis. *BMJ* **346,** f324 (2013).
3. de Zeeuw, D., Parving, H. H. & Henning, R. H. Microalbuminuria as an early marker for cardiovascular disease. *J Am Soc Nephrol* **17,** 2100–2105 (2006).
4. Brenner, B. M. *et al.* Effects of losartan on renal and cardiovascular outcomes in patients with type 2 diabetes and nephropathy. *N Engl J Med* **345,** 861–869 (2001).
5. Haller, H. *et al.* Olmesartan for the delay or prevention of microalbuminuria in type 2 diabetes. *N Engl J Med* **364,** 907–917 (2011).
6. Pohl, M. A. *et al.* Independent and additive impact of blood pressure control and angiotensin II receptor blockade on renal outcomes in the irbesartan diabetic nephropathy trial: clinical implications and limitations. *J Am Soc Nephrol* **16,** 3027–3037 (2005).
7. Izuhara, Y. *et al.* Renoprotective properties of angiotensin receptor blockers beyond blood pressure lowering. *J Am Soc Nephrol* **16,** 3631–3641 (2005).
8. Lewis, E. J. *et al.* Renoprotective effect of the angiotensin-receptor antagonist irbesartan in patients with nephropathy due to type 2 diabetes. *N Engl J Med* **345,** 851–860 (2001).
9. Ruggenenti, P., Perna, A., Gherardi, G., Gaspari, F., Benini, R. & Remuzzi, G. Renal function and requirement for dialysis in chronic nephropathy patients on long-term ramipril: REIN follow-up trial. Gruppo Italiano di Studi Epidemiologici in Nefrologia (GISEN). Ramipril Efficacy in Nephropathy. *Lancet* **352,** 1252–1256 (1998).
10. Bohlen, L., de Courten, M. & Weidmann, P. Comparative study of the effect of ACE-inhibitors and other antihypertensive agents on proteinuria in diabetic patients. *Am J Hypertens* **7,** 84S–92S (1994).
11. The GISEN Group. Randomised placebo-controlled trial of effect of ramipril on decline in glomerular filtration rate and risk of terminal renal failure in proteinuric, non-diabetic nephropathy. The GISEN Group (Gruppo Italiano di Studi Epidemiologici in Nefrologia). *Lancet* **349,** 1857–1863 (1997).

12. Axelsson, J., Rippe, A., Oberg, C. M. & Rippe, B. Rapid, dynamic changes in glomerular permeability to macromolecules during systemic angiotensin II (ANG II) infusion in rats. *Am J Physiol Renal Physiol* **303,** F790–799 (2012).

13. Hoffmann, S., Podlich, D., Hahnel, B., Kriz, W. & Gretz, N. Angiotensin II type 1 receptor overexpression in podocytes induces glomerulosclerosis in transgenic rats. *J Am Soc Nephrol* **15,** 1475–1487 (2004).

14. Kriz, W. Podocytes as a target for treatment with ACE inhibitors and/or angiotensin-receptor blockers. *Kidney Int* **65,** 333–334 (2004).

15. Quack, I. *et al.* beta-Arrestin2 mediates nephrin endocytosis and impairs slit diaphragm integrity. *Proc Natl Acad Sci USA* **103,** 14110–14115 (2006).

16. Quack, I. *et al.* PKC alpha mediates beta-arrestin2-dependent nephrin endocytosis in hyperglycemia. *J Biol Chem* **286,** 12959–12970 (2011).

17. Soda, K. *et al.* Role of dynamin, synaptojanin, and endophilin in podocyte foot processes. *J Clin Invest* **122,** 4401–4411 (2012).

18. Macconi, D. *et al.* Permselective dysfunction of podocyte-podocyte contact upon angiotensin II unravels the molecular target for renoprotective intervention. *Am J Pathol* **168,** 1073–1085 (2006).

19. Hsu, H. H. *et al.* Mechanisms of angiotensin II signaling on cytoskeleton of podocytes. *J Mol Med* (*Berl*) **86,** 1379–1394 (2008).

20. Greka, A. & Mundel, P. Cell biology and pathology of podocytes. *Annu Rev Physiol* **74,** 299–323 (2012).

21. Yu, M., Ren, Q. & Yu, S. Y. Role of nephrin phosphorylation inducted by dexamethasone and angiotensin II in podocytes. *Mol Biol Rep* **41,** 3591–3595 (2014).

22. Ayoub, M. A. *et al.* Functional interaction between angiotensin II receptor type 1 and chemokine (C-C motif) receptor 2 with implications for chronic kidney disease. *PLoS One* **10,** e0119803 (2015).

23. Mu, F. T. *et al.* EEA1, an early endosome-associated protein. EEA1 is a conserved alpha-helical peripheral membrane protein flanked by cysteine "fingers" and contains a calmodulin-binding IQ motif. *J Biol Chem* **270,** 13503–13511 (1995).

24. Jones, N. *et al.* Nck adaptor proteins link nephrin to the actin cytoskeleton of kidney podocytes. *Nature* **440,** 818–823 (2006).

25. New, L. A. *et al.* Nephrin Tyrosine Phosphorylation Is Required to Stabilize and Restore Podocyte Foot Process Architecture. *J Am Soc Nephrol* **27,** 2422–2435 (2016).

26. Buter, H., Navis, G., Dullaart, R. P., de Zeeuw, D. & de Jong, P. E. Time course of the antiproteinuric and renal haemodynamic responses to losartan in microalbuminuric IDDM. *Nephrol Dial Transplant* **16,** 771–775 (2001).

27. Brenner, B. M. & Anderson, S. The Gordon Wilson lecture. Why kidneys fail: an unifying hypothesis. *Trans Am Clin Climatol Assoc* **98,** 59–70 (1987).

28. Davis, B. J., Cao, Z., de Gasparo, M., Kawachi, H., Cooper, M. E. & Allen, T. J. Disparate effects of angiotensin II antagonists and calcium channel blockers on albuminuria in experimental diabetes and hypertension: potential role of nephrin. *J Hypertens* **21,** 209–216 (2003).

29. Abecasis, G. R. *et al.* A map of human genome variation from population-scale sequencing. *Nature* **467,** 1061–1073 (2010).

30. Garcia, J. A. *et al.* A phase 2, single-arm study of ramucirumab in patients with metastatic renal cell carcinoma with disease progression on or intolerance to tyrosine kinase inhibitor therapy. *Cancer* **120,** 1647–1655 (2014).

31. Jhaveri, K. D., Flombaum, C. D., Kroog, G. & Glezerman, I. G. Nephrotoxicities associated with the use of tyrosine kinase inhibitors: a single-center experience and review of the literature. *Nephron Clin Pract* **117,** c312–319 (2011).

32. Ruebner, R. L., Copelovitch, L., Evageliou, N. F., Denburg, M. R., Belasco, J. B. & Kaplan, B. S. Nephrotic syndrome associated with tyrosine kinase inhibitors for pediatric malignancy: case series and review of the literature. *Pediatr Nephrol* **29,** 863–869 (2014).

33. Kandula, P. & Agarwal, R. Proteinuria and hypertension with tyrosine kinase inhibitors. *Kidney Int* **80,** 1271–1277 (2011).

34. Collino, F. *et al.* Preeclamptic sera induce nephrin shedding from podocytes through endothelin-1 release by endothelial glomerular cells. *Am J Physiol Renal Physiol* **294,** F1185–1194 (2008).

35. Sellin, L., Huber, T. B., Gerke, P., Quack, I., Pavenstadt, H. & Walz, G. NEPH1 defines a novel family of podocin interacting proteins. *FASEB J* **17,** 115–117 (2003).

36. Zheng, L., Baumann, U. & Reymond, J. L. An efficient one-step site-directed and site-saturation mutagenesis protocol. *Nucleic Acids Res* **32,** e115 (2004).

37. Feng, Y. H., Ding, Y., Ren, S., Zhou, L., Xu, C. & Karnik, S. S. Unconventional homologous internalization of the angiotensin II type-1 receptor induced by G-protein-independent signals. *Hypertension* **46,** 419–425 (2005).

38. Mundel, P. *et al.* Rearrangements of the cytoskeleton and cell contacts induce process formation during differentiation of conditionally immortalized mouse podocyte cell lines. *Exp Cell Res* **236,** 248–258 (1997).

39. Okamura, M., Takano, Y., Saito, Y., Yao, J. & Kitamura, M. Induction of nephrin gene expression by selective cooperation of the retinoic acid receptor and the vitamin D receptor. *Nephrol Dial Transplant* **24,** 3006–3012 (2009).

Acknowledgements

Author Contributions

E.K. – performed experiments, analyzed data, statistical analyses, preparation and correction of the manuscript; U.Z. – performed experiments, analyzed data; M.R. - performed experiments, analyzed data; S.A.P. – performed experiments, analyzed data; J.S. – designed experiments, performed experiments, analyzed data; M.W. – provided experimental techniques, read and corrected the manuscript; I.Q. – provided experimental techniques, read and corrected the manuscript; L.C.R. – read and corrected the manuscript; L.S. – designed the research, analyzed data, wrote, corrected and managed the manuscript.

Additional Information

Supplementary information accompanies this paper at http://www.nature.com/srep

Competing financial interests: The authors declare no competing financial interests.

How to cite this article: Königshausen, E. *et al.* Angiotensin II increases glomerular permeability by β-arrestin mediated nephrin endocytosis. *Sci. Rep.* **6**, 39513; doi: 10.1038/srep39513 (2016).

Publisher's note: Springer Nature remains neutral with regard to jurisdictional claims in published maps and institutional affiliations.
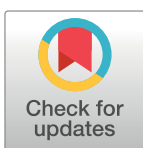
A novel *in vivo* method to quantify slit diaphragm protein abundance in murine proteinuric kidney disease

Raphael Haase[1], Sebastian Alexander Potthoff[1], Catherine Meyer-Schwesinger[2], Clara Frosch[1], Thorsten Wiech[3], Ulf Panzer[2], Eva Königshausen[1], Johannes Stegbauer[1], Lorenz Sellin[1], Lars Christian Rump[1], Ivo Quack[1☯]*, Magdalena Woznowski[1☯]

1 Department of Nephrology, Medical Faculty, Heinrich-Heine University, Düsseldorf, Germany, 2 III. Medical Clinic University Hospital Eppendorf, Hamburg, Germany, 3 Institute of Pathology, University Hospital Eppendorf, Hamburg, Germany

☯ These authors contributed equally to this work.
* ivo.quack@med.uni-duesseldorf.de

Abstract

Injury of the glomerular filter causes proteinuria by disrupting the sensitive interplay of the glomerular protein network. To date, studies of the expression and trafficking of glomerular proteins have been mostly limited to *in vitro* or histologic studies. Here, we report a novel *in vivo* biotinylation assay that allows the quantification of surface expression of glomerular proteins in mice. Kidneys were perfused *in situ* with biotin before harvest. Afterwards glomeruli were isolated and lyzed. The protein of interest was separated by immunoprecipitation and the amount of surface-expressed protein was quantified by Western blot analysis with streptavidin staining. As proof-of-concept, we examined the presence of nephrin in the slit diaphragm in two well-established murine models of proteinuric kidney disease: nephrotoxic nephritis and adriamycin nephropathy. In proteinuric animals, significantly less nephrin was detected in the slit diaphragm. When proteinuria decreased once again during the course of disease, the amount of surface nephrin returned to the baseline. Our present results suggest that our assay is a valuable tool to study the glomerular filter in proteinuric kidney diseases. Note that the assay is not limited to proteins expressed in the slit diaphragm, and all surface proteins that are accessible to biotin perfusion and immunoprecipitation qualify for this analysis.

Introduction

Injury to a single layer of the glomerular filter is sufficient to induce albuminuria. If podocytes and the slit diaphragm are involved, albuminuria easily reaches nephrotic ranges. Albuminuria is a main driver of the progression of kidney disease [1] and is associated with a markedly increased cardiovascular risk [2]. Several studies have suggested that altered trafficking of slit diaphragm proteins causes filter leakage. We previously demonstrated that nephrin, the backbone of the slit diaphragm, undergoes β-arrestin2-dependent endocytosis in healthy and

diseased states [3, 4]. Meanwhile the concept of nephrin endocytosis has been confirmed and extended by other groups (reviewed in [5–7]). Newly identified regulatory mechanisms of nephrin endocytosis involve planar cell polarity pathways, e.g. Wnt5a and Vangl2 [8, 9]. CIN85/RukL controls nephrin turnover by ubiquitination [10, 11]. Some studies demonstrated dynamin- and clathrin-dependent uptake whilst others showed that raft-dependent endocytosis might be an alternative pathway [4, 12, 13]. Recent work suggests that reduction of endocytotic processes is also detrimental to the podocyte [14].

Studies of podocyte protein trafficking have been hampered by the lack of a suitable *in vivo* model of the glomerular filter. To elucidate the complex interplay of the filter structures mainly two different techniques have been used so far. First, the classical immunofluorescence labeling approach using antibodies that recognize epitopes in the extracellular domains of the receptors being studied [15]. Second, covalent modification of cell surface receptors with biotin as a valuable technique for monitoring surface protein trafficking. Biotinylation enables labeling of the cell surface protein at a particular time point, but instead of using a specific antibody, all surface proteins are tagged with biotin. The protein of interest is then separated by immunoprecipitation followed by SDS-PAGE and Western blotting. The biotinylated fraction can be visualized by staining with streptavidin and quantified by densitometry. So far biotinylation has been limited to *in vitro* experiments. Satoh et al. recently described a method in which glomeruli are extracted first and are then biotinylated in vitro [16]. However, it is known that the complex architecture of the glomerular filter is altered by mechanical stress. We learned from our previous work that especially the molecular composition of the slit diaphragm changes rapidly. Based on these observations we developed an *in vivo* biotinylation assay because we were convinced that biotinylation of glomerular extracellular proteins *in situ* yields more accurate results.

Applying the assay in an acute and a chronic proteinuric disease model, we demonstrate that the amount of surface nephrin can be reliably quantified with the biotinylation assay introduced.

Materials and methods

Animal care

Mice were obtained either from an in-house breed at a local animal care facility or from Janvier Labs, France. This study was carried out in strict accordance with the recommendations in the Guide for the Care and Use of Laboratory Animals of the National Institutes of Health. The protocol was approved by the local Institutional Animal Care and Use Committee: Landesamt für Natur, Umwelt und Verbraucherschutz Nordrhein-Westfalen, Recklinghausen, Germany; Permit Number: AZ: 84–02.04.2012.A099. If necessary analgesia was performed with Carprofen 5 mg/kg s.c. Animals were sacrificed by decapitation under anesthesia performed with Ketamin 100mg/kg bodyweight and Xylazin 5mg/kg bodyweight.

Induction of nephrotoxic serum nephritis (NTN)

C57Bl/6 male mice (8 weeks of age) were injected intraperitoneally with 500–800 μL NTN serum. Control animals received an equal amount of normal saline. Following the collection of urine, mice were weighed and examined on day 1 or 18 after injection.

Induction of adriamycin-induced nephropathy (ADR)

BALB/c male mice (6 weeks of age) were injected intravenously with adriamycin (10 mg/kg bodyweight; ADR, Sigma-Aldrich, Steinheim, Germany), and control animals were

administered an equivalent volume of water for injection (aqua ad injectabilia). Following the collection of urine, mice were weighed and examined 7 days after injection.

Analysis of proteinuria

Twelve hour urine collection was performed in single metabolic cages. Proteinuria was assessed using a 10% polyacrylamide gel. Urinary albumin and creatinine excretion were measured using standard laboratory protocols, and proteinuria was normalized based on creatinine excretion.

In vivo biotin labeling and immunoprecipitation (IP)

First, kidneys were perfused via the abdominal aorta with 5ml ice-cold PBS (rate 2mL/min) supplemented with 1 mM $MgCl_2$ and 0.1 mM $CaCl_2$ (PBSCM). Then, perfusion was repeated with 5 mL PBSCM (rate 2mL/min) supplemented with 0.5 mg/mL EZ-Link™ Sulfo-NHS-LC-Biotin (Thermo Scientific, Rockford, USA) for surface protein labeling. Afterwards, unspecific biotin binding was quenched with 5mL PBSCM (rate 2mL/min) supplemented with 100 mM glycine. Finally, kidneys were perfused with 5 mL PBSCM (rate 2mL/min) containing 16 x 10^6 Dynabeads/mL (Invitrogen, Oslo, Norway). After perfusion, kidneys were immediately minced and digested for 40 minutes at 37°C with 1.5 mg/mL Collagenase A (Roche, Mannheim, Germany). Cell suspensions were filtered through 100 µm cell strainers (Greiner Bio-One, Frickenhausen, Germany), separated by centrifugation (5.000 ×*g* for 5 min at 4°C), and washed with PBSCM using a Dynamag magnet. When a purity of >95% glomeruli was achieved, glomeruli were collected by centrifugation (6.800 ×*g* for 5 min at 4°C). Samples were immediately homogenized using a TissueRuptor (Qiagen, Hombrechtikon, Switzerland), and were lysed for 30 min on ice. Insoluble cellular material was removed by centrifugation (15.000 ×*g* for 30 min at 4°C). Protein concentrations from the supernatant were measured using a BCA Protein assay kit (Thermo Scientific, Rockford, USA), and were subsequently adjusted to ensure equal total protein content.

IP analysis: samples were incubated with anti-nephrin antibodies overnight at 4°C, followed by a 3-h incubation with protein A-Sepharose (GE LifeSciences, Freiburg, Germany) or with or streptavidin agarose beads directly (Pierce, Thermo Fisher Scientific, Waltham, USA). Due to N-linked glycosylation nephrin appears as a double band [17]. The immunoprecipitates were extensively washed with CHAPS buffer. Bound proteins were resolved using 2× Laemmli sample buffer, separated on 10% polyacrylamide gel, and electroblotted onto nitrocellulose membranes. The blots were blocked in 5% bovine serum albumin (BSA) in TBST before incubation with primary antibodies (nephrin: Progen GP-N2, Heidelberg, Germany; beta-actin: Sigma, St. Louis, USA; streptavidin-HRP: Thermo Scientific, Rockford, USA; p44/42 MAPK (Erk1/2): Cell Signaling Technologies, Danvers, USA; Podocalyxin: R&D Systems, Minneapolis, USA) overnight at 4°C. After washing with TBST for 30 min, the blots were incubated for 60 min with HRP-coupled secondary antibodies, and excessive antibodies were removed by washing with TBST for 30 min. ECL SuperSignal (Thermo Scientific, Rockford, U.S.A.) was used for chemiluminescence visualization (FluorChem FC2 Imager; Alpha Innotec, USA), and the densitometric analysis was performed (AlphaView SA; Cell Biosciences Inc., version 3.3.1, Alpha Innotec, USA).

Immunofluorescence

Biotin—Streptavidin. For immunofluorescent stainings, 2 µm paraffin sections were deparaffinized and antigen retrieval was performed by boiling at 98°C in 0.05% citraconic acid anhydride (Sigma, St. Louis, USA), pH7.4 for 20 min. Unspecific binding was blocked in 3%
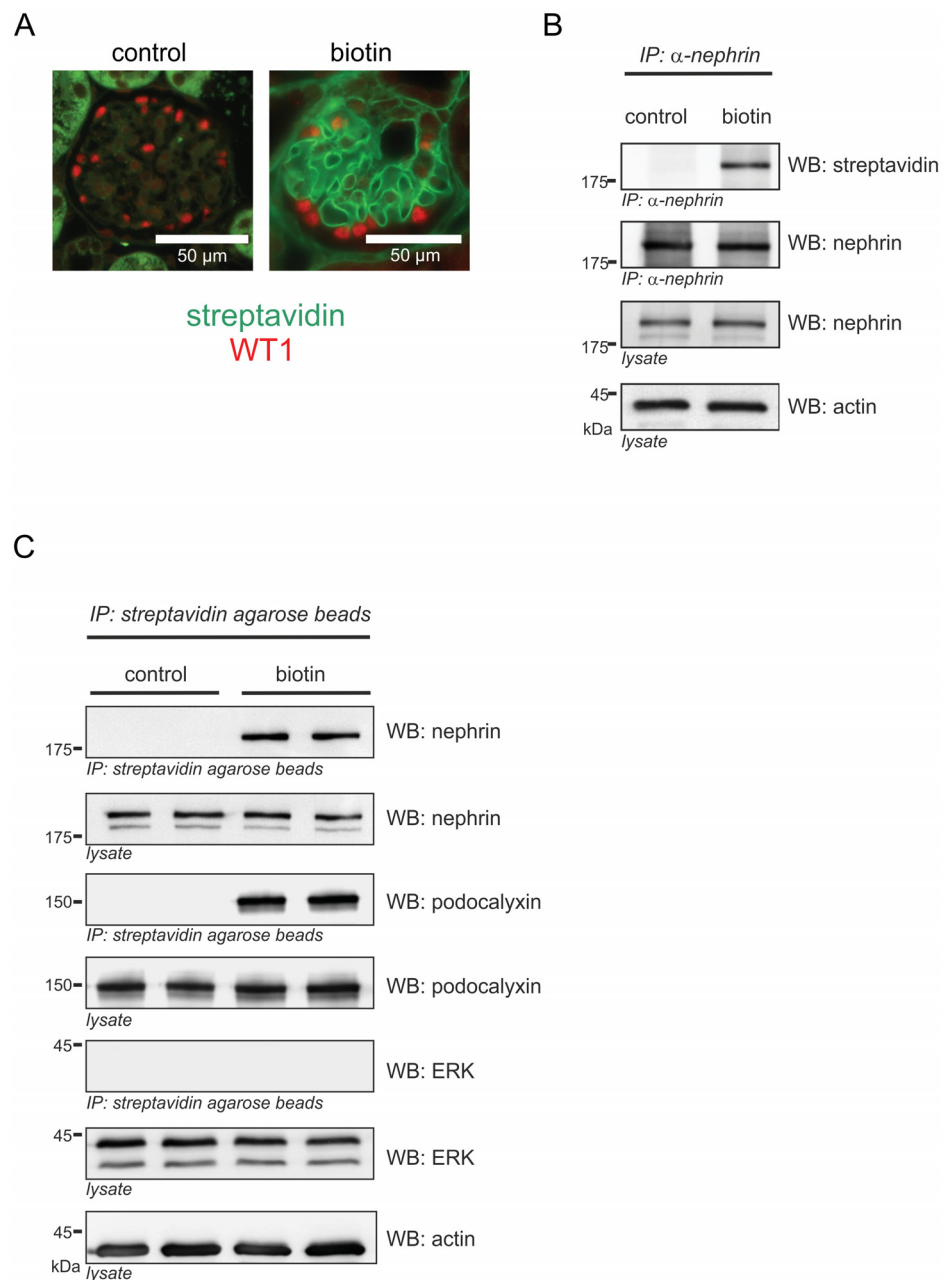
Fig 1. Detection of biotin in murine glomeruli. (A) Representative immunofluorescence staining of kidney sections of C57Bl/6 mice. Podocyte nuclei were labeled by WT1 staining (red). Biotin was detected with streptavidin (green). In biotin-perfused mice (biotin), biotin was detected along the glomerular capillaries. PBS-perfused mice (control) did not show any biotin deposition. **(B)** Western blot analysis after immunoprecipitation of nephrin (IP α-nephrin) from biotin-perfused (biotin) and PBS-perfused (control) murine kidneys. A biotinylated fraction of nephrin (WB streptavidin) was only detectable in biotin-perfused mice. Total nephrin immunoprecipitates and lysates (WB nephrin) showed equal expression of total nephrin. Beta-actin (actin) was used as a loading control. **(C)** Western blot analysis after immunoprecipitation of biotinylated surface proteins (IP streptavidin agarose beads) from biotin-perfused (biotin) and PBS-perfused (control) murine kidneys. Biotinylated nephrin (WB nephrin) and podocalyxin (WB podocalyxin) were only detectable in biotin-perfused mice. Extracellular-signal regulated kinases p42 and p44 (ERK) could not be detected at all. Total nephrin, podocalyxin and ERK lysates (WB nephrin, WB podocalyxin and WB ERK) showed equal expression of nephrin, podocalyxin and ERK. Beta-actin (actin) was used as a loading control.
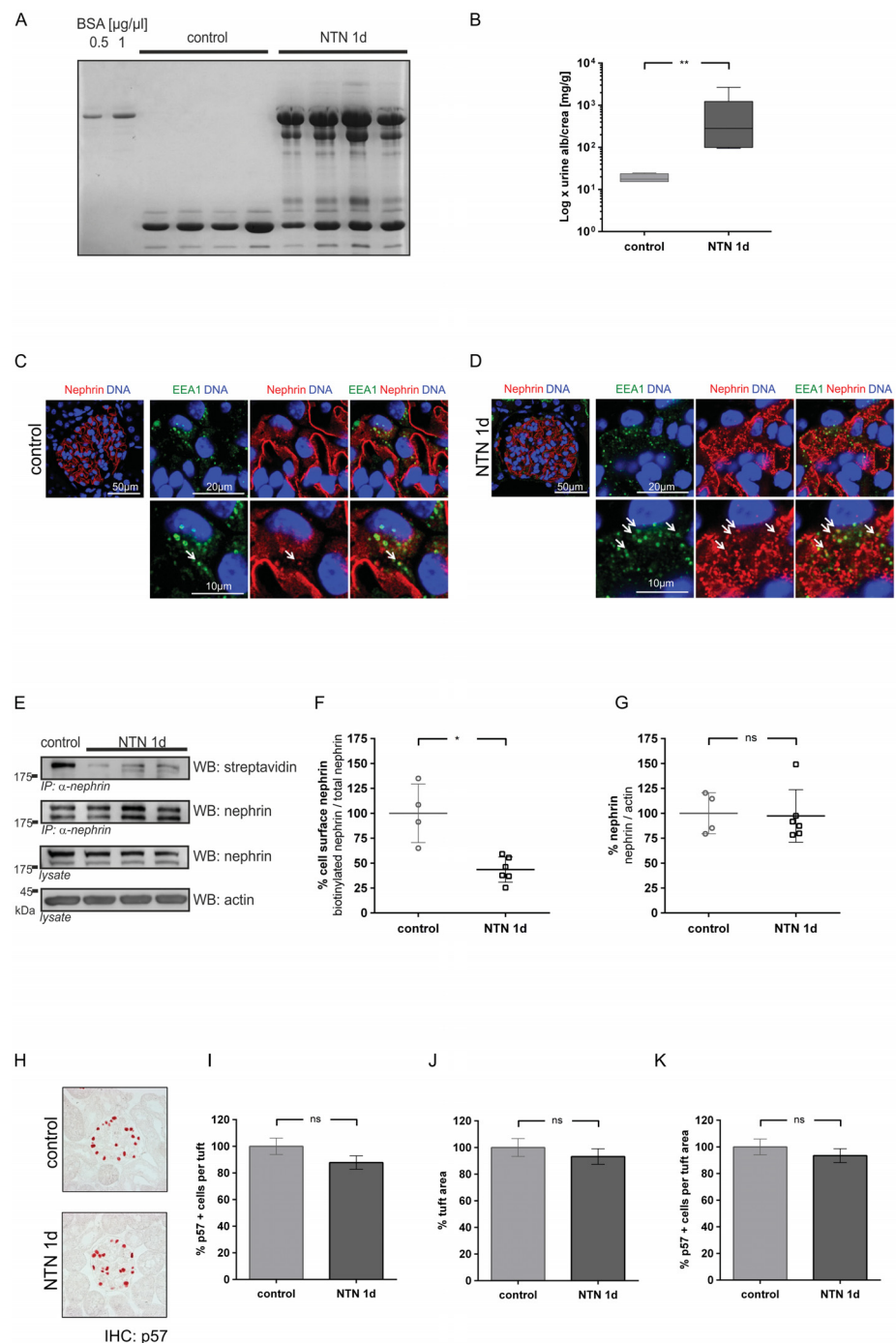
https://doi.org/10.1371/journal.pone.0179217.g001

Fig 2. Albuminuria and nephrin surface abundance in early nephrotoxic nephritis. (A) Coomassie gel shows albuminuria in mice injected with NTN serum (NTN 1d). No albuminuria was detected in mice injected with normal saline (control). **(B)** Quantitative evaluation of albumin-creatinine excretion in healthy mice (control) and NTN mice (NTN 1d). Statistical analysis: Mann-Whitney U test, ** p < 0.01 (control: n = 4; NTN: n = 6). **(C, D)** Immunofluorescence staining of murine kidney sections of healthy mice (control) and mice injected with NTN serum (NTN 1d). Staining was performed with an anti-nephrin antibody (red), an anti-EEA1-antibody (green) and nuclear DNA with Draq5 (blue). White arrows indicate colocalization of nephrin with EEA1 positive vesicles. **(E)** Representative western blot of total and biotinylated nephrin detected with streptavidin (streptavidin). In comparison to untreated mice (control) less surface nephrin (WB: streptavidin) was detected in NTN mice (NTN 1 d). Total nephrin immunoprecipitates and lysates (WB: nephrin) showed

equal expression of total nephrin in both groups. β-actin (WB: actin) was used as loading control. **(F, G)** Densitometric analysis of western blots: **(F)** Amount of nephrin at the cell surface graphed as biotinylated nephrin to total nephrin ratio; **(G)** Amount of total nephrin graphed as total nephrin to β-actin ratio. **(H)** Immunohistochemistry: staining of p57 indicates podocytes in healthy mice (control) and NTN mice (NTN d1). **(I)** Number of p57 positive cells per glomerular tuft **(J)** Glomerular tuft area (μm^2) **(K)** Percentage of p57 positive cells in relation to tuft area. (40 gloms per mouse quantified). Western Blot data show means ± SD. Podocyte counts show means ± SEM. Statistical analysis: unpaired *t*-test with Welch's correction. Significance level was set to 5%, *p < 0.01, ** p<0.001, (non-significant differences (ns)).

goat serum for 60 min at RT. Primary antibody incubation (rabbit α-WT1 1:800, Santa-Cruz, Santa-Cruz, USA) was performed in blocking buffer o/n at 4˚C. Binding was visualized by incubation with TRITC-α-rabbit coupled secondary antibodies (Abcam, Eugene, USA) diluted 1:300 in blocking buffer for 60 min at RT. Stainings were evaluated with a Zeiss Axio Observer microscope using the LSM software (Zeiss, Jena, Germany).

Nephrin—EEA1. For immunofluorescent stainings, 2 μm paraffin sections were deparaffinized and antigen retrieval was performed by boiling at 98˚C in 0.05% citraconic acid anhydride (Sigma, St. Louis, USA), pH7.4 for 40 min. Unspecific binding was blocked in 5% horse serum with 0.05% Triton X-100 for 30 min at RT. Primary antibody incubations (guinea-pig α-nephrin (IF 1:200, Acris, Rockville, USA) and rabbit α-EEA1 (IF 1:400, Santa Cruz, Santa Cruz, USA) were performed in blocking buffer o/n at 4˚C. Binding was visualized by incubation with AF488-α-guinea pig or Cy3-α-rabbit coupled secondary antibodies (all affinity-purified donkey antibodies Jackson ImmunoResearch, West Grove, USA) diluted 1:400 in blocking buffer for 30 min at RT. Stainings were evaluated with a Zeiss LSM 510 meta microscope using the LSM software (all Zeiss, Jena, Germany).

Quantification of podocyte loss

As described before staining of the CDK-inhibitor p57 was used to measure the number of healthy podocytes [18, 19]. Two μm thick paraffin sections were deparaffinized and antigen retrieval was performed by boiling for 30 min in 10 mM citrate buffer pH 6.1 at constant 98˚C in a steam cooker. Unspecific binding was blocked (5% horse serum, 30 min RT). Rabbit anti-p57 (Santa Cruz, Santa Cruz, USA) diluted 1:400 in 5% horse serum was incubated o/n at 4˚C. Color development was performed with the ZytoChem-Plus AP Polymer-Kit (Zytomed, Berlin, Germany) according to the manufacturers' instructions with neufuchsin. Stainings were evaluated under an Axioskop and photographed with an Axiocam HRc using the Axiostar software (all Zeiss, Jena, Germany). Quantification of podocyte loss was performed using a serpentine movement from cortex to medulla and vice versa. The outlines and p57-positive nuclei of 40 consecutively encountered capillary tufts were traced and counted manually at a 400-fold magnification in a blinded manner. The mean podocyte number per glomerular random cross-sectional area was calculated.

Results

Quantification of nephrin surface expression in mice

Mice were perfused with either biotin or phosphate buffered saline (PBS). In kidneys perfused with biotin, linear staining along the glomerular capillaries was visualized. No staining was detected in controls perfused with PBS (Fig 1A). To quantify the surface fraction of nephrin two different approaches have been used. First, nephrin was separated by immunoprecipitation with a nephrin specific antibody, followed by SDS-PAGE and western blot analyses. The biotinylated fraction of nephrin, was then visualized by staining with streptavidin. No
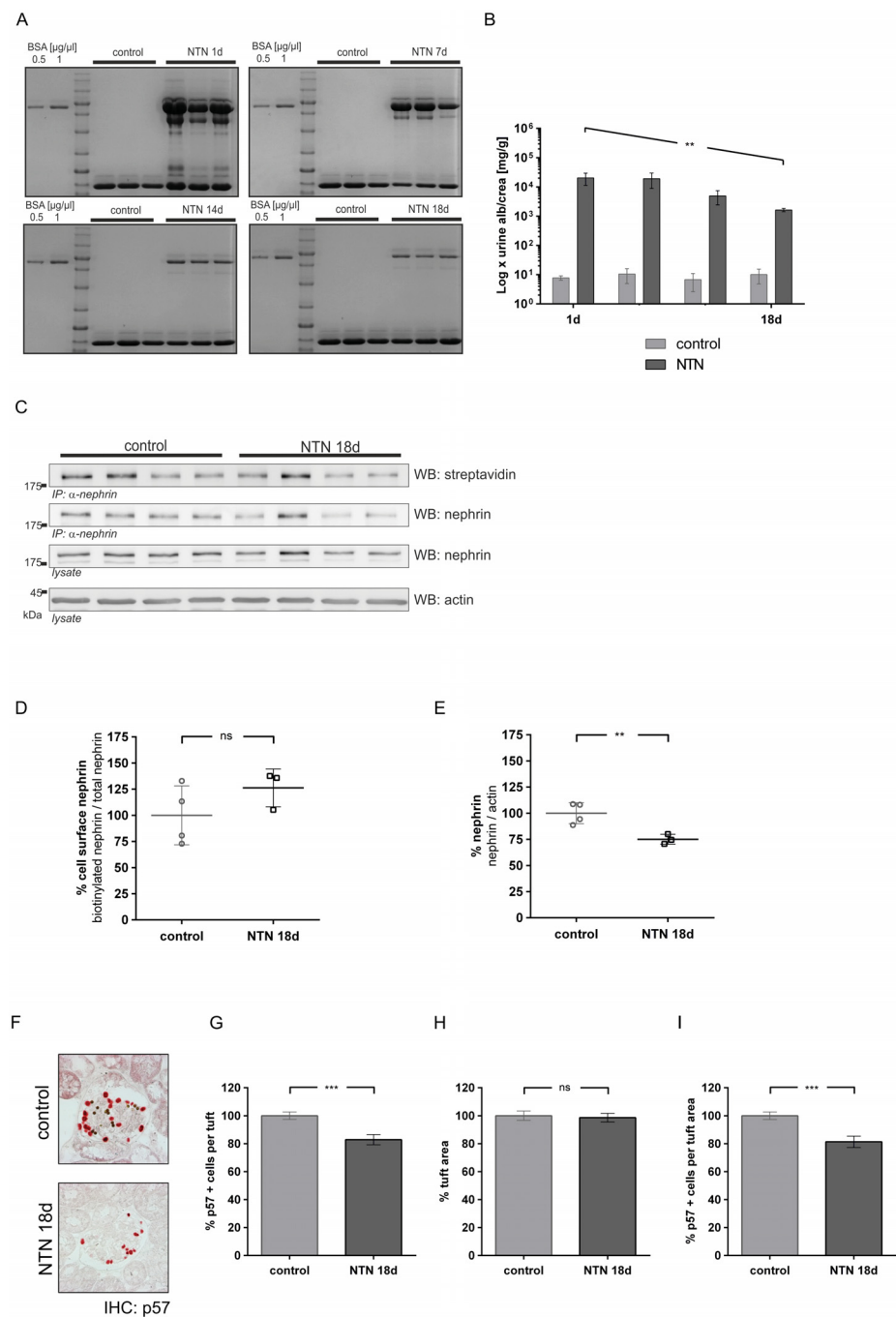
Fig 3. Albuminuria and nephrin surface abundance in late nephrotoxic nephritis. (A) Coomassie gel loaded with urine samples collected on days 1, 7, 14, and 18 after serum injection (BSA standard, left). In NTN mice, albuminuria decreased over the course of 18 days. **(B)** Quantitative analysis of albumin to creatinine excretion in healthy (light grey) and NTN mice (dark grey) on days 1, 7, 14, and 18. Statistical analysis: one-way ANOVA test for linear trend, ** $p < 0.005$ (control: n = 4; NTN: n = 3). **(C)** Western blot analysis of total nephrin and biotinylated nephrin (streptavidin) from control mice (control) versus NTN mice 18 days (NTN 18 d) after serum injection. In comparison to control mice (control), less surface nephrin (WB: streptavidin) was detected in NTN mice (NTN 18 d). Total nephrin immunoprecipitates and lysates (WB: nephrin) demonstrated less expression of total nephrin after 18 days. β-actin (WB: actin) was used as the loading control. **(D, E)** Densitometric analysis of western blots: **(D)** Amount of surface nephrin graphed as biotinylated nephrin to total nephrin ratio; **(E)** Amount of total nephrin graphed as total nephrin to β-actin ratio. **(F)** Immunohistochemistry:

staining of p57 (red) indicates podocytes in healthy mice (control) and NTN mice (NTN 1d). Magnetic beads appear as black dots. **(G)** Number of p57 positive cells per glomerular tuft **(H)** Glomerular tuft area (μm^2) **(I)** Percentage of p57 positive cells in relation to tuft area (control n = 2, NTN n = 2, 40 gloms per mouse quantified). Western blot data show means ± SD. Podocyte counts show means ± SEM. Statistical analysis: unpaired *t*-test with Welch's correction. Significance level was set to 5%, ** p < 0.001, *** p<0.0001, (non-significant differences (ns)).

biotinylated nephrin was detected in PBS perfused controls. Lysate controls indicated equal amounts of protein (Fig 1B). Second, the reverse experiment has been performed. Biotinylated proteins were separated by pull-down with strepatividin agarose beads, followed by SDS-PAGE and western blot analyses. The nephrin fraction was visualized by staining with a nephrin specific antibody. To demonstrate that the assay allows the detection of other glomerular surface proteins podocalyxin was detected. The intracellular control proteins extracellular-signal regulated kinases p42 and p44 (ERK) could not be detected. Further, no biotinylated proteins were detected in PBS perfused controls. Lysate controls indicated equal amounts of protein. (Fig 1C).

Nephrin surface expression in nephrotoxic nephritis

Early nephrotoxic nephritis. Nephrotoxic nephritis (NTN) rapidly induces severe proteinuria in its heterologous phase [20]. One day after injection of the NTN serum, proteinuria in mice significantly increased 3–4 log ranks (Fig 2A and 2B). In comparison to untreated kidneys induction of NTN led to a transformation of the linear staining of nephrin to a punctate pattern. High resolution images show an enhanced colocalization of nephrin with early endosomal antigen 1 (EEA-1) (Fig 2C and 2D), suggesting increased endocytosis of the nephrin molecules. Loss of nephrin from the slit diaphragm was then quantified using the biotinylation assay (Fig 2E). At day 1, densitometric analysis of the western blot results indicated a 57% decrease of biotinylated nephrin in NTN mice (Fig 2F), but equal amounts of total nephrin were detected (Fig 2G). In line with this finding the podocyte numbers remained stable in the NTN mice compared to untreated animals (Fig 2H–2K).

Late nephrotoxic nephritis. Albuminuria decreased significantly over the course of 18 days (Fig 3A and 3B). At day 18, the results of the western blot analysis conducted after biotinylation indicated the recovery of surface nephrin (Fig 3C). At day 18, the densitometric results showed no significant differences between the percentage of cell surface nephrin in either group (Fig 3D). However, total nephrin was reduced by 25% in NTN mice at day 18 (Fig 3E). Podocyte numbers were reduced by approximately 19% in NTN mice (Fig 3F–3J).

Adriamycin induced nephropathy

Adriamycin induced nephropathy (ADR) is a model of focal segmental sclerosis [21]. Six days after injection, a significant four log rank increase of proteinuria (compared to controls) was detected (Fig 4A and 4B). In comparison to healthy mice adriamycin induced a disruption of the linear staining pattern of nephrin, which was replaced by a fragmented and granulated cytoplasmic staining pattern. High resolution images show an enhanced colocalization of nephrin with EEA-1, suggesting endocytosis of nephrin (Fig 4C and 4D). These findings were confirmed in the *in vivo* biotinylation assay that was conducted using a western blot analysis (Fig 4E). Densitometric evaluation of the results at day 7 revealed that, despite a reduction of total nephrin by 71% (Fig 4F), biotinylated nephrin was still significantly decreased by 53% (Fig 4G). Podocyte numbers were reduced by approximately 40% (Fig 4H–4K).
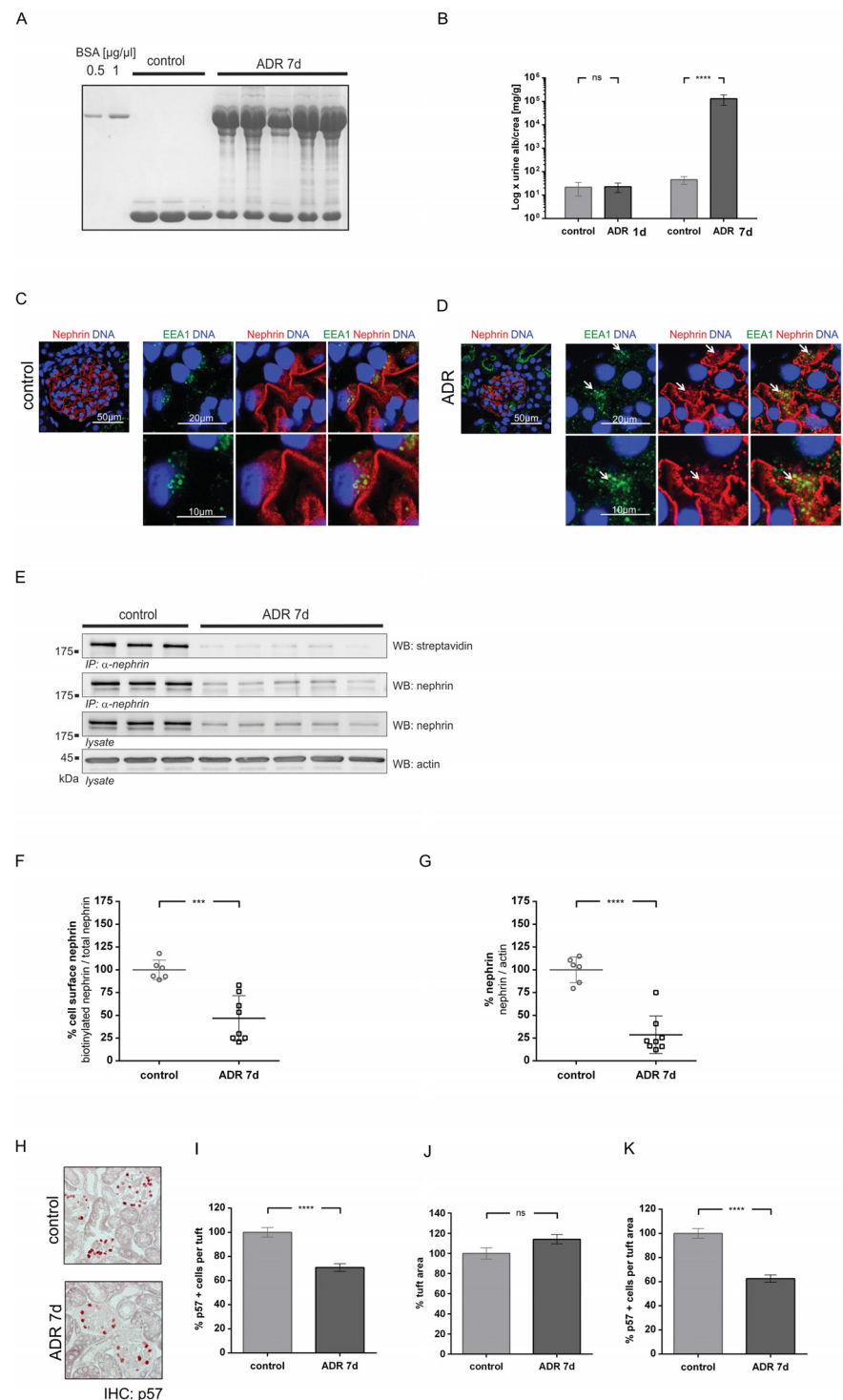
Fig 4. Nephrin surface abundance in adriamycin nephropathy at day 7. (A) Coomassie gel shows albuminuria in ADR mice at day 7 (ADR 7d), which was not detected in healthy mice (control). **(B)** Quantitative analysis of the albumin to creatinine ratio in healthy mice (control) versus ADR mice on days 1 and 7 (ADR1 and ADR 7). Statistical analysis: *t*-test with Welch's correction was performed on day 1 and 7. **** p < 0.0001 (non-significant differences (ns); control: n = 9; ADR: n = 12). **(C, D)** Immunofluorescence staining of glomeruli from healthy mice (control) or ADR mice (ADR 7 d). Staining was performed with an anti-nephrin antibody

(red), and nuclei were stained with DAPI (blue). White arrows indicate colocalization of nephrin with EEA1 positive vesicles. **(E)** Western blot analysis of surface nephrin (streptavidin) and total nephrin immunoprecipitates and lysates (WB nephrin). In comparison to healthy mice (control), less surface nephrin (WB: streptavidin) was detected in ADR mice at day 7 (ADR 7d). Total nephrin immunoprecipitates and lysates (WB: nephrin) showed less expression of total nephrin at day 7. β-actin (WB: actin) was used as loading control. **(F, G)** Densitometric analysis of western blots: **(F)** Amount of cell surface nephrin graphed as biotinylated nephrin to total nephrin ratio; **(G)** Amount of total nephrin graphed as total nephrin to β-actin ratio. **(H)** Immunohistochemistry: staining of p57 indicates podocytes in healthy mice (control) and NTN mice (NTN d1). **(I)** Number of p57 positive cells per glomerular tuft **(J)** Glomerular tuft area (μm^2) **(K)** Ratio of p57 positive cells in relation to tuft area (control n = 2, ADR n = 3, 40 gloms per mouse quantified). Western blot data show means ± SD. Podocyte counts show means ± SEM. Statistical analysis: unpaired *t*-test with Welch's correction. Significance level was set to 5%, *** p < 0.0001, **** p<0.00001, (non-significant differences (ns)).

Discussion

The *in vivo* biotinylation assay allowed the quantification of nephrin abundance at the glomerular slit diaphragm of mice. This method is useful as a complementary technique to immunofluorescence, and expands the possibilities of studies focusing on the expression and trafficking of glomerular surface proteins. As proof of principle the hallmark proteins of the podocyte nephrin and podocalyxin have been detected. To demonstrate the usefulness of the assay, we quantified nephrin surface abundance in two different and well-established models of proteinuric kidney disease.

NTN led to the rapid induction of albuminuria, which was nearly reversible in the course of disease. Quantification of nephrin revealed that more than half of the molecules were lost from the slit diaphragm at the peak of albuminuria, while the amount of total nephrin was preserved. In addition, the results of immunofluorescence studies showed a change of the linear distribution of nephrin to a punctate pattern. Colocalization experiments revealed that nephrin was translocated from the podocyte surface to the early endosome suggesting endocytosis of nephrin. Besides endocytosis changes in podocyte morphology and loss of podocytes presumably contribute to the observed pattern change. These findings are in line with previous results [8]. When albuminuria decreased once again, the surface abundance of nephrin was restored. However, after 18 days, nephrin abundance was diminished by approximately 25%. Histologic analysis of podocyte numbers suggested that this reduction in total nephrin was most likely caused by loss of podocytes. Our finding is also in line with previous reports of nephrotoxic nephritis [22]. Regarding ADR, albuminuric animals also showed significant reductions of surface nephrin. Immunofluorescence revealed an enhanced translocation of nephrin in vesicles of the early endosome. Moreover, there was a marked reduction of total nephrin most likely due to the loss of podocytes. This finding has been reported for ADR earlier [23], and is supported by our observation that podocyte numbers are strongly reduced in ADR at day 7. It should be kept in mind that an impaired perfusion with the magnetic particles due to advanced damage of the glomerular tuft could lead to a biased quantification of glomerular proteins. However, it might be questioned whether the inside of damaged capillary tufts would be adequately covered with biotin when extracted glomeruli are bathed in biotin like described by Satoh et al. [16]. To account for fluctuations in total protein yield and to ensure accurate quantitation and comparability between different experiments, all Western blot replicates have been normalized to beta actin.

Conclusion

In both models of proteinuric kidney disease nephrin surface abundance correlated inversely with proteinuria. In nephrotoxic nephritis we could show that proteinuria and nephrin loss

were reversible. Taken together this proof-of-concept study shows the potential of the *in vivo* biotinylation assay to gain more insight into the function of the glomerular filter.

Acknowledgments

Author Contributions

Conceptualization: IQ MW.

Data curation: RH MW IQ.

Formal analysis: RH MW IQ.

Funding acquisition: IQ MW.

Investigation: RH SAP CMS CF TW EK JS.

Methodology: MW RH CMS IQ SAP.

Project administration: MW RH.

Resources: UP.

Supervision: MW IQ.

Validation: MW IQ.

Visualization: CMS MW IQ.

Writing – original draft: IQ MW RH.

Writing – review & editing: LCR LS EK TW UP JS EK.

References

1. Tsai WC, Wu HY, Peng YS, Ko MJ, Wu MS, Hung KY, et al. Risk Factors for Development and Progression of Chronic Kidney Disease: A Systematic Review and Exploratory Meta-Analysis. Medicine. 2016; 95(11):e3013. Epub 2016/03/18. https://doi.org/10.1097/MD.0000000000003013 PMID: 26986114;

2. Kalaitzidis R, Bakris G. Pathogenesis and treatment of microalbuminuria in patients with diabetes: the road ahead. J Clin Hypertens (Greenwich). 2009; 11(11):636–43. Epub 2009/11/03. https://doi.org/10.1111/j.1751-7176.2009.00184.x PMID: 19878372.

3. Quack I, Rump LC, Gerke P, Walther I, Vinke T, Vonend O, et al. beta-Arrestin2 mediates nephrin endocytosis and impairs slit diaphragm integrity. Proceedings of the National Academy of Sciences of the United States of America. 2006; 103(38):14110–5. Epub 2006/09/14. https://doi.org/10.1073/pnas.0602587103 PMID: 16968782;

4. Quack I, Woznowski M, Potthoff SA, Palmer R, Konigshausen E, Sivritas S, et al. PKC alpha mediates beta-arrestin2-dependent nephrin endocytosis in hyperglycemia. The Journal of biological chemistry. 2011; 286(15):12959–70. Epub 2011/02/16. https://doi.org/10.1074/jbc.M110.204024 PMID: 21321125;

5. Inoue K, Ishibe S. Podocyte endocytosis in the regulation of the glomerular filtration barrier. American journal of physiology Renal physiology. 2015; 309(5):F398–405. Epub 2015/06/19. https://doi.org/10.1152/ajprenal.00136.2015 PMID: 26084928;

6. Soda K, Ishibe S. The function of endocytosis in podocytes. Current opinion in nephrology and hypertension. 2013; 22(4):432–8. Epub 2013/05/25. https://doi.org/10.1097/MNH.0b013e3283624820 PMID: 23703394;

7. Swiatecka-Urban A. Endocytic Trafficking at the Mature Podocyte Slit Diaphragm. Front Pediatr. 2017; 5:32. https://doi.org/10.3389/fped.2017.00032 PMID: 28286744;

8.   Babayeva S, Rocque B, Aoudjit L, Zilber Y, Li J, Baldwin C, et al. Planar cell polarity pathway regulates nephrin endocytosis in developing podocytes. The Journal of biological chemistry. 2013; 288 (33):24035–48. Epub 2013/07/05. https://doi.org/10.1074/jbc.M113.452904 PMID: 23824190;

9.   Babayeva S, Zilber Y, Torban E. Planar cell polarity pathway regulates actin rearrangement, cell shape, motility, and nephrin distribution in podocytes. American journal of physiology Renal physiology. 2011; 300(2):F549–60. Epub 2010/06/11. https://doi.org/10.1152/ajprenal.00566.2009 PMID: 20534871.

10. Teng B, Schroder P, Muller-Deile J, Schenk H, Staggs L, Tossidou I, et al. CIN85 deficiency prevents nephrin endocytosis and proteinuria in diabetes. Diabetes. 2016. Epub 2016/08/18. https://doi.org/10.2337/db16-0081 PMID: 27531950.

11. Tossidou I, Teng B, Drobot L, Meyer-Schwesinger C, Worthmann K, Haller H, et al. CIN85/RukL is a novel binding partner of nephrin and podocin and mediates slit diaphragm turnover in podocytes. The Journal of biological chemistry. 2010; 285(33):25285–95. Epub 2010/05/12. https://doi.org/10.1074/jbc.M109.087239 PMID: 20457601;

12. Waters AM, Wu MY, Huang YW, Liu GY, Holmyard D, Onay T, et al. Notch promotes dynamin-dependent endocytosis of nephrin. Journal of the American Society of Nephrology: JASN. 2012; 23(1):27–35. Epub 2011/11/05. https://doi.org/10.1681/ASN.2011010027 PMID: 22052054;

13. Qin XS, Tsukaguchi H, Shono A, Yamamoto A, Kurihara H, Doi T. Phosphorylation of nephrin triggers its internalization by raft-mediated endocytosis. Journal of the American Society of Nephrology: JASN. 2009; 20(12):2534–45. Epub 2009/10/24. https://doi.org/10.1681/ASN.2009010011 PMID: 19850954;

14. Soda K, Balkin DM, Ferguson SM, Paradise S, Milosevic I, Giovedi S, et al. Role of dynamin, synaptojanin, and endophilin in podocyte foot processes. The Journal of clinical investigation. 2012; 122 (12):4401–11. Epub 2012/11/29. https://doi.org/10.1172/JCI65289 PMID: 23187129;

15. Dundas CM, Demonte D, Park S. Streptavidin-biotin technology: improvements and innovations in chemical and biological applications. Applied microbiology and biotechnology. 2013; 97(21):9343–53. Epub 2013/09/24. https://doi.org/10.1007/s00253-013-5232-z PMID: 24057405.

16. Satoh D, Hirose T, Harita Y, Daimon C, Harada T, Kurihara H, et al. aPKClambda maintains the integrity of the glomerular slit diaphragm through trafficking of nephrin to the cell surface. J Biochem. 2014; 156 (2):115–28. https://doi.org/10.1093/jb/mvu022 PMID: 24700503;

17. Yan K, Khoshnoodi J, Ruotsalainen V, Tryggvason K. N-linked glycosylation is critical for the plasma membrane localization of nephrin. Journal of the American Society of Nephrology: JASN. 2002; 13 (5):1385–9. PMID: 11961028.

18. Hiromura K, Haseley LA, Zhang P, Monkawa T, Durvasula R, Petermann AT, et al. Podocyte expression of the CDK-inhibitor p57 during development and disease. Kidney Int. 2001; 60(6):2235–46. https://doi.org/10.1046/j.1523-1755.2001.00057.x PMID: 11737597.

19. Taniguchi Y, Pippin JW, Hagmann H, Krofft RD, Chang AM, Zhang J, et al. Both cyclin I and p35 are required for maximal survival benefit of cyclin-dependent kinase 5 in kidney podocytes. American journal of physiology Renal physiology. 2012; 302(9):F1161–71. https://doi.org/10.1152/ajprenal.00614.2011 PMID: 22262481;

20. Assmann KJ, Tangelder MM, Lange WP, Schrijver G, Koene RA. Anti-GBM nephritis in the mouse: severe proteinuria in the heterologous phase. Virchows Archiv A, Pathological anatomy and histopathology. 1985; 406(3):285–99. Epub 1985/01/01. PMID: 3923705.

21. Lee VW, Harris DC. Adriamycin nephropathy: a model of focal segmental glomerulosclerosis. Nephrology (Carlton). 2011; 16(1):30–8. Epub 2010/12/24. https://doi.org/10.1111/j.1440-1797.2010.01383.x PMID: 21175974.

22. Sussman AN, Sun T, Krofft RM, Durvasula RV. SPARC accelerates disease progression in experimental crescentic glomerulonephritis. The American journal of pathology. 2009; 174(5):1827–36. Epub 2009/04/04. https://doi.org/10.2353/ajpath.2009.080464 PMID: 19342370;

23. Pereira Wde F, Brito-Melo GE, de Almeida CA, Moreira LL, Cordeiro CW, Carvalho TG, et al. The experimental model of nephrotic syndrome induced by Doxorubicin in rodents: an update. Inflammation research: official journal of the European Histamine Research Society [et al]. 2015; 64(5):287–301. Epub 2015/03/20. https://doi.org/10.1007/s00011-015-0813-1 PMID: 25788426.